DESIGN AND MODELLING OF A MINIATURISED ULTRASONIC MACHINING SYSTEM

Thesis submitted in accordance with the requirements of the University of Liverpool for the degree of Doctor in Philosophy

by

Wanwanut Boongsood

December 2012

ABSTRACT

Ultrasonic Machining (USM) is the outstanding manufacturing process for producing complex cavities for all materials subjected to brittle fracture without the requirements of electrical/thermal conductivity or chemical reactivity. As a result, a wide range of materials can be fabricated efficiently. Even though the process benefits a variety of applications, the use of this method is not widespread because of the complexity of a large number of interacting parameters affecting the machining operation. Additionally, commercial machines available in the market tend to be rather large. In an age of micro-manufacturing and nanotechnology, as well as sustainable development, it is wasteful to machine hard and brittle materials in meso/micro scale geometries with the large equipment currently available.

This research developed a miniaturised USM system. The effects of each of the different design parameters were considered and organised effectively using the Axiomatic Design approach to understanding the behaviour of a complex system. The system components were designed, modelled and then simulated with Finite Element Analysis software to characterise their responses, and were also optimised using a Design and Experiments method for a robust design. Prototypes were built and tested to validate the design. The dynamic characteristics based on prototype testing did not agree well with the computer simulation results. It was believed that this was the result of non-linearity behaviour caused by electrical impedance mismatching. Glass ceramic machining was investigated. A prediction equation of machining rates was proposed in a simple form. Through the novel miniature design, the material removal rates were comparatively superior compared with conventional systems while the size of the proposed transducer and horn assembly was reduced to half that of typical horn shapes.

ACKNOWLEDGEMENT

This thesis would not have been possible without the kind support and supervision of Professor Bernard Hon and Professor Hugh Clare.

Besides, I am indebted to several individuals who contributed and extended their valuable assistance to this project, namely Dr. Gary Seiffert, Dr. Carl Hopkins and everyone in the Acoustic Research Unit; Derek Neary; Stephen Boyes, Duncan Smith, Dr. Anthony Deakin and others in the Department of Electrical Engineering and Electronics; Dr. Chris Sutcliffe and his students; and Professor Margaret Lucas and her students in the University of Glasgow.

I also wish to thank all my colleagues and staff in the School of Engineering.

Last but not least, a special thought goes to all my family, students in the Liverpool Thai Society, and colleagues in Suranaree University of Technology for giving me the strength. You are my vitality.

CONTENTS

LIST OF FIGURES

Number *Page*

LIST OF TABLES

Number *Page*

LIST OF ACRONYMS AND ABBREVIATIONS

AD	Axiomatic Design Approach
AJM	Abrasive Jet Machining
ANOVA	Analysis of Variance
AWJM	Abrasive and Water Jet Machining
C	Capacitor
CAD	Computer-Aid Design
CCD	Central Composite Design
CHM	Chemical Machining
CNC	Computer Numerical Control
DOE	Design of Experiments
DP	Design Parameter
EBM	Electron Beam Machining
ECG	Electrochemical Grinding
ECM	Electrochemical Machining
EDM	Electrical Discharge Machining
FEA	Finite Element Analysis Method
FEM	Finite Element Modelling
FFD	Full Factorial Design
FFT	Fast Fourier Transform
FR	Functional Requirement
F-test	A statistical test having an F-distribution under the null hypothesis.

GMM	Giant Magnetostrictive Composite Material
IBM	Ion Beam Machining
L	Inductor
LBM	Laser Beam Machining
LDV	Laser Doppler Vibrometry
MRR	Material Removal Rate
MS	Machining Speed
PAC	Plasma Arc Cutting
PCM	Photochemical Machining
PSI	Phase Shifting Interferometry
P-value	The smallest level of significant that would lead to the rejection of the null hypothesis with the given data.
PZT	Piezoelectric Material (Lead Zirconate Titanate)
Q-factor	Quality Factor
R	Resistor
Ra	Roughness Average of a Surface
RSA	Response Surface Analysis
S/N	Signal-to-Noise Ratio
SLM	Selective Laser Melting
USM	Ultrasonic Machining
VSI	Vertical Scanning Interferometry
WJM	Water Jet Machining
WLI	White-Light Interferometry

Chapter 1

Introduction

There is a drive for products today to have a variety of functions and to be smaller in size. The underlying drive is sustainability and the need to preserve the Earth's precious resources. The integration of functions and miniaturisation of components is being driven by the development of micro-fabrication technology.

Ultrasonic Machining (USM) is a means of mechanical material removal from a work-piece which would benefit from miniaturisation. USM does not need electrical conductivity or chemical reactivity of a work-piece to enable material removal. The method is especially suitable for hard and brittle materials which are normally difficult to machine. To develop a miniaturised ultrasonic machining device would revolutionise its use, enabling it to become a household tool as well as being a more efficient industrial tool.

This chapter is divided into six sections. Section 1.1 to 1.3 is the explanation of the background of USM and related processes. Section 1.4 is the motivation behind the project. The objectives and scope of the work are presented in Section 1.5. Section 1.6 is research methodology. The outline of this thesis is presented in Section 1.7.

1.1 Conventional Machining Processes

The classification of machining processes is shown in Figure 1.1. Generally, material shaping is carried out by creating a chip with an applied shear force between a strong cutting tool placed against a work-piece. The excess material can be removed from solid objects and what remains is the desired profile. A

number of various geometries can be made by many kinds of conventional machining operations.

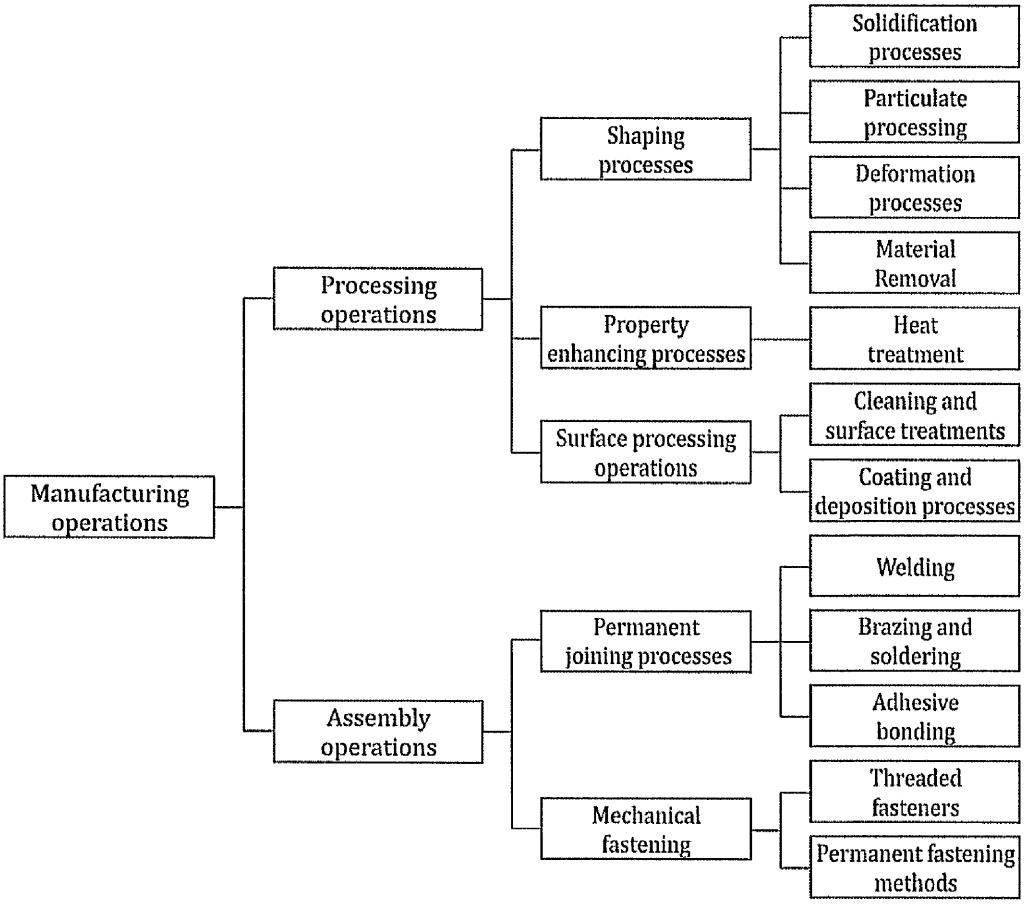

Figure 1.1: Classification of Manufacturing Processes (Groover 2011).

They are usually applied as a secondary process to achieve higher precision than solidification, particulate, and deformation processing. Examples of conventional machining processes are turning, drilling, milling, and grinding performed by lathes, drill presses, milling, and grinding machines. These conventional machines normally rely on electric motors for their power and are

controlled by a skilled operator called a machinist to load and unload the work-piece, as well as set-up and adjust cutting and feeding speed during an operation. The design of these classic machines are almost the same as the early ones developed in the 18th century during the Industrial Revolution (Groover 2011). Modern machining is carried out using computer numerical control (CNC) machines.

1.2 Non-conventional Machining Processes

Machining is one of the most important material removal processes in industry, and generally is the means of material shaping by creating a chip through shear force between a strong cutting tool placed against a work-piece. The excess material can be removed from solid objects to give a number of desired shapes by various types of machines such as turning, drilling, milling, and grinding.

Products today generally require more complexity and durability. In this new era, a lot of new materials are being developed and some of them have much higher strengths. Thus, manufacturing techniques have been challenged. New methods based on material removal which have been developed for this challenge can be grouped into 'Non-conventional Machining Processes'.

Non-conventional machining processes have been developed enormously since the 1940s. During the World War II, many new applications forced manufacturing technologies to introduce new tools and new forms of energy to fulfil unusual requirements. The non-traditional machining processes since then have been developed increasingly to meet the demands including (Benedict 1987; Groover 2011);

- The development of new materials with special properties which normally are harder and tougher which is more difficult or almost impossible to be fabricated by old-fashioned methods.

- The complexity of new products and their components that calls for a more effective method beyond the performance of conventional machining.
- The requirement of surface damage avoidance that is commonly caused by traditional machining processes.
- The need for more accuracy, repeatability, and reliability to reduce the number of rejects and increase removal rates, results in the cost efficiency of production being enhanced.

Among a variety of non-conventional machining processes, they may be classified into 4 groups as shown in Figure 1.2 based on the types of energy used for fabrication (Groover 2011; Singh 2007) which are as follows:

(i) **Mechanical.** Some forms of mechanical energy rather than the operation of the usual cutting tool. For instance, high velocity liquid or particles are applied to create shear forces or erosion on the work-piece. The processes in this group include water jet machining (WJM); abrasive & water jet machining (AWJM); abrasive jet machining (AJM); and Ultrasonic Machining (USM). Since these processes have a mechanical base, they are able to machine almost every kind of material. WJM uses high pressure and high velocity of a water stream to create a fine cutting line on the work. A thick work-piece which is very difficult to cut by a single pass can be cut deeper by multi-passes. Abrasive particles can be added to the stream to enable a higher cutting capacity, called AWJM, to cut harder materials. AJM is usually used for surface finishing and de-burring caused by a high velocity gas stream mixed with abrasives. USM, the main process of this thesis, is a very useful method to create complex cavities on hard and brittle surface materials and will be explained further in Section 1.3.

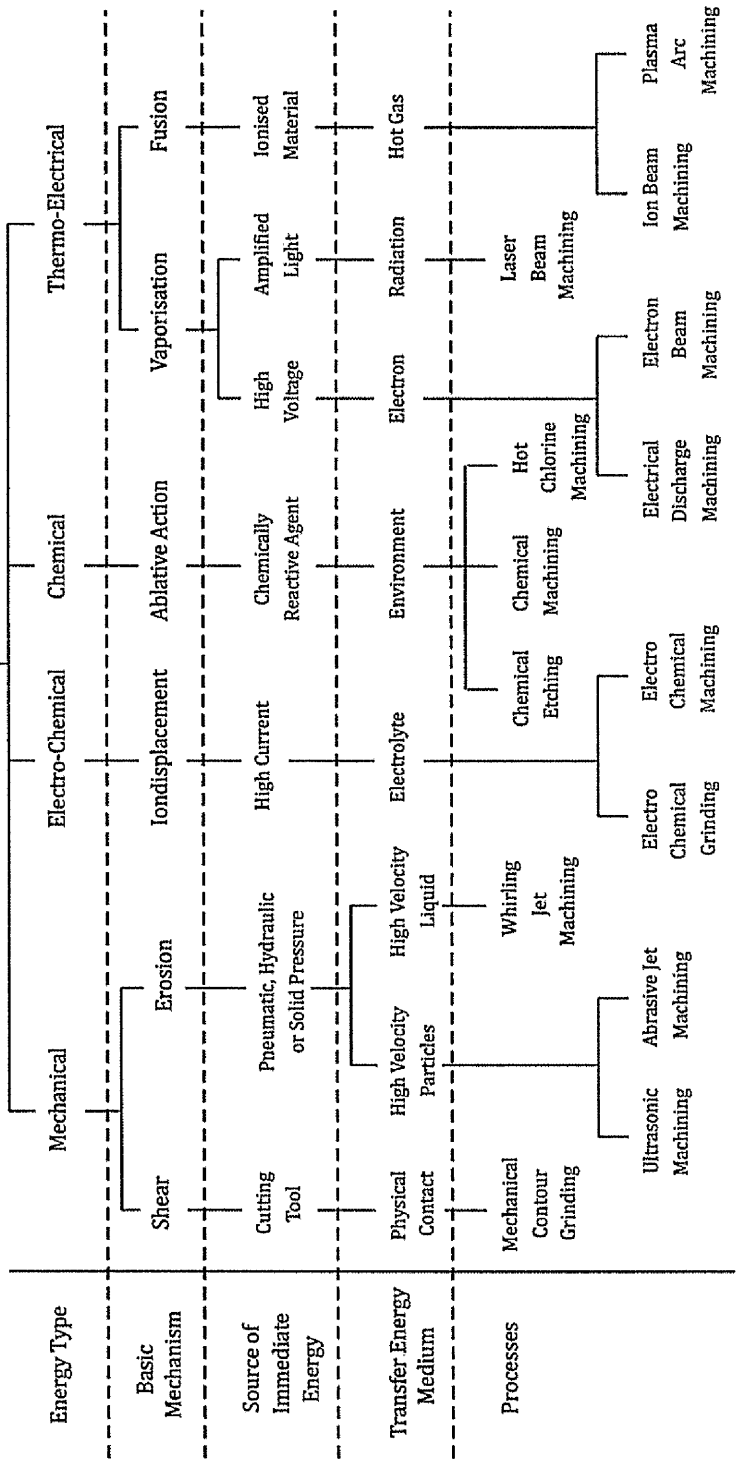

Figure 1.2: Classification of Non-Conventional Manufacturing Processes (Singh 2007).

(ii) **Electro-chemical.** The basic mechanism of this group is ion-displacement for material removal of a conductive work-piece in an electrolyte. Electrochemical machining (ECM) and electrochemical grinding (ECG) are examples of the processes in this group. ECM is normally used for creating deep or difficult to produce cavities in electrically conductive materials. The electrically conducting material is used as the negative pole in an electrical circuit, and a formed tool is used as the positive pole. ECG uses electro-chemical reactions so the life of grinding wheels is a lot longer.

(iii) **Chemical.** This group of machining processes such as chemical machining (CHM) and photochemical machining (PCM) requires a chemical reaction using reactive agents (strong acidic or alkali solution) to remove selected surfaces off a work piece while other areas are covered by a mask. The resolution of machining depends on masking technologies. The material removal rate is controlled by a selection of reactive agents and time of reaction. A depth of cut of 12.5 mm is possible but for most applications in the electronics industry making circuits and semiconductor wafers require depths of a few hundred microns.

(iv) Thermo-electrical. These processes include electrical discharge machining (EDM); electron beam machining (EBM); laser beam machining (LBM); ion beam machining (IBM); and plasma arc cutting (PAC). They use high thermal energy from various sources (high voltage, amplified light, or ionised material) to create a vaporisation or fusion on the work material. Thermal or electrical conductivity of materials influence the machining efficiency of these methods. Materials with low melting points can be machined faster and consume lower energy. EDM is one of the most commonly applied processes. It produces a complex cavity shaped by a formed tool electrode on the work submerged in dielectric fluid. Sparks occur at a small gap between the electrode (negative pole) and the work-

piece (positive pole). This process requires electrical conductivity of the work-piece materials. EBM, LBM, IBM, and PAC are similar but energy of cutting comes from different sources. They are able to cut any known materials but the limit of the cutting depth is usually limited to around a few to 20 millimetres. Among these examples, PAC is the most powerful method; when its heat is high enough it can cut to a depth of 150 mm thick, but is restricted only to conductive materials.

1.3 Ultrasonic Machining Process (USM)

Ultrasonic vibrations have been applied in many ways for the purpose of material processing, for example, ultrasonic vibrations assisted machining and ultrasonic welding. Ultrasonic assisted machining can be classified as the method using ultrasonic oscillations added to the tool heads of conventional machining systems such as drilling, latching, and milling machines in order to improve machining speed. Ultrasonic welding is the technique of applying ultrasonic vibrations to the work-pieces being held together under pressure to create a solid-state weld.

In this thesis, USM is defined as the manufacturing process during which a cavity in a work surface is shaped by either an axially vibrating tool or work-piece at ultrasonic frequencies. The tool bit has the same shape and size as that of the desired shape of the cavity. The resonance of the oscillations is essential for efficient machining. Abrasive particles mixed with liquid can be spread between the tool and work-piece to increase the rate of machining. Machining without abrasives involved is possible but the rate of machining tends to be slower. A variety of different shapes of cavities including round, square, and odd-shaped thru-holes, and cavities of varying depths can be made. As material is removed by mechanical action, material properties of the work-piece such as electrical conductivity and chemical reactivity have no effect on the process. Thus, various types of materials can be machined by USM.

Most of the non-conventional machining processes can be used on metals but not so effective when the processes are used for machining non-metals. The comparison of machining characteristics is presented in Table 1.1 and Table 1.2. Metals are excellent in electrical conductivity which is required for machining by EDM, ECM and PAC and their reactions to chemical solutions are also superior for CHM and PCM.

Table 1.1: Machining Characteristics of Non-Conventional Machining Processes (Groover 2011; Singh 2007).

Machining Characteristic	Non-conventional Processes								Conventional Processes	
	Mech		Elec	Ther				Chem		
	USM	WJM	ECM	EDM	EBM	LBM	PAC	CHM	Milling	Grinding
Material removal rate	C	C	B	C	D	D	A	C	A	B
Dimension control	A	B	B	A-B[b]	A	A	D	A-B[b]	B	A
Surface finish	A	A	B	B-D[b]	B	B	D	B	B-C[b]	A
Surface damage[a]	B	B	A	D	D	D	D	A	B	B-C[b]

Rating A = Excellent, B = Good, C = Moderate, D = Poor.

[a] Good rating means low surface damage. [b] Rating depends on cutting conditions.

Table 1.2: Applicability of Non-Conventional Machining Processes to Selected Work Materials (Groover 2011; Singh 2007).

Work Material	Non-conventional Processes								Conventional Processes	
	Mech		Elec	Ther				Chem		
	USM	WJM	ECM	EDM	EBM	LBM	PAC	CHM	Milling	Grinding
Aluminium	C	C	B	B	B	B	A	A	A	A
Steel	B	D	A	A	B	B	A	A	A	A
Super Alloys	C	D	A	A	B	B	A	B	B	B
Ceramics	A	D	D	D	A	A	D	C	D	C
Glass	A	D	D	D	B	B	D	B	D	C
Silicon			D	D	B	B	D	B	D	B
Plastics	B	B	D	D	B	B	D	C	B	C
Cupboard	D	A	D	D			D	D	D	D
Textiles	A	A	D	D			D	D	D	D

Rating A = Excellent, B = Good, C = Moderate, D = Poor.

The other methods given as examples in section 1.2 can be utilised for both metals and non-metals. However, AJM, AWJM, WJM, EBM and IBM are mainly used for cutting sheet materials. LBM is widely used for both cutting sheet materials and printing details onto flat surface, but the surface quality can be harmed caused by high temperatures. Therefore, USM is the best choice for producing shallow pockets, marking details, and cutting non-metals with excellent dimension control, outstanding surface finish and low surface damage. Figure 1.3 shows some parts that have been made by USM.

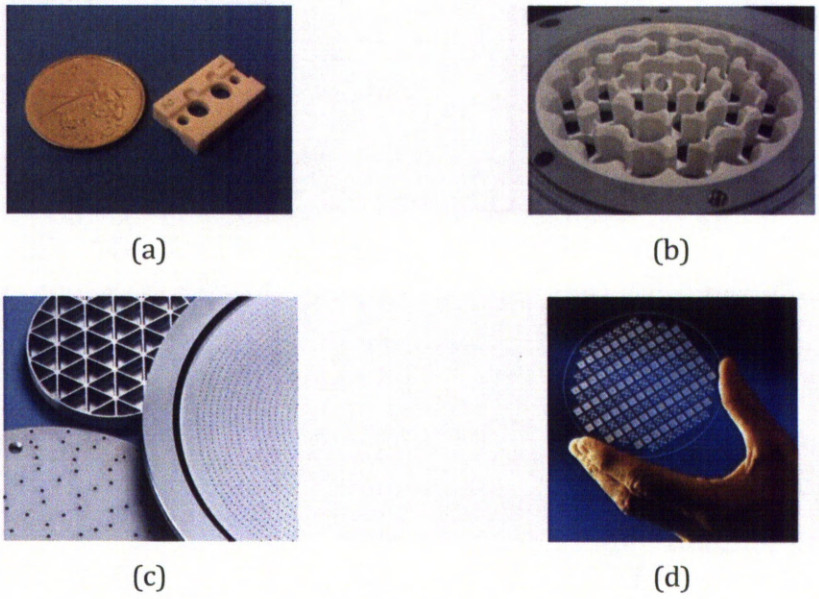

(a) (b)

(c) (d)

Figure 1.3: Some Examples of Parts Made by USM. (a) and (b) Ceramics; (c) Metal; (d) Glass. Photos from Bullen Inc. (2010).

If EDM is the most preferable for machining complex geometries on metals, USM should be the option for all other materials that are prone to brittle fracture, from advanced ceramics to glass, graphite, and some fibre-reinforced plastics (Jahanmir, Ramulu & Koshy 1999). The tool is sometimes shaped to produce multiple holes with either rounded or non-rounded shapes and is fed slowly with a constant force downwards into the work-piece. Material removal

occurs when abrasive particles, suspended in the slurry between tool and work-piece, impact the work-piece due to vibration of the tool or work holder at sufficient amplitude and high frequency. In special applications, the machining can be carried out without abrasive slurry called dry machining. The amplitude of machining vibrations can be varied (Komaraiah & Narasimha Reddy 1993) generally in the range of a few hundredth of millimetres (Jahanmir, Ramulu & Koshy 1999; Singh & Khamba 2006), and the frequencies are just beyond the audible range, approximately 20 kHz (Benedict 1987; Gilmore 1991; Groover 2011; Jahanmir, Ramulu & Koshy 1999; Singh & Khamba 2006).

The mechanisms of material removal for USM are somewhat uncertain and can be classified as described briefly below which are summarised from (Ichida et al. 2005; Jahanmir, Ramulu & Koshy 1999; Khairy 1990; Lee & Chan 1997; Singh & Khamba 2006; Soundararajan & Radhakrishnan 1986; Thoe, Aspinwall & Wise 1998):

- Hammering: It is direct or indirect hammering of abrasive grains localised in the gap between the tool and the work surface as shown in Figure 1.4 (a) and (b), respectively.
- Impacting: For micro grains, they are forced to impact the work-piece by the vibrating tool end as shown in Figure 1.4 (c).
- Rolling: It happens in the side gap of the tool and the work surface which is similar with the conventional lapping method as shown in Figure 1.4 (d).
- Cavitation: At high vibrations in a liquid, bubbles can be formed and collapse which cause the breakage on the work-piece as shown in Figure 1.4 (e).
- Chemical action: It is employed with some types of liquids mixed with abrasives that cause chemical reaction on the work surface.

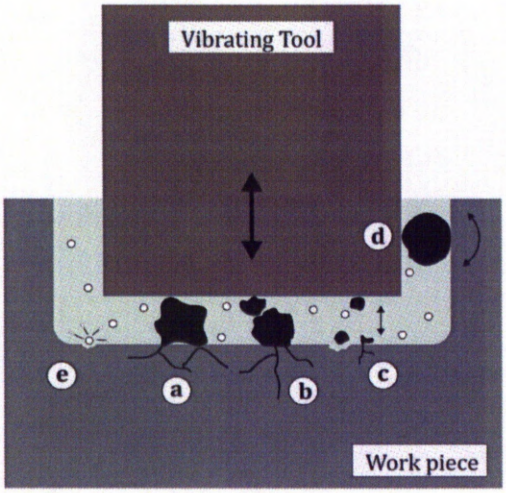

Figure 1.4: Material Removal Mechanisms in USM. (a) and (b) Hammering; (c) Impacting; (d) Rolling; (e) Cavitations.

The first two methods, hammering and impacting, are considered to be the major mechanisms (Kainth, Nandy & Singh 1979; Khairy 1990; Komaraiah & Narasimha Reddy 1993; Singh & Khamba 2006; Soundararajan & Radhakrishnan 1986; Thoe, Aspinwall & Wise 1998) in which individual or combined effects of them result in the desired surface area on the work-piece removed by shear.

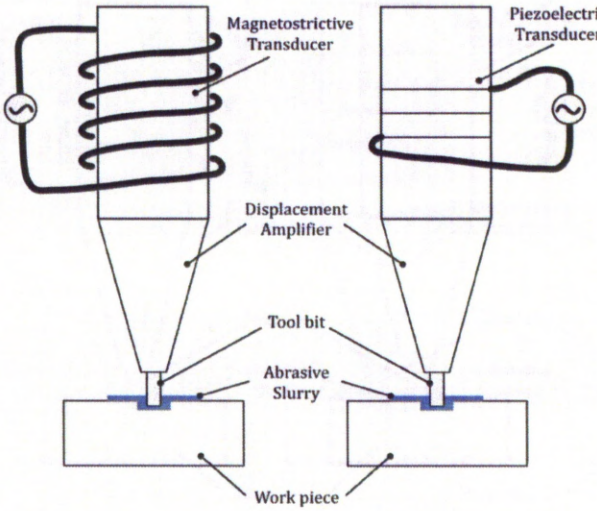

Figure 1.5: The Basic Set-up of USM System.

The common set-up of USM system is presented in Figure 1.5 including;

- Ultrasonic Transducers: The ultrasonic vibrations are generated from either magnetostrictive or piezoelectric materials which transform electrical signals to mechanical displacements.
- Displacement Amplifier: Also called sonotrode and horn, it works as a wave transmission line. Generally, the mechanical displacements are needed to be amplified because very low amplitude (only a few microns) is created by the vibrating generators. This is insufficient to remove material from the work surface. Displacement amplifiers are made from metals because their properties are suitable for wave energy transformation. The magnification ratio depends on its shape.
- Tool Bit: The forming tool is attached to the end of the displacement amplifier. It is normally made from metals because of wave

transmission quality and its ductility enables it to withstand the vibrations and impact forces.

- Abrasive Slurry: It is a mixture of liquid and abrasive grains which are spread throughout the machining area.
- Work Material: The work-piece will be first positioned close, not touching, to the tool end allowing a little space for vibration.

The key of machining effectively is the resonance of the system. At that point, maximal amplitude of vibration is generated with minimal power input. The incorporating mechanical parts including mechanical vibrating generator, displacement amplifier, and tool bit are required to vibrate at longitudinal modes of vibrations at the desired resonant frequency. Resonant conditions are changed by varying the shape and geometries of the mechanical components.

Figure 1.6, obtained, from The University of Tokyo (2012) and Femto-st (2012), shows commercial USM machines which are typically quite large. The mechanical vibrating generator itself is rather complicated. The low frequencies of the energy source (typically 50-60 Hz), need to be transformed to ultrasonic frequencies. To excite the materials used for the vibrating generator, the current (for magnetostrictive materials) or voltage (for piezoelectric materials) has to be amplified to a higher level. Accordingly, the electrical signal generator (not presented in Figure 1.5) is often designed separately as a control box from the other components.

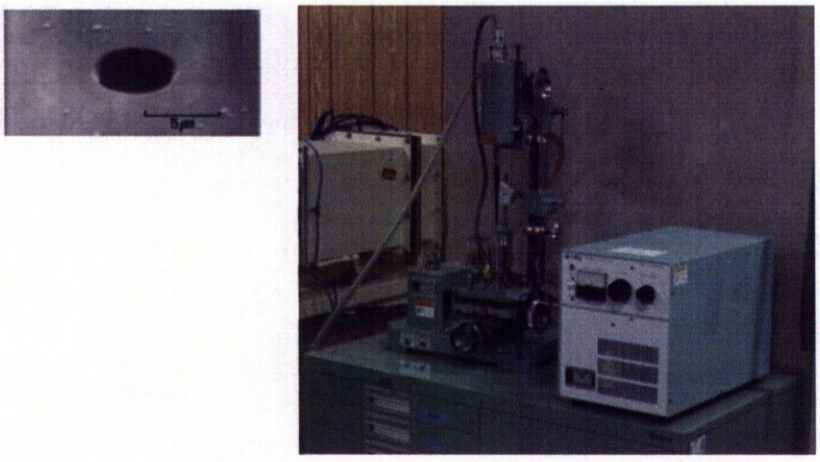

(a) MEMS Facility in the Department of Mechanical Engineering (The University of Tokyo 2012).

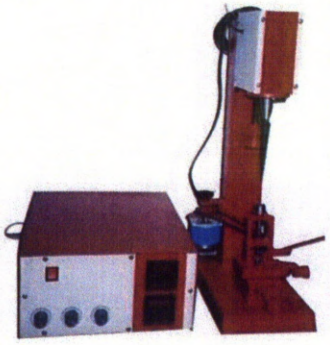

(b) Ultrasonic Abrasive Machining (Femto-st 2012).

Figure 1.6: Examples of USM Systems.

1.4 Demands for Miniaturisation

In the modern world, miniaturisation of products is demanded, and plays an important role in our lives. This is caused by a number of reasons.

It is a trend. We can see many products such as computers, cameras, medical devices and others which are being built smaller, with strong customer demand. This is especially true for the electronics market where miniaturisation is the key to success. Not only has the size of components been reduced, but they have more functionality through integration. For instance, all-in-one printers combine functions of printer, scanner, and fax machine. Smart phones can work as a mobile phone, a camera, a torch, a calculator and a small computer.

A major driver is the concern for sustainability of the Earth's precious resources and the environment. Global Warming is set to affect many parts of the world in the future if mankind does not heed the warnings. Green technology and sustainable development are very important topics around the world. An EU annual policy strategy for 2010 states clearly the need to improve the environment and combat climate change (Communities 2009). Engines used in transport are taking account of cost-effective and energy-effective considerations (European Communities 2007). Products need to be designed smarter with more effective materials usage and energy consumption throughout their complete life-cycle, including disposal.

This approach is also beneficial to economics. Every enterprise prefers to gain higher profits. Miniature means greater things in economics. When the cost of production is reduced it means higher profits. The direct impact of miniaturisation is a reduction of raw material cost. Moreover, as the size of goods or parts become miniature, compact space is sufficient for storage allocation; and less space is taken up during transportation. Management of inventory as well as parts or material handling are more effective.

Micromachining is the base technology to satisfy those requirements for reduced product size. The demands force manufacturing technologies to move forward. To miniaturise the USM system is not only to follow the trends but also leads to benefits by extending micro-machining technologies.

1.5 Research Objectives

In an age of micro-manufacturing and nanotechnology, as well as sustainable development, it is wasteful to machine hard and brittle materials in meso/micro scale geometries with the large equipment currently available. To bridge the gap between wasting our limited world resources by using big machine and the requirement of meso/micromachining, the development of a miniaturised USM system is the solution. The basic aim of this research is to minimise a USM system maintaining compatible performance with the conventional systems.

The objectives of the project include;

- To design a miniaturised USM system with rational and scientific methods throughout the whole design and development process including design, modelling, prototyping, and testing.
- To apply the Axiomatic Design Approach (AD) to the concept design and to use Design of Experiments Method (DOE) in manipulating and optimising many different interacting parameters for the detailed design.
- To investigate USM process parameters and interactions affecting machining performance in micro/meso scale manufacturing.

1.6 Overall Methodology of the Project

The need to design a miniaturised USM system effectively has motivated the following studies:

(i) **Literature Survey.** As the first step, the literature related to ultrasonic machining and its aspects were reviewed. Studying and understanding of various fields were necessary in order to design and miniaturise the system successfully. For USM, the waves travel in a medium at frequencies higher than audible range and have some effects on the medium which they pass through (Blitz 1967; Calderwood 1968), so the principle of high power ultrasonics is the basic theory used to describe vibrations. Moreover, the process itself is complex and has uncertainty (Komaraiah & Reddy 1993; Soundararajan & Radhakrishnan 1986). Thus, clarification of key parameters was needed to effectively design a machining system for meso/micro-machining. Also, understanding of the functions of USM components, ideas of horn miniaturisation, and how to assemble them was very important to optimise the process and minimise the size of the system.

(ii) **Development of a Framework for Designing USM Components.** To achieve a better understanding of system behaviours, the Axiomatic Design Approach (AD) was applied for the design activities of a USM system. The approach is a design methodology developed to establish a universal rational basis for design (Melvin & Suh 2002; Yu et al. 2010). It has been applied to many products and systems (Bang & Heo 2009; Cavique & Gonçalves-Coelho 2009; Durmusoglu & Kulak 2008; Jang et al. 2002) but this is the first time that this theory has been applied to USM system design. Function requirements of the USM system and subsystems are defined. Using AD, design parameters which satisfy the requirements were considered systematically. As a result, the system has been designed effectively, and organised properly.

(iii) **Experimental Design for Simulation.** Tools facilitating detailed design were utilised in order to design components cleverly. Careful planning of simulation experiments is generally a great help to estimate the effects of changes in a model's inputs on its outputs (Kelton 2000). The key components of the miniaturised USM have been modelled by using 3D Computer-Aid Design (CAD) software Pro Engineer and the dynamic characteristics of the design at no-load conditions were determined by Finite Element Analysis Method (FEA) using computer simulation software COMSOL Multiphysics. To ensure a robust design, the proposed geometries were considered using Design of Experiments Methods (DOE). A number of interacting parameters were taken into account only for significant combinations using Fractional Factorial Design or Full Factorial Design depended on the complexity of the geometries. These were then used to optimise the value of dimensions using Response Surface Methodology. The novel horn design has been proposed to optimise machining rate with minimised exciting energy and size, and a reasonable operating life cycle.

(iv) **Investigating and Verifying the Characteristics of the System Prototype.** Finally, prototypes were built and tested to verify the simulation results. Dynamic characteristics of vibrating components were demonstrated and measured at no load condition to confirm the design generated from the computer simulation. Experiments on the machining of a selective hard and brittle material were carried out. Statistical analysis tools were used to investigate the system performance. In a choice of machining conditions, the machining performance of the proposed design was compared with USM commercial machines. Finally, the novel design characters were discussed and some recommendations were presented for the possibility of further developments.

1.7 Thesis Outline

This thesis includes seven chapters and references.

In Chapter 2, literature on principles and techniques used for designing and modelling of miniaturised USM system are presented. This can help designers and readers to better understand the system based on up to date research findings.

In Chapter 3, Axiomatic Design is presented to organise the functions required for a USM system. The interrelationship among USM subsystems is examined and considered in the Design Structure Matrix. After that, the details in the matrix are rearranged to a systemised AD Matrix.

Chapter 4 and Chapter 5 show the design of USM subsystems and performance evaluations of Prototype-I and Prototype-II. Machine performance testing is explained in Chapter 6. Conclusions of the whole project and suggestions for future work are presented in Chapter 7.

Chapter 2

Literature Review

Ultrasonic machining is not a newly invented process. It is used to create complex cavities on hard, brittle, and difficult to machine materials such as glass, engineering ceramics, and titanium effectively. However, the complication of parameters involved impedes the widespread use of this technology, limiting it to prototype manufacture or laboratory use. Oversized components are normally designed for commercial USM machines to reduce effects from changing tool bits and for other reasons. As a result, the machines are sizable in relation to the work-piece.

In the era of sustainable development, designing for optimal use is essential. An oversized machine means waste of materials and energy consumption. Publications and patents related to USM have been reviewed in order to efficiently design a miniaturized USM system for machining small cavities. In this chapter, the general ideas of the process including system components and parameters effecting to removal rates have been reviewed in Sections 2.1 to 2.3, the ideas to reduce the system size are discussed in Section 2.4, and the design tools used for miniaturisation are explained in Sections 2.5 and 2.6.

2.1 High Energy Ultrasonic Applications

The term wave motion is used to describe the transmission of a disturbance through a medium in a way that energy is passed. Ultrasonics is the name given when the energy pitches above the audible range, generally having frequencies higher than 16 kHz, where the limit is merely up to the ability of signal generators.

Ultrasonic applications can be divided into 2 sections, low and high energy. Basically, low energy waves are applied to a medium for measuring its propagation constants occupied for the purpose of non-destructive testing and measurements, medical imaging, and communications. Whereas, for high energy ultrasonic waves, the nonlinear term in the wave equation becomes important when the applied stress and consequential strain are no longer a linear relationship, which causes some changes (Blitz 1967; Gooberman 1968), i.e. the frequency dependence of Young's modulus and Poisson's ratio for sedimentary rocks presented by Tutuncu et al. (1998). The physical changes may be caused by heat, steady ultrasonic forces, cavitations, and large mechanical stresses.

Some applications of high energy ultrasonics are able to be performed at audible frequencies, roughly 20 to 20 kHz, but the inaudible option is preferred. Such applications tend to use vibration amplitude as high as possible. Consequently, the range of high power ultrasonic applications is from 18 kHz, to avoid unpleasant noise, up to about 100 kHz, where the levels of motion amplitudes are practicable. Some applications of high energy ultrasonics are presented in Table 2.1. Ultrasonic applications are safe and environmentally friendly (Siddiq & Ghassemieh 2008; Statnikov, Korolkov & Vityazev 2006). Amplitudes of applications range from a few microns to about 50 μm only. It sounds small but, for example, it means we can make use of the acceleration of 8,000g at the displacement amplitude of just 5 μm and the frequency of 20 kHz. Also, ultrasonics improves the capability of conventional processes where energy consumption is reduced.

2.2 The Process

USM is a mechanical material removal process. It has been well established since 1950 (Benedict 1987; Thoe, Aspinwall & Wise 1998), and was first invented about 20 years earlier (Jahanmir, Ramulu & Koshy 1999; Neppiras 1964; Thoe, Aspinwall & Wise 1998). The process is particularly suitable for

brittle and hard to machine materials. It is comparable to EDM for the production of complex cavities but USM is more versatile as it can be used for machining both electrical conductive or non-conductive materials. All materials that are subject to brittle fracture can be successfully machined by USM.

Table 2.1: Applications of High Energy Ultrasonics (Neppiras 1960).

Medium	Application			Frequency (kHz)	Acoustic intensity ($W \cdot cm^{-2}$)
Gas	Separation of gas mixtures Production of aerosols-spraying Coagulation of aerosols			10-100 1-25	Any
Liquid	Shaking-mixing-flow promotion Thermal effects-therapy Precipitation of hydrosols			500-2000	0.5–1.5
	Cavitation				
	Degassing Tensile strengths of liquids Sonoluminescence-sonochemiluminescence Hot-spot chemistry Fundamental oxidation reactions			0-40 500-2000	Any 1-5 1-5
	Disruptive	*Dispersive*	*Acceleration of rate processes*		
	Erosion studies Descaling Tinning Cell disruption Bactericidal Sterilization Pasteurization Depolymerization	Emulsification Dispersing solids Cleaning fabrics Degreasing Cleaning solids Electrolytic dispersion Grain refinement of metals	Chemical reactions Maturing Surface reactions Diffusion Tanning-dyeing Extraction Accelerated solution Emulsion polymerization	5-40	1.5
Solid	Shaking-mixing-flow promotion			0-50	Any
	Investigation non-linear effects Destructive testing-fatigue-adhesive bonds-wear			Any	102-106
	Cold welding Machining-drilling-taping-polishing			20-25	102-104

There are only 3 main basic elements for the USM process which are (1) a tool bit to create a cavity or cavities onto (2) a work-piece by the use of (3) ultrasonic vibrations of either the tool or work-piece. However, abrasive slurry, a mix of abrasive powder and liquid, is generally applied by spreading it between the tool and the work-piece (Figure 1.5) to increase cutting speed. The process where abrasive slurry is not used is called Dry Machining. Although

there are only a few elements involved, the mechanical properties of the materials, the conditions of combining those elements, and the contributions of the abrasive slurry, all affect machining rates. The parameters involved in machining are summarised and shown in Figure 2.1. The complexity of those parameters may be a drawback and limits USM to mostly fabricating prototypes or in laboratory use (Jahanmir, Ramulu & Koshy 1999).

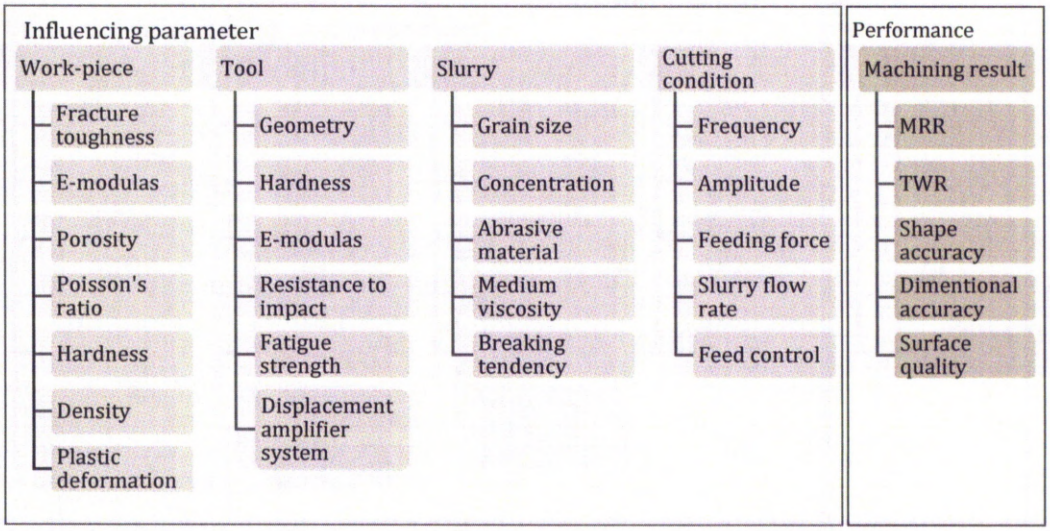

Figure 2.1: Parameters Affecting USM Material Removal and Tool Wear Rates.

Many researchers have aimed to model relationships among those parameters to express a formula for predicting material removal rates for the USM process. They derived the material removal rate (MRR) from the mechanisms based on their assumptions or findings, which are mainly based on hammering and impacting. The following are some of the well-known USM process models.

Shaw (1956), cited in Kainth, Nandy and Singh (1979), modelled the USM process assuming that the material was removed by both hammering and impacting forces and the abrasive grains were assumed to be spherical shapes,

$$MRRMRRMRR \propto (d_A h)^{\frac{3}{2}} N f_V \qquad \text{Eq. 2-1}$$

$$h = \left(\frac{8 F_S A_V d_A}{\pi K H_W C \left(1 + \frac{H_W}{H_T}\right)} \right)^{\frac{1}{2}} \qquad \text{Eq. 2-2}$$

where, d_A is the size of the abrasive particles, h is the depth of indentation, N is the number of abrasive particles making impact per cycle, f_V is the frequency of vibration, F_s is the steady feeding force to hold against each other between the tool and the work-piece (sometimes called static force), A_V is the amplitude of vibration, K is a constant of proportionality, H_W is the hardness of the work-piece, C is the concentration of abrasive particles in the slurry by weight, and H_T is the hardness of the tool tip. However, the MRR prediction equation that Kainth, Nandy and Singh (1979) developed was very specific. It was specified for one particular tool, work, and abrasive material varying values of static force and oscillation amplitude.

Miller (1957) derived a machining rate equation based on plastic deformation for the special case where a solid circular tool was used for machining the work-piece in a pool of cube-shaped abrasive slurry. The model was

$$MRR \propto \left(\frac{P_S f_V d_A}{G b} \right)^{\frac{1}{q}} \cdot \left(\frac{d_T \rho_A V_A (C+1)}{A_V F_Y C} \right)^{\left(\frac{1}{q}\right)-2} \cdot \frac{1}{q} \qquad \text{Eq. 2-3}$$

where P_s is the steady feeding pressure, G is the shear modulus, b is the Burgers vector, q is work hardening capacity, d_T is the size of the tool tip, ρ_A is the

density of the abrasive material, V_A is the volume of the abrasives, and F_Y is the atmospheric force on the surface of the slurry.

Neppiras (1964) surveyed USM machining characteristics and proposed the following equation:

$$MRR \propto (A_V f_V)^2 P_S d_A \qquad \text{Eq. 2-4}$$

However, Neppiras explained that Eq. 2-4 is not applicable when A_V and f_V are very large, P_S is higher than an optimum value, and A_V is much smaller than d_A.

Kazantsev and Rosenberg (1965) studied the mechanisms of USM using a high speed camera and established Eq. 2-5 after conducting series of experiments on machining glass material with a steel tool tip using boron carbide as the abrasive material.

$$MRR \propto \left(\frac{P_S}{C}\right)^{K_1} C f_V \qquad \text{Eq. 2-5}$$

where K_1, the exponent of P_S/C, depends on the abrasive material.

Cook (1966), cited in Komaraiah and Narasimha Reddy (1993), proposed an equation linking the machining speed (MS) with the MRR:

$$MS = 5.9 \frac{f_V P_S}{H_W} A_V^{1/2} R_A^{1/2} \qquad \text{Eq. 2-6}$$

where R_A is the average radius of abrasive grains.

Soundarajan and Radhakrishnan (1986) machined several types of work materials using a mild steel tool with boron carbide abrasive. The MRR and machined surfaces were observed. They found that there was no machining when the working gap between the tool tip and the work-piece surface was larger than the mean size of the abrasive particles. They concluded that the prime mechanism for USM was hammering.

Komaraiah and Narasimha Reddy (1993) proposed a new MRR model based on experimental results. When the fracture toughness of the work-piece material is T_W, the machining rates could be calculated as

$$MRR \propto \frac{P_S^2}{T_W^{3/2} H_W^{1/2}} \cdot \frac{f_A}{N} \qquad \text{Eq. 2-7}$$

Wang and Rajurkar (1996) described the MRR in the USM process as the consequence of the dynamic impact mechanics caused by abrasive grits.

$$MRR \propto S d_A (\rho^4 f_V^8 A_V^8)^{\frac{1}{5}} \qquad \text{Eq. 2-8}$$

where S is the cutting area of machining zone and ρ is the density of the work material. They confined their equation for perfect brittle materials only.

Lee & Chan (1997) established an MRR model according to the test results of ceramic indentation as follows:

$$MRR \propto \frac{f_V}{N} \cdot (K_2 F_S + K_3 A_V) \qquad \text{Eq. 2-9}$$

when K_2 and K_3 are the coefficients determined by the machining conditions. They discussed that the MRR could be increased by increasing all parameters in Eq. 2-9 but the developing was limited by optimum values of the static feeding force and grit size.

The MRR also depends on the tool shape, the aspect ratio (the ratio of the length to the size of cut), and the flow of the abrasive slurry (McGeough 1988; Thoe, Aspinwall & Wise 1998). When the cutting areas of the tools are similar, the shapes of cut having larger perimeters show greater machining rates. The aspect ratio also shows the same effect as the shape of cut; the MRR is reduced at a deeper cut. These are the cause of the flow resistivity of the machining conditions. The abrasive particles are degraded under the repeated hammering

force without the new particles' replacement. Therefore, the MRR drops with the condition that tends to resist the flow of the abrasive slurry.

Although the MRR can be expressed in many ways, Shaw's work seems to be an inspiration for later researchers. Cook's equation is well recognised (El-Hofy 2006; Komaraiah & Narasimha Reddy 1993; Sun, Masuzawa & Fujino 1996) because it is not excessively complex, includes sensible parameters and can be used for all types of materials. The MRR of the USM process is generally 300 mm^3/min (Boothroyd & Knight 1989; Singh 2007). However, it can have a wider range varying from 0.5 (for machining titanium) to 1300 (for machining graphite) mm^3/min (Gilmore 1991; Jianxin & Taichiu 2002; Komaraiah & Reddy 1993; Kumar & Khamba 2010; McGeough 1988; Singh & Khamba 2006) depending on materials and machining conditions involved.

The knowledge about predicting the MRR is still limited. This study was, therefore, designed to fill this knowledge gap. Equations Eq. 2-1 to Eq. 2-9 affirm the complexity of the USM parameters affecting the rates of machining and it can be seen that no equation well represents all machining conditions. Most of the published equations were in complex forms, and are markedly different. Any parameters can be included in the equations subject to the authors' assumptions without a clear evidence to support that those parameters are critically important to calculating MRR. Coefficients of the parameters, such as materials and machining conditions, are always involved and have not been clearly publicised. Basically, these coefficients are barely able to be known without a series of experiments. Most researchers noted that, in practice, the MRR rises and decreases after reaching an optimum value. The maximum MRR is related to process parameters in a complex manner. For instance, the optimum value of abrasive grit size depends on the amplitude of tool vibration. Also, the increasing of the steady feeding force (or pressure) and/or the higher concentration of the abrasive slurry increase the MRR, then, after reaching their optimum values, the

MRR drops. These reasons make the USM process still difficult to be predicted by a user.

In order to describe the performance of a machining process, the quality of surface finish is comparatively important to the rates of machining. The USM parameters affecting the surface finish have been summarised in previous publications (Benedict 1987; El-Hofy 2006; Kazantsev & Rosenberg 1965; Khairy 1990; Komaraiah et al. 1988; Komaraiah & Reddy 1993; Lee & Chan 1997; McGeough 1988; Neppiras 1964; Thoe, Aspinwall & Wise 1998; Venkatesh 1983; Yu, Hu & Rajurkar 2006). The machined surface quality is mostly under the influence of the abrasive slurry, amplitude of vibration, and the fracture behaviours of the work and tool materials.

Dimensional accuracy of USM operation depends on abrasive particle size, the support of the tool and the work-piece, and the fracture toughness of the tool material. Since the process makes use of the abrasive particles to create a cavity onto the work-piece surface, the cavity is always slightly larger than the tool. When the tool and work-piece are supported rigidly and positioned accurately, the oversize of the cavity produced is approximately 1.5 times the average size of the abrasive particles (Kremer et al. 1981). When the machined cavity is deeper, slight tapering is present. The size reduction from the original contour is due to the side wear of the tool and the degradation of the working abrasive particles.

The particle size of the abrasive and the fracture behaviours of the materials involved play very important roles on the roughness of the machined surface. The greatest influence is due to the abrasive size. Typically, as the abrasive becomes larger, the surface roughness increases due to deeper indentation. While the tool material is fixed, the surface roughness values vary for different abrasive and work materials. It has been reported that a better surface finish is obtainable from harder tools (Komaraiah et al. 1988; Komaraiah

& Reddy 1993). The roughness of the surfaced machined by USM is around 0.5 to 2.5 μm Ra.

In conclusion, USM is a complex process. There are plenty of parameters affecting the performance of the process and the relationships among parameters are nebulous. As a result, the process has not been applied on a business scale. In general, if the rate of machining is increased by deeper indentation per impact, the surface finish will be inferior. The MRR can be higher by increasing: the frequency of vibration; amplitude of vibration; size of the abrasive particles; hardness of the tool and abrasive materials; flow, circulation, and concentration of the abrasive slurry; and static feeding force. However, the increase of the MRR is not linear as it will decrease after a maximum value is reached, depending on the combination of the process parameters. Therefore, the challenge lies in clarifying the process to make it predictable.

2.3 The System Components

The ultrasonic machining system principally consists of the vibration generator, tool bit, and abrasive slurry feeder. The ultrasonic vibrations are generated from materials having exclusive properties that can be inevitably provoked into action by external boosters, smart materials. However, at such a high frequency, the vibrations produced from the smart materials have insufficient displacement amplitude for machining a work-piece effectively; so, there is always a need for amplifying the amplitude of vibrations. Afterwards, the tool bit is connected to the vibration amplifier to define the shape of the cavity onto the surface of a work-piece. Then, the USM process can function properly with the use of abrasive slurry between the tool bit and the work-piece.

Some of the machining set-ups summarised and practised by researchers are presented in Table 2.2. Although many parameters affect the machining performance, there are two primary parameters directly controlled by the USM system components, which are frequency and amplitude of vibrations. The

amplitude of vibrations can be varied by adjusting electrical power input. The amplitude can be a very small amount or as large as the oscillator materials can withstand before dielectric breakdown and mechanical fracture. The frequency of vibrations normally is a resonant frequency in order to generate sufficient amplitude for cutting.

Table 2.2: USM Process Parameters and Machining Performances.

Parameter		Unit	[1]	[2]	[3]	[4]	[5]	[6]
Amplitude of vibration	A_V	µm	62.5		~25	37.5	40	25 to 50
Frequency of vibration	F_V	kHz	25.5	18 to 22	~20	19 to 25	20	~20
Size of abrasive particles	d_A	#Mesh size*	#400	#280 to #600	#240 to #800	#220	#400	#200 to #800
Slurry concentration	C	% weight	16.8	20	30 to 60	28.5	20 (% volume)	
Static feeding force	F_S	N	9.3	1 to 10		15	12	
Machine power		W	200	900	40 to 2400	250	1100	
MRR:TWR**					1 to 100:1			500 to 1500:1
Aspect ratio					40:1			35:1
MRR		mm^3/min	350					400 to 1300
Work-piece material**			Glass	Glass			Glass	Graphite
Tool material**			Mild steel	Mild steel Silver steel Stainless steel WC				Titanium Steel Aluminium
Abrasive material**			B_4C	SiC B_4C		SiC		SiC SiO_2 Al_2O_3 B_4C

[1]= Kainth, Nandy and Singh (1979), [2]= Venkatesh (1983), [3]= Benedict (1987), [4]= Komaraiah et al. (1988), [5]= Khairy (1990), [6]= Gilmore (1991)

* See Appendix for converting mesh size to µm.

** Names: MRR = Material removal rate, TWR = Tool wear rate, WC = Tungsten carbide, B_4C = Boron carbide, SiC = Silicon carbide, SiO_2 = Silicon dioxide, Al_2O_3 = Aluminium oxide

Table 2.2: USM Process Parameters and Machining Performances (Cont.)

Parameter		Unit	[7]	[8]	[9]	[10]	[11]***	[12]
Amplitude of vibration	A_V	μm	40		50 to 150	5 to 50	<1	20 to 30
Frequency of vibration	F_V	kHz	19 to 25	~20	16 to 25	>20		19 to 23
Size of abrasive particles*	d_A	#Mesh size	#220	#240 to #800	#80 to #240		0.2 μm	#180 to #400
Slurry concentration	C	% weight	28.5 (by volume)	Up to 40 (by volume)	10 to 15	~30		25 to 35
Static feeding force	F_S	N	5	Up to 50		0.1 to 30	0.1 to 0.6m	
Machine power		W	250	Up to 900	250	50 to 3000		
MRR:TWR**							2 to 100:1	
Aspect ratio				40:1				
MRR		mm^3/min	10 to 20	40 to 650	2.8 to 46.8			
Work-piece material**			Glass Ferrite Alumina WC		Ferrite		Quartz glass Silicon	Ceramics Glass Graphite Fibre-reinforced plastic
Tool material**					Steel		WC	Steels Polycrystalline diamond
Abrasive material**					B_4C		Diamond	B_4C SiC Diamond

[7]= Komaraiah and Narasimha Reddy (1993), [8]= Dorf and Kusiak (1994), [9]= Lee and Chan (1997),[10]= Thoe, Aspinwall and Wise (1998), [11]= Egashira and Masuzawa (1999), [12]= Jahanmir, Ramulu and Koshy (1999)

* See Appendix for converting mesh size to μm.

** Names: MRR = Material removal rate, TWR = Tool wear rate, WC = Tungsten carbide, B_4C = Boron carbide, SiC = Silicon carbide

*** Micro-machining

Table 2.2: USM Process Parameters and Machining Performances (Cont.)

Parameter		Unit	[13]	[14]	[15]	[16]***	[17]	[18]
Amplitude of vibration	A_V	μm	6 to 12	5 to 20	40 to 80	1 to 1.5		25.3 to 25.8
Frequency of vibration	F_V	kHz	17 to 23	16 to 25	18 to 20	39.5	>20	21
Size of abrasive particles*	d_A	#Mesh size	#80 to #160	#80	#280 to #800	0.25 to 1.3μm		#220 to #500
Slurry concentration	C	% weight			30 to 50	3	30 to 60	20 to 30
Static feeding force	F_S	N	25 to 65	10	30	0.01 to 0.12	0.1 to 30	16.3
Machine power		W	50 to 100	250			50 to 3000	100 to 400
MRR:TWR**							1 to 100:1	
Aspect ratio								
MRR		mm^3/min		0.4 to 1				0.11 to 0.57
Work-piece material**			Alumina	Aluminium based ceramic				Titanium
Tool material**				Mild steel				High carbon steel High speed steel Titanium Titanium alloy Cemented carbide
Abrasive material**			Diamond	B_4C				Al_2O_3 SiC B_4C

[13]=Zhang et al. (2000), [14]=Jianxin and Taichiu (2002), [15]=El-Hofy (2006), [16]=Yu, Hu and Rajurkar (2006), [17]=Singh and Khamba (2006), [18]=Kumar and Khamba (2010)

* See Appendix for converting mesh size to μm.

** Names: MRR = Material removal rate, TWR = Tool wear rate, B_4C = Boron carbide, Al_2O_3 = Aluminium oxide, SiC = Silicon carbide

*** Micro-machining

A transducer is a device converting one form of energy into another. There are many types of transducers used for generating vibrations (Blitz 1967; Gooberman 1968; Park et al. 2007):

- Piezoelectric Transducers: These utilise a reverse piezoelectric effect. When an electric field is applied across a piezoelectric object, a crystalline material, in the direction of a polar axis, the material is mechanically strained.
- Magnetostrictive Transducers: The principle is based on reverse magnetostriction. Ferromagnetic materials or ferrites change their length when they are subjected to a magnetic field.
- Electrostrictive Transducers: The principle of these transducers can be compared with magnetostriction. Specific materials in curtain dielectrics, ferroelectrics, possess this effect. Ferroelectric materials are under a mechanical strain when an electric field is applied.
- Purely Mechanical Transducers: Mechanical transducers make use of high kinetic energy in a stream of fluid propagated into acoustic energy. They are commonly called whistles or sirens.
- Electromagnetic Transducers: This kind of transducers requires the movement of a magnet material under a magnetic field generated from an electric coil with an alternating current through it or from a moving coil.
- Electrostatic Transducers: The phenomenon behind these transducers is electrostatics, which causes the attraction or repulsion between two parallel metal plates due to the presence of surface charge imbalance.
- Miscellaneous Transducers: These include the transducers utilising thermal, chemical, and optical effects of materials.

In USM, the two main types of transducers are piezoelectric and magnetostrictive transducers (Thoe, Aspinwall & Wise 1998) while the others seem to be less common. Even if piezoelectric and electrostrictive materials are similar in terms of producing mechanical strains under electric fields, the primary difference is the nature of the electromechanical coupling (Jalili 2009; Leo 2007). Piezoelectric materials exhibit a linear relationship between electric and mechanical variables while electrostrictive materials show polarisation saturation resulting in a non-linear strain response. Purely mechanical transducers can only generate a frequency lower than 100 kHz and are suitable for low power applications. Electromagnetic transducers are typically used for applications at acoustic frequencies and are used as receivers or sensors at megacycle frequencies. Electrostatic transducers are generally used for low power works. In addition, the sensitivity of miscellaneous transducers, e.g. shape memory alloys/polymers, photomechanical materials, and pH-sensitive materials are too slow to respond at ultrasonic frequencies.

In the early days of the development of ultrasonic transducers for machining, nickel stacks, one of the magnetostrictive-type transducers, were generally used (Clark 1954; Neppiras 1964; Soundararajan & Radhakrishnan 1986; Venkatesh 1983). The high frequency current is fed into the laminated nickel core wound around by a coil. Although laminating the core's material can reduce eddy current losses, water cooling is a common requirement necessary for minimising or removing the heat produced at higher frequencies. The high Curie temperature and reasonable cost of material versus electro-mechanical coupling coefficient are the reasons behind the popularity of the nickel transducers.

When the nickel transducers were commonly used, a new piezoelectric ceramic material, lead zirconate titanate (PZT) was being developed and later became an even more attractive material for ultrasonic machining and other oscillating applications. The piezoelectric transducer construction is simpler

than the magnetostrictive type because the high frequency alternating voltage is applied directly to the electrodes coated onto each side of the poled piezoelectric ceramic. By the time that the material was newly developed, it had a comparative Curie temperature; the coupling coefficient was approximately double; and it had a lower relative cost, compared with the nickel transducers (Neppiras 1960). Today's piezoelectric transducers have 90-96% energy efficiency and can operate continuously without any cooling system (Thoe, Aspinwall & Wise 1998).

Since the 1960s, giant magnetostrictive composite materials (GMM), especially rare-earth iron, have been discovered and developed for high frequencies and high power applications (Clark 1993). These materials can be the candidates for a wide range of ultrasonic applications. Among them, Terfenol-D offers the best choice between a large magnetostrain and a low magnetic field (Claeyssen, Lhermet & Maillard 2002). It has high power energy conversion efficiency and can generate mechanical strain three times higher than can piezoelectric transducers. Moreover, it is a metal based material so it has a better mechanical overload property. However, the GMM transducers are limited to some kHz applications due to their current losses. They are typically in a rod or bulk shape since the cost to produce them as lamination cores is still high. Also, considering output energy with respect to material volume/mass, per active material volume/mass, per unit cost (Giurgiutiu & Rogers 1997; Liu et al. 2006; Olabi & Grunwald 2008; Yamamoto, Eda & Shimizu 1999), piezoelectric transducers seem to have an advantage. Piezoelectric transducers could maintain a large commercial scale in the foreseeable future; on the other hand, the rare-earth iron material mainly has been developed by NASA, US Navy, and French Navy funding and has very good potential (Claeyssen, Lhermet & Maillard 2002; Dapino, Flatau & Calkins 2006).

Constructions of each type of transducer for high power and high frequency applications are different. Both piezoelectric and GMM transducers

have one similar basic construction: that they usually need an optimum mechanical pre-stress in order to ensure dynamic operations under compressive load (for the piezoelectric types) and a large dynamic strain and high power output (for the GMM types) (Abdullah, Shahini & Pak 2009; Ando & Kagawa 1992; Claeyssen et al. 1997; Greenough & Jenner 1994; Kellogg & Flatau 2004; Park & Yim 2004). Generally, piezoelectric transducers are simple in design as the active material which is a single piece or stack, is secured between two metal plates. The nickel-type transducers have only a coil wound around the laminated nickel core. There is an external component used for amplifying mechanical strain displacement. However, GMM transducers can be versatile in their constructions to enhance the oscillating efficiency. A direct current (DC) (Dapino, Flatau & Calkins 2006; Dhilsha et al. 1997; Dhilsha, Rajeshwari & Rajendran 2005; Kellogg & Flatau 2008) or permanent magnet (Liu et al. 2006; Park & Kim 2004; Ueno, Qiu & Tani 2004; Wing Or, Nersessian & Carman 2003) can be added as a bias to the system. Their field strength and the position of the magnet enormously affect the performance of the transducers.

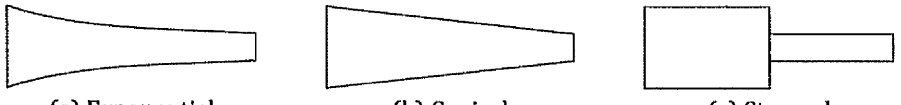

Figure 2.2: Basic Horns with Circular Cross Sections.

A horn or waveguide is a component in an USM system for amplifying the amplitude of vibrations produced from a transducer. Basically, by tapering a horn the wave motion increases from one end to another. Figure 2.2 shows the most frequently used conventional horns which are in exponential, conical, and stepped shapes (Neppiras 1960; Seah, Wong & Lee 1993; Sherrit et al. 2002; Singh & Khamba 2006). The horn material and geometry influence largely the resonant frequency and waves' transformation. Thus, the structure of the

transducer and horn unit must have a certain length where mechanical longitudinal resonance at the desired ultrasonic frequency of operation occurs, generally a half wavelength of the fundamental frequency of the material or multiples of half wavelengths. Also, it is essential to have materials with matching acoustic properties to ensure that the waves propagate efficiently from the transducer to the horn. For the same resonating frequency, material, and sizes of the horn ends, the stepped horn that the shape is reduced to at the node shows the greatest amplification. However, the amplification is limited to the dynamic strength of the horn materials.

The ideas for amplifying displacement of vibrations at high frequencies have been reviewed and are presented below.

Fletcher and Thwaites (1992) proposed a design for matching a thick piezoelectric transducer to an air medium by replacing a single horn with a pack of smaller exponential horns. The gain was approximately 10 dB (amplitude ratio of 3) in a range from 30 to 90 kHz.

In a series of papers related to the Mars Exploitations Technologies under a contract with NASA, the use of ultrasonic vibrations was discussed (Badescu et al. 2005a; Badescu et al. 2005b; Bar-Cohen et al. 2005; Bar-Cohen et al. 2007; Chang et al. 2005; Chang et al. 2004; Sherrit et al. 2002; Sherrit et al. 2004; Sherrit 2004). Sherrit et al. (2002) presented several designs for reducing the overall length of titanium horns at around 22 kHz but maintaining the acoustic length. The standard stepped, invert stepped, flipped and folded horns were modelled by computer modelling, and all the designs gave comparable results. It was found that the folded horn, whose length was half of the standard stepped horn, had the mechanical quality factor (Q-factor) as low as a tenth of the standard one due to the bolt connection between the base plate and the outer shell of the horn. However, the authors did not give the output of the folded horn without the bolt connection. Chang et al. (2004) aimed to increase the cutting rates. A free mass was added between the dog-bone shaped horn and the tool

bit. The MRR was improved by increasing the cutting force but the frequency of vibrations was reduced from ultrasonic at the drive to tens of Hz to 1000 Hz. Unfortunately, this frequency level is not preferable for USM machining. Later, Chang et al. (2005) improved the folded horn, first suggested by Sherrit et al. (2002), by proposing a planar folded horn. The design can be manufactured and assembled without any component touching the outer shell of the horn. Their computer simulation results showed that the planar folded horn had lower resonant frequency at the first mode while other qualities were comparable to the standard stepped horn. Iula et al. (2005) and Iula (2009) proposed a power ultrasonic actuator including a new horn design attached to a conventional sandwich transducer. The new horn utilised flexural vibrations to maximise the axial displacement which strongly developed at the centre of the front end of the horn. The displacement amplification of the new horn was about 50% higher than that of a stepped horn. Wevers et al. (2005) proposed an ultrasonic sandwich transducer for ultrasonic field generation to produce the enlargement of the bubbles in water. They realised that, to have a device working properly with high acoustical power at low ultrasonic frequency and broad bandwidth, the transducer must have: the acoustical reflection quality at the back end; the matched acoustical impedance between the front end and the medium; and the low quality factor, to be big, and many layers of a PZT material. Novel horn designs proposed by Cardoni, Harkness and Lucas (2010) had closer longitudinal and torsional frequencies. As a result, the large displacement was a combination of both modes at the given resonant frequency.

Most of the designs mentioned in the previous paragraph show that the presence of cavities or slits in a horn can increase vibration amplitude, but this reduces the ability of the structure to withstanding dynamic application, so both constraints need to be considered collectively.

Not only physics of waves can amplify amplitude of vibrations, a larger displacement can be achieved by the influence of an external mechanical

amplifier. Le Letty et al. (1997), Juuti et al. (2005), Ouyang, Zhang and Gupta (2008), proposed flexural lever-hinge mechanisms together with transducers for the purpose of displacement amplification. The amplification was greatly involved in the strength of the hinges and levers. Yoon et al. (2006) increased the stroke of motions through a combination of a piezo-stack actuator and a self-contained hydraulic system. The amplification ratio of the design was about 79.6 and the block force reduced from the piezo-stack actuator at 25000 N to 314 N at the output shaft. Kommepalli et al. (2009) developed a piezoelectric microactuator by using the mechanisms of different flexural motions of different materials attached partially together to produce the large displacement at the centre of the bridge structure.

Although the idea of using an external mechanical amplifier to increase the displacement of vibrations is viable, the limitations due to the dynamic strength of flexural hinges and the natural frequency of the system means that the resultant vibration is limited to only hundreds of Hertz.

Another key element of a USM system is the feeding of abrasive slurry into the cutting zone. It can be implemented either by pumping the abrasive slurry to the machining area or submerging the work-piece in a pool of slurry. As summarised in Table 2.2, abrasive slurry is a mixture of abrasive particles and fluid with a concentration of around 20 to 50% by weight. In general, the fluid used for the purpose is water (Guzzo, Shinohara & Raslan 2004; Khairy 1990; Thoe, Aspinwall & Wise 1998), because it is easily available and exhibits low viscosity and good wetting property.

2.4 Challenges of Miniaturisation

Miniaturisation is important. It is known that the demand for products with variety in functions and a reduction in dimensions is growing. Many commercial and scientific products can take advantages from miniaturisation

(Liu 2006). Those companies who can successfully develop miniaturised products gain enormous competitiveness.

For micro scale machining, how small the range of 'micro' or 'miniature' has not been well defined. However, 'micro' and 'miniature' mean small. Hence, any products that are not easily fabricated, are significantly reduced in scales, or very small examples of their kinds, can be referred to as miniaturised in this context (Masuzawa 2000).

Miniaturised products cannot be developed easily without the support of micro-manufacturing technologies and strategies. It is crucial to overcome challenges such as accuracy, precision, tool wear, burr formation, part handling and fixturing, and inspection methods. When a product needs to be made considerably smaller than a usual size, a manufacturing process is required to produce the less dimensional error which sometimes is likely to be impossible. Burr formation of a few microns may be negligible for conventional machining, but when the edge radius of the holes of hundreds microns is so diminutive it is significant. The chip sizes should be minimal for the same reason as the burr and for the purpose of the quality of machined surfaces. Accordingly, the cutting conditions for micro-manufacturing are different from the traditional purpose because high precision is a key requirement.

Masuzawa (2000) summarised micro-machining technologies and applications. He introduced that many conventional machining processes would be utilised in micromachining if the process can satisfy two guidelines which are reducing unit removal and improving equipment precision. Rahman et al. (2007), Li, Wang and Li (2007) and Li et al. (2008) studied micro-manufacturing; the high accuracy, precision, and resolution of equipments were underlined decisively. Based on Masuzawa's guidelines, USM responds to the first requirement as it could machine hard and brittle materials. The unit removal per cut of the process is small and machining force to form chips is low. The depth of cut can be managed to be as small as the combination of the

vibration amplitude and the size of abrasives used. Therefore, USM can be a promising process for micro-machining.

Machining smaller holes induces a larger tool wear. When tiny tools are used, wear resistance of tool materials is vital and the static feeding force needs to be small to avoid breakage of the tool (Boy et al. 2010; Boy et al. 2006; Egashira & Masuzawa 1999; Zhang, Rentsch & Brinksmeier 2005). The high-precision set-up was required for manufacturing micro holes. Using USM, Egashira and Masuzawa (1999) managed to vibrate the work-piece using a rotational cutting tool instead of the vibrating tool as in the conventional set-up. This is because it was more difficult to attach the tool to a transducer, fabricate the tool, and control the out-of-roundness of the massive tool. A hole of 5-mm diameter has been created successfully.

At present, this topic is promising with regard to miniaturisation of a product. Also, the components of a USM system and parameters affecting the machine performance are complex. Therefore, this project was aimed at scientifically developing a relatively smaller version of USM transducer and horn assembly (compared with conventional geometries) without altering its basic functions for micro/meso scale machining, and to propose the feasible electrical components which are practically able to be used for this purpose.

2.5 AD for System and Product Design

One of the most important stages of product development is conceptual design. It is known that 70% to 80% of the total life cycle cost is determined during the concept development stage (El-Haik 2005; Liu et al. 2009). Unfortunately, developing concepts for a product is not an easy task. It requires the designer's creativity, experience, and knowledge.

Axiomatic Design (AD) has been introduced to facilitate the product design process. The approach was proposed by N.P. Suh in 1990 (Gonçalves-Coelho & Mourão 2007; Jang et al. 2002; Suh 1990). It is believed that the design process

can be managed systematically and scientifically with the use of the AD approach.

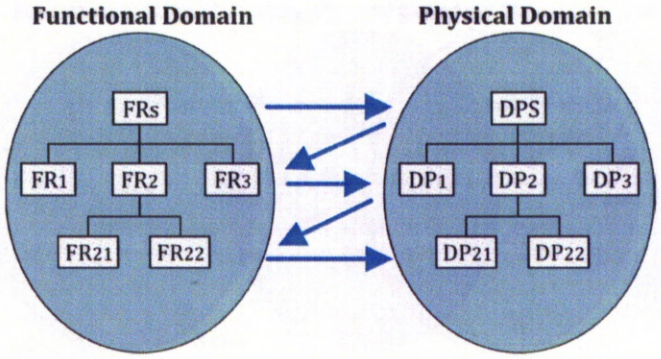

Figure 2.3: Fundamental of AD.

AD consists of several fundamental concepts (Gonçalves-Coelho & Mourão 2007; Jang et al. 2002; Suh 1999; Suh 2001). The AD design process focuses on the generation of objectives 'what we want to achieve' and solutions 'how they can be achieved'. In the terminology of AD, the objectives are defined as Functional Requirements (FRs) in the functional domain and the solutions are expressed as Design Parameters (DPs) in the physical domain. Figure 2.3 illustrates the AD approach between the functional and physical domains. Each FR and DP needs to be mapped. Their relationships can be stated as a matrix, which is known as a design matrix. Higher requirements and solutions can be broken down to more detailed levels, called decomposition. Any decisions made at higher levels result in the change of lower levels. Thus, the process goes by zigzagging between the domains. In order to select solutions, two design axioms are utilised.

Axiom 1. The Independent Axiom: Maintain the independence of FRs.

Axiom 2. The Information Axiom: Minimise the information content of the design.

The first axiom can be stated as, in a good design, each FR can be satisfied without affecting the other FRs. If this goal can be achieved, the matrix will be a diagonal matrix and the design is uncoupled, which is most preferable. This means that each DP will affect only its associated FR and can be determined independently without consideration of other components. In many designs, where the independence is unachievable, two possibilities of decoupled and coupled designs exist. Firstly, a design is decoupled (partially coupled) when the arranged design matrix is either upper or lower triangular. As a result, the order of designing each DP is important. The DPs of a decoupled design must be considered following their priorities. Lastly, when a matrix cannot be rearranged into a triangular shape, the design is coupled. A coupled matrix indicates that the design is complex, undesirable, unstable, and lacks robustness. An iterative approach to design is required and extensive methods of solutions should be sought. An uncoupled, decoupled, and coupled design matrix is shown in Figure 2.4.

$$\begin{Bmatrix} FR_1 \\ \vdots \\ FR_n \end{Bmatrix} = [A] \begin{Bmatrix} DP_1 \\ \vdots \\ DP_n \end{Bmatrix}$$

	DP1	DP2	DP3
FR1	X		
FR2		X	
FR3			X

Uncoupled

	DP1	DP2	DP3
FR1	X		
FR2	X	X	
FR3	X	X	X

Decoupled

	DP1	DP2	DP3
FR1	X	X	
FR2	X	X	
FR3	X	X	X

Coupled

Figure 2.4: Design Matrix and Coupling.

The second axiom states that the best design is the one having minimum information content. Alternatively, it can be said that among all possible DPs for satisfying a specified FR, the one with the most possibility of success is the best solution. The information content is the consideration of an accuracy (or tolerance). The information content (I) is defined in Eq. 2-10. Figure 2.5 shows that the design range is defined by the upper and lower bounds for the target value, the system range is the capability of the available system, and the common range defines the probability of the success of this specific design solution. However, this axiom can be inferred in some different ways, for examples; the simplest design is the best or the design with minimum number of parts is the best (Suh 2001).

$$I = log\left(\frac{system\ range}{common\ range}\right) \qquad \text{Eq. 2-10}$$

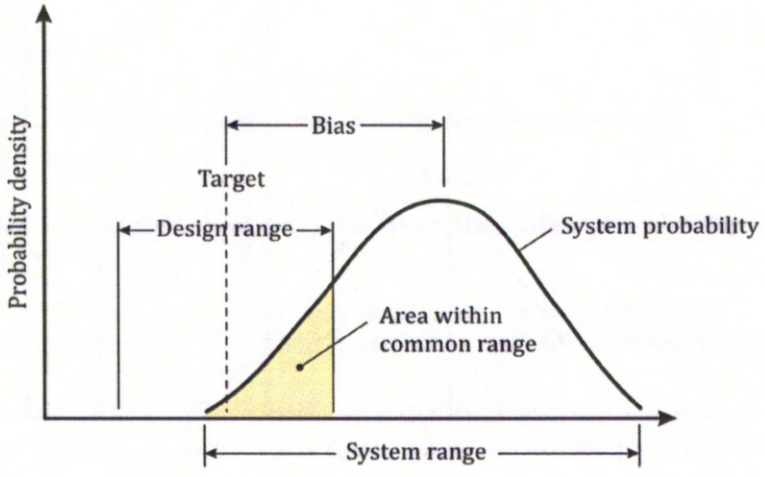

Figure 2.5: The Probability of Success for a One-FR and One-DP Design.

In the product development field, generally there are four domains: customer needs in the customer domain, functional requirements in the functional domain, design parameters in the physical domain, and process

variables in the process domain. The customer domain can be mapped with the functional domain by converting customer needs (general terms) to functional requirements (scientific terms). For the follow domains, mapping and zigzagging following the AD principles should be put forward.

AD has been applied in various products and systems. Jang et al. (2002) illustrated the use of AD for marine design problems. Lee and Suh (2005) presented the applications of AD for fabrication of composite structures. Gonçalves-Coelho and Mourão (2007) applied AD for the selection of the most appropriate manufacturing process for producing a mechanical component. Bang and Heo (2009) applied AD to nanofluid coolants. The system was found to be naturally coupled due to the characteristics of thermal-fluid system at the parametric level, but possibly the degree of couplings would be reduced or eliminated by the support of the AD approach. Cavique and Gonçalves-Coelho (2009) studied the common design of heat ventilation and air conditioning systems. They focused on the comfort and energy consumption of the systems used in commercial buildings in South European climates. A few subsystems were found to be coupled designs. Leu, Wu and Liu (2009) applied AD for the design of mechatronic products. They claimed that the use of AD principles for multiple disciplinal tasks, e.g., electronic, mechanical, and software designs, improved communication and understanding between the team. Designers were able to co-design and co-analyse the products layer-by-layer. Consequently, both functionalities and structures of the mechatronic products could be developed and integrated concurrently.

As the parameters affecting USM process and the system components are complex, the priority of design activities is important in order to develop a miniaturised USM system effectively. AD, as proved by many researchers mentioned earlier, can be very helpful for managing the activities. The framework of the design tasks can be constructed following AD guidelines.

Moreover, this study provides the first that a USM system has been developed using an AD approach.

2.6 Applied Statistics for Engineering Problems

In the analysis of nearly all engineering tasks, models play an important role for problem formation and solution. A mechanistic model is a type of model which is built from knowledge of the basic physical mechanism. It might be expressed as

$$y = f(x_1, x_2, \dots, x_n) \qquad \text{Eq. 2-11}$$

where y is a parameter of interest which is related to variables $x_1, x_2, \dots, x_n$ and can be formed in a function f. However, when an experimental process is performed more than once, the outcomes are slightly different due to small changes or variation in factors that are unable to be controlled completely, as presented in Figure 2.6. Therefore, a more realistic model for parameter y might be

$$y = f(x_1, x_2, \dots, x_n) + \epsilon \qquad \text{Eq. 2-12}$$

where ϵ is a term added to the model to compensate for the fact that the observed values are effected by sources of variability.

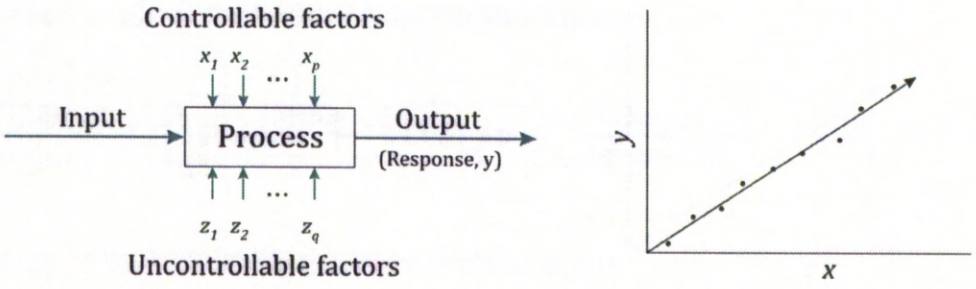

Figure 2.6: The Realistic Output from Experiments.

Sometimes, engineers deal with problems that are not simple or well understood, and for which it is not easy to form mechanistic models. The models for those problems could be developed from engineering and scientific knowledge but not directly from the theoretical understanding of the principles of the fundamental mechanism. This type of model is called an empirical model (Figure 2.7). By observation study and collecting a lot of data, the expected value of y, $E(y)$, can be predicted. The model of the relationship between the variables is

$$E(y) = f(x_1, x_2, \dots, x_n) \qquad \text{Eq. 2-13}$$

For the same reasons that have been described previously, all experiments always have uncontrolled factors, so the model should be written as

$$E(y) = f(x_1, x_2, \dots, x_n) + \epsilon \qquad \text{Eq. 2-14}$$

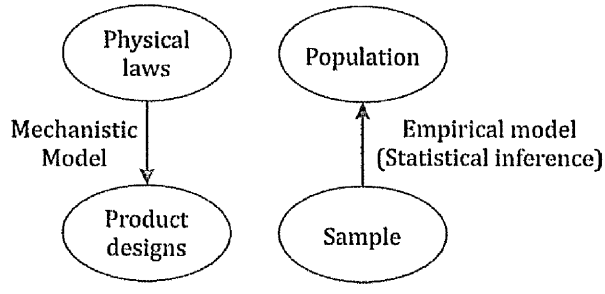

Figure 2.7: Type of Models (Montgomery 2009).

Design of experiments (DOE) or experimental design is a strategy to gather empirical knowledge. It can be applied when investigating a phenomenon in order to gain an understanding of, or identify critical factors impacting a system. Building a design means carefully choosing a small number of experiments that are to be performed under controlled conditions. The data tables are generated which contain an important amount of structured variation. The chances of

extracting useful information from the data are increased by selecting the sample wisely. As a result, problems can be better understood, important variables can be highlighted, and optimum conditions of a system can be found.

2.6.1 Using DOE for Observational Study

Experiments are an important part of learning about how systems work. A factorial experiment is one of the experimental techniques used in observation when problems with two or more factors are being considered. A factor means a controlled independent variable or a variable whose levels are set by the experimenter. Generally, the technique is performed for all or partial combinations of factor levels. The advantages of factorial designs over one-factor-at-a-time experiments are that they are more efficient and they allow interactions to be detected. An interaction effect exists when the effect on one factor is not at the same levels.

For an example, suppose there are 2 factors, A and B, considered with 2 levels, low and high. The number of runs for this case of experimentation is $2^2=4$ without replication of runs. The outcomes that could occur are 8 possibilities, which are as listed in Table 2.3. However, making good decisions, an analysis of which factors or relationships have significant effects on the system, is not a simple task. A check of assumptions is important, therefore probability models for statistical inference are involved in the assessments.

Table 2.3: Possibilities of Main Effects and Interaction Effects of Analysis of 2 Factors and 2 Levels.

Kinds of Effects	Example of data output
1. Nothing	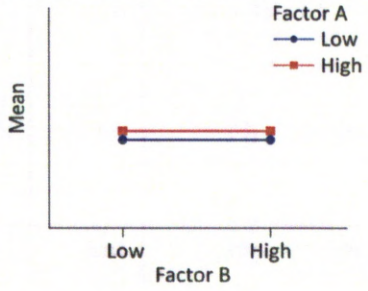
2. Main effect of factor A	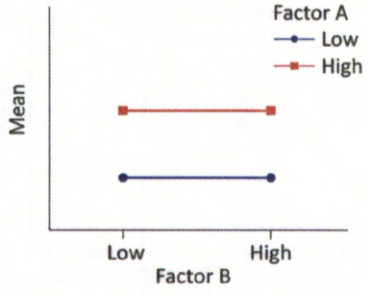
3. Main effect of factor B	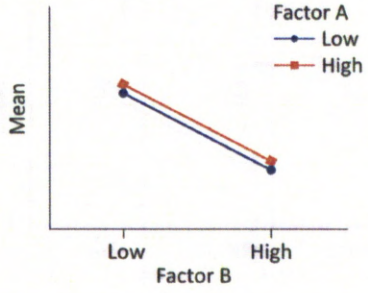
4. Both main effects (factors A and B)	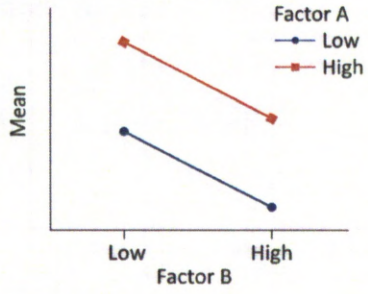

Table 2.3: Possibilities of Main Effects and Interaction Effects of Analysis of 2 Factors and 2 Levels. (Cont.)

Kinds of Effects	Example of data output
5. AB interaction	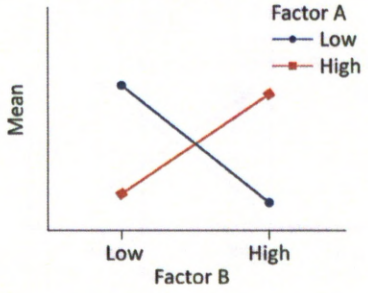
6. AB interaction and main effect of factor A	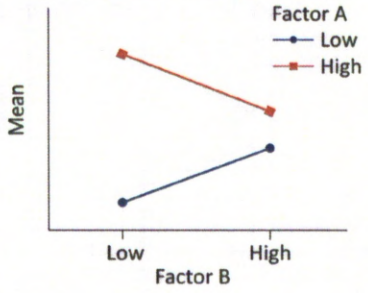
7. AB interaction and main effect of factor B	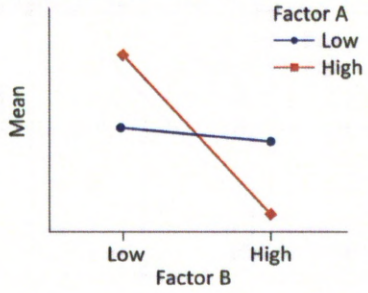
8. AB interaction and both main effects (factors A and B)	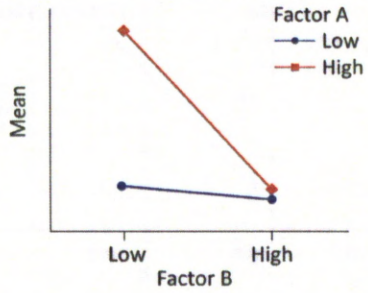

Many problems require decisions to be made regarding whether to accept or reject a statement about some parameters. The statement is called a hypothesis. For example, suppose that resonant frequency of an ultrasonic machining system is the focus, an exciting frequency is a random variable, and the decision is whether or not the resonant frequency of the system is 21 kHz. Then the problem can be expressed as

$$H_0: \mu = 20\ kHz$$
$$H_1: \mu \neq 20\ kHz \qquad \text{Eq. 2-15}$$

The statement H_0 is called the null hypothesis and the statement H_1 is called the alternative hypothesis. The decision making procedure about the hypothesis is called hypothesis testing. The test statistic is computed to make a decision and, in this example, it is the sample mean, $\bar{x}$, of resonant frequency which is observed from some specimens. Suppose if $19 \leq \bar{x} \leq 21$, we will not reject the null hypothesis and this region is called the acceptance region. If either $\bar{x} < 19$ or $\bar{x} > 21$, we will reject the null hypothesis in favour of the alternative hypothesis and this region is called the critical region. The boundaries between the critical regions and the acceptance region are called the critical values.

Hypothesis testing procedures rely on using the information in a random sample from the population of interest. Thus, the truth or falseness of a particular hypothesis can never be known without performing an experiment on the entire population. The decision can be either of two wrong conclusions.

Type I error is rejecting the null hypothesis H_0 when it is true. The probability of making a type I error is donated by α.

$$\alpha = P(\text{type I error}) = P(\text{reject } H_0 \text{ when } H_0 \text{is true}) \qquad \text{Eq. 2-16}$$

Sometimes, the type I error is called the significant level or the α-error. The probability of making this type of error is shown in the shaded area of the normal distribution in Figure 2.8.

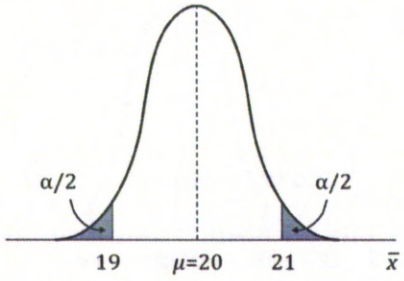

Figure 2.8: The Probability of Type I Error when $\mu = 20$.

Type II Error is failing to reject the null hypothesis H_0 when it is false. The probability of making a type II error is donated by β.

$$\beta = P(\text{type II error}) = P(\text{fail to reject } H_0 \text{ when } H_0 \text{ is false}) \qquad \text{Eq. 2-17}$$

The type II error, sometimes called the β-error, is shown in Figure 2.9.

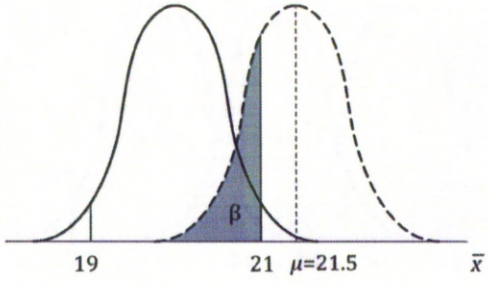

Figure 2.9: The Probability of Type II Error when $\mu = 21.5$.

Type I and type II errors are related. A decrease in probability of one type always results in an increase of the other. However, generally type I error is more preferable for some reasons (Montgomery & Runger 2006). Analysts can directly control the type I error probability when they select the critical value. The decrease of a sample size increases β-error but α is held constant.

To judge whether any parameter affects the response, F-test from the analysis of variance (ANOVA) table is widely used (Park 1996). F-test considers a decomposition of the variability in a collection of data in terms of sums of squares. The test statistic in an F-test is the ratio of two scaled sums of squares reflecting different sources of variability. These sums of squares are constructed so that the statistic tends to be greater when the null hypothesis is not true. The formula for the simple ANOVA F-test statistic (F_0) is

$$F_0 = \frac{between\ group\ variavility}{within\ group\ variability} \qquad \text{Eq. 2-18}$$

And the critical value (F-critical or F_α) follows the F-distribution with numbers of degree of freedom under the null hypothesis.

One other way to report the hypothesis testing results is the P-value approach. The definition of the P-value is the smallest level of significance that would lead to the rejection of the null hypothesis with the given data. The null hypothesis would be rejected for any P-value less than α.

$$\text{P-value} = 1 - P(\text{lower critical value} < \bar{x} < \text{upper critical value}) \qquad \text{Eq. 2-19}$$

It is not always easy to compute the exact P-value but in practice the value can be reported by using most modern statistical analysis software which is adopted widely.

Another technique used for analysing factorial experiments is a normal probability plot of factor effects (Antony 2003). The effects of factors are plotted against cumulative probability (percent). The plots are useful for evaluating the

normality of factor effects. Those inactive main and interaction effects tend to fall roughly along a straight line whereas active effects tend to appear as extreme points falling off each end of the line. Figure 2.10 is an example of a normal probability plot showing significant effects of factors B and C, and interaction between factors A and C on a response.

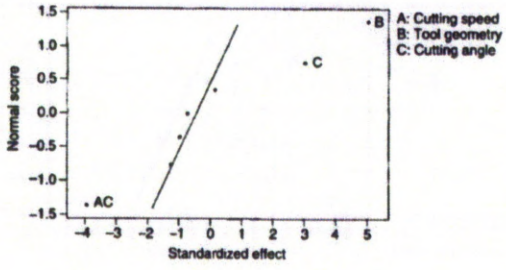

Figure 2.10: Example of Normal Probability Plot of Effects (Antony 2003).

When the number of factors increases, the number of runs required becomes very large. Also, very often time, resources, and budget for investigations are insufficient. A fractional factorial design is an effective technique used to draw out valuable conclusions from fewer runs. Generally, a fraction such as ½ and ¼ of the runs is picked from full factorial designs.

2.6.2 Using DOE for Design Optimisation Problems

Parameter design is one of three steps in the product design phase of functional design, parameter design, and tolerance design. The first design step in the design of a miniaturised USM system has already been discussed in Section 2.5, the last step is particularly essential for manufacturing a product in mass volume so it will not be involved in this thesis, while the parameter design step will be discussed below.

In order to find optimum levels for the quality of a product, fractional factorial designs using tables of orthogonal arrays are often used in case there are too many parameter combinations to be observed (Park 1996). When there

are many parameters under consideration, full factorial or fractional factorial designs can be used, depending on the situation, to select or screen out the few important main effects from the many less important ones. For this purpose, the type of design, according to the experimental objective, is called a screening experiment or main effects design. The DOE analysis tools used for the screening objective include the tools already explained in 2.6.1: main and interaction effect plots, P-value, F-test, and normal probability plots.

Later, after the parameters potentially influencing the quality characteristic of a product or process have already been identified, contour and surface plots can be created from the data collected following DOE. They can help experimenters or designers to understand the nature of the relationship between two significant factors. The examples of the plots gathered from Antony (2003) are presented in Figure 2.11 where the relation of cutting speed and cutting angle affecting tool life can been seen. The plots show that the tool life is increased when the cutting angle is increasing and the cutting speed is decreasing. Moreover, a response surface can be mapped mathematically as a response function (Eq. 2-14) used to find a direction of potential improvement for a problem, which is a proper method to seek the direction of improvement in optimization problems. This method is called Response Surface Methodology (RSM) (Antony 2003; Lawson & Erjavec 2001; Myers, Montgomery & Anderson-Cook 2009).

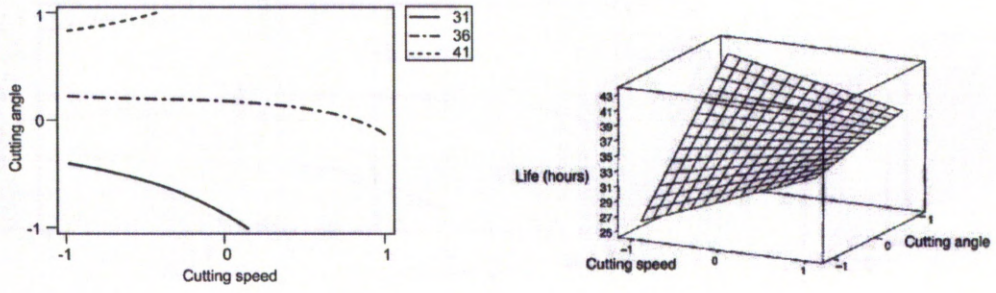

(a) (b)

Figure 2.11: Examples of (a) Contour and (b) Surface Plots (Antony 2003).

In summary, statistical design of experiments is a very useful and valuable technique for investigating processes or systems and also for optimising problems with many design variables. The technique requires fewer experiments to analyse systems scientifically and has been applied extensively. There are over nine hundred thousand publications found on ScienceDirect, one of the largest online collections of published scientific research, when the words 'design of experiments' are used as searching keywords. Some of the works of researchers who have employed statistics for analysing or optimising problems relating to USM systems have been explored. The important parameters affecting machining performances seemed to depend on the machine and work material used in investigations. In the early 1960s, Wu used RSM for tool life prediction (Wu 1962). Benkirane, Kremer and Moisan (1999) studied the machining rates of a contour machining system in the selection of important process parameters using a neural network approach. They examined the effect of varying several of the process parameters while keeping the tool stationary. Dapino, Flatau and Calkins (2006) studied the variations of the properties of Terfenal-D, a material for a transducer, when drive amplitude sensitivity, mass load sensitivity, and repeatability were investigated. Jain, Jain and Deb (2007) optimised process parameters of several advanced mechanical-type machining

processes using genetic algorithm under the economic, efficient, and effective utilization concerns. Singh and Khamba (2007) optimised the MRR for their selected USM machine for the machining of pure titanium and titanium alloy. Kumar, Khamba and Mohapatra (2009) developed a model for the prediction of tool wear rate for the machining of pure titanium.

Since DOE is a very useful tool for solving engineering problems, it has been used in the project for the design of a miniaturised horn and investigation of the proposed USM system. This is because it would take a long time to achieve an optimum solution if every dimension and process parameter had to be taken to account. The literature review reflected that the horn geometry can be optimised more effectively than considering one dimension at a time such as had been made by Nicholson and McDicken (1996) and Cardoni, Harkness and Lucas (2010). Also, the MRR prediction equation of the proposed USM system can be created by well-planned experiments in order to obtain a simple form of equation involved with significant parameters only.

Chapter 3

Axiomatic Design of the Miniaturised USM System

3.1 The Purpose of Using AD

Axiomatic Design (AD) has been used for product development processes in order to design products or systems effectively, scientifically, and logically as reviewed in Section 2.5. Product or system development is not an easy task, and this applies to the design of a USM system. As presented in Sections 2.2 and 2.3, a USM system is a complex system. There are a number of components and parameters involved affecting machining outputs. Design each component with the wrong order might cause project delay.

AD has been found to be one of the most effective tools in defining and analysing a problem but is not an innovative solution generator (Shirwaiker & Okudan 2008). In addition, when using AD (the 2nd Axiom), sufficient information needs to be obtained from every design candidate in order to select the best solution. However, obtaining that information was impractical for the project where almost every component was made as a new system prototype. Therefore, the project aimed to implement AD to analyse the design of a conventional USM machining system in order to prioritise the tasks of the design of the components for a miniaturised USM system. In this way, the researcher could be assured that, like the existing conventional USM system, the proposed miniaturised USM system fulfilled the essential functions for micro-machining. Note that the solutions presented in this chapter were abstract and conceptual only.

3.2 FRs, DPs, Constraints, and Design Matrix for a USM System

With the intention of developing a system effectively by following AD principles, FRs and DPs of the system need to be determined. For a proper design, the number of DPs is recommended to be equal to the number of FRs (Suh 2001). Otherwise, the design is a coupled design or the FRs cannot be satisfied when the number of DPs is less than the number of FRs. In addition, when the number of DPs is more than FRs, the design is a redundant or coupled design.

Level 0

The highest level of FRs can be initially denoted by thinking what functions are most essential to be achieved. Therefore, there was only one FR to be fulfilled at this level (Level 0): 'Develop a machining system utilising ultrasonic vibrations'. Next, constraints were developed so the thinking process could be focused on a specific area. For this thesis the scope was set for a miniaturised system (*Ca*) capable of creating a maximum cavity of 5×5 mm² (*Cc*) on glass material (*Cb*). The FRs, DPs, and the constraints for the highest level can be stated as in Table 3.1.

Table 3.1: AD Level 0.

FR0:	Develop a machining system utilised ultrasonic vibrations.	***DP0:***	Miniaturized USM system.
Ca:	Miniaturise the system.		
Cb:	Focus on machining glass material.		
Cc:	Create the cavity of 5x5 mm² (maximum).		

The design equation is

$$\{FR\} = [X]\{DP\} \qquad \text{Eq. 3-1}$$

Level 1

Next, the FRs for the lower level (Level 1) were generated as well as the associated DPs. By considering the USM principle, the process can effectively be used to machine a hard and brittle work-piece by the influence of vibrations, abrasive slurry, and feeding force. Accordingly, those were the requirements for the system Level 1. A concern over the user safety of a user was also included. Thus, the requirements and their DPs are given in Table 3.2.

Table 3.2: AD for the Proposed USM System at Level 1.

FR1:	Identify shape/size of cavity on a work-piece.	***DP1:***	Tool bit.
FR2:	Generate vibrations.	***DP2:***	Vibration generating system.
FR3:	Feed abrasive slurry into the machining zone.	***DP3:***	Abrasive slurry feeder.
FR4:	Force the machining system and the work-piece against each other.	***DP4:***	Feeding mechanism.
FR5:	Prevent the user from harmful effects caused by the machining system	***DP5:***	Case.

C1a: Ultrasonic frequencies ($f_V \sim 20kHz$).
C1b: Maximise amplitude of vibrations (A_V).
C1c: The force of FR3 is varied depending on cutting conditions (F_S).

The design equation can be written in a matrix form as

$$\begin{Bmatrix} FR1 \\ FR2 \\ FR3 \\ FR4 \\ FR5 \end{Bmatrix} = \begin{bmatrix} X & & & & \\ X & X & & & \\ & & X & & \\ X & X & & X & \\ X & X & X & X & X \end{bmatrix} \begin{Bmatrix} DP1 \\ DP2 \\ DP3 \\ DP4 \\ DP5 \end{Bmatrix} \quad \text{Eq. 3-2}$$

The constraints for the design Level 1 have been determined. First, the vibrations generated for machining must be at ultrasonic levels preferred to be just beyond the audible range, approximately 20 kHz (*C1a*). Second, the amplitude of vibrations must be maximised (*C1b*). The last constraint requires

that the cutting force may vary depending on cutting conditions (*C1c*) in order to achieve a specific surface quality or machining rate.

Eq. 3-2 shows that the design of Level 1 was a decoupled design. *DP1*: 'Tool bit' is used to define the shape and size of cavity to be created on the work surface. *DP2*: 'Vibration generating system' responds to generating vibrations for cutting a work-piece. The USM process can be performed by either vibrating the tool or the work-piece but the constraint *Ca* states that the system must be minimised. Accordingly, it was better to excite the tool because the work-piece might be large or complex and the subsequent design of vibrating the work-piece would be more difficult. Moreover, *DP2* needs to be able to drive *DP1*: 'Tool bit' at ultrasonic frequencies with sufficient amplitude of vibrations. *DP2* is the main part of the system (and the focal part of this thesis) because it is related to many items and its construction is complicated. Based on the theory of vibrations, every part connected within the system has an effect on waves travelling through the media. Thus, *DP2* results from *DP1*. Also, *DP2* affects to *DP4*: 'Feeding mechanism' and *DP5*: 'Case' because these two components are connected. *DP3*: 'The abrasive slurry feeding system' is required to feed abrasive slurry to the cutting zone. It can be designed to be either separated from or included in the vibration generating system.

At this stage, the idea of separation was more preferable to avoid a coupled design and so *DP3* can be considered independently. For a machining operation, it is necessary to have a force between the cutting tool and the work-piece, so *DP4*: 'Feeding mechanism' is responsible for this task. The last DP of Level 1 is *DP5*: 'Case'. It is used to cover the machining system in order to prevent the user from any kind of harmful damages that might happen. *DP5* can be designed at last once the decision for the concepts of *DP1, DP2, DP3*, and *DP4* have been finalised because its design is affected by every component. For example, the case could be affected by the size of the tool bit and vibration generating system;

the means of feeding abrasive slurry; and the force required for holding the components.

In summary, the decoupled design matrix in Eq. 3-2 suggests the sequence of the design tasks. The concept of *DP1*: 'Tool bit' must be decided first, then *DP2*: 'Vibration generating system' and *DP4*: 'Feeding mechanism' respectively, while *DP3*: 'The abrasive slurry feeding system' can be designed independently, and the last one is the design of *DP5*: 'Case'.

Level 2

The requirements and their correlated solutions for each FR/DP in Level 1 were decomposed to a lower level (Level 2). Table 3.3 shows the functions required for designing a tool bit for USM process. The design can be a decoupled design and the design equation can be written as Eq. 3-3. The tool bit should have one end with a desired shape (*DP11*) and another end with a part for receiving energy transferred from the vibration generator (*DP12*). In general for USM applications, each part can be connected to each other by screw, taper fitting, or soldering (Abdullah, Shahini & Pak 2009; Singh & Khamba 2006; Thoe, Aspinwall & Wise 1998). The soldering method seems to be the most favourable for energy transmission between parts whereas the screw is better for convenience, the ease of tool changing, and cost of production. For the choices of tool materials, the quality to withstand dynamic stress and strain (*DP13*) comes as the most important. Then, its machinability properties (*DP14*) are essential for lead time and cost considerations.

Table 3.3: AD for the Proposed USM System at Level 2: *FR1/DP1* Tool bit.

FR11:	Create a breakage on a work-piece.	***DP11:***	Tool bit end.
FR12:	Obtain energy from vibrations generating system.	***DP12:***	Screw thread.
FR13:	Withstand frequentative strain/stress.	***DP13:***	Toughness of tool material.
FR14:	Be machined to complex shape.	***DP14:***	Machinability of tool material.

$$\begin{Bmatrix} FR11 \\ FR12 \\ FR13 \\ FR14 \end{Bmatrix} = \begin{bmatrix} X & & & \\ & X & & \\ & X & X & \\ X & X & X & X \end{bmatrix} \begin{Bmatrix} DP11 \\ DP12 \\ DP13 \\ DP14 \end{Bmatrix} \quad \text{Eq. 3-3}$$

Decomposition of *DP2*: 'Vibration generating system' is shown in Table 3.4. There were four main physical components which are *DP21*: 'Plug' for receiving power from a source, *DP22*: 'Signal generator' for generating alternating signals, *DP23*: 'Transducer' for converting the signals to mechanical vibrations, and *DP24*: 'Screw' for transmitting the mechanical vibration energy to the tool bit (*DP1*).

The relationships of each component can be expressed as Eq. 3-4 where it shows a coupled design. The relationships are based on the general knowledge of common types of signal generators and transducers. Typically, power rating of a normal power source is too high for the power required for a signal generator and the strength of the signal output generated from a signal generator is too low for a transducer. For example, in the UK the standard power rating is 230 V, whilst the power output of a function generator is around ±5 V, and a piezoelectric transducer requires the power rating of several hundreds to a thousand Volts to drive it.

Table 3.4: AD for the Proposed USM System at Level 2: *FR2/DP2*, Vibration generating system.

FR21:	Receive power input.	***DP21:***	Power receiver/Plug.
FR22:	Generate electrical alternating signals.	***DP22:***	Signal generator.
FR23:	Generate mechanical vibrations.	***DP23:***	Transducer.
FR24:	Transfer vibration energy to the tool bit.	***DP24:***	Screw.

$$\begin{Bmatrix} FR21 \\ FR22 \\ FR23 \\ FR24 \end{Bmatrix} = \begin{bmatrix} X & X & & \\ X & X & X & \\ & X & X & \\ & & X & X \end{bmatrix} \begin{Bmatrix} DP21 \\ DP22 \\ DP23 \\ DP24 \end{Bmatrix} \quad \text{Eq. 3-4}$$

Moreover, the required signal is defined by the type of transducers used. For example, piezoelectric transducers require signals with high voltage/low current while magnetostructive transducers need low voltage/high current signals. The design of the vibration generating system for USM applications is a coupled design as long as it needs vibrations at resonant frequencies and if the ultrasonic frequencies must be obtained by using smart materials converting electrical signals to mechanical vibrations. Therefore, the source of power, signal generator, and transducer for generating ultrasonic frequencies need to be matched to each other in order to maximise the efficiency, especially to generate vibrations at resonances.

The complex vibration generating system in Table 3.4 can be considered in a simpler way as a decoupled design when one constraint is chosen to be the most important. Hence, the maximum amplitude of vibrations (*C1b*) is a critical requirement. In order to gain the highest amplitude of vibration, losses need to be minimal. Therefore, the FRs and DPs of the vibration generating system, determined to have minimal losses, can alternatively be deployed. The re-written FRs and DPs are shown in Table 3.5. The choices of mechanical components affects electrical behaviour of a system as expressed in Eq. 3-5 so it was noted that materials and fabricating processes involved in the vibration generating system take priority.

Table 3.5: AD Level 2: Re-written *FR2/DP2*, Vibration generating system.

FR21':	Minimise mechanical losses.	***DP21':***	Mechanical impedance matching.
FR22':	Minimise electrical losses.	***DP22':***	Electrical impedance matching.

$$\begin{Bmatrix} FR21' \\ FR22' \end{Bmatrix} = \begin{bmatrix} X & \\ X & X \end{bmatrix} \begin{Bmatrix} DP21' \\ DP22' \end{Bmatrix} \qquad \text{Eq. 3-5}$$

For the abrasive slurry feeding system, the FRs and DPs can be decomposed as presented in Table 3.6. The design equation can be written as Eq. 3-6. The size of *DP31*: 'Container' could limit the means of mixing and feeding. Therefore, the design of the abrasive slurry feeder was decoupled and *DP31* was the first followed by *DP32* 'Feeder' in the design sequence. DP33 'Mixer' was the last in the design order because if the feeder is too long, the mixer might need to maintain equal concentration for the entire slurry media.

Table 3.6: AD for the Proposed USM System at Level 2: FR3/DP3 Abrasive slurry feeder.

FR31:	Contain the mix between abrasive particles and fluid.	***DP31:***	Container.
FR32:	Feed abrasive slurry into the machining zone.	***DP32:***	Feeder.
FR33:	Mix abrasive particles and fluid.	***DP33:***	Mixer.

$$\begin{Bmatrix} FR31 \\ FR32 \\ FR33 \end{Bmatrix} = \begin{bmatrix} X & & \\ X & X & \\ X & X & X \end{bmatrix} \begin{Bmatrix} DP31 \\ DP32 \\ DP33 \end{Bmatrix} \qquad \text{Eq. 3-6}$$

The next component to be considered was *DP4*: 'Feeder'. Ideally, either the tool or the work-piece can be a moving part. The idea of moving the tool to the work-piece was preferable for the ease of use and design. Generally, the size and weight of a work-piece can be in a wider range than the tool so moving a work-piece might be more difficult and complex.

The functions for *DP4*: 'Feeder', as shown in Table 3.7, include *FR41*: 'Maintain desired feeding force' satisfied by *DP41*: 'Set weight' and *FR42*: 'Move the tool' corresponded by *DP42*: 'Tool feeder'. The means of maintaining feeding force might be engaged with the structure of tool feeder, so the design matrix can be presented as Eq. 3-7. However, the force must be changeable within a range (as under the constraint *C1c*) depending on cutting conditions.

Table 3.7: AD for the Proposed USM System at Level 2: FR4/DP4 Feeding mechanism.

FR41:	Move the tool.	***DP41:***	Tool feeder.
FR42:	Maintain desired feeding force.	***DP42:***	Set weight.

$$\begin{Bmatrix} FR41 \\ FR42 \end{Bmatrix} = \begin{bmatrix} X & \\ X & X \end{bmatrix} \begin{Bmatrix} DP41 \\ DP42 \end{Bmatrix} \quad \text{Eq. 3-7}$$

Finally, the functions of *DP5*: 'Case' to prevent a user from harmful effects caused by the machining system' were listed in Table 3.8. It is required to hold the system rigidly in a proper place and to allow the tool to contact the work-piece. Most importantly, it should protect a user from any unsafe consequences caused by the system. These requirements were fulfilled by *DP51*: 'Clamper', *DP52*: 'Case mouth', and *DP53*: 'Body cover', respectively. The connections between functions and components is expressed in Eq. 3-8 where *DP51* and *DP52* were independent to each other and both had an effect on the design of *DP53*.

Table 3.8: AD for the Proposed USM System at Level 2: FR5/DP5 Case.

FR51:	Hold the machining system in place.	***DP51:***	Clamp.
FR52:	Allow the tool bit to contact the work-piece.	***DP52:***	Case mouth.
FR53:	Prevent the harmful areas from a user.	***DP53:***	Body cover.
C2a:	Minimise energy losses from the system to external components.		

$$\begin{Bmatrix} FR51 \\ FR52 \\ FR53 \end{Bmatrix} = \begin{bmatrix} X & & \\ & X & \\ X & X & X \end{bmatrix} \begin{Bmatrix} DP51 \\ DP52 \\ DP53 \end{Bmatrix} \quad \text{Eq. 3-8}$$

3.3 Product Framework

This section presents the use of AD for the design of a miniaturised USM system adapted from designing a standard USM system. The AD was used for managing design tasks by considering the relationships of functional and physical domains. By following the AD approach, the components of a USM system were identified as decoupled and coupled designs. Therefore, it is very important that these components must be designed in order, otherwise, some components could not be adjusted without affecting other functions.

The framework for the design tasks is depicted in Figure 3.1. The AD approach allows the interrelationships between each task to be well defined from the highest level to the lower activities. This ensures that all objectives can be fulfilled. As this is a conceptual study, only the main components of a miniaturised USM system have been included. The details of the designs that are within the scope of this thesis will be presented in Chapter 4 and Chapter 5. Every step taken follows the framework based on the AD approach.

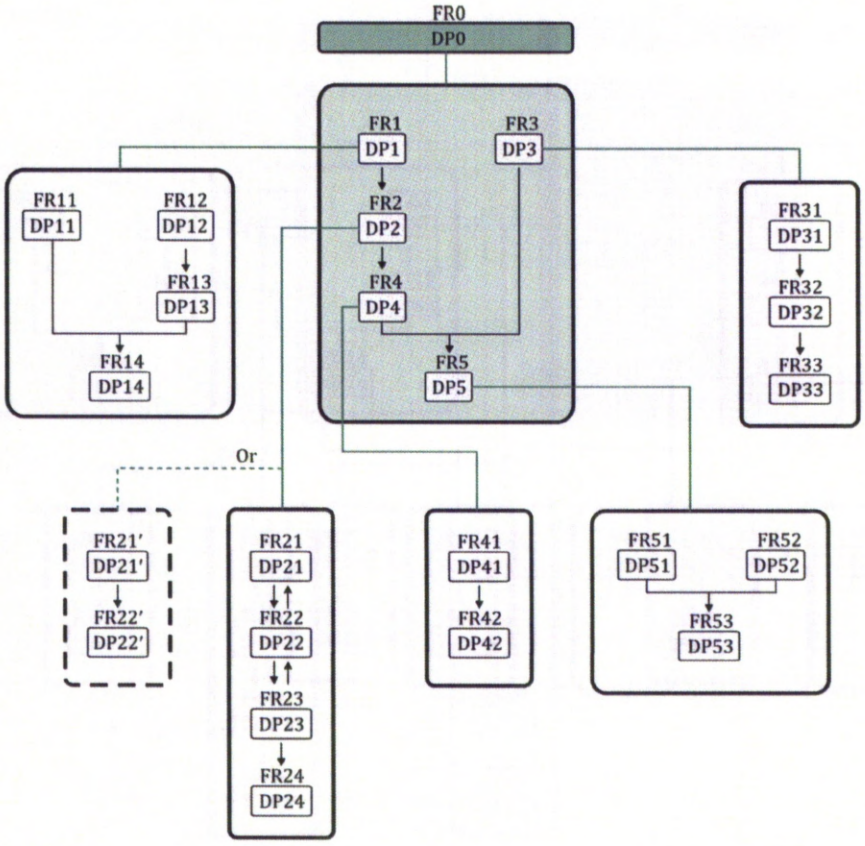

FR0: Develop a machining system utilised ultrasonic vibrations.
FR1: Identify shape/size of cavity on a work-piece.
FR2: Generate vibrations.
FR3: Feed abrasive slurry into the machining zone.
FR4: Force the machining system and the work-piece against each other.
FR5: Prevent the user from harmful effects caused by the machining system
FR11: Create a breakage on a work-piece.
FR12: Obtain energy from vibrations generating system.
FR13: Withstand frequentative strain/stress.
FR14: Be machined to complex shape.
FR21: Receive power input.
FR22: Generate electrical alternating signals.
FR23: Generate mechanical vibrations.
FR24: Transfer vibration energy to the tool bit.
FR21': Minimise mechanical losses.
FR22': Minimise electrical losses.
FR31: Contain the mix between abrasive particles and fluid.
FR32: Feed abrasive slurry into the machining zone.
FR33: Mix abrasive particles and fluid.
FR41: Move the tool.
FR42: Maintain desired feeding force.
FR51: Hold the machining system in place.
FR52: Allow the tool bit to contact the work-piece.
FR53: Prevent the harmful areas from a user.

DP0: Miniaturized USM system.
DP1: Tool bit.
DP2: Vibration generating system.
DP3: Abrasive slurry feeder.
DP4: Feeding mechanism.
DP5: Case.
DP11: Tool bit end.
DP12: Screw thread.
DP13: Toughness of tool material.
DP14: Machinability of tool material.
DP21: Power receiver/Plug.
DP22: Signal generator.
DP23: Transducer.
DP24: Screw.
DP21': Mechanical impedance matching.
DP22': Electrical impedance matching.
DP31: Container.
DP32: Feeder.
DP33: Mixer.
DP41: Tool feeder.
DP42: Set weight.
DP51: Clamp.
DP52: Case mouth.
DP53: Body cover.

Figure 3.1: Decomposition of FRs and DPs for USM System.

Chapter 4

Design and Performance Evaluation of Prototype-I

Design of main components of the USM system is discussed in this chapter. A USM system is a complex system and there are interrelationships between the electrical and mechanical components which were already explained in Chapter 3. In order to miniaturise the system effectively, the components must be designed to match each other. In this project, the focus was on designing and prototyping the mechanical components including transducer and horn. However, without the electrical components such as power supply and signal generator, the system could not work and was unable to be validated, so the prototype of the electrical components were made but they were not the central part of this project.

4.1 Design of Mechanical Components

4.1.1 Material Selection

4.1.1.1 Transducer

There are two main types of materials employed in transducer technology for high power ultrasonic applications; namely, piezoelectric and magnetostrictive materials. Piezoelectric and electrostrictive materials are both ferroelectric and have a number of features in common but the former is used more commonly because degradation of the properties of electrostrictive materials tends to be dramatically increased at high frequency applications. Accordingly, only piezoelectric and magnetostrictive materials are candidates

and their important characteristics that affect a transducer performance are summarised, weighted, and decided in Table 4.1.

Piezoelectric transducers utilize the piezoelectric property of a material to convert electrical energy directly into mechanical energy thus their coupling factors are generally high. When an electrical field is applied across a piezoelectric material, it expands or contracts in its lattice structure which is not isotropic but polar alignment dependent. A typical piezoelectric material is Lead Zirconate Titanate (PZT) discovered in the 1950s (King et al. 1990). Two types of PZT are available, hard and soft. Typically, hard PZT is more suitable for high power applications despite giving less displacement. The hard PZT has a good extension rate, with good temperature, and time stability. PZT is a ceramic, with poor tensile strength, so operating under a preload is necessary. Fortunately the displacement attained for a given applied voltage is not significantly affected by the degree of preload if the preload is under the limit recommended by the PZT ceramic manufacturer.

Magnetostrictive transducers utilize the magnetostrictive property of a material to convert the energy in a magnetic field into mechanical energy. The magnetic field is provided by a coil of wire which is wrapped around the magnetostrictive object. Nickel was the earliest material used for magnetostructive transducers. Even though Nickel gives a high force, the major disadvantages in transducer uses are its high electrical losses and low coupling efficiency (around 30% only) so high heat will be generated from the transducer and the power output is relatively low. However, the development of new magnetostrictive material breaks through the limits of Nickel. Rare earth-iron called Terfenol-D or Giant Magnetostrictive Material (GMM) discovered by A.E.Clark (Olabi & Grunwald 2008; Park et al. 2007) attributes high magnetostrains larger than Nickel and its coupling efficiency is equivalent to PZT.

Table 4.1: Transducer Material Selection for Miniaturized USM System.

Material Characteristic	Unit	Transducer Characteristic	Type of Transducer					
			Piezoelectric		Magnetostrictive			Electrostrictive
			PZT		Terfenol-D		Nickel	PMN
Static strain Dynamic strain	ppm ppm	Displacement/Blocked force	100 - 600 Up to 1600		800 – 2000 Up to 4000	✓	-40 to -50	1500 Up to 2500
Young's modulus	GPa	Displacement/Blocked force	48 - 116	✓	25 - 80		225	
Coupling coefficient		Conversion efficiency	0.65 – 0.85	✓	0.6 – 0.85		0.3	0.6 – 0.9
Sound velocity	m/s	Length to resonance	2600 - 3600		1395 – 2444	✓	5600	
Curie Temperature	°C	Operating temperature range	80 – 350 (Irreversible)		340 – 380 (Reversible)	✓	580	
Quality factor		Amplitude sensitivity	20 – 2500		3 - 20	✓	132 - 360	
Density x 10^3	kg/m^3	Weight	7.6 – 8.1	✓	9.1 – 9.5		8.7 - 9.5	
Driving voltage or current		Power consumption	kV	✓	kA		kA	Higher than PZT
Cost	$/$cm^3$	Cost	200 (£130)*	✓	400 (£260)*			
Bias Mechanism		System complexity	Electric field	✓	Magnetic field		Magnetic field	Electric field
Degradation		Life span	Depoling		Melting and mechanical shock	✓	Melting and mechanical shock	Depoling

✓ means preferable.
* $ 1 = £0.65

As presented in Table 4.1, important characteristics for developing a miniaturised ultrasonic machining system are summarised and discussed below.

- Speed of operation: PZT has a significantly wider range of frequencies (up to MHz) for applications than does Terfenol-D because the generation of magnetic field and eddy current loss induces a frequency limitation of Terfenol-D to some kHz (Claeyssen, Lhermet & Maillard 2002; Yamamoto, Eda & Shimizu 1999).
- Broadband: In machining applications, oscillating systems are very sensitive to applied loads (Claeyssen et al. 1997; Xu, Hu & Chan 2002) such as a static force holding a USM device against a work-piece or the different weights of cutting tools. When high mechanical quality factor (Q factor) PZT is operating off resonance, its output and efficiency decrease markedly. Low Q factor Terfenol-D (Olabi & Grunwald 2008) performs well over a frequency broadband and beats the narrowband limitations of PZT (Ceratec North America Corp. 2011; Fuji Ceramics Corp. 2011).
- Amplitude of vibrations: Terfenol-D tends to be better than PZT in its ability to produce displacements (Claeyssen, Lhermet & Maillard 2002; Yamamoto, Eda & Shimizu 1999). The lower stiffness of Terfenol-D can generate higher maximum displacement (non-loaded) at a static bias and even higher at resonance. To get a high material removal rate, one of the most important factors is achieving high amplitude of vibrations. The displacement generated by Terfenol-D at the resonant frequency is possibly ten times higher than that of PZT. This issue can be overcome since there are various techniques to magnify the amplitude. For a PZT device, it is necessary to design an effective horn in order to gain superior displacements.

- Available blocked force: The blocked force is the maximum force exerted at a given voltage level when the displacement is totally blocked. The highest displacement is a force-free condition. The relationship between force and displacement shows linear behaviour (Claeyssen et al. 1997; Kellogg & Flatau 2004). Consequently, PZT can deliver higher maximum force at a given stroke because of its high stiffness.

- Compactness: Generally, the diameter of magnetostrictive transducers is larger because of the need to have a coil wrapped around the magnetostrictive material. Moreover, sometimes a mechanical pre-stress and a permanent magnet are used to enlarge the amplitude of vibrations. However, because a resonant frequency correlates to the speed of sound in a medium, at the same resonant frequency the slower sound velocity in Terfenol-D benefits from a shorter transducer length.

- Life: Transducer materials lose their property when operated beyond their Curie temperature. After cooling down, PZT material loses its piezoelectric property permanently whereas Terfenol-D is reversible and can be degraded permanently by melting or mechanical shock. The Curie temperature of Terfenol-D is 340-380°C, so it can work at the 200°C high temperature zone freely. Unlike metal based materials, PZT is ceramic, so, without a proper preload it is likely to fail under tension (Abdullah, Shahini & Pak 2009) where high amplitude of vibrations is needed. Terfenol-D is not sensitive to voltage, while higher voltage shortens the life of a PZT transducer. Also, PZT is likely to lose its poling mechanism at a bias voltage of about 1000V/m (PI Ceramics 2011); but there is no de-poling mechanism within Terfenol-D material after a number of vibrations.

- Cost: The cost of PZT is cheaper because it has been widely used for the past half decade (Olabi & Grunwald 2008).
- Power consumption: PZT needs kV and mA where Terfenol-D requires mV and kA for operation. However, Terfenol-D seems to consume more energy for the same frequency (Liu et al. 2006).

In summary, despite the fact that Terfenol-D is suitable for a miniaturised USM system; the potential for developing high strain rate, having short length for resonance, and the ability to function in a wide range of temperature and frequencies, PZT is selected for this project. The material cost is cheaper, and power consumption is less. In addition, because PZT has been used widely for many years, there are more knowledge and information on material properties. Accessible to suppliers, design information, and support tools are plentiful. The most important, using PZT, the displacement can be amplified by connecting to a proper horn where the bias mechanism is a lot simpler than a wrapped coil used for exciting Terfenal-D which this advantage is very suitable for design for miniaturisation.

4.1.1.2 Horn and Backing

Since PZT was chosen as the material for the miniaturised ultrasonic transducer, the choice of material to amplify the displacements was considered in relation to a PZT transducer design. The sandwich piezoelectric transducer, also known as the Langevin composite piezoelectric transducer is widely used for high power purposes (Abdullah, Shahini & Pak 2009; Iula 2009; Xian & Lin 2008). This means that the PZT plates or rings are sandwiched between metal plates or rings.

The amplitude of vibrations depends on the combination of the two end sections. The front end section of the device where the amplitude is amplified is known as the 'horn' and the other section is the 'backing'. An ultrasonic horn is

required to work as a wave transmission line to amplify the displacement of vibrations generated from an ultrasonic transducer.

Unlike choosing a material for the vibration generator where two options can be compared and weighted, each option for the horn and backing needs to be a pair of matched materials in order to benefit the whole system. Generally, the requirement of a USM transducer is to produce high amplitude vibrations so the useful energy form the vibrating PZT is directed forward to the horn. Properties of materials such as acoustic impedance, damping properties, density, and sound velocity of materials play very important roles in the transmission efficiency.

Mechanical impedance is a measure of the motion resistivity of a structure when force-driven. At resonance, the mechanical impedance will be lower so the greatest amplitude is developed. The backing should have high mechanical impedance to ensure the maximum amount of energy is transferred to the other end of the device; along with the horn which should have impedance matching the source of vibrations so the wave energy can be transmitted efficiently.

It is preferred for the horn to have a low damping capacity. Damping is a dynamic property of materials and although damping occurs for all types of vibrations, its presence is undesirable for the horn. Damping results in a conversion of mechanical energy into heat (heating can occur during continuous high amplitude operations). Due to high energy loss, the amplitude of vibrations of a high-damping object tends to become less at a resonance.

High power ultrasonic applications are performed at low frequencies compared with the whole range of periodics in solids. Each part of the ultrasonic assembly contributes its share to the overall resonant frequency. Consequently, the backing lowers the resonant frequency of the whole system. As the frequencies of resonance vary directly with sound velocity and elasticity but

inverse to the density of materials, the sound velocity and elasticity of a backing material should be low and the density high.

Considerations should be given to the use of high fatigue strength material under the condition of continuous oscillations. In USM, the resonant frequency of a horn is affected by the change of temperature mentioned earlier because heat can occur due to energy losses and continuous oscillations. Thus, the properties of horn and backing materials should remain satisfactory within varying temperatures.

Other desirable properties of materials for miniaturisation include, good machinability, light weight, and high strength to weight ratio. These are important for a novel horn design since it is likely to be a complex shape in order to minimise the overall size.

The materials in Table 4.2 have been suggested for use with ultrasonic transducers. Aluminium and magnesium are suitable materials for the horn and the rest for the backing. Apart from material acoustic and mechanical properties, tool steel and aluminium are the most desirable based on cost consideration.

Table 4.2: Materials Used in Transducers (Cremer, Heckl & Petersson 2005; Ensminger & Stulen 2008b; Morgan technical ceramics 2011; Neppiras 1960).

Material	Density (kg/m^3)	Velocity of Sound (m/s)	Impedance (MRayls)*	Fatigue strength (MPa)	Loss Factor
Aluminium	2700	6420	17.3	100	10 (10^{-5})
Brass	8450	4700	40.6	50	1 (10^{-3})
Ductile iron	7100	5900	46.4	42	4 (10^{-4})
Magnesium	1740	5800	10.0	50	
Tool steel	7850	5240	46.0		
Stainless steel	7720	5790	45.7	270	3 (10^{-4})
Titanium	4510	6070	27.3	720	

* MRayls = $kg/(s \cdot m^2) \times 10^6$

4.1.1.3 Tool Bits

In USM, the shapes of tool bits define the shapes of cavities. They are used in conjunction with abrasive particles at the interface with the work-piece. These abrasive particles are normally equal to or harder than the work-piece. As a consequence, tool wear is a general phenomenon. Tool wear is important since it influences both MRR and machining accuracy (Kumar, Khamba & Mohapatra 2009; Zhang, Rentsch & Brinksmeier 2005). As well as MRR, many parameters affect tool wear rates including static loads, types of abrasives and work-piece, abrasive slurry concentrations, amplitude and frequencies of vibrations. Consequently, the choice of material for tool bits essentially depends on machining conditions, complexity of tool geometry, work materials, machining accuracy and surface finishing requirements.

One of the advantages of USM is the possibility for hard objects to be machined by softer materials, for example, cutting ceramics (Mohs hardness=9) by a mild steel tool (Mohs hardness=5) because the work-piece surfaces are acted on by very hard abrasive particles. Both tool and work surfaces are worn during machining but minimising tool wear is desirable. The tool surfaces need to be rigid and stiff in contact with the particles in order to achieve high MRR. In addition, the tool surfaces should resist deformation to gain fine and accurate finished surfaces. Hard and high stiffness materials benefit MRR and surface finish but have a drawback when machining complex cavities because of the difficulty of producing a tool with complex geometry. Materials that have proved suitable for tool-bits include structural steels, stainless steels, tool steels, and high speed steels (Jahanmir, Ramulu & Koshy 1999; Seah, Wong & Lee 1993).

Since the end face and the edge of the form tool have the highest wear rate due to impact, hammering stresses, and cavitations, a two-piece unit with a metal core and cemented carbide outer layer is used for machining simple cavities. By sintering a hard alloy layer onto a tool tip, tool wear rate can be reduced thereby maintaining dimensional accuracy and surface quality. The tool

life will be longer but it is more expensive comparing with steel tools. However, the two-piece unit might face the issue of vibration amplitude reduction caused by energy loss or mismatched mechanical impedance between parts.

In conclusion, the selection of tools must be considered for each individual case. In this project, tool steels were used for machine performance evaluation.

4.1.2 Finite Element Analysis

The piezoelectric effect is the connection between the electrical and mechanical domains of a material as shown in Figure 4.1 (Adriaens, De Koning & Banning 2000). Each of piezoelectric materials exhibits its own electrical and mechanical properties. Ultrasonic systems can be designed using either a relatively simple theoretical approach for a simple system or finite element analysis (FEA) for more complex systems.

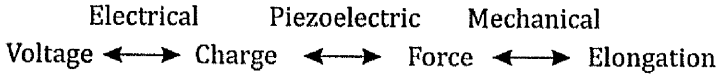

Figure 4.1: Piezoelectric Effect (Adriaens, De Koning & Banning 2000).

FEA is a numerical method used to model, analyse, and predict the performance of physical systems. For a physical system the accuracy of the model depends greatly on the system geometry, material properties, boundary conditions, and external loads. The system is divided into elements. An element contains a single material so the behaviour of the element is controlled by material laws and equations. The element geometry is defined by nodes where loads (or some types of forcing function driving the system) and boundary conditions are applied.

The basics of FEA of structural and piezoelectric elements presented in Section 4.1.2.1 and 4.1.2.2 are summarised from Ensminger & Stulen (2008a). Alternative designs have been analysed using FEA software COMSOL

Multiphysics, and the comparison of different designs is given in Section 4.1.3. 3D elements are used in the simulations throughout the thesis.

4.1.2.1 Structural Analysis

The formation of FEA is based on the principle of virtual work which can be stated in the mathematical form as

$$\iiint_V \delta S^T [c] S dV = \iiint_V \delta \boldsymbol{u}^T [\boldsymbol{F} - \rho \ddot{\boldsymbol{u}} - k\dot{\boldsymbol{u}}] dV + \iint_{S_1} \delta \boldsymbol{u}^{S_1 T} \boldsymbol{T} dS_1 + \delta \boldsymbol{u}^{iT} \boldsymbol{R}_c^i \quad \text{Eq. 4-1}$$

In Eq. 4-1, a bold letter indicates a column vector, a superscript T assigns its transpose, a bracket donates a matrix, and the quantity following δ is a variational quantity. The displacement components, as a function of position in the volume, are donated by vector $\boldsymbol{u}$. The vector of strains is donated by $\boldsymbol{S}$. The vector of stresses the product of the stiffness matrix, $[c]$, and $\boldsymbol{S}$. The left side of Eq. 4-1 relates to the potential energy stored in the volume. The first term on the right side contains the body forces including the bulk force, $\boldsymbol{F}$, acting on the volume, the inertial force from the mass, and the initial damping forces. The second term indicates the traction forces, $\boldsymbol{T}$, acting over surface, S_1. The last term relates to the concentrated loads, $\boldsymbol{R}_C^i$, applied at a single point.

The body is divided into a number of volumes as is the integral representation of Eq. 4-1. The individual volumes are the finite elements. The quantities within an element are defined by interpolation functions operating on the values at the nodes

$$\boldsymbol{u}^m(x, y, z) = [\boldsymbol{H}_u^m(x, y, z)]\boldsymbol{U} \quad \text{Eq. 4-2}$$

where $\boldsymbol{U}$ is the vector of global displacement at the nodes, $\boldsymbol{u}^m(x, y, z)$ refers to the continuous displacements within the m^{th} finite element, $[\boldsymbol{H}_u^m(x, y, z)]$ is the

interpolation matrix to estimate the displacements within the m^{th} element from the displacements at the nodes. The subscript u donates the matrix with the association to displacements.

$$\boldsymbol{S}^m(x,y,z) = [\boldsymbol{B}_u^m(x,y,z)]\boldsymbol{U} \qquad \text{Eq. 4-3}$$

The estimate of strain in the m^{th}element, $\boldsymbol{S}^m(x,y,z)$, can be taken from the nodal displacement $\boldsymbol{U}$ with the transformation matrix $[\boldsymbol{B}_u^m(x,y,z)]$. The displacements and strains are then put back into Eq. 4-1.

$$\delta\boldsymbol{U}^T\sum_m\left[\iint\int_{V^m}[\boldsymbol{B}_u^m]^T[\boldsymbol{c}][\boldsymbol{B}_u^m]\boldsymbol{U}dV^m\right] \qquad \text{Eq. 4-4}$$

$$= \delta\boldsymbol{U}^T\sum_m\left[\int\int_{V^m}[\boldsymbol{H}_u^m]^T\left[\boldsymbol{F}-[\boldsymbol{H}_u^m]\rho\ddot{\boldsymbol{U}}-[\boldsymbol{H}_u^m]\kappa\dot{\boldsymbol{U}}\right]dV^m\right]$$

$$+\delta\boldsymbol{U}^T\sum_m\left[\int\int_{S_1^m}[\boldsymbol{H}_u^m]^T\boldsymbol{T}dS_1^m\right]+\delta\boldsymbol{U}^T\boldsymbol{R}_c^i$$

$\delta\boldsymbol{U}^T$is a full vector of global variation nodal displacements which, in Eq. 4-1, $\delta\boldsymbol{u}^{S_1T}$and $\delta\boldsymbol{u}^{iT}$are the subsets of $\delta\boldsymbol{U}^T$. $\boldsymbol{U},\dot{\boldsymbol{U}}$, and $\ddot{\boldsymbol{U}}$ are the vectors of global displacement, velocity, and acceleration and they have no connection to the individual finite elements. Therefore, Eq. 4-4 can be rewritten as Eq. 4-5, and Eq. 4-6 is the reduced form where the matrices of the consistent mass $[\boldsymbol{M}]$, damping $[\boldsymbol{C}]$, and stiffness $[\boldsymbol{K}]$ are presented in Eq. 4-6 to Eq. 4-8 respectively and $\boldsymbol{R}$ is a vector of the sum of all equivalent loads acting at the nodes.

$$U\sum_m\left[\iint\int_{V^m}[\boldsymbol{B}_u^m]^T[\boldsymbol{c}][\boldsymbol{B}_u^m]dV^m\right]=\sum_m\left[\iint\int_{V^m}[\boldsymbol{H}_u^m]^T\boldsymbol{F}dV^m\right] \quad \text{Eq. 4-5}$$

$$-\ddot{U}\sum_m\left[\iint\int_{V^m}\rho[H_u^m]^T[H_u^m]dV^m\right]$$

$$+\dot{U}\sum_m\left[\iint\int_{V^m}\kappa[H_u^m]^T[H_u^m]dV^m\right]$$

$$+\sum_m\left[\int\int_{S_1^m}[\boldsymbol{H}_u^m]^T\boldsymbol{T}dS_1^m\right]+\boldsymbol{R}_c^i$$

$$[\boldsymbol{M}]\ddot{U}+[\boldsymbol{C}]\dot{U}+[\boldsymbol{K}]U=\boldsymbol{R} \quad \text{Eq. 4-6}$$

$$[\boldsymbol{M}]=\sum_m\left[\iint\int_{V^m}\rho[H_u^m]^T[H_u^m]dV^m\right] \quad \text{Eq. 4-7}$$

$$[\boldsymbol{C}]=\sum_m\left[\iint\int_{V^m}\kappa[H_u^m]^T[H_u^m]dV^m\right] \quad \text{Eq. 4-8}$$

$$[\boldsymbol{K}]=\sum_m\left[\iint\int_{V^m}[\boldsymbol{B}_u^m]^T[\boldsymbol{c}][\boldsymbol{B}_u^m]dV^m\right] \quad \text{Eq. 4-9}$$

$$\boldsymbol{R}=\sum_m\left[\int\int_{S_1^m}[\boldsymbol{H}_u^m]^T\boldsymbol{T}dS_1^m\right]+\sum_m\left[\int\int_{S_1^m}[\boldsymbol{H}_u^m]^T\boldsymbol{T}dS_1^m\right]+\boldsymbol{R}_c^i \quad \text{Eq. 4-10}$$

In the case of the design of power ultrasonic systems, the resonant frequency and modal vibration are of most interest, so there are the

correspondence of eigenvectors and eigenvalues. Thus, the damping is assumed to be light; in other words, $[\boldsymbol{C}]\dot{\boldsymbol{U}}$ can be ignored when the model is used for determining resonant frequencies. A no-load situation of Eq. 4-6 can then be replaced by Eq. 4-11.

$$[\boldsymbol{M}]\ddot{U} + [\boldsymbol{K}]U = 0 \qquad \text{Eq. 4-11}$$

The solution to Eq. 4-11can be assumed to be in the form of

$$\boldsymbol{U} = \phi sin[\omega(t - t_0)] \qquad \text{Eq. 4-12}$$

where ϕ is a vector of order n, t is the time variable, t_0 is a time constant and ω is the radian frequency of vibration of the vector ϕ. Then Eq. 4-11 becomes a generalised eigenproblem

$$[\boldsymbol{K}]\phi = \omega^2[\boldsymbol{M}]\phi \qquad \text{Eq. 4-13}$$

or

$$([\boldsymbol{K}] - \lambda[\boldsymbol{M}])\varphi = 0 \qquad \text{Eq. 4-14}$$

where λ is the eigenvalue, which equals to the radian frequency squared, ω^2, and ϕ is the eigenvector. Eq. 4-14 has a solution only if the characteristic polynomial of $([\boldsymbol{K}] - \lambda[\boldsymbol{M}])$ equals zero as given by

$$|[\boldsymbol{K}] - \lambda[\boldsymbol{M}]| = 0 \qquad \text{Eq. 4-15}$$

The solution is n pairs of eigenvalues and corresponding eigenvectors. The set of solutions can be written

$$[\boldsymbol{K}][\boldsymbol{\Phi}] = [\boldsymbol{M}][\boldsymbol{\Phi}][\boldsymbol{\Omega^2}] \qquad \text{Eq. 4-16}$$

where $[\boldsymbol{\Phi}]$ is a matrix of the eigenvectors ϕ_i and $[\boldsymbol{\Omega^2}]$ is a diagonal matrix listing the corresponding eigenvalues ω_i^2.

The eigenvectors are M-orthonormal, so $[\boldsymbol{\Phi}]^T[\boldsymbol{K}][\boldsymbol{\Phi}] = [\boldsymbol{\Omega^2}]$ and $[\boldsymbol{\Phi}]^T[\boldsymbol{M}][\boldsymbol{\Phi}] = [\boldsymbol{I}]$. The matrix $[\boldsymbol{\Phi}]$ would be in a basic form $\boldsymbol{U} = [\boldsymbol{\Phi}]\boldsymbol{X}$ where $\boldsymbol{X}$ is referred as generalised displacements. Then, Eq. 4-6 becomes

$$\ddot{\boldsymbol{X}} + [\boldsymbol{\Phi}]^T[\boldsymbol{C}][\boldsymbol{\Phi}]\dot{\boldsymbol{X}} + [\boldsymbol{\Omega}]^2\boldsymbol{X} = [\boldsymbol{\Phi}^T]\boldsymbol{R} \qquad \text{Eq. 4-17}$$

At time 0, there can be

$$\boldsymbol{X}_0 = [\boldsymbol{\Phi}]^T[\boldsymbol{M}]U_0 \qquad \text{Eq. 4-18}$$

$$\dot{\boldsymbol{X}}_0 = [\boldsymbol{\Phi}]^T[\boldsymbol{M}]\dot{U}_0 \qquad \text{Eq. 4-19}$$

and the forcing function $r_i(t)$ is

$$r_1(t) = \phi_i^T\boldsymbol{R}(t) \qquad \text{Eq. 4-20}$$

When damping is included, it is assumed that

$$[\boldsymbol{\Phi}]^T[\boldsymbol{C}][\boldsymbol{\Phi}] = 2\omega_i\xi_i\delta_{ij} \qquad \text{Eq. 4-21}$$

where ξ_i is a modal damping parameter and δ_{ij} is the Kronecker delta ($\delta_{ij} = 1$ for $i = j, \delta_{ij} = 0$ for $i \neq j$). From Eq. 4-21, $[\boldsymbol{\Phi}]$ and $[\boldsymbol{C}]$ are assumed to be orthogonal, so Eq. 4-17 can be reduced to n equations of the form

$$\ddot{x}_i + 2\omega_i\xi_i\delta_{ij}\dot{x}_i + \omega_i^2x_i = r_i \qquad \text{Eq. 4-22}$$

The conventional damping model is Rayleigh damping as given in Eq. 4-23 when α and β are constants to be determined.

$$[\boldsymbol{C}] = \alpha[\boldsymbol{M}] + \beta[\boldsymbol{K}] \qquad \text{Eq. 4-23}$$

The response can be calculated using

$$x_i = \frac{1}{\bar{\omega}_i}\int_0^t r_i(\tau)e^{-\xi_i\omega_i(t-\tau)}sin\bar{\omega}_i(t-\tau)d\tau + e^{-\xi_i\omega_i t}(\alpha_i sin\bar{\omega}_i t + \beta_i cos\bar{\omega}_i t) \quad \text{Eq. 4-24}$$

$$\bar{\omega}_i = \omega_i\sqrt{(1-\xi_i^2)} \quad \text{Eq. 4-25}$$

where $\alpha_i$and β_i are constants determined from the initial conditions of $x_i$and $\dot{x}_i$.

4.1.2.2 Piezoelectricity

Electrical and mechanical properties coupled piezoelectric materials follow these equations;

$$T_{ij} = c_{ijkl}^E S_{kl} - e_{mij}E_m \quad \text{Eq. 4-26}$$

$$D_n = e_{nkl}S_{kl} - \varepsilon_{mn}^S E_m \quad \text{Eq. 4-27}$$

Each index in Eq. 4-26 and Eq. 4-27 runs from 1 to 3. S_{kl} is the strain tensor, T_{ij} is the stress tensor, D_n is the electrical displacement, and E_m is the electric field. The coefficients C_{ijkl}^E are the elastic stiffness constants determined under constant field, $\varepsilon_{mn}^S$is the dielectric constants indicated under constant strain. e is the piezoelectric tensor coupling the mechanical and electrical properties of the material. These forms of constructive relations can be written in engineering matrix forms which each index running from 1 to 6;

$$T_\nu = [c_{\nu\mu}^E]S_\mu - [e_{m\nu}]E_m \quad \text{Eq. 4-28}$$

$$D_n = [e_{n\mu}]^T S_\mu - [\varepsilon_{nm}^S]E_m \quad \text{Eq. 4-29}$$

Alternatively, the relations can be reduced to a single matrix equation;

$$\begin{bmatrix}[T]\\ [D]\end{bmatrix} = \begin{bmatrix}[c]_{6\times6} & -[e]_{6\times3}\\ [e]^T_{3\times6} & [\varepsilon]_{3\times3}\end{bmatrix}\begin{bmatrix}[S]\\ [E]\end{bmatrix} \qquad \text{Eq. 4-30}$$

The constituent matrix in Eq. 4-30 can be separated into four matrices including a purely elastic matrix $[c]$, piezoelectric coupling matrix $[e]$ and its transpose, and dielectric matrix $[\varepsilon]$. The subscripts indicate the size of matrix sufficient to define the relation of an elastic material.

Then, the effects of piezoelectricity are added to the principal equation, Eq. 4-1;

$$\iiint_V [\delta \boldsymbol{S}^T[\boldsymbol{c}]\boldsymbol{S} - \delta \boldsymbol{S}^T[\boldsymbol{e}]\boldsymbol{E} - \delta \boldsymbol{E}^T[\boldsymbol{e}]^T\boldsymbol{S} - \delta \boldsymbol{E}^T[\boldsymbol{\varepsilon}]\boldsymbol{E}]\, dV \qquad \text{Eq. 4-31}$$

$$= \iiint_V [\delta \boldsymbol{u}^T F - \rho \delta \boldsymbol{u}^T \ddot{\boldsymbol{u}} - \delta\varphi\sigma]\, dV + \iint_{S_1} \delta \boldsymbol{u}^{S_1 T}\boldsymbol{T} dS_1$$

$$- \iint_{S_2} \delta\varphi\sigma' dS_2 + \delta \boldsymbol{u}^{iT}\boldsymbol{R}_c^i - \delta\varphi \boldsymbol{Q}_c^i$$

where $[\boldsymbol{e}]$ is the the matrix of piezoelectric constants, $\boldsymbol{E}$ is the vector of electric fields, $\boldsymbol{\varphi}$ is the electric potential, $\boldsymbol{\sigma}$ is the body charge, $\boldsymbol{\sigma'}$ is the surface charge, $\boldsymbol{Q}$ is the point charge, $\boldsymbol{F}$ is analogous to the body force, $\boldsymbol{T}$ is the surface traction, and $\boldsymbol{R}_c^i$ is the contracted force.

Similar to the displacement and strains given in Eq. 4-2 and Eq. 4-3, the electrical potential and field are given by;

$$\varphi^m(x,y,z) = \left[\boldsymbol{H}_\varphi^m(x,y,z)\right]\Phi \qquad \text{Eq. 4-32}$$

$$\boldsymbol{E}^m(x,y,z) = -\left[\boldsymbol{B}_\varphi^m(x,y,z)\right]\Phi \qquad \text{Eq. 4-33}$$

As in the case of $[B_u^m]$, the matrix $[B_\varphi^m]$ is calculated by differentiating elements of $[H_\varphi^m]$.

$$[K_{u\varphi}] = \sum_m \left[\iint \int_{V^m} [B_u^m]^T [e][B_\varphi^m] dV^m \right] \quad \text{Eq. 4-34}$$

$$[K_{\varphi u}] = \sum_m \left[\iint \int_{V^m} [B_\varphi^m]^T [e][B_u^m] dV^m \right] \quad \text{Eq. 4-35}$$

$$[K_{\varphi\varphi}] = -\sum_m \left[\iint \int_{V^m} [B_\varphi^m]^T [\varepsilon][B_\varphi^m] dV^m \right] \quad \text{Eq. 4-36}$$

$$\boldsymbol{Q} = \sum_m \left[\iint \int_{V^m} [\boldsymbol{H}_\varphi^m] \sigma dV^m \right] + \sum_m \left[\int \int_{S_2^m} [\boldsymbol{H}_\varphi^m]^T \sigma' dS_2^m \right] + \boldsymbol{Q}_c^i \quad \text{Eq. 4-37}$$

Then, these definitions are substituted into Eq. 4-31;

$$\delta \boldsymbol{U}^T \left[[\boldsymbol{M}]\ddot{\boldsymbol{U}} + [\boldsymbol{C}]\dot{\boldsymbol{U}} + [\boldsymbol{K}_{uu}]\boldsymbol{U} + [\boldsymbol{K}_{u\varphi}]\boldsymbol{\Phi} - \boldsymbol{R} \right] \quad \text{Eq. 4-38}$$

$$+ \delta \boldsymbol{\Phi}^T \left[[\boldsymbol{K}_{\varphi u}]\boldsymbol{U} + [\boldsymbol{K}_{\varphi u\varphi}]\boldsymbol{\Phi} - \boldsymbol{Q} \right] = 0$$

and it can be reduced into;

$$\begin{bmatrix} [\boldsymbol{M}] & 0 \\ 0 & 0 \end{bmatrix} \begin{bmatrix} \ddot{\boldsymbol{U}} \\ \ddot{\boldsymbol{\Phi}} \end{bmatrix} + \begin{bmatrix} [\boldsymbol{C}] & 0 \\ 0 & 0 \end{bmatrix} \begin{bmatrix} \dot{\boldsymbol{U}} \\ \dot{\boldsymbol{\Phi}} \end{bmatrix} + \begin{bmatrix} [\boldsymbol{K}_{uu}] & [\boldsymbol{K}_{u\varphi}] \\ [\boldsymbol{K}_{\varphi u}] & [\boldsymbol{K}_{\varphi\varphi}] \end{bmatrix} \begin{bmatrix} \boldsymbol{U} \\ \boldsymbol{\Phi} \end{bmatrix} = \begin{bmatrix} \boldsymbol{R} \\ \boldsymbol{Q} \end{bmatrix} \quad \text{Eq. 4-39}$$

The matrix $[\boldsymbol{K}_{uu}]$ is the same matrix $[\boldsymbol{K}]$ as defined in Eq. 4-9, and the subscript uu donates the elastic stiffness matrix and is consistent with the

arrangement used with the other matrices. The matrices $[\boldsymbol{K}_{u\varphi}]$ and $[\boldsymbol{K}_{\varphi u}]$ are the piezoelectric stiffness matrices, and $[\boldsymbol{K}_{\varphi\varphi}]$ is the dielectric stiffness matrix.

4.1.3 Idea Generation of Prototype-I

The main concepts of miniaturising a USM system include minimising the size, maximising the amplitude of vibrations and optimising the frequency of working resonance to 18 kHz – 25 kHz which is suitable for cutting hard and brittle materials. The conventional horn designs are shown in Figure 2.2. Their cross sectional areas are reduced from the driven end to the tool end. The deformations at points along the length of the USM device will be accompanied by a stress, σ; and with the reducing cross section the displacement amplitude can be magnified from one end of the device to the other.

$$\sigma_x = E\frac{\partial \xi}{\partial x} \qquad \text{Eq. 4-40}$$

The basic horn equation in terms of particle displacement, ξ, is as follows:

$$\frac{1}{c^2}\frac{\partial^2 \xi}{\partial t^2} - \frac{1}{S}\frac{\partial S}{\partial x}\frac{\partial \xi}{\partial x} - \frac{\partial^2 \xi}{\partial x^2} = 0 \qquad \text{Eq. 4-41}$$

In terms of particle velocity, v, and implying harmonic motion, the following equation is used:

$$\frac{\partial^2 v}{\partial x^2} + \frac{1}{S}\frac{\partial S}{\partial x}\frac{\partial v}{\partial x} + \frac{\omega^2}{c^2}v = 0 \qquad \text{Eq. 4-42}$$

where x is the distance from one end of the horn to the reference position; S is the cross-sectional area of the horn at distance x; ω is the angular frequency $(= 2\pi f)$; f is the frequency of vibrations; and c is the velocity of sound in the medium of the horn.

Comparison between conventional designs shows that the stepped horn has the highest amplitude gain when the cross section is reduced at the nodal position (or the quarter wavelength position).

In order to maximise the amplitude of vibrations while the size of the system is minimised, the ideas of several designs discussed in Section 2.3 were considered.

The overall length of a horn can be reduced and can maintain acoustic length by folding or flipping the horn (Chang et al. 2005; Sherrit et al. 2004; Sherrit 2004). The folded horn could shorten the horn length by a half but the horn tip displacement was found to be a factor of ten below a standard horn design. These researchers claimed that this was because their prototype did not have a one-piece horn, but was made of two parts connected by screw threads.

The strain displacement can be increased whilst maintaining the overall length by introducing slits in the horn construction (Cardoni, Harkness & Lucas 2010; Iula 2009). Cardoni, Harkness and Lucas (2010) wanted to increase the displacement amplitude in order to raise material cutting rates. They made use of diagonal silts for combining longitudinal and torsional modal vibrations. The diagonal slit idea functioned effectively for drilling a round hole. However, the associated torsional vibrations causes misshapes and size inaccuracy (Jahanmir, Ramulu & Koshy 1999) when machining a rectangular or more complicated cavity.

In summary, the reduction of the cross sectional area and introduction of slitting in the horn increases amplitude of vibration because both can reduce the stiffness of the body. As the definition of stiffness is the capacity of a mechanical system to sustain loads without excessive changes of its geometry, so any horns that lower stiffness should produce higher amplitudes when other conditions are similar. However, the strength and the available force generating from the

horn should always be taken into account when designing a horn for ultrasonic machining purpose.

In order to determine the amplitude of vibration at a resonance, viscous damping ($\alpha = 0$ and $\beta > 0$, where α is mass damping and β is stiffness damping) is used for modelling since the mechanism is commonly used in vibration analysis when the system is operated in a fluid medium such as air, gas, water, and oil (Rao 2004). The stiffness damping of a material is frequency dependent which has been estimated from a mechanical loss factor of the material, η, and the exciting frequency, f, as the following equation (Bhalla & Soh 2004).

$$\beta = \frac{\eta}{2\pi f} \qquad \text{Eq. 4-43}$$

Several designs were modelled (after ascertaining that it was possible to manufacture their shapes) to study their dynamic characteristics for a range of frequencies. The designs and their resonant frequencies obtained from FEA are presented in Table 4.3. The pictures of designs 1A to 1F are presented as a quarter symmetry sector of the horns. All designs have an identical total length and smallest cross sectional area. The length was equal to the stepped horn presented by Iula et al. (2005) so the modelling of stepped horn 1A was validated, and the rest can be compared at an identical length. Then the dynamic characteristics are influenced by the shapes of cavities in the horns. Letters L, F, and T represent longitudinal, flexural, and torsional mode of vibrations, respectively.

Table 4.3: Comparison of Horns with an Identical Length.

No.1A Stepped	No.1B Conical	No.1C Hollow with aligned holes	No.1D Hollow with unaligned holes	No.1E Beam	No.1F Beam with side supports
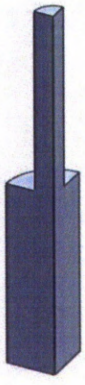		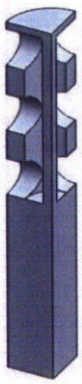		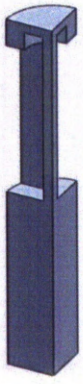	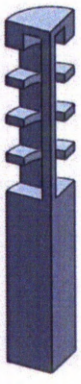
Resonant Frequencies in the range of 0 – 35000 Hz					
4594 (F)	5334 (F)	5059 (F)	5091 (F)	3317 (F)	4303 (F)
8519 (F)	11477 (F)	11329 (F)	11379 (F)	5882(T)	8542 (T)
19519(F)	20796 (F)	16014 (T)	16127 (T)	8398 (F)	9241 (F)
20523 (T)	21884 (T)	21268 (F)	21313 (F)	16005 (F)	19130 (F)
28907 (F)	30883 (L)	25841 (T)	26156 (T)	16792 (F)	20467 (T)
31333 (L)	32452 (F)	27053 (L)	27139 (L)	20105 (F)	22737 (F)
33046 (T)		31969 (F)	32258 (F)	20235 (T)	27443 (L)
				22298 (F)	31143 (T)
				23485 (F)	
				27327 (T)	
				28522 (L)	
				34232 (F)	

Conventional horns represented by, Design 1A and Design 1B were taken as references. Design 1C and Design 1D are alike but have holes with different alignment. The aim of having hole-like cavities is to control the displacement of the horn only in the axial direction when it is resonating in longitudinal mode. The modelling results showed the alignment of the holes had no effect on resonant frequencies. Design 1E is similar to the work of Iula (2009). Each beam of Design 1E seems to resonate individually apart from the whole system as the frequencies of those individual resonances are highlighted in bolded font in Table 4.3. The existence of too many resonant frequencies next to each other is

not desirable because a complex mode of vibration may appear. Thus, it was demonstrated that a number of resonant frequencies can be reduced by linking each beam together as shown in Design 1F.

The simulation results for the initial horn designs concluded that cavities in a horn reduce resonant frequencies compared to conventional horn designs. When the length and smallest cross sectional area are fixed, different horns tend to resonate longitudinally at the equivalent frequency. Long and thin sections in a horn increase the number of resonant frequencies of the system. To minimise these numbers, a horn should have less cavities and avoid thin and long geometries. Otherwise, it is preferable to have a design linking those sections together to ensure that they vibrate as a unit.

As a result of the literature survey, and the modelling work described above, a novel horn design is purposed (Figure 4.2). The horn is tapered and folded backwards and forwards into the centre in order to reduce the total length significantly. Four holes are located in the outer wall of the horn for ease of manufacturing. Accordingly, the total length can be shortened significantly whilst still amplifying the amplitude effectively. The circular cavity was chosen because it does not cause individual resonance and is easier for manufacturing.

The transducer and horn (with features mentioned above) assembly was modelled and simulated. The resonant frequency was expected to be 18.5 kHz when a tool bit is attached. The vibration amplitude is hard to predict with the limitations of FEA because of the complexity of real geometries and losses in joints and microstructure of materials. Hence, the vibration amplitude in the range of ±100 Hz from the resonant frequency was simulated and the resolution was set at 10 Hz to reduce the computer processing time. At the tool bit end the amplitude in the axial direction was expected to be about 40 μm as this value is the one-third of maximum amplitude at resonance (Figure 4.3).

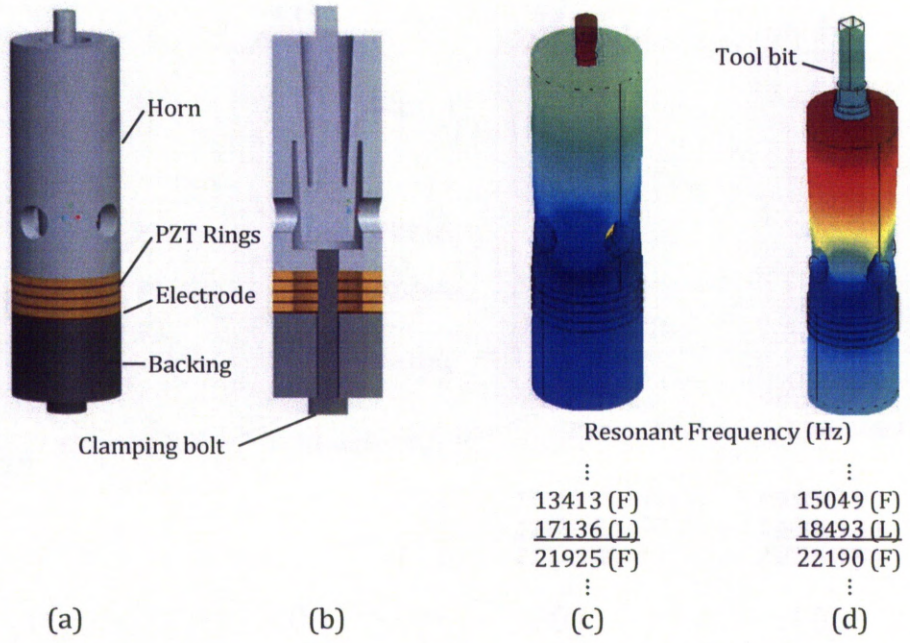

Figure 4.2: Prototype-I. (a) 3D Model; (b) Half section; (c) and (d) First Longitudinal Vibration Mode without and with Tool Bit.

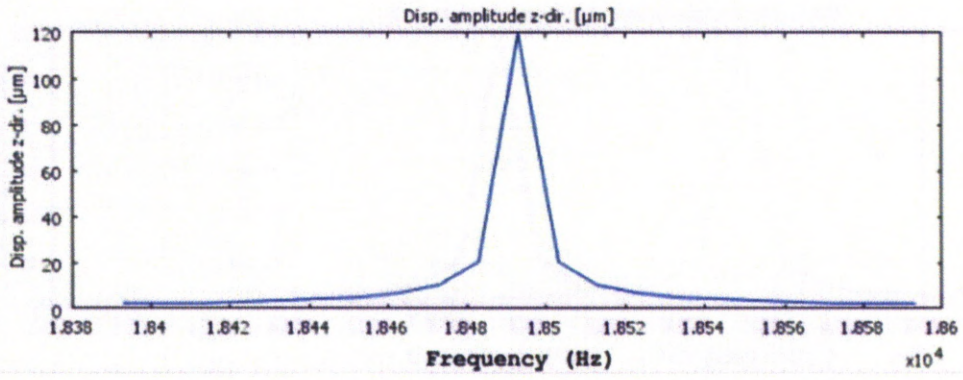

Figure 4.3: The Displacement Amplitude Computed at the End of the Tool Bit as a Function of Frequency.

4.1.4 Design Optimisation Techniques

Statistical analysis methods are effective means for dealing with complex problems. When a simple system is studied, such as a sandwich transducer combining a conical horn or stepped horn, the equations of the relationships between the cross-sectional areas of each component and the system resonant frequency, amplitude, or other dynamic characteristics can be constructed readily using statistical analysis methods. Optimisation of the objective function can be achieved mathematically. On the other hand, when the system is more complex, mathematic modelling and solving is more difficult.

4.1.4.1 Screening Parameters by Factorial Design

The concept of a novel USM transducer assembly was determined to be a sandwich type. The shape of the assembly and material for each component has already been discussed. At this stage, their dimensions will be determined to maximise the performance of the USM system. A statistical analysis method, Factorial Design, has been applied to solve the problem by screening only important parameters from a number of factors. Three methods of factorial designs as listed below were used to determine whether important parts of the components significantly anticipate the overall system performance. The analysis tools included ANOVA, main effects plots, interaction plots, and a normal probability plot which were already explained in Section 2.6.

- Full Factorial Design (FFD): This allows the investigation of the effects of factors under consideration, as well as the interactions among the factors. The number of experiments may be large because all possible combinations have to be considered.
- Fractional Factorial Design: Only a fraction of all possible combinations of factors of interest are tested, so the number of runs required is less than FFD. These types of designs are used when five or more factors are

under investigation, cost of experiments is high, or the study is time-consuming.

- Taguchi Designs: These methods, developed by a Japanese engineer, Genichi Taguchi, can be classified as fractional factorial designs using two, three, and mixed levels designs.

4.1.4.2 Optimising Key Parameters by Response Surface Analysis Method

Once the important parameters affecting a response have been screened from inactive parameters by factorial designs; a more complicated design, the response surface designs, can be used for establishing desirable response values and operating conditions. Response functions (Eq. 2-13) of outputs of interest such as resonant frequency and amplitude of vibrations can be modelled. Then the optimum solution under constraints can be determined.

To form an effective response surface plot, Central Composite Designs (CCD) was used. CCD is one of the most popular RSM designs due to the following properties (Lawson & Erjavec 2001; Myers, Montgomery & Anderson-Cook 2009);

- From Figure 4.4, first, the design allows estimation of all main effects and interactions. Then, axial points combined with the centre point are added to this design to estimate linear effects equivalent to one-at-a-time experiments for estimating curvature effects.
- The design allows a reasonable amount of information for fitting a surface while not involving a large number of design points.
- It is flexible. The axial points can be adjusted to enable investigation into different experimental regions of interest.

Figure 4.4: Central Composite Design.

4.1.5 Optimising Prototype-I

A stack of 4 layers of PZT rings was used for the prototype. The rings had an outer diameter (OD) of 25 mm, an inner diameter (ID) of 16 mm, and a thickness of 2 mm. Also, it was decided to construct the backing out of steel, and the horn out of aluminium. The development of the particular features of the backing and horn is explained in Section 4.1.3. Next, optimisation of the geometry was made in order to confirm the most favourable shape.

4.1.5.1 Factorial Analysis to Clarify Effects of Holes and Confirm Critical Parameters

The dimensions listed in Table 4.4 were considered as the control factors to be analysed. Each dimension of interest was levelled for applying fractional factorial design to establish which dimensions have a significant effect on frequencies and vibration amplitude. FFD is possible in this case because there are only a few control factors. All eight combinations of the factors were modelled and simulated.

The summary of the computing results is shown in Table 4.5. ANOVA was applied and the P-value from the statistical analysis software (Table 4.6) shows the key factors. These are the horn length, backing length, and the size and shape of the holes on the horn, which affect the amplitude of vibration. Figure 4.5 shows that the mean responses of the main factors and some interactions lay away from the normal trend line as reflected in the ANOVA table. In addition,

Figure 4.6 illustrates that the main factors also affect the resonant frequencies of the systems.

Table 4.4: Factors Affecting Transducer Performances Focused on Holes Effects.

Factor	Level		Unit
A: Backing length	20	30	mm
B: Horn length	45	55	mm
C: Holes	0, Without holes	1, With holes	-

Table 4.5: Simulation Results Using FFD (3 factors with 2 levels, $2^3 = 8$ combinations)

Factor			Resonant Frequency (Hz)	Amplitude at off Resonance	
				-100 Hz (μm)	+100 Hz (μm)
A	B	C			
40	55	1	17565	186	178
20	45	0	24276	140	138
40	55	0	19120	158	155
20	55	1	18865	214	206
40	45	0	22089	125	122
20	55	0	21003	175	168
40	45	1	20117	143	138
20	45	1	21706	165	161

Table 4.6: Considering Effects of Holes: ANOVA for Displacement Amplitude at the Tool Bit End.

Analysis of Variance for Disp at Fr+/-0.1kHz

Source	DF	Seq SS	Adj SS	Adj MS	F	P
Main Effects	3	10325.5	10325.5	3441.83	229.46	0.000
2-Way Interactions	3	238.5	238.5	79.50	5.30	0.026
3-Way Interactions	1	9.0	9.0	9.00	0.60	0.461
Residual Error	8	120.0	120.0	15.00		
Pure Error	8	120.0	120.0	15.00		
Total	15	10693.0				

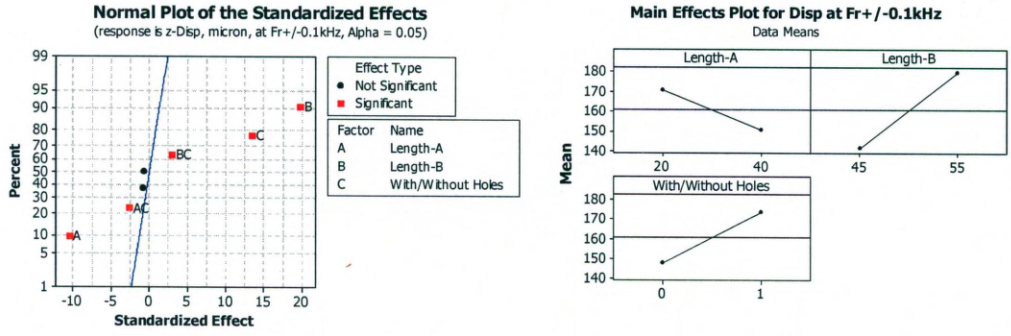

(a) Normal Plot (b) Main Factors Effects

Figure 4.5: Considering Effects of Holes: The Plots of Effect A, B, and C on the Displacement Amplitude at the Tool Bit End.

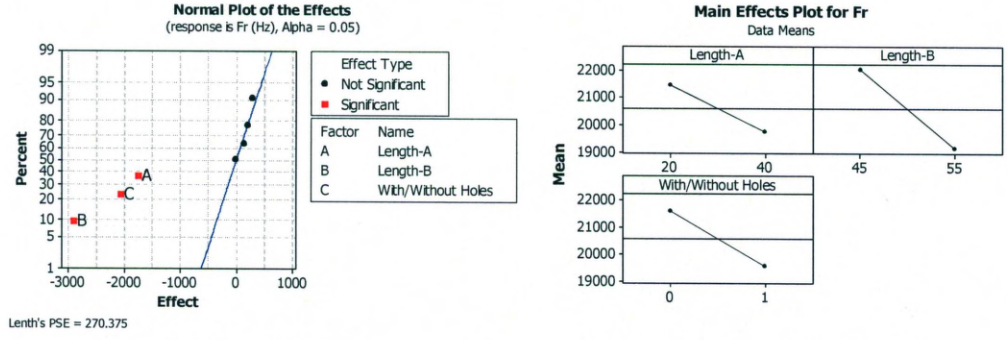

(a) Normal plot (b) Main factors effects

Figure 4.6: Considering Effects of Holes: The Plots of Effect A, B, and C on Resonant Frequency.

From the analysis results, there are some conflicting requirements when considering Figure 4.5 (b) and Figure 4.6 (b). In order to maximise the vibration amplitude the backing length should be short, the horn length should be long and there should be holes on the horn. However, for the system to resonate around 18 kHz – 25 kHz, the horn length should be kept short without holes.

4.1.5.2 *Factorial Analysis to Define Critical Parameters and Effects of Various Holes Types*

Based on the results obtained in the previous section that the holes and their combinations with the backing or horn length affect the performance of the transducer significantly, next, different sizes and types of holes were considered. Three main factors of interest and their levels are presented in Table 4.7. The examples of transducer models are demonstrated in Figure 4.7. Using the full factorial analysis method, 27 combinations of parameters have been modelled and simulated. The statistical analysis results are shown in Figure 4.8.

Table 4.7: Factors Affecting Transducer Performances Focused on Types of Holes.

Factor	Level			Unit
A: Backing length	20	30	40	mm
B: Horn length	45	55	65	mm
C: Holes	2 mm, Single row	2 mm, Multi rows	8 mm, Single row	-

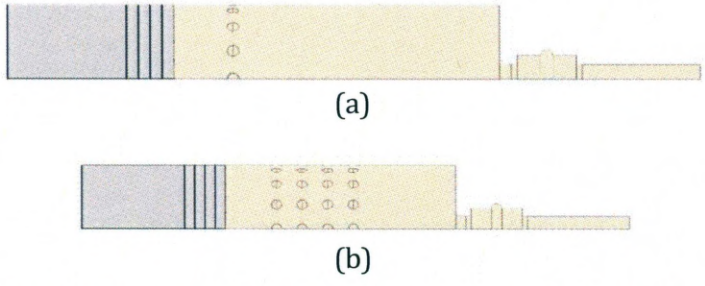

Figure 4.7: Models for Considering Effects of Types of Holes. (a) Horn with Single Row; (b) Horn with Multi Rows.

Analysis of Variance for Disp. at Fr+/-0.1kHz

Source	DF	Seq SS	Adj SS	Adj MS	F	P
Length-A	2	4148.9	4148.9	2074.5	91.15	0.000
Length-B	2	21432.9	21432.9	10716.5	470.86	0.000
Holes	2	3681.8	3681.8	1840.9	80.89	0.000
Length-A*Length-B	4	22.3	22.3	5.6	0.24	0.910
Length-A*Holes	4	109.4	109.4	27.4	1.20	0.333
Length-B*Holes	4	137.4	137.4	34.4	1.51	0.227
Length-A*Length-B*Holes	8	28.4	28.4	3.5	0.16	0.995
Error	27	614.5	614.5	22.8		
Total	53	30175.6				

(a)

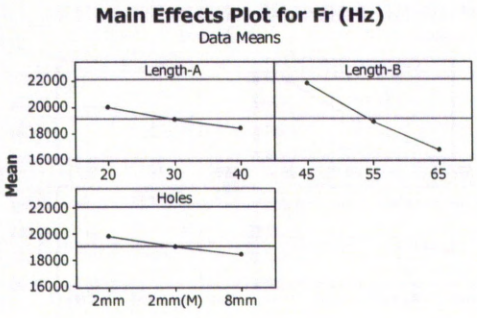

(b)

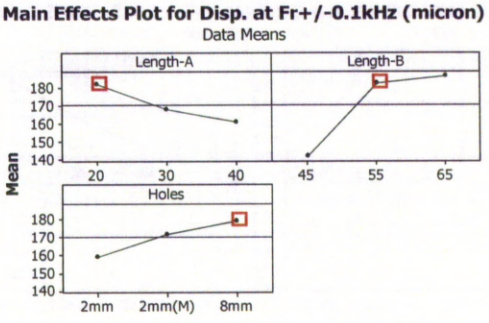

(c)

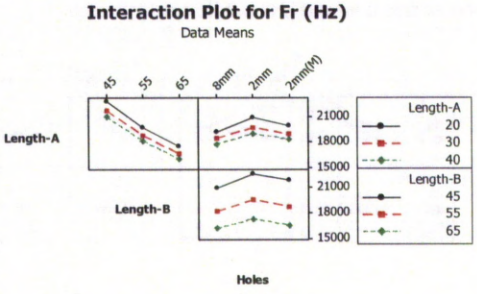

(d)

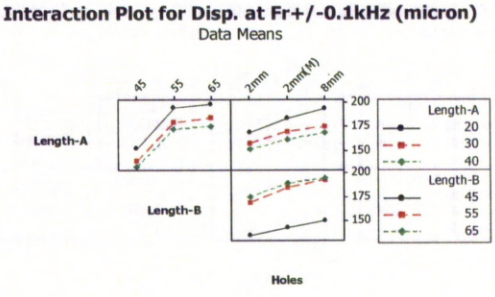

(e)

Figure 4.8: Statistical Analysis of Holes Types. (a) ANOVA Table; (b) Main Effects on Resonant Frequency and (c) on Amplitude; (d) Interaction Effects on Resonant Frequency and (e) on Amplitude.

The ANOVA table in Figure 4.8 (a) agrees with the analysis in Section 4.1.5.1 which confirms the significant effects of the backing length, horn length,

and types of holes on the transducer. However, from Figure 4.8 (b) to Figure 4.8 (e) on the effects of hole types on transducer performance, the level of amplitude is not much different whether it is generated by the system with an 8 mm single-row or 2 mm multi-rows holes. For horn length of 55 mm and 65 mm, the displacement amplitude is similar but the resonant frequency drops to nearly 16 kHz when using a horn of 65 mm length. Consequently, based on manufacturing and material considerations, a transducer with a backing length of 20 mm and a horn length of 55 mm with 8-mm single-row holes was chosen as the centre point for response surface analysis.

4.1.5.3 Response Surface Analysis to Optimise Parameters for Prototype-I

The three key factors including the backing length, horn length, and hole diameter were used for as the centre point for response surface analysis (RSA) and optimisation. The levels of each factor were specified following RSA design guidance which indicated that the response would express a maxima or minima within the study variable ranges. The simulation plan is shown in Table 4.8. The response surface plots obtained by simulating 20 combinations are presented in Figure 4.9 (a) and Figure 4.9 (b) which show the effects of the key parameters on frequencies of resonance. There are some interactions between the factors. From Figure 4.10 (a), when the length of the horn is kept constant and the holes were enlarged, the amplitude of vibrations increases. However, Figure 4.10 (b) shows that the resonant frequency will drop to an audible range at some combinations, and will be higher if the holes are made smaller and the horn is shorter.

Table 4.8: Factors Levelled Following RSA Guidance.

Factor	Level					Unit
A: Backing length	16.6	18	20	22	23.4	mm
B: Horn length	51.6	53	55	57	58.4	mm
C: Holes diameter	6.3	7	8	9	9.7	mm

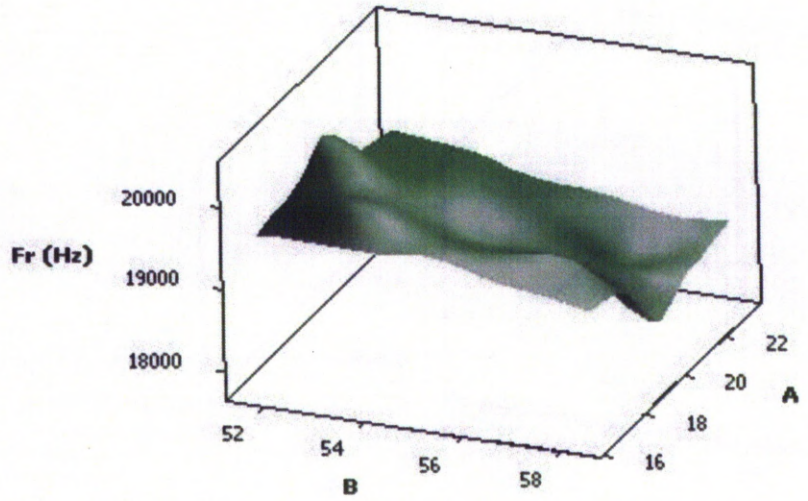

(a)

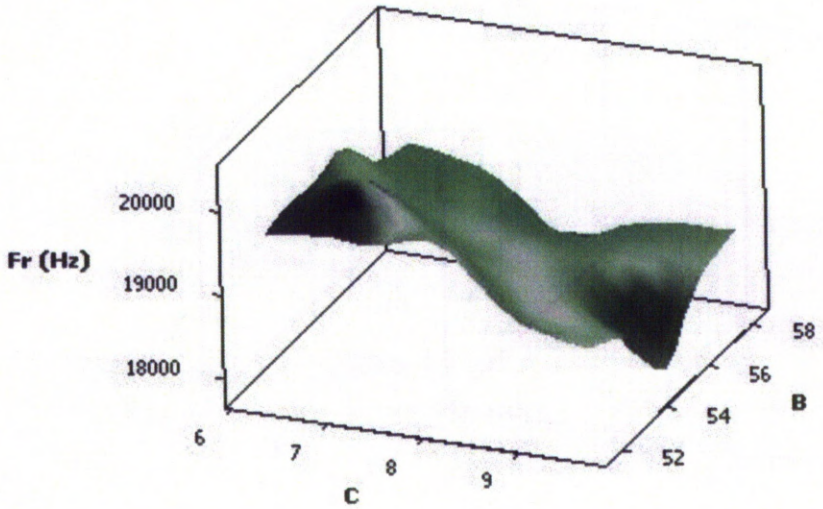

(b)

Figure 4.9: RSA Results. Surface Plot of Frequency Responding to (a) Factors A & B, and (b) Factors B & C.

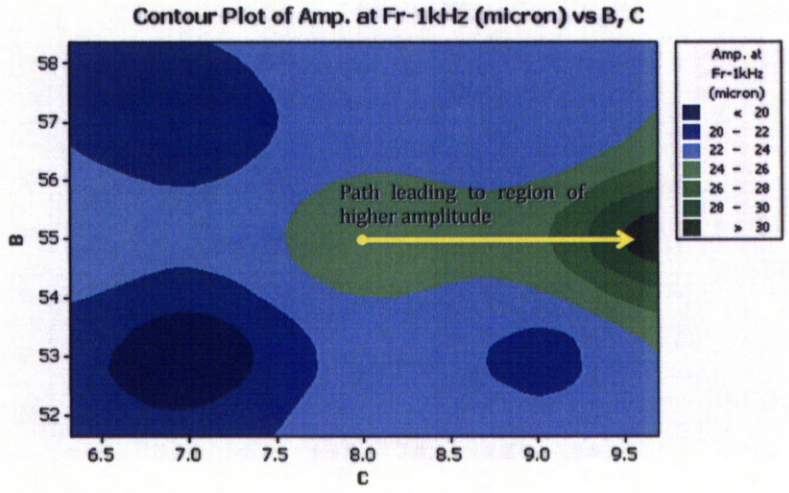

(a)

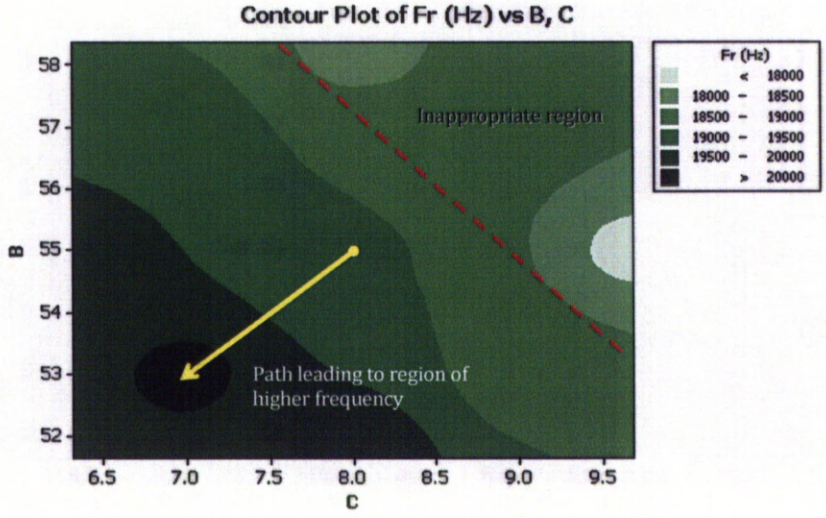

(b)

Figure 4.10: RSA Results. Contour Plot of (a) Amplitude and (b) Resonant Frequency Responding to Factors B & C.

Because there are considerable disagreements over the effects of the factors on the frequencies and amplitudes, the response optimiser in the statistical software has been applied to find the optimum point on the response surfaces for maximising displacement amplitude within the range of 18 kHz – 25

kHz of resonant frequency. The optimisation results are shown in Figure 4.11 (crossed sections of the response surfaces) which the size of the optimised backing, horn, and holes should be 19.5, 54.8, and 8.6 mm, respectively. As the new dimensions obtained by the RSA are very similar to the FFD, the simulating outputs from both methods are comparable. A backing length 20 mm, horn height 55 mm, and holes size 8 mm was chosen as the final design of Prototype-I for ease of manufacturing.

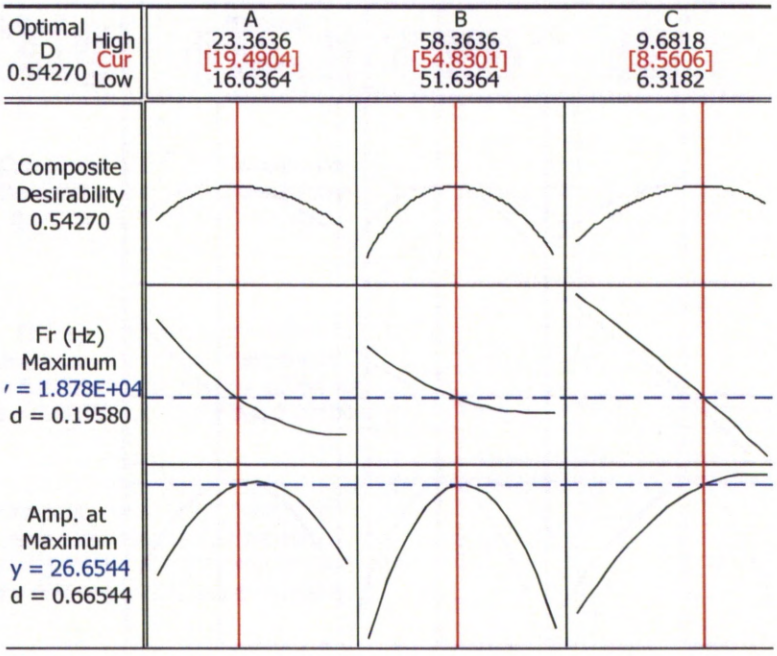

Figure 4.11: Optimisation Using RSA for Prototype-I.

4.2 Electrical Components and Abrasive Slurry Circulation System

4.2.1 Signal Generator and Power Amplifier Controlling the Miniaturised USM System

Normally the signal for driving a transducer is generated at low level of power by a signal generator, and then it is amplified to a desired level of voltage by a power amplifier. For the case of driving a piezoelectric transducer, the signal needs to be increased to hundreds of volts. An example of the circuit is presented in Figure 4.12. The size of electronics and electrical assembly is not small as it consists of a number of parts. Generally, a signal generator is not so big for generating frequencies in the range from 18 kHz to 25 kHz for the purpose of ultrasonic machining. While it is possible to produce a palm-size generator, it is not feasible to produce a miniaturised transformer because of its metal core and copper coils constructions.

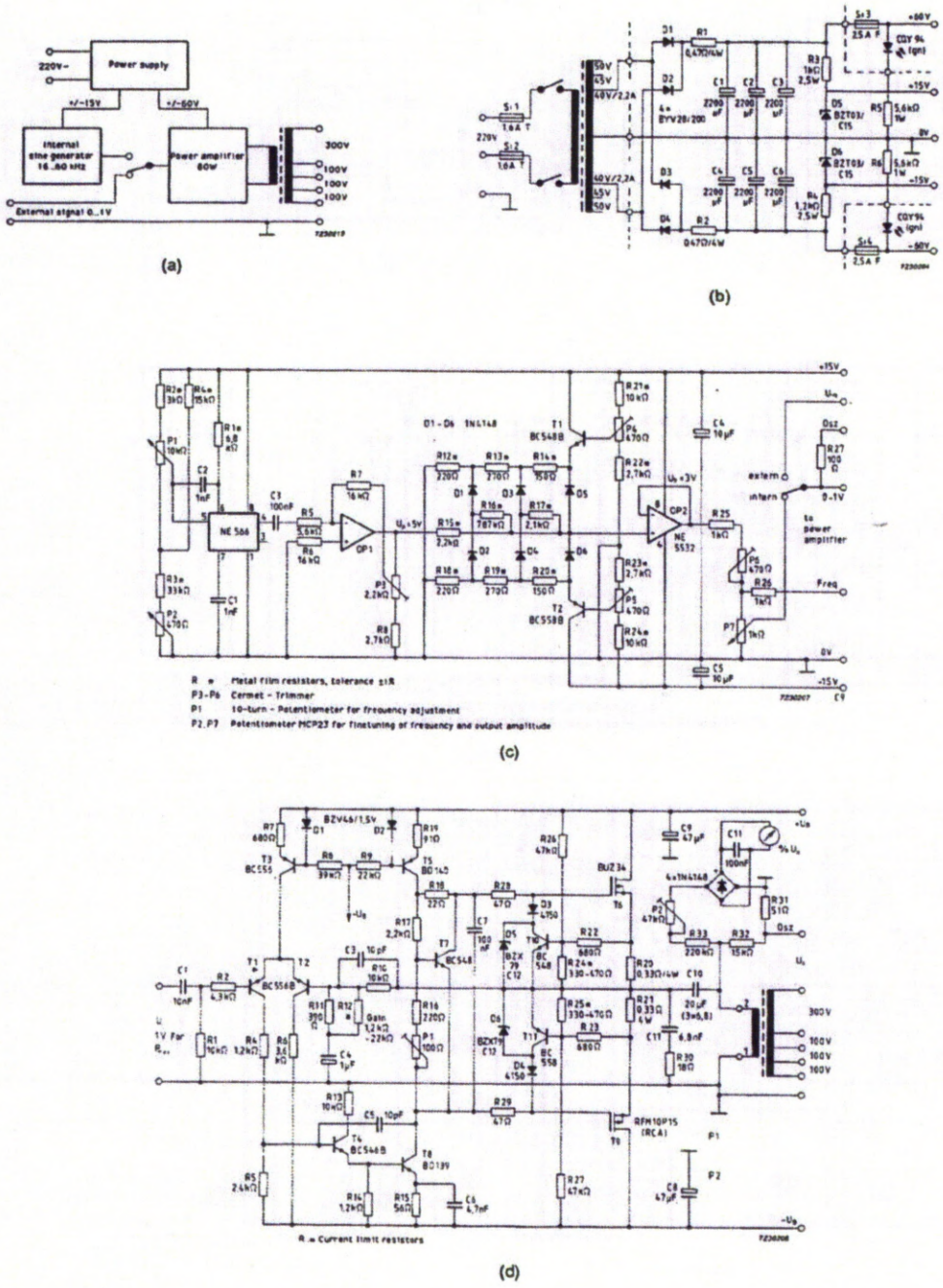

Figure 4.12: Example of Drive Circuit for High-Intensity Transducer; (a) Block Diagram, (b) Power Supply, (c) Sinewave Generator, and (d) Power Stage with Output Transformer. Diagrams from Morgan technical ceramics (2011).

Based on the modern technology, the use of a piezoelectric transformer as a high voltage transformer could be a promising alternative. Currently, the transformer power capability is up to 100 watts with 4 amps and expected to reach 200 watts (Carazo 2004). It also has a resonant frequency of 30 kHz to 300 kHz (Fuji & Co. 2012) which is not so far from the appropriate range of frequency for ultrasonic machining. The size of Fuji & Co's transformer is small, i.e. 50 mm long, 13 mm wide and 2.7mm thick for a resonant frequency of 33 kHz and even smaller for higher resonant frequencies. The variety of design, construction, and poling (Horsley, Foster & Stone 2007) gives room for improvement for piezoelectric transformers to a wider range of applications. However, through an interview with Carazo in 2010, it was noted that the piezoelectric transformers for such high power level like USM application were not yet commercialised since they were developed by and under the rights of U.S. Navy and Agents (Carazo 2010).

Without the electrical components, the performance test of a miniaturised USM system prototype could not be completed because they are the prime driver of a USM system. Common test equipments in the Laboratory were used in this investigation. A function generator was available but a new power amplifier suitable for driving a piezoelectric transducer was built in house. PB58A, a programmable power booster amplifier from Cirrus Logic, Inc. was selected as the main element for amplifying the power. It was able to boost power supplies up to 280 Vp-p in high power bandwidth. Moreover, the cost and size of around 25-mm wide, 7-mm thick, 45-mm long of the chip was very attractive for the project. Unfortunately, a large heat-sink was necessary for keeping the temperature of the running chip under the limit. Therefore, the power amplifier box was massive compared with the booster chip itself.

4.2.2 Abrasive Slurry Circulation System

The slurry, which is a mixture between abrasive particles and liquid, is normally pumped (Figure 4.13 (a)) or poured to the cutting area (Guzzo, Raslan

& De Mello 2003; Komaraiah & Narasimha Reddy 1993; Singh & Khamba 2006; Thoe, Aspinwall & Wise 1998). In feed method as shown in Figure 4.13 (b) is possible (Thoe, Aspinwall & Wise 1998) but the position of the tube is crucial since it affects vibration characteristics and causes an imprint on the machined surface. The abrasive can be any material with hardness higher than the work material. The common abrasive materials include aluminium oxide (Al_2O_3), silicon carbide (SiC), and boron carbide (B_4C). The common types of liquid are water and oil. Using water is more preferable since it has high fluidity, high thermal conductivity, and there is plenty.

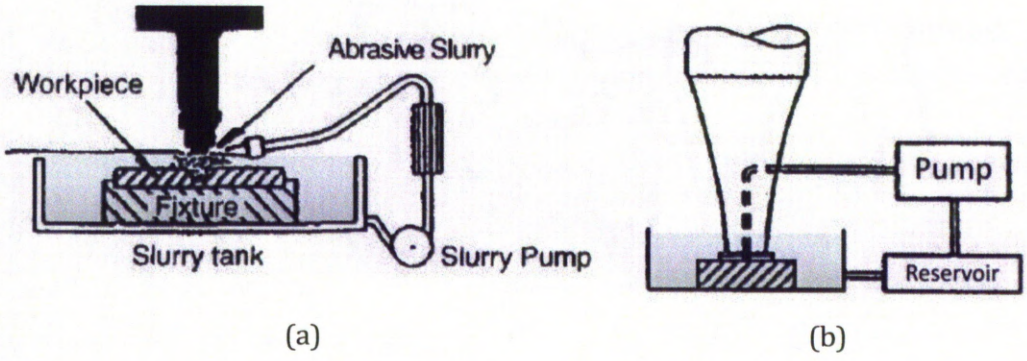

Figure 4.13: Abrasive Slurry (a) Pumping and (b) In-Feeding to a Cutting Zone. Pictures from Thoe, Aspinwall and Wise (1998).

It was decided in Section 3.2 that the abrasive slurry feeding system had to be independent from the vibration generating unit, so the system as shown in Figure 4.13 (b) was impractical because of its complex geometry. Using the amount of slurry filling the entire chamber with the slurry is wasteful of materials for micro/meso scale machining. Moreover, pumping abrasive slurry through the pump will cause massive wear in the pumping system. Consequently, it was decided to pour the slurry into the cutting zone because of the small scale of operation and small amount of material removal.

4.3 Dynamic Characteristics Based on Experiments

FEA has been recognised as an effective method of characterising the behaviour of vibrating structures (Abdullah, Shahini & Pak 2009; Chang et al. 2005; Iula 2009; Lerch 1990; Seah, Wong & Lee 1993; Xian & Lin 2008). Nevertheless, experimental validation is still required to evaluate the accuracy of computer simulation modelling. Determining the modal characteristics of a proposed prototype of an ultrasonic transducer and horn combination was performed in order to improve the design. The modal parameters include natural frequencies and mode shapes of vibrations. The modal data will present the true characteristics of the systems and can assist the design studies. By modal parameter analysis, the weak areas of the designs can be indentified and improved.

The proposed prototypes of the transducer-horn assembly were validated by the following procedure (Figure 4.14);

- Determination of the frequencies of resonances.
- Measurement of the vibration amplitude at the expected frequency and its mode shape.
- Verification of the experimental and computer simulation results.
- Feedback of the outputs for model and design improvement.

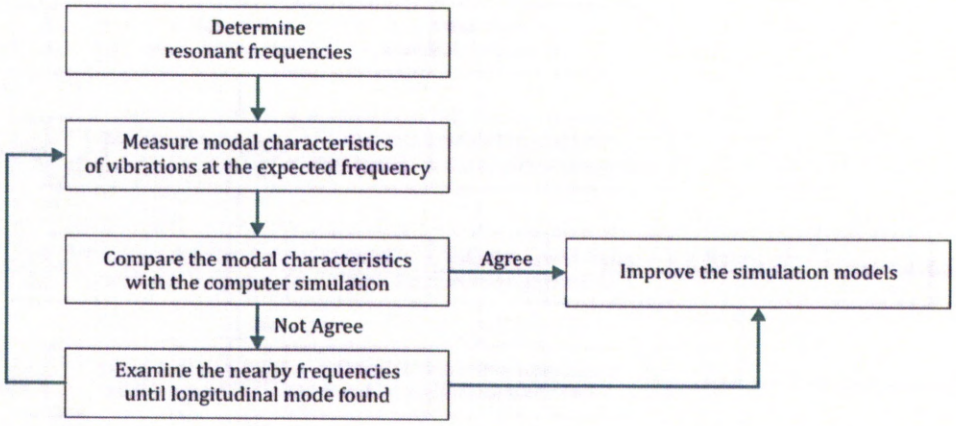

Figure 4.14: The Procedure of Experimental Set-Up for Validation of a Transducer-Horn Assembly.

4.3.1 Experimental Set-Up

Resonances of any structure can be determined by various methods. In the present case, an electrical signal induces mechanical displacement in a piezoelectric transducer-horn assembly which expands when a positive voltage is applied and contracts under a negative voltage. By applying alternating signals, the assembly will oscillate and when the signals are driving at frequencies approximately equal to the natural frequencies of the system, resonance occurs. At the natural frequencies, the vibration amplitude increases sharply as distinct from other frequencies.

The occurrence of resonances can be determined by electrical phenomenon, not only by measuring large displacements of vibrations. Electrical resonance occurs at a particular frequency when the impedance of a circuit drops to the minimum level which allows the electrical current flow at the highest level. The phase difference between the driving voltage and the response will be in phase.

Sections 4.3.1.1 and 4.3.1.2 are two experimental methods to determine the resonant frequencies of a prototype of the proposed piezoelectric transducer-horn assembly in this project.

4.3.1.1 Determining Electrical Resonances

In summary, electrical properties of piezoelectric materials behave as follows under resonant frequency excitation.

- Minimum electrical impedance
- Maximum current flow
- Operating current in phase with supplied voltage

These behaviours can be explained by an electrical circuit model. As an alternating voltage causes expansions and contractions in the assembly of piezoelectric transducer and horn, the dynamic performance of the piezoelectric material behaves accordingly under the alternating stresses. Since the simple form of the equivalent electric circuit of piezoelectric transducer can be represented by Figure 4.15 consisting of resistance (R), inductance (L) and capacitance (C) (Blitz 1967), the resonant frequencies can be identified from the frequency response of a series-RLC circuit behaviour when a voltage of fixed amplitude with varying driving frequency is applied.

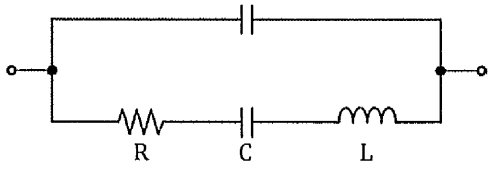

Figure 4.15: The Equivalent Electric Circuit of a Piezoelectric Transducer.

When a sinusoidal signal is connected to the series RLC circuit, a mathematical description of the circuit behaviour can be written as;

Inductive reactance: $X_L = 2\pi fL = \omega L$ Eq. 4-44

where f is the frequency and ω is the angular frequency.

Capacitive reactance: $X_C = \frac{1}{2\pi fC} = \frac{1}{\omega C}$ Eq. 4-45

When $X_L > X_C$ the circuit is inductive.

When $X_L < X_C$ the circuit is capacitive.

Total circuit reactance: $X_T = X_L - X_C$ or $X_C - X_L$ Eq. 4-46

Total circuit impedance: $Z = \sqrt{R^2 + {X_T}^2} = R + jX$ Eq. 4-47

where the real part of impedance is the resistance R, the imaginary part is the reactance X, and $j = \sqrt{-1}$.

From Eq. 4-44 and Eq. 4-45, it can be seen that the values of these resistances depend on the supplied frequency. Figure 4.16 shows the relationship of inductive and capacitive reactance against frequency where the former is a straight line and the latter is a hyperbolic curve. The resonant frequency (f_r) occurs when the resistance is at the minimum value and can be calculated as follows.

$$X_L = X_C \rightarrow 2\pi fL = \frac{1}{2\pi fC}$$

$${f_r}^2 = \frac{1}{4\pi^2 LC}$$

$$f_r = \frac{1}{2\pi\sqrt{LC}} \text{ or } \omega_r = \frac{1}{\sqrt{LC}} \quad \text{Eq. 4-48}$$

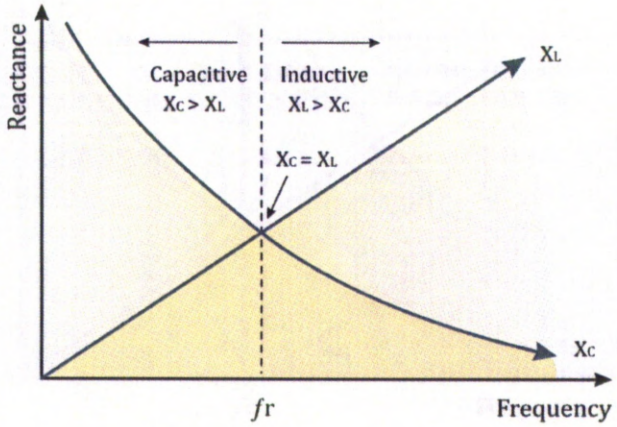

Figure 4.16: The Curve of Inductive and Capacitive Reactance Against Frequency.

At resonance, there are some remarkable electrical characteristics such as the drop of impedance and the peak of current. From Eq. 4-46 and Eq. 4-47, at the resonant frequency, no imaginary impedances exist in the complex form since they are cancelled out, so the total impedance of the series circuit becomes just the value of the resistance, Z = R. Therefore, at resonance the impedance of the circuit is at its minimum value and equals to the resistance of the circuit. The impedance at resonance is called the dynamic impedance of the circuit as shown in Figure 4.17. Also, the current flowing through a series resonance circuit is the product of voltage divided by impedance. The current will be at its maximum value at resonance as shown in Figure 4.18. In addition, the current circuit must be in phase with the source voltage at resonance as shown in Figure 4.19 because the current through the circuit is only affected by the resistance.

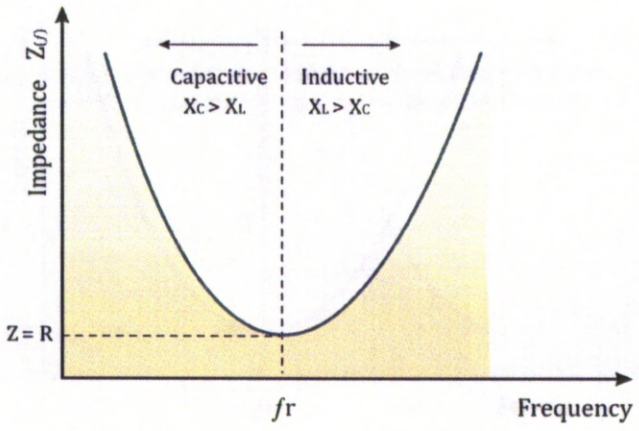

Figure 4.17: The Curve of the Impedance of a Series Resonance Circuit.

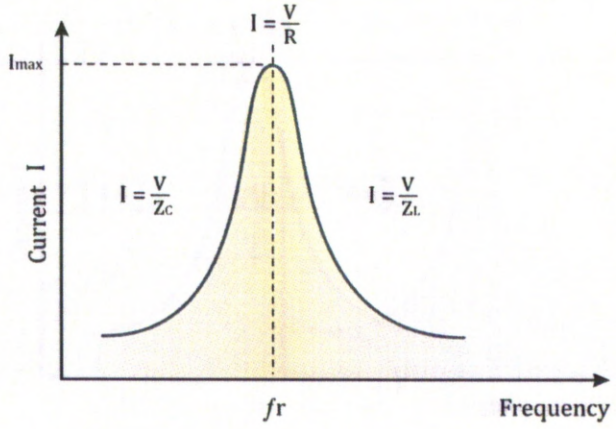

Figure 4.18: The Curve of the Current of a Series Resonance Circuit.

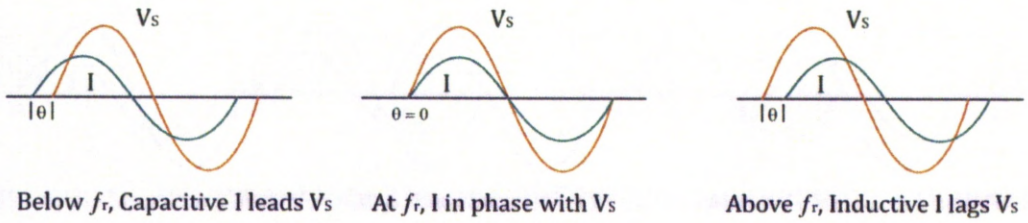

Figure 4.19: The Phase Angle of a Series Resonance Circuit.

Even if the equivalent circuit of the proposed assemblies is more complicated than the circuit in Figure 4.15, the behaviour at resonant frequencies are similar. Thus, resonant frequencies of the assemblies can be determined from the behaviour of the series RLC circuit mentioned before, by monitoring the electrical characteristics such as the peak voltage or current, impedance drop, and the change of phase angle while varying voltage frequency.

The set-up for determining electrical resonant frequencies of the proposed transducers is shown in Figure 4.20 and the main components of the test system include;

- Signal generator: It is the source of alternating voltages used to drive the assembly.
- Oscilloscope: This item is used to observe the voltage response to an electrical signal.
- Resistors: There are 3 resistors in the circuit for determining electrical resonant frequencies.

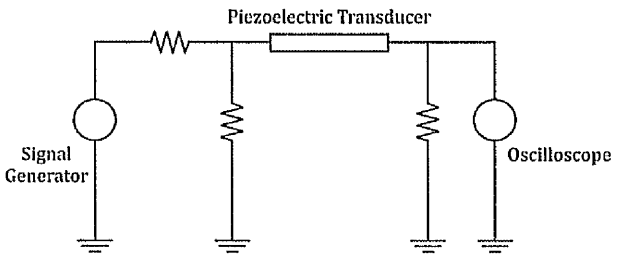

Figure 4.20: The Electrical Resonance Testing System.

4.3.1.2 Determining Mechanical Resonances

A vibrating system can be illustrated in a simple graphical way by using electromechanical analogy where the mechanical system can be replaced by an electrical circuit. One of the most logical methods is force-voltage analogy as presented in Table 4.9.

Table 4.9: Force-Voltage Analogy Correspondences Table (Harris 1970; Paganelli et al. 2010).

Mechanical quantity		Equivalent electrical quantity	
Exciting force (N)	F	Exciting voltage (V)	V
Velocity (m/s)	v	Current (A)	i
Displacement (m)	x	Charge (C)	q
Mass (kg)	M	Inductance (H)	L
Damping constant (Ns/m)	D	Resistance (Ω)	R
Elastic compliance (m/N)	C_m	Capacitance (F)	C
Power (W = Nm/s)	$F \cdot v$	Power (W = V A)	$V \cdot i$
Mechanical Impedance (Ns/m)	F/v	Electrical Impedance (Ω)	V/i

For a transducer, an electrical signal induces mechanical displacement. Since the behaviour of a structure undertaking forced vibrations is equivalent to an electrical circuit excited by an alternating electromagnetic field, the velocity, v, corresponds to the current, i, and the applied forced, F, to the voltage V (Blitz 1967; Kim, Wang & Brennan 2011; Paganelli et al. 2010). When a force F_0

applied at any time, t, a period force $F = F_0 \sin \omega t$, and the equation of motion is given by

$$F = M\frac{\mathrm{d}^2x}{\mathrm{d}t^2} + D\frac{\mathrm{d}x}{\mathrm{d}t} + \frac{x}{C_m} \qquad \text{Eq. 4-49}$$

where the wave motion of the structure is aligned in the direction x. An elastic compliance, C_m equals to $1/k_v$, where k_v is the dynamic stiffness of material.

Eq. 4-49 can be written in the term of velocity as

$$F = M\frac{dv}{dt} + Dv + \frac{1}{C_m}\int v\,\mathrm{d}t \qquad \text{Eq. 4-50}$$

which is equivalent to a simple electrical circuit composed of RLC in series applying voltage $V = V_0 \sin \omega t$ as written by

$$V = L\frac{di}{dt} + Ri + \frac{1}{C}\int i\,\mathrm{d}t \qquad \text{Eq. 4-51}$$

Under steady conditions the velocity, v , at a given time will be

$$v = \frac{F}{D + j\left(\omega M - \frac{1}{\omega C_m}\right)} \qquad \text{Eq. 4-52}$$

Mechanical impedance: $Z_m = D + j\left(\omega M - \frac{1}{\omega C_m}\right)$ Eq. 4-53

Mechanical reactance: $X_m = \omega M - \frac{1}{\omega C_m}$ Eq. 4-54

As happens in the electrical circuit, the term X_m is equal to zero at the resonant frequency, so, $Z_m = D$. The velocity and displacement amplitude reaches their maximum level where the exciting frequency is

$$f_r = \frac{1}{2\pi\sqrt{MC_m}} \text{ or } \omega_r = \frac{1}{\sqrt{MC_m}} = \sqrt{\frac{k_m}{M}} \qquad \text{Eq. 4-55}$$

In fact, most real structures are multi-degree of freedom systems. They are continuous and have an infinite number of degrees of freedom. For a system with n degrees of freedom, there are n natural frequencies where each frequency has its own mode shape. The equation of motion, Eq. 4-50, can be expressed in a matrix form as shown in Eq. 4-56. Determining resonant frequencies of an infinite degrees of freedom system is more difficult.

$$\vec{F} = [M]\frac{\mathrm{d}^2\vec{x}}{\mathrm{d}t^2} + [D]\frac{\mathrm{d}\vec{x}}{\mathrm{d}t} + \left[\frac{1}{C_m}\right]\vec{x} \qquad \text{Eq. 4-56}$$

In experimentation, the resonance of a system can be monitored by observing the peaks of the frequency response of the acceleration, velocity, or displacement created by force excitation. The main components of the test system consist of the following items;

- Exciter: It could be a hammer or any shaker that creates vibrations with a flat power spectral density in the frequency domain.
- Sensor: It is used to measure acceleration, velocity, or displacement of a moving part.
- Analyser: This may be called a Fast Fourier Transform (FFT) analyser. By using suitable software, the voltage signals from the sensor can be analysed to find the natural frequencies, mode shapes, and damping ratios.

As the system to be determined for resonant frequencies is an ultrasonic machining system, mechanical vibrations are generated from exciting a stack of piezoelectric rings (part of ultrasonic transducer and horn assembly), so the stack can be used as an exciter of the testing system. A white noise generator is

connected to the assembly for generating a random signal with a flat power spectrum.

Since the size of the ultrasonic transducer is compact, any sensors attached should better have less effect on the system so the measurement will be more accuracy. The measuring devices used were a miniature accelerometer (Type 4374, Brüel & Kjær, Figure 4.21) and Laser Doppler Vibrometer (VH300+, Ometron, Figure 4.22) where the range of frequency was limited to 26 kHz and 25 kHz respectively.

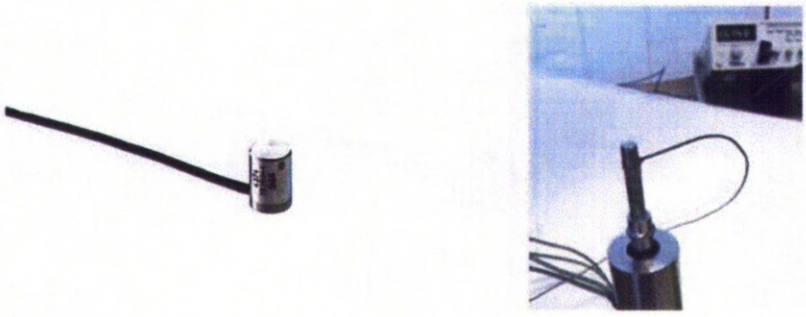

(a) (b)

Figure 4.21: (a) Brüel & Kjær 4374 Accelerometer (b) Measuring a Vibrating Object.

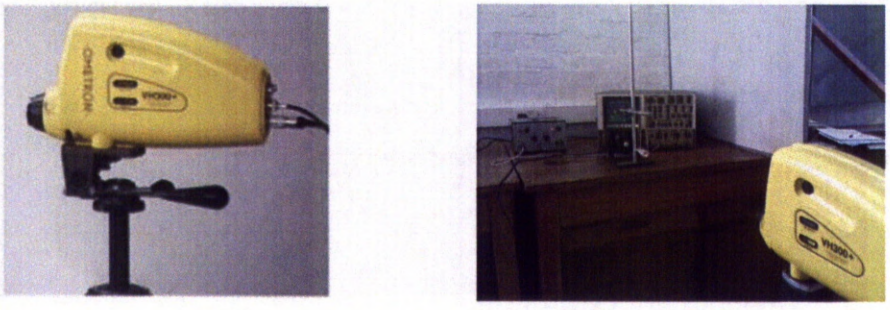

(a) (b)

Figure 4.22: (a) Ometron VH300+ Laser Doppler Vibrometer (b) Measuring a Vibrating Object.

Initially, the plan was to use 3 accelerometers. One accelerometer should be mounted at a point on the structure and the others mounted at other several points with different directions in order to determine resonant frequencies and also define the modal shapes of vibrations. However, this idea was found to be impractical because the sensors dropped off the vibrating horn very often, causing damage to the accelerometers and gave non-consistent feedbacks. The plan to use accelerometers was therefore abandoned.

A Laser Doppler Vibrometer (LDV) is more preferable as an ultrasonic vibration sensor because it is a non-contact, fast, and efficient method of measuring surface vibration velocities and displacement. The Ometron VH300+ is a single-point LDV, 1D-LDV, used for measuring vibration velocities. The principle of the measurement (Brüel & Kjær 2011) as shown in Figure 4.23 is based on a Michelson interferometer in which a laser beam is divided into a reference beam and a signal beam. The signal beam is directed onto a vibrating test structure, and the back-reflected light is recombined with the internal reference beam. The frequency of the signal beam is shifted when the test structure moves resulting in intensity modulation of the recombined beam due to interference between the reference and signal beams. The recombined light is split into two paths, and a quarter-wave plate is used so that the two signals are in quadrature (sine and cosine) allowing the direction of motion to be determined. This allows both the speed and direction normal to the surface of motion to be determined.

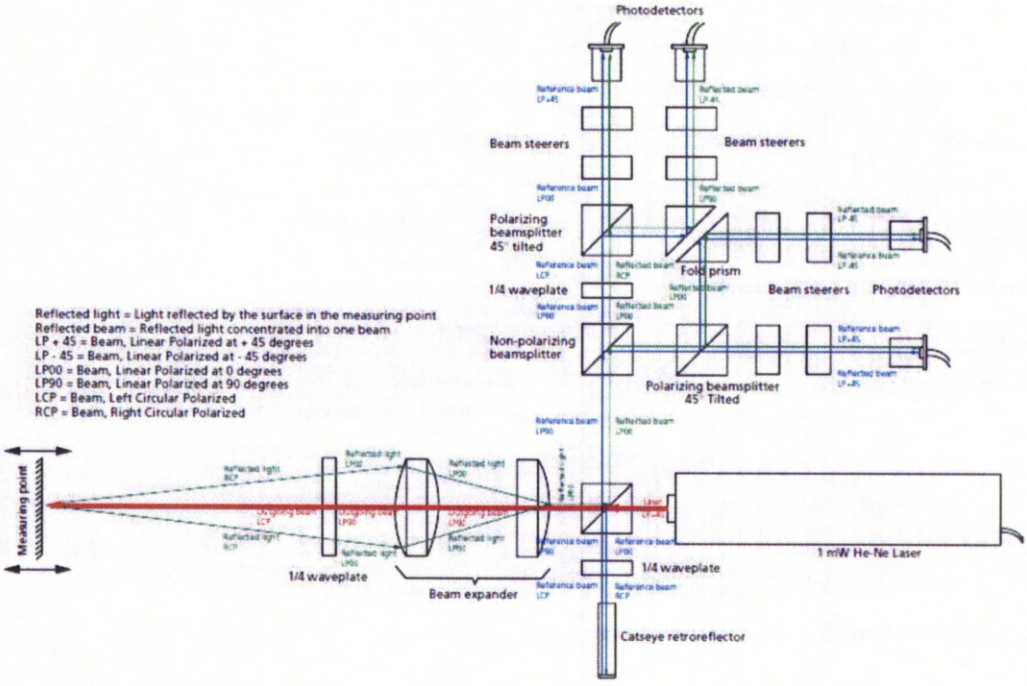

Figure 4.23: Optical Principle of the Type 8329 LDV.

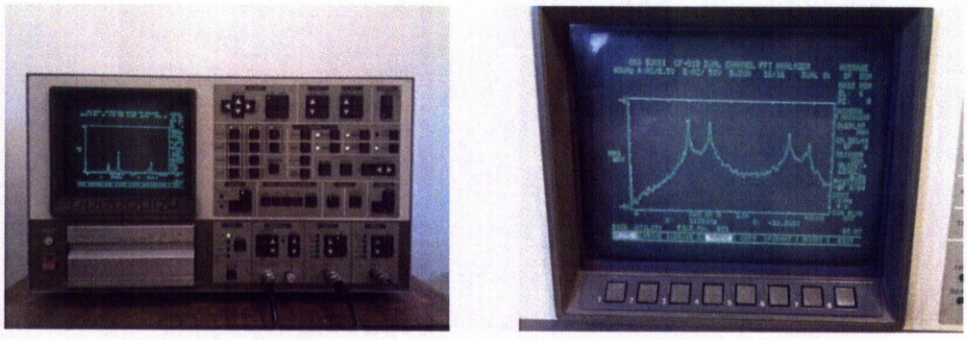

(a) (b)

Figure 4.24: (a) Ono Sokki CF-940 FFT Analyser. (b) Peaks of Resonance.

The laser beam was pointed at and focused on a surface of a vibrating object and the response signal was sent to an Ono Sokki CF-940 dual channel FFT analyser (Figure 4.24) for processing. Then, resonant frequencies of a system could be determined by the peaks in a frequency response function plot. An example of the plot is illustrated in Figure 4.24 (b).

The measurement devices used in this project were calibrated with a Brüel & Kjær 4294 calibration exciter (Figure 4.25) before performing any tests and the accuracy of the equipment set-ups were more than 95%. The final set-up for determining resonant frequencies is shown in Figure 4.26.

(a) (b)

Figure 4.25: (a) Brüel & Kjær 4294 Calibration Exciter and (b) Specification.

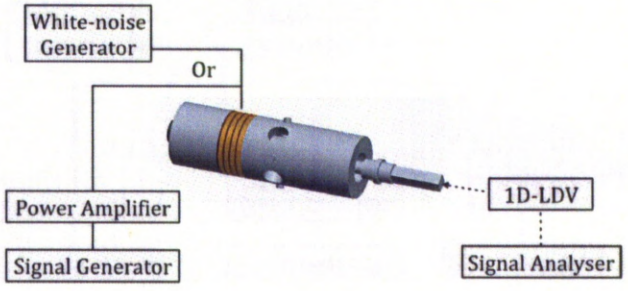

Figure 4.26: The Mechanical Resonance Testing System.

4.3.2 Measuring Amplitude and Determining Mode Shapes of Vibration

To validate the prototypes of ultrasonic transducer and horn assemblies, two characteristics of vibrations in response to exciting frequencies, the amplitude and mode shapes, have been determined. The measurement equipments mentioned in Section 4.3.1.2 were used with the purpose of determining the amplitude of vibrations. The non-contact measuring instrument has no load effect on the test system and the 1D-LDV is able to measure on high or low temperature surfaces while the available accelerometer could not be attached properly on the exciting object during the pilot test.

In order to identify a mode of vibration at a specified frequency, generally at least a single row or column of measurement points on an object is required as shown in Figure 4.27. It is important to include sufficient points with proper positions to describe a mode shape completely. However, the set-up shown in Figure 4.27 was impracticable for the project since there was only one sensor available at a time. Fortunately, the set-up as shown in Figure 4.28 is feasible for the test of a USM when the longitudinal modes of vibrations are the most interesting and only they need to be clarified from other modes in a frequency range. The equipment for determining longitudinal modes of vibrations included;

- Signal Generator: The exciting signals were generated by the generator.
- Power Amplifier: The signals generated from the signal generator are not sufficient to drive the USM system for machining purpose, thus, a power amplifier as explained in Section 4.2.1 was used for driving the USM prototypes.
- Exciter: In this case, a stack of piezoelectric rings, a component in the USM system, acts as the exciter.
- Sensor: The 1D-LDV was used for measuring the amplitude and determining the modes of vibrations.

- Analyser: An analyser as described in Section 4.3.1 was used.

There were a few steps required for determining longitudinal mode of vibrations using the set-up as shown in Figure 4.28. Firstly, the resonant frequencies of the system in the range of interest were determined by means of either electrical or mechanical resonance. Secondly, at a given frequency, the amplitude of vibration in the axial direction (z-axis) was measured. Thirdly, the amplitude of vibrations in 2 different directions (x and y-axis) was measured at the same resonant frequency for the second step. Lastly, the mode of vibrations at the given resonant frequency was identified as a longitudinal mode or a mode having strong vibrations in the axial direction when the amplitude obtained from the second step was significantly higher than the third step.

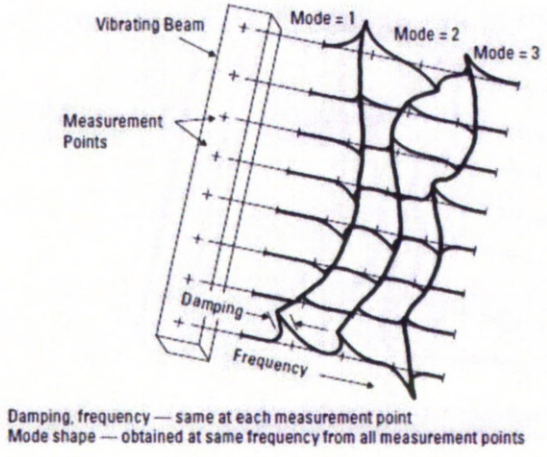

Figure 4.27: Concepts of Modal Parameters.

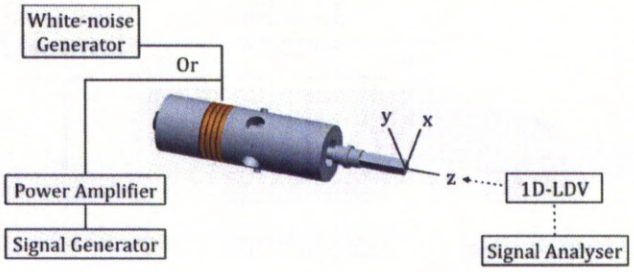

Figure 4.28: The System for Measuring Amplitude and Identifying Longitudinal Modal Shape of Vibrations.

4.3.3 Building Prototype-I, Testing, and Results

The components of the first prototype of the miniaturised USM system included a signal generator, a power amplifier, and a set of ultrasonic transducers and horn assembly. The signal generator can produce sine waves of 10 Vp-p at maximum. The power amplifier has a fixed voltage gain of 13 but the output voltage is limited to 115 V due to the maximum voltage limit of a power booster chip inside the power amplifier. The components of the prototype ultrasonic transducer and horn assembly included; the tool bit, horn coupling, steel backing part, stack of 4 PZT rings, sintered stainless steel horn, and copper electrodes.

Initially, the prototype of the horn was planned to be made of two aluminium parts using EDM and joined together as a rigid body by metal brazing. However, due to practical limitations, the horn was made from 316L stainless steel powder by an additive manufacturing technique, Selective Laser Melting (SLM).

SLM method is a process of additive manufacturing enabling the production of light-weighted complex structured components directly from layer-by-layer laser melted metal powder with a design defined by 3D model data with no need for specific tooling (Buchbinder et al. 2011; Louvis, Fox &

Sutcliffe 2011; Wong et al. 2009). However, building dense and homogeneous aluminium alloy objects by SLM is difficult and requires high laser powers, slow scanning speeds, and appropriate defined scanline spacing (Buchbinder et al. 2011; Louvis, Fox & Sutcliffe 2011), so 316L stainless steel was chosen as the material for the ultrasonic horn due to power considerations.

Figure 4.29 shows the fabrication of the ultrasonic horns. The horns were built by using a 50 W SLM machine called SLM-100. The SLM scanning layer aligns on the radial plane of the horn and develops in the direction of the horn axis on the top of a metal bed plate which later was machined off. The fabrication was performed under an argon atmosphere to prevent fire and oxidation.

A set of the novel ultrasonic transducer-horn assembly is illustrated in Figure 4.30. The mechanical parts were bolted together from the backing part through a stack of the PZT rings, with each layer separated by a copper electrode, into the horn. Since the tensile strength of PZT materials is inadequate for the high mechanical stress involved, the PZT ceramics should always be kept under compression, pre-stress, during an operation especially for dynamics applications such as USM. The pre-stress was controlled to a defined amount by using a torque wrench.

The first experiment was to determine resonant frequencies of the system by identifying the peaks of the responses. Prototype-I was excited by a white-noise generator, the laser beam was pointed to the end of the tool bit in 5 different directions, then the response from the laser vibrometer was sent to the FFT analyser.

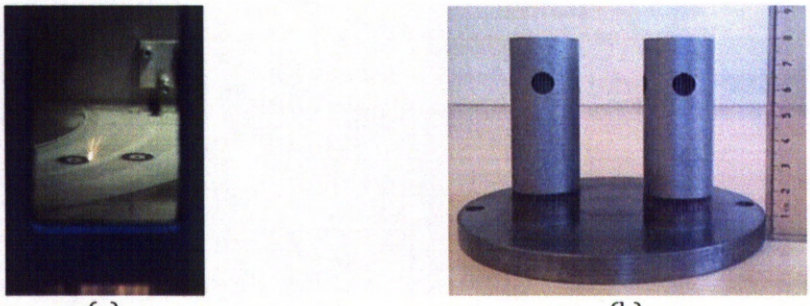

(a) (b)

Figure 4.29: Rapid Prototyping of the USM Horn by SLM; (a) Metal Powder Being Melted and (b) Horns Made on a Bed Plate.

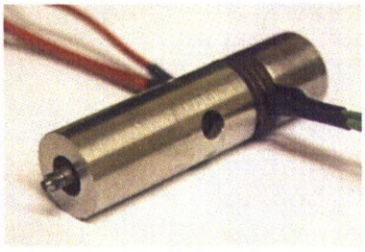

Figure 4.30: The Transducer-Horn Assembly of Prototype-I.

Since the horn for Prototype-I was designed to be aluminium rather than stainless steel, the FEA model had to be simulated again by changing the materials. The comparison between the modal frequencies predicted by the FEA software and observed by exciting with a white-noise generator is shown in Table 4.10. At the frequencies of 11.3 and 16 kHz, Prototype-I showed very strong responses. Thus both these frequencies were the next points of focus. The assembly was excited again by using the power amplifier at the exciting voltage of 190 Vp-p at the fixed frequencies. The 1D-LDV was applied for measuring the vibration responses. The responses in the z-direction were 12.3 dBV at 11.3 kHz and 9.7 dBV at 16 kHz while the responses in the other directions were -11.8 dBV at 11.3 kHz and -17.4 dBV at 16 kHz. These results showed that the vibrations in the z-direction were really stronger than the other directions, and the longitudinal vibrations should occur at the frequencies of 11.3 and 16 kHz.

However, there were noticeably different system behaviours at 11.3 and 16 kHz considering the plots of the frequency responses in Table 4.10. The 16.0 kHz should be the frequency of a longitudinal mode unquestionably because it could be monitored in every direction of the observations and the responses detected in the z-direction were found reasonably stronger than the other directions. Although the Prototype-I also showed the strong response in the axial direction at 11.3 kHz, possibly it might not be a pure longitudinal vibration. The frequency of 11.3 kHz was likely to be a complex mode as the outcome of combining two non-axial modal frequencies of around 10.9 and 11.9 kHz.

Table 4.10: Modal Frequencies of Prototype-I in the Range of 0 – 26 kHz.

(a) Plot of Response

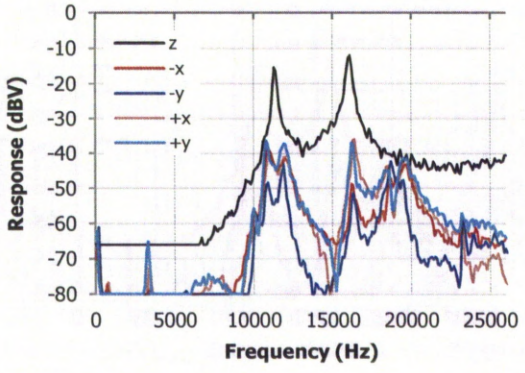

(b) Modal frequency (kHz)

FEA	Experiment, measured in the direction of				
	z	-x	+x	-y	+y
0.7 (F)		3.6	3.5	3.5	3.5
2.6 (F)		10.8	10.7	10.6	10.8
4.6 (F)	11.3	12.2	11.7	11.6	12.1
5.8 (F)	16.0	16.0	16.2	16.0	16.2
6.6 (T)		18.7	18.4	18.6	18.3
7.8 (L)		19.8	19.3	19.2	19.4
9.6 (T)		23.2	22.6	23.3	23.2
10.8 (F)					
14.0 (T)					
14.3 (L)					
14.5 (F)					
16.6 (F)					
20.6 (L)					
23.3 (F)					
24.7 (F)					

Unfortunately, the test results did not agree well with the FEA. First, the longitudinal modes were not occurring at the expected frequencies. Instead of 11.3 and 16.0 kHz, they had been expected to be 7.8, 14.3, and 20.6 kHz. Also, there was no evidence of a longitudinal modal frequency in the range of 18 to 25 kHz which is the appropriate range for machining. Moreover, the amplitude of the actual vibrations was significantly less than one third of the expected value. Therefore, the machining rate would be very slow under these conditions. For

the given reason, improvements to the prototype were necessary in order to obtain higher longitudinal resonant frequency with higher amplitude.

4.3.4 Investigating Causes of Poor Dynamic Characteristics of Prototype-I

In order to improve the USM system, the causes of the poor dynamic characteristics of the system were investigated.

4.3.4.1 Comparison between the Results of FEA and Experiment on Longitudinal Modal Frequencies

There were two longitudinal modal frequencies found by testing but three frequencies predicted by FEA in the range of interest. A comparison of longitudinal modal vibrations between the FEA and actual test results is given in Table 4.11. The deformed shapes simulated from the FEA software were plotted and the z-vibrations at the points P1 and P2 were measured to identify the relationship of vibrations between these two points and the tool bit end (E).

Table 4.11: Investigation of Longitudinal Modal Frequencies.

FEA	Experiment			
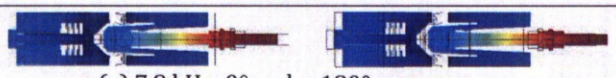 (a) 7.8 kHz; 0° and 180°	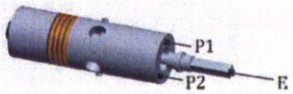			
 (b) 14.3 kHz; 0° and 180°	Freq. (kHz)	E-Resp. (dBV)	P1-Resp. (dBV)	P2-Resp. (dBV)
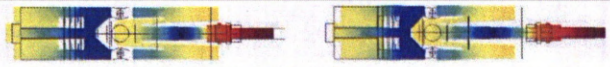 (c) 20.6 kHz; 0° and 180°	11.3	12.3	-23.6	-27.0
	16.0	9.7	1.5	1.0

The first comment from the data in Table 4.11 is that the modal frequency of 14.3 kHz by FEA would be equivalent to 11.3 kHz from actual testing because the responded signals at P1 and P2 were very low compared to the vibrations at the tool end. In Table 4.10 the results from the FEA showed that there were lateral modal frequencies around 14.3 kHz which was similar to the response-

frequency plot where the non-axial vibrations around 11.3 kHz were detected by testing. Therefore, the frequency of 20.6 kHz predicted by the FEA would be 16.0 kHz when the prototype was tested and the first longitudinal mode found by FEA would be missing because the movement of the horn was affected by the clamping method.

4.3.4.2 The Effects of Pre-Stresses

The effects of varying pre-stresses on the resonant frequencies and the vibration amplitude of Prototype-I were investigated. Although PZT ceramic materials can withstand pressures larger than 250 MPa without breaking, it was recommended that the PZT materials should be kept under compression below 30 MPa (beyond this load there is no displacement produced) (Abdullah, Shahini & Pak 2009; Morgan technical ceramics 2011; PI Ceramics 2011). However, for the safe operation of the central bolt the pre-stress was typically lowered to 25 MPa (Abdullah, Shahini & Pak 2009; Morgan technical ceramics 2011).

The pre-stress was controlled using a torque wrench and varied by changing the applied torques. In the previous tests Prototype-I was assembled with a tightening torque of 7 N·m which was the torque required for 25 MPa compression when using a M5 bolt. The resonant frequencies and the vibration amplitude of Prototype-I with different tightening torques are shown in Figure 4.31. The results show that the pre-stress in the range of 5 to 8 N·m has insignificant effect on the characteristics of the prototype.

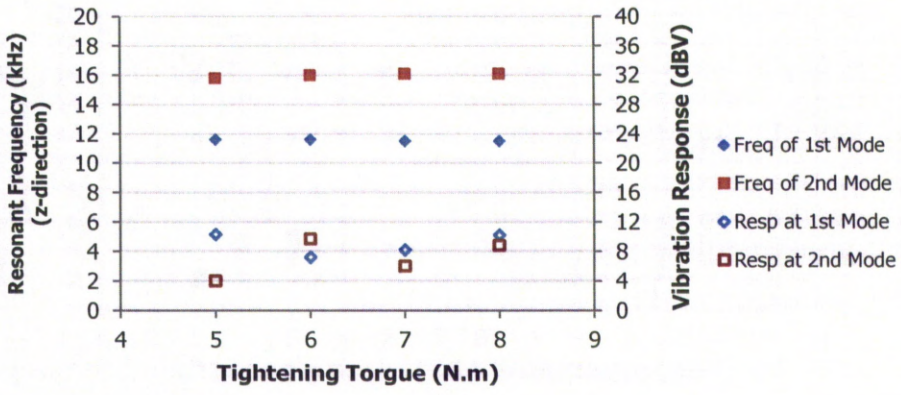

Figure 4.31: The Influence of Pre-Stress.

4.3.4.3 Measuring the Property of the PZT Material

The aim was to check whether the quality of the PZT material was as claimed by the manufacturer. The parameter involved was piezoelectric charge constant (d_{33}), the mechanical strain experienced by a piezoelectric element per unit of electrical energy applied. The property of the parameter mentioned in the datasheet was determined at 1000±200 Hz according to European Standard EN 50324-2 but the d_{33} Piezo meter, a system for testing piezoelectric parameters available in the Department only operated at the test frequency of 110 Hz.

Figure 4.32 shows the test results obtained from two different sets of the same PZT material. Each set consisted of three PZT rings. The first set was the damaged PZT rings, which were accidently forced cracks at their edges at the first trial of assembly, and the other set was the rings in good conditions. The mean value of the d_{33} of the damaged rings was smaller than the good rings and both were averagely larger than the value mentioned in the datasheet (265 pC/N). However, considering that the tests were done under the different frequencies and the test machine typically had an error about 10%, the quality of the material could not be rejected that it was not as claimed.

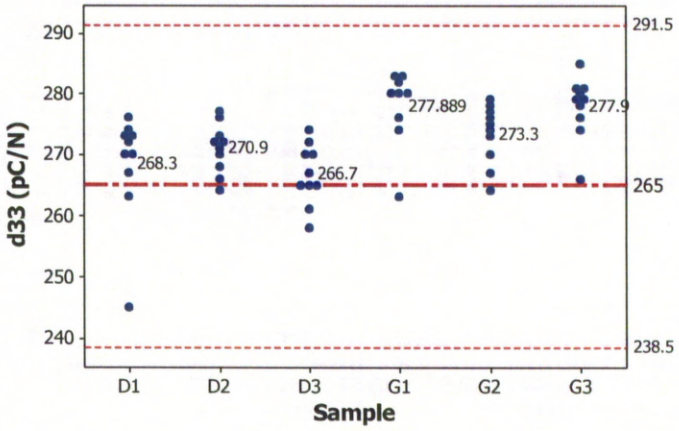

Figure 4.32: Piezoelectric Charge Constant.

4.3.4.4 Measuring the Displacement Amplitude of Single PZT Rings under Static Charges

Not only was the property of the PZT material relating to the strain displacement under an electric charge investigated, measurement of the actual expansion and contraction of the material was also attempted. It was planned that while the PZT material was being charged, its height would change until the charge was removed. Therefore, the test set included two PZT rings, one was the object under test and another one was a reference object, which were placed with small space next to each other. If there was a change in height of the object under test, the change could be detected by a high resolution measuring instrument.

A Wyko NT3300 white-light interferometer (WLI), an optical surface profiling system, was used for the measurement. The WLI technology overview was summarised in the manufacturer technical note and manual (Lamb & Zecchino 1999; Olszak, Schmit & Heaton 2001). The equipment was used to produce the image of nm-resolution static measurement in the z-range (along the optical path) and μm-resolution measurements in the x-axis and y-axis. The WLI provides two interferometric measurement techniques which are Phase

Shifting Interferometry (PSI) and Vertical Scanning Interferometry (VSI). PSI is typically used to measure smooth surfaces in very high precision for sub-nanometer features. VSI works well for rough surfaces where the light source is changed for the best focus position. However, VSI measures in the nanometer range rather than sub-nanometer range.

The VSI mode was applied because the surfaces of the PZT objects under test were not smooth and had discontinuities. Figure 4.33 shows the surfaces data scanned by using the WLI. Figure 4.33 (a) and Figure 4.33 (b) show the images at magnification ratios 1:5 and 1:10 respectively where discontinuous surfaces between the silver film electrodes (area 1), PZT ceramics (area 2) and space (area 3) can be seen. The low quality images were caused by the different light reflection characteristic of the materials. It was decided that the surface profiling focused on the test set at magnification 50x as presented in Figure 4.33 (c) where there were only two regions of PZT ceramics separated by a space. Figure 4.33 (d) shows an example of the result of analysis of regions. The two largest regions were compared, for example, regions 1 and 41. The region 1 was set as a reference level. Then, the mean height of region 41 was compared to the reference level which represented the deformed surface of the test object under a voltage charge.

Figure 4.34 shows the comparison plots between theory and experiment of the PZT material deformation under DC voltage charges. The surface roughness of the PZT ceramics under test was about 0.1 μm Ra. The theory was calculated from the applied voltages and the piezoelectric charge constant (or strain coefficient) of the PZT material which was 265 pC/N (or m/V). Considering the trend of the experimental results, it was noted that the deformation was proportional to the voltage charge. In addition, the distortion of the experiment data from the theory line was acceptable even it was fairly high because the surface roughness of the PZT objects under test was higher than the highest distortion in the range (around 0.08 μm Ra).

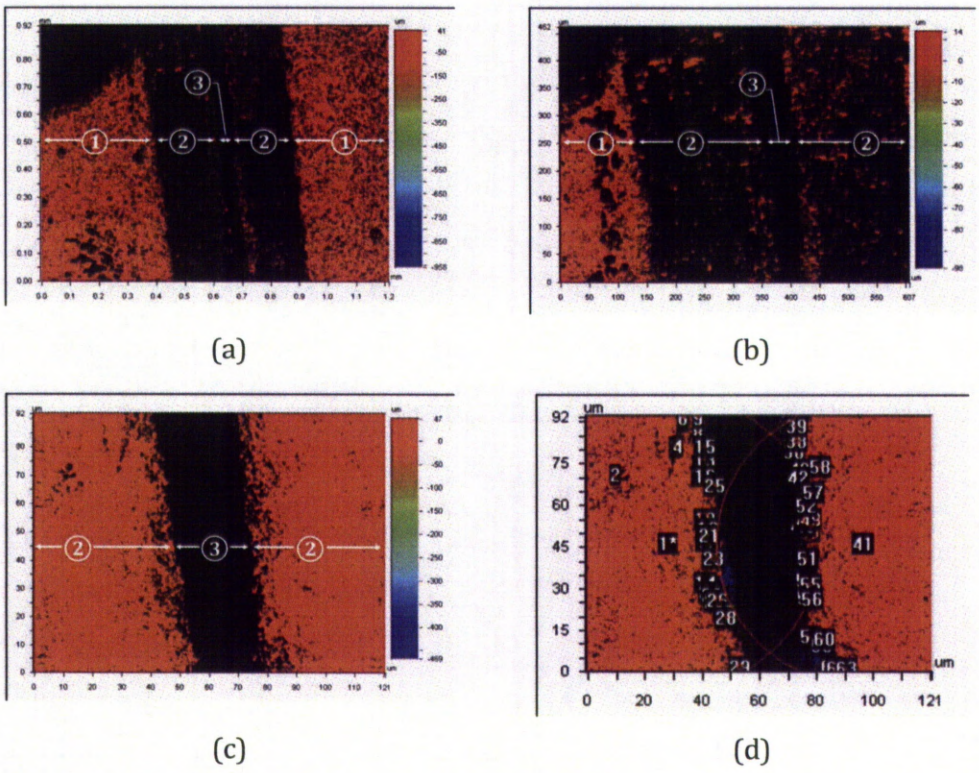

Figure 4.33: Surface Data of PZT Rings at the Magnification of (a) 5x, (b) 10x, and (c) 50x; and (d) Multi-Region Analysis

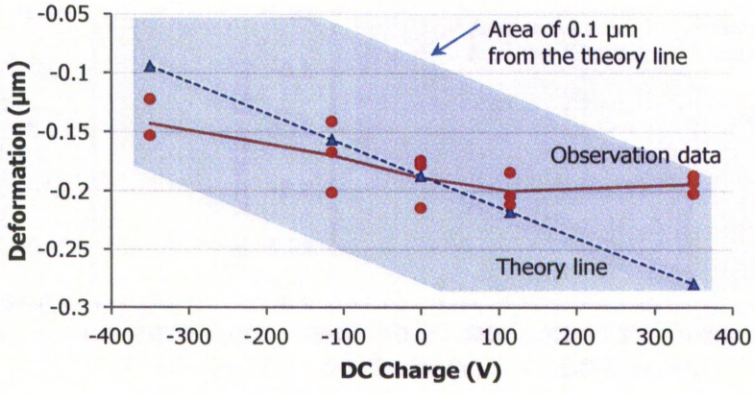

Figure 4.34: Deformation of a PZT Material Under DC Voltage Charges.

4.3.4.5 Determining the Damping Property of the SLM Horn

Using FEA, the accuracy of the FEA results depends on how well the input data of materials represented their actual properties in the simulation. In the early stage of detailed design for the miniaturised USM system, the material properties collected from literatures and manufacturers datasheets which were understandingly obtained by following any appropriate standard test methods. However, properties of materials sometimes depend on shapes, specific applications, and environment, which are somehow quite different from standard conditions. Therefore, the determination of damping characteristics of a SLM part for the prototype was necessary because the properties of the part made by such a special method might vary from conventional manufacturing processes. Several methods for determining damping properties of materials were considered including following standard test methods, impact hammer testing, and shaker testing.

The first standard for testing was ASTM E-756-04, Standard Test Method for Measuring Vibration-Damping Properties of Materials (ASTM International 2004). Two transducers are required in the measurement, one to cause vibrations, and one to measure the response of the test specimen to the excitation force. A massive rigid test fixture is required for holding one end of the test specimen in an environmental chamber to control temperature. This test method measures the loss factor (η), a frequency-dependent vibration damping property of various types of materials, which can be defined as

$$\eta = \frac{(\Delta f_n)}{(f_n)} \qquad \text{Eq. 4-57}$$

where f_n is the resonant frequency for mode n and Δf_n is the half-power bandwidth of mode n. This method is useful over a frequency range of 50 to 5000 Hz. The test method was found to produce good results when used for

testing homogeneous materials, and in some damping applications, materials consisting of two or more layers with different characteristics.

Although ASTM E-756 is very useful; this method is not practicable for measuring the loss factor of the SLM horn used in this project due to several reasons. The beam dimensions that a width of 10 mm, a free length of 180 to 250 mm, and a thickness of 1 to 3 mm are required by the standard. Such dimensional requirements could not be met by the SLM machine as its largest dimension is limited to only 100 mm. Moreover, it was not possible to conduct the tests using a non-contact exciter which could minimise all sources of damping except the material under investigation. Instead, an impact hammer, a miniature force transducer designed to excite and measure impact forces, was used for the Prototype-I SLM horn. By using the hammer impacting method, the specimen generally must be hit a number of times until the average value of the responses seen was consistent. The frequency was not a problem since the chosen hammer covered the frequency range of interest but using the hammer was found very difficult to control hitting the test specimen without double hits.

The second standard test method was ISO 16940:2004, Glass in Building – Glazing and airborne sound insulation – Measurement of the mechanical impedance of laminated glass (International Organization for Standardization 2004). Similar to ASTM E-756, it is a method for measuring the loss factor in a frequency range of 0 to 5000 Hz but especially for laminated glass test pieces. The recommended geometry for the test sample is a beam of 25 mm x 300 mm with a nominal 4 mm thickness. A shaker driven by a white-noise generator is used for exciting the test beam which is glued at its mid length onto an impact button of the shaker.

ISO 16940 was found to be similar to ASTM E-756 for the project in the terms of sample size requirement. Flat steel beams of 1.5 m and 300 mm length were tested following the guidelines of ISO 16940. The loss factor of the material was in the acceptable range comparing the property of the material cited in the

standard. Unfortunately, when the test was performed on a shorter beam of steel, which was equivalent to the length possible to be made by the SLM machine, the loss factor observed was outside the practical range.

Since following most parts of the test standards were not successful due to practical constraints, the test for determining loss factor of materials was prepared based on the available tools and instruments. The test was set up as a general test system configuration. Figure 4.35 (a) shows a viable test configuration (Agilent Technologies 2011) and Figure 4.35 (b) shows the actual test arrangement. The test specimen was attached to a beam and excited by a shaker driven by a white-noise generator. The vibrations were detected by the 1D-LDV and analysed by the FFT analyser.

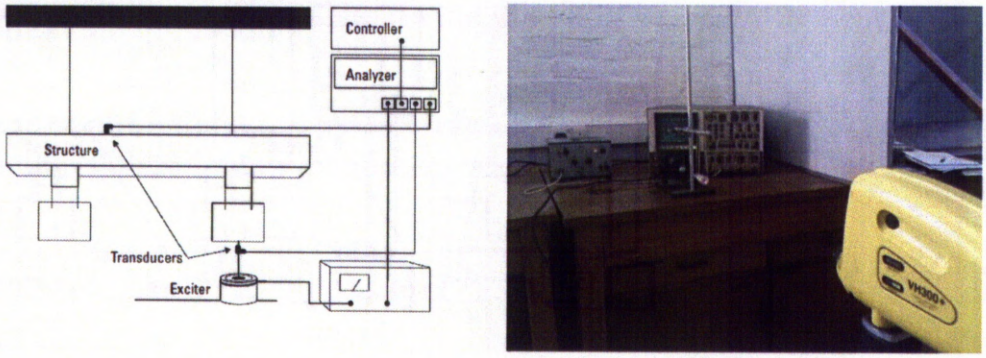

(a) (b)

Figure 4.35: Test Configurations for Determining Loss Factor of Materials; (a) General Test Configuration (Agilent Technologies 2011); (b) Experimental Set-Up.

Unfortunately, the set-up did not work effectively. The pilot test was performed on a steel part machined from a cold rolled bar. The measured loss factor of the steel part was acceptable compared to the standard data. However, the experiment showed abnormal results when various types of materials were

tested for validating the set-up. The loss factors of different materials including cold-rolled copper and aluminium were found to be similar to steel.

The causes of error were investigated and expected to be affected by the limitations of the measuring equipment. The signals detected by the 1D-LDV were weak and too close to the noise floor of the measuring equipment. Moreover, the resolution of the analyser was excessively coarse for this purpose. Therefore Δf_n used for calculating the loss factor in Eq. 4-57 was similar in every resonant frequency and for this reason the damping property of materials was inaccurately measured.

Since the various set-ups for explaining the damping property of materials have been carried out and failed, the characteristics of a SLM part was reviewed from literatures. It is clearly understood that material damping is affected significantly by its microstructures. Zhang et al. (1994) illustrated the use of relationship between damping properties and materials microstructures adopted by physicists as a means of detecting the presence of defects and predicting phase transformations in crystalline materials. Göken et al. (2006) explained that different phases like ferrite, pearlite, bainite and martensite in steel could be revealed by damping measurements. Pechersky (1991) stated that cast metals had higher damping coefficients than formed metals and showed the plots of damping loss factor as a function of frequency for wrought bronze, cast bronze, and T6 aluminium over the range 0 to 16 kHz. These three materials re-arranged the sequence of the material loss factor at around 4 kHz where the damping property rose up rapidly. This phenomenon, the sudden rise in acoustic radiation, was called the coincidence frequency which was proportional to the square root of the ratio of the mass density to Young's modulus and inversely proportional to the thickness of material. Rohatgi et al. (1994) also confirmed that damping properties were frequency dependent and revealed that the damping capacity of metal-matrix composites strongly related to volume

fraction, size, shape, nature of particles, the processing technique, porosity, and interfacial bond.

Parts made by SLM methods show high damping which is a drawback to its ability to generate high vibration amplitude at resonance. To fabricate an object by the SLM process, high energy from a laser beam is applied to melt loose metal powder selectively layer-by-layer to form a rigid model which might not be 100% dense. Therefore, the mechanical properties of the parts made by this method are more similar to the parts fabricated by casting rather than cold working method. For powder metallurgy and casting, it has been known that porosity is a typical issue. It happens because during solidification, there could be unfulfilled gaps between particles or unmolten powder particles. Those pores, voids, and discontinuities of material microstructure impede velocity of the waves travelling in the object and then damp amplitude of oscillations (Pechersky 1991; Schneider 1997).

To support that a material with high damping characteristics naturally presents lower vibration amplitude at resonance, the vibrations generated from the similar conventional horns made from different materials were measured. A comparison was made on two conical horns which were machined from wrought aluminium and wrought stainless steel and were driven at similar excitation conditions.

Table 4.12 shows the comparison of the vibration amplitudes at resonance between conical horns and Prototype-I and also presents the loss factors of the materials collected from Cremer, Heckl and Petersson (2005). The test on conical horns affirmed the theory that; higher damping material decreases velocity of waves travelling in a medium (Eq. 4-52) and reduces amplitude of vibrations. For the same geometry, the object with a higher density (Aluminium has a lower density than stainless steel) will be resonate at a lower frequency (Eq. 4-55).

Table 4.12: Comparison of Different Horns*.

Material	**Horn shape**	**Amplitude**	**Loss factor**
Aluminium	Conical	6.5 μm at 20 kHz	0.3 to 10 (10^{-5})
Stainless steel	Conical	3.2 μm at 16 kHz	0.2 to 3 (10^{-4})
SLM Stainless Steel	Folded with holes (Prototype-I without tool bit attached)	6.9 μm at 14 kHz 3.1 μm at 22 kHz **	

* Horns with no tool bit attached.

** Strongest signal was at 23.2 kHz but it was much distorted which was unreadable.

The SLM horn failed during the test, the micrographs of the failure horn is given in Figure 4.36. It happened because of the parts were incapable of working under dynamic conditions. Residual stresses were found to be very general in SLM components (Mercelis & Kruth 2006; Shiomi et al. 2004) which was due to thermal effects caused by rapid melting and cooling. Moreover, porosity in SLM parts could induce stress concentration in the microstructures of materials. These caused fatigue failure on the horn after only a short period of operations under dynamic excitations.

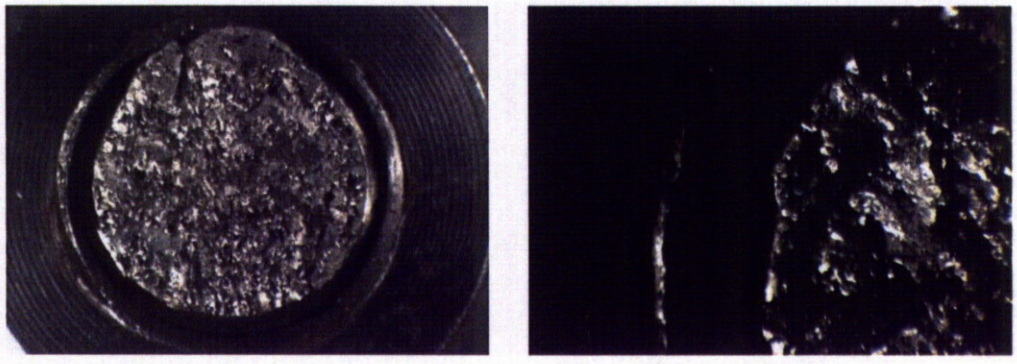

(a) (b)

Figure 4.36: Failure of the Horn; (a) 18x and (b) 50x Magnification.

4.4 Conclusions

Dynamic characteristics of ultrasonic machining systems are closely related to the quality of material structure and component connections. Displacement amplitude of vibration, the product of velocities of ultrasonic waves in a medium, was influenced by micro-structural elements caused by manufacturing processes. Moreover, the operational lifespan of transducers and vibrating parts are shortened as numbers of the discontinuous in the medium increase. A number of defects in material will slow down speed of waves resulting in high mechanical impedance. By matching the mechanical impedance, the ultrasonic waves would propagate through the structure more effectively. The selection of materials played an important role in matching mechanical impedance.

Initially, the new horn design for Prototype-I was planned to be made from two parts sintered together as one rigid body. The first part, having very deep grooves was to be made by EDM. The second part, a simple shape, was intended to be made by a conventional machine. The preferred material was wrought aluminium. Due to practical considerations, the horn was made from stainless steel powder by SLM. The experimental results showed that the vibration amplitude was very low, the longitudinal resonance occurred at lower frequency than expected. The horn failed after short times of use. These proved that SLM horn were not suitable to be the prototype. Referring to Table 4.12, if the horn was made from wrought aluminium, it was possibly that the vibration amplitude could be doubled, the longitudinal resonant frequency could be higher, and the operating life could be longer.

Chapter 5

Design and Performance Evaluation of Prototype-II

5.1 Idea Generation of Prototype-II

Since the performance and mechanical characteristics of the first design attempt were not particularly good for USM, a new design of horn was necessary. The new design was restricted the use of CNC machining while aluminium was chosen as the material for the horn.

Copper electrodes were made thinner. In order to minimise damping in the system, the thickness of copper electrodes were reduced. To protect the PZT rings from breakage, the electrodes, horn, and backing part were made oversize to prevent uneven loading applied to the rings. Also, the horn was divided into two parts in order to decrease the number of assembly changes required during the planned experiments. If the transducer and horn are assembled repeatedly, the chance of the PZT rings to be damaged is increased, and even worse if the alignment of the PZT stack is poor. It was suspected that this was one of reasons that caused the failure of the original PZT rings. The additional part will be called the front. Some ideas for improvement have been generated and modelled as shown in Table 5.1.

Table 5.1 shows the comparison of the candidate horns for Prototype-II. Most of the models are presented in quarter section cut, except Design 2A and Design 2E which are half cut and full section respectively. Design 2A is an improved transducer assembly and it was simulated as a reference. The first longitudinal resonance is quite high because its total length is short (no horn attached). Design 2B is a modification of Prototype-I which has the folded back-

and-forth horn with holes. Design 2C and Design 2D are purposely alternative shapes. It was expected that the flexibility of their shapes would create high amplitude. Design 2E is intended to make use of transitive wave motions. The horn of Design 2F has been flipped back to reduce the overall size.

Table 5.1: Comparison of the Candidate Horns for Prototype-II.

	No.2A Transducer	No.2B Modified Prototype-I	No.2C Double bent beam	No.2D Flexible bent beam	No.2E Transverse	No.2F Backward
Model		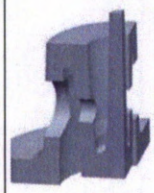			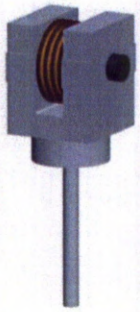	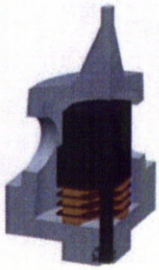
Simulation Results	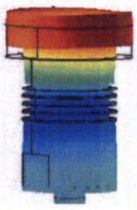		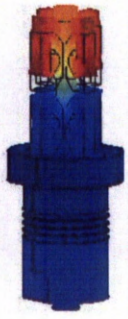			
Resonant Frequency, f, (Hz)						
	⋮ 30422 (F) 33369 (L) **44412 (B)** ⋮	⋮ 16459 (T) 16579 (L) 17195 (F) ⋮	⋮ 17038 (F) 17785 (L) **18485 (F)** ⋮	⋮ 10343 (T) 11406 (L) 16706 (T) ⋮	⋮ **18868 (F)** **23953 (L)** 26684 (T) ⋮	⋮ 17184 (F) 19738 (L) 20827 (F) ⋮
Displacement amplitude z-direction, A, at 100 Hz off resonance (μm)						
		5.4	4.8	6.1	0.14	2.8
Stiffness, k, of the structure z-direction (N/μm)						
		39	92	26	17	60
Max. Available blocked force, $F = kA$ (N)						
		50	443	160	3	169
Relative MRR comparing to Prototype-I ($MRR \propto f \cdot A^{3/4}$)						
		85%	83%	64%	8%	62%

At this stage, each design was modelled without tuning its dimensions to an operating frequency. Each design was analysed and the overall characteristics compared in order to determine optimal USM conditions. Design 2E was eliminated first because transverse waves do not have efficient power to generate motions in the axial direction. Next, Design 2F was eliminated, because it is wider and heavier, and the wave transfer is slightly inefficient; whereas Design 2B and Design 2C have promising outputs but there modes of vibration are very close to each other. Design 2D was the best choice because of its potential to produce high amplitude. In addition, its length can be shortened for a tuned frequency and its MRR could be higher at higher frequencies.

Table 5.2 shows the simulation results of a horn model whose is revised from Design 2D. In summary, the top half of the horn of Design 2D has been cut to produce a higher frequency of resonance; the bent beams part is kept in the design for magnifying amplitude of vibrations (Part A in Table 5.2) and shortening the total length of the horn (Part B in Table 5.2); the beams are not too long or too thin for gaining proper stiffness; and most importantly, the geometry lends itself to ease of manufacture by CNC machining.

Table 5.2: Prototype-II.

Model	Characteristic
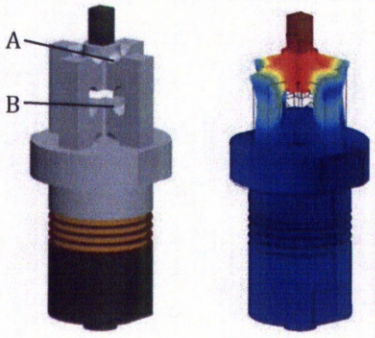	Resonant Frequency, f, (Hz)
	⋮
	20136 (F)
	22663 (L)
	28823 (F)
	⋮
	Displacement amplitude z-direction, A, at 100 Hz off resonance (μm)
	7.1
	Stiffness, k, of the structure z-direction (N/μm)
	97
	Max. Available blocked force, $F = kA$ (N)
	687
	Relative MRR comparing to Prototype-I ($MRR \propto f \cdot A^{3/4}$)
	143%

The dimensions of Prototype-II were determined in a wider context than Prototype-I. When Prototype-I was designed, its dimensions were determined to maximise the vibration amplitude at a given frequency. Prototype-II was designed for minimising horn weight; maximising amplitude, available blocked force, and the relative MRR at the desired resonant frequency; and maximising the gaps between the expected longitudinal resonant frequency and the other modal frequencies at the lower and higher resonant frequency. The details of obtaining the dimensions of Prototype-II are presented in Section 5.2. The tested results of Prototype-II are explained in Section 5.3

5.2 Optimising Prototype-II

The purpose of this step is to propose the optimised geometry of a horn for Prototype-II which should be equivalent to or better than Prototype-I and made of a rolled aluminium bar by CNC machining. The tested results of Prototype-I (Section 4.3.3) suggested that only optimising the displacement amplitude of vibrations within a range of resonant frequencies is inadequate for developing a robust ultrasonic transducer. It was proved that the properties of materials as well as a power generator played very important roles regarding the transducer performance. The optimisation for Prototype-II was performed using fractional factorial design.

The objectives of the optimisation were to design for minimising horn weight; maximising amplitude, available blocked force, and the relative MRR at the desired resonant frequency; and maximising the gaps between the expected longitudinal resonant frequency and the other modal frequencies at the lower and higher resonant frequency. A table of Taguchi's fractional factorial design for 5 factors with 2 levels was constructed. The factors and levels considered are explained in Table 5.3. Twelve data points of the factors and combinations, and their simulated results are shown in Table 5.4. The displacement amplitudes were calculated at 100 Hz off resonance, which the amplitudes were also used

for determining the available blocked forces. The MRRs, $MRR \propto f \cdot {A_V}^{3/4}$ obtained from Shaw (1956) cited in Kainth, Nandy and Singh (1979), are the relative values compared with the simulated resonant frequency and amplitude of Prototype-I which are both slightly different from the values in Section 4.1.5.3 because some input properties of materials were updated after the prototype had been made.

Table 5.3: Factors and Levels used in Optimisation for Prototype-II.

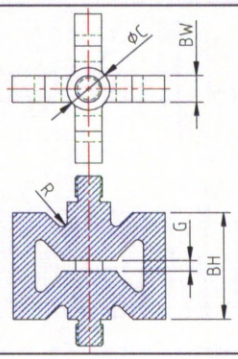

Factor	Level		Unit
BH: Beam height	20	25	mm
BW: Beam width	5	8	mm
R: Fillet radius	1.5	2.0	mm
G: Gap width	5	3	mm
C: Core Diameter	8	10	mm

Table 5.4: Table of Taguchi's Fractional Factorial Analysis and Responses.

Factor					Response					
BH	BW	R	G	C	Freq. (kHz)	Disp. (μm)	Force (N)	MRR (%)	Wt. (g)	Dist. (kHz)
25	5	2.0	5	8	21.3	6.5	551	125	14.9	0.5
25	8	2.0	3	10	24.0	7.6	1041	159	23.7	0.3
25	8	1.5	5	10	23.7	8.4	1065	169	22.9	1.2
20	8	2.0	5	8	22.9	7.2	679	146	15.6	2.6
25	8	1.5	5	8	23.0	7.4	794	149	21.9	3.8
20	5	2.0	5	10	22.0	6.6	574	131	11.4	0.3
20	8	1.5	3	8	22.4	6.9	639	138	16.1	3.1
25	5	2.0	3	8	21.4	6.5	570	126	15.3	0.8
25	5	1.5	3	10	21.9	6.6	670	130	16.3	1.2
20	8	2.0	3	10	24.1	7.8	908	163	17.0	1.0
20	5	1.5	5	10	22.1	7.0	614	138	11.3	0.3
20	5	1.5	3	8	20.4	5.8	408	110	10.9	1.2
Prototype-I (Model)					18.5	5.8	419	100		
Prototype-I (Actually made from sintered stainless steel)					13.7	6.3				

Initially, only the resonant frequency, amplitude, available blocked force, MRR, and weight were investigated. However, it was found later that some combinations of the factors cause another modal resonance very close to the longitudinal resonance, so the distance between 2 resonant frequencies was brought into account. The data was analysed and the graphical analysis in Figure 5.1 shows that the beam width has effects to many responses and the next factor is the gap width which means improvement should focus on changing the sizes of both factors. The resonant frequencies generated by all combinations of interest lay within the range of 18 kHz - 25 kHz, which contains the appropriate frequencies for machining by USM. Therefore, these data were used to generate response surfaces for the optimisation. Figure 5.2 shows the optimum dimensions of the horn for Prototype-II which has the beam height 21mm, beam width 8 mm, fillet radius 1.5 mm, gap 5 mm, and core diameter 8.5 mm.

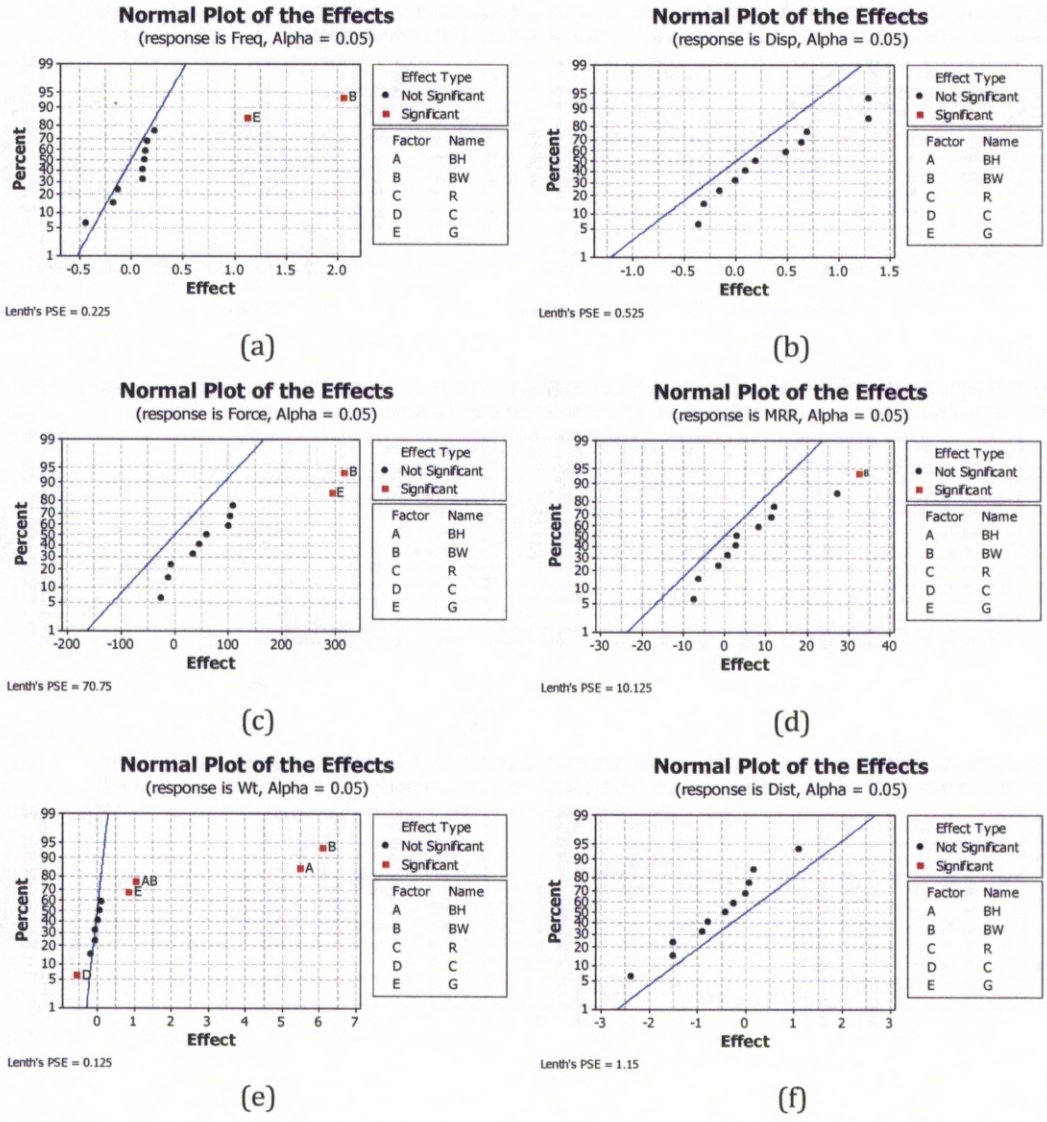

Figure 5.1: Normal Plots of Responses. (a) Frequency; (b) Displacement Amplitude; (c) Available Blocked Force; (d) Relative MRR. (e) Weight of Horn; and (f) Distance of the Nearest Resonance.

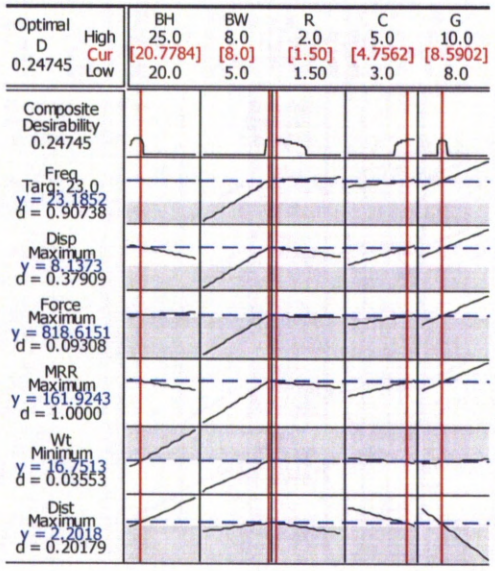

Figure 5.2: Optimisation Using RSA for Prototype-II.

5.3 Building Prototype-II, Testing, and Results

Prototype-II consisted of a stack of four PZT rings sandwiched between a tool steel backing end and the machined aluminium horn which was re-designed for better dynamics performance than Prototype-I. Each layer of PZT rings was separated by a 0.05-mm copper electrode. The diameters of the horn, backing end, and electrodes were made oversize relative to the PZT rings to avoid uneven surfaces which might have caused damage to the rings from unbalanced force during operation. Unlike the horn of Prototype-I which was made by SLM, a CNC machine was used for manufacturing the horn for Prototype-II (butterfly shape) as described in Section 5.2. Consequently, the microstructure and mechanical properties of the horn material could be similar to an extruded aluminium bar. The signal generator and power amplifier were kept unchanged.

5.3.1 Electrical System Resonance

By the time Prototype-II was ready for testing, the 1D-LDV was returned to the manufacturer for calibration. Therefore, the test of electrical system resonance was conducted to observe electrical characteristics of Prototype-II. The experiments were set up as explained in Section 4.3.1.1 by monitoring the voltage over a series resistor connected to the USM system.

Figure 5.3 (a) shows the voltages measured across the 100-Ω series resistor compared to the input admittance on a piezoelectric surface obtained by computer simulation. The exciting voltage was set to be low only 3.8 V_p (peak value) to prevent overloading of the resistor and the frequency of excitation was from 5 kHz to 26 kHz in steps of 1 kHz. The voltage plot shows that there is only one voltage peak of voltages representing resonance at 21 kHz. For the admittance plot, the sign of resonance at 11 kHz was ignored since the simulation showed the whole transducer moving backward/forward to the fixed point while it showed expansion/contraction at 22 kHz. When comparing the voltage and admittance responses, it could be seen that the variation of resonant frequencies was about 1 kHz which was acceptable.

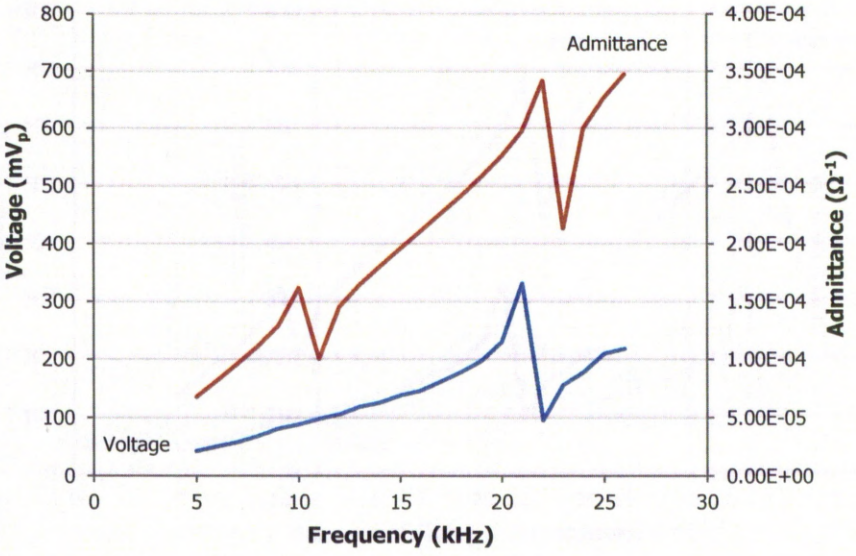

(a)

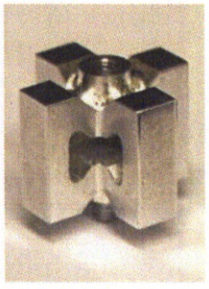

(b)

Figure 5.3: (a) Electrical Characteristics; (b) Horn Prototype-II.

The resonant frequency of 21 kHz was only 1 kHz away from the expected value of 22 kHz, it was an acceptable characteristic for the design of a transducer and horn for USM machining. However, the results were unable to be repeated satisfactorily. More detail on unrepeatability is explained in the next sections.

5.3.2 Non-Linearity Characteristics

In order to examine closely the characteristics of Prototype-II and because the electrical current flowing in the system was found to be small, the 100-Ω series resistor as connected shown in Figure 4.20 was replaced by the circuit in Figure 5.4. The detected response waveforms showed behaviours of non-linearity.

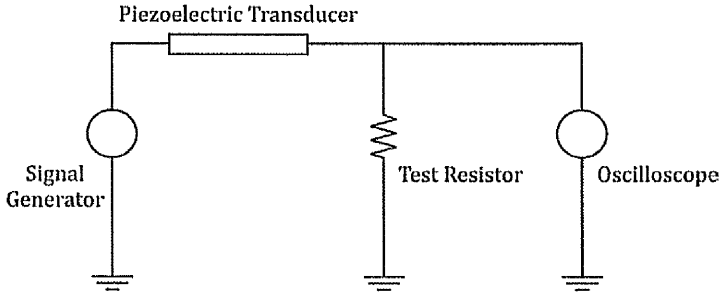

Figure 5.4: The Simplified Circuit for Determining Electrical Resonance.

The frequencies of electrical system resonance of Prototype-II were varied relative to power input. The first sign of non-linearity was observed when it was excited at higher power rating resulting in lower resonant frequencies as presented in Figure 5.5. Further, by observation at resonant frequencies, the waveforms of the signals measured across the 27-Ω series resistor appeared not to be regular smooth sine curves at power input greater than 30 V and worse at even higher power.

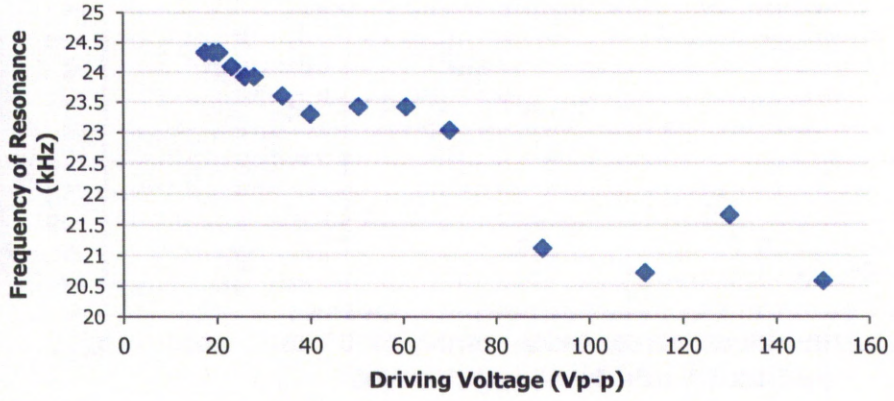

Figure 5.5: The Change of Resonant Frequency Subjected to Driving Voltages.

At higher electrical input levels, the response curves changed and showed different routes over a range of resonant frequency when the driving frequency was increased and decreased. Such phenomena are shown in Figure 5.6 (a) to Figure 5.6 (d) for four different levels of driving voltages.

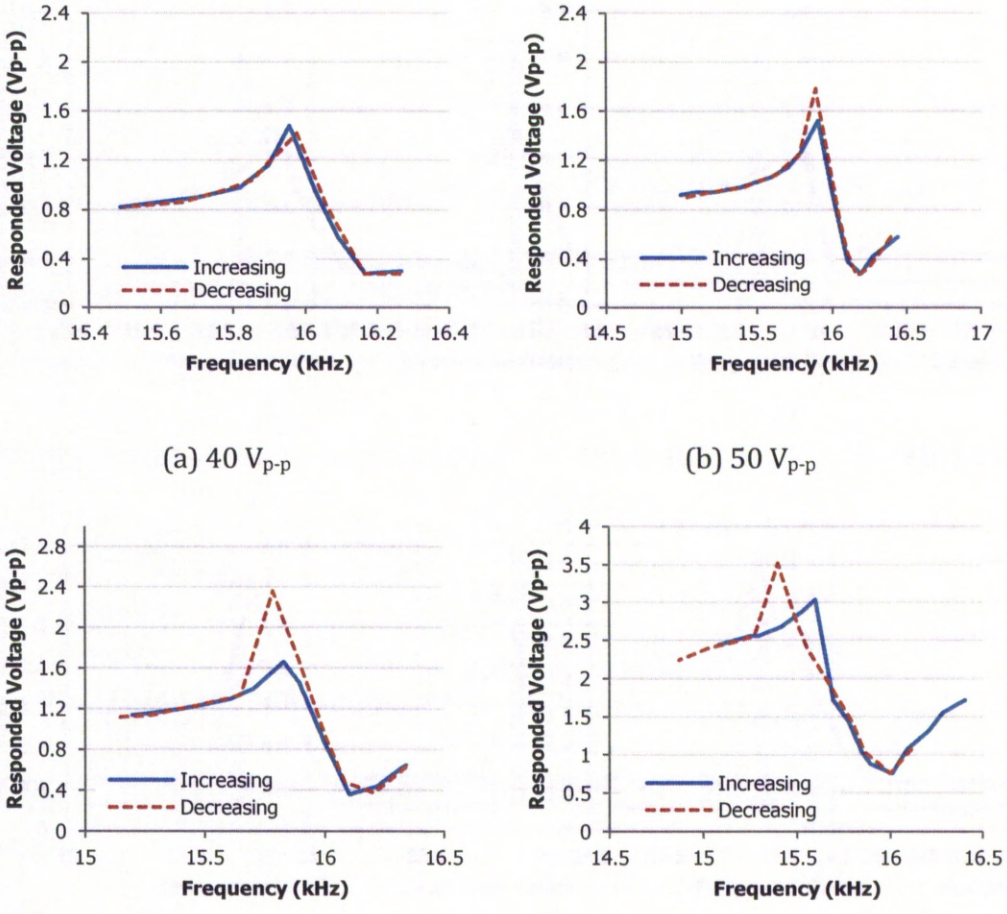

(a) 40 $V_{p\text{-}p}$ (b) 50 $V_{p\text{-}p}$

(c) 60 $V_{p\text{-}p}$ (d) 120 $V_{p\text{-}p}$

Figure 5.6: Unrepeated Routes of Responses at Different Driving Voltages.

A series of tests for investigating temperature effects on Prototype-II were also conducted. It was assumed that the responded voltages would be affected by a change of temperature. The system was tuned to resonance and kept at the resonant frequency. The temperature of the transducer and the voltage across the series resistor were measured over a period of time. The responses at the low and high levels of driving voltages, 25 V and 190 V were shown in Figure 5.7

(a) and Figure 5.7 (b). For a driving voltage of 25 V, the transducer temperature seemed to be stable, whilst the temperature increased nearly 4°C, when the voltage was increased to 190 V. At high driving voltages, the transducer vibrated at higher amplitude than at low driving voltages, so the temperature of the transducer driven at 190 V reached saturation at higher temperature than 25 V. However, it was interesting to note that the responded voltages dropped by 50% even when the temperature of the transducer changed only slightly, as shown from Figure 5.7 (a). This value of such voltage drop was significant.

It was found that the temperature of a high power booster chip which was a main component used in the HV power amplifier affected the responded voltages. As there was limited space inside the HV power amplifier, one terminal of the thermocouple was placed onto the heat sink attached to the chip instead of placing it directly to the chip. However, the position of the terminal was very close to the chip. With this arrangement, the temperature of the heat sink could represent the temperature of the chip. The responded voltage, transducer temperature, and chip temperature over a period of time is given in Figure 5.7 (c). Unfortunately, the drop of responded voltages did not seem to be caused by the chip. In fact, the temperature of the chip reached a maximum after less than 5 minutes with an increase of merely 2°C, while the responded voltage still decreased continuously and become stable after 20 minutes.

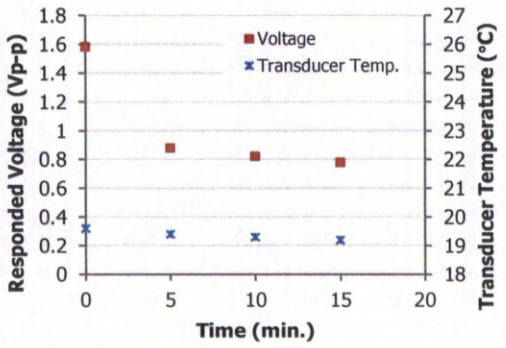

(a) At Driving Voltage 25 V_{p-p}

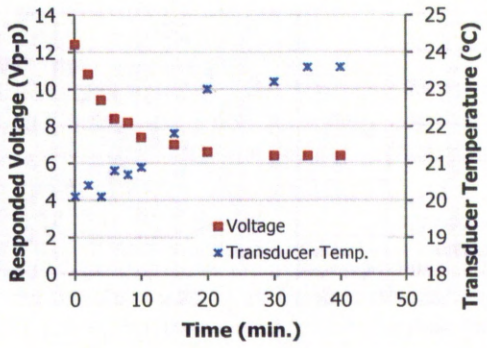

(b) At Driving Voltage 190 V_{p-p}

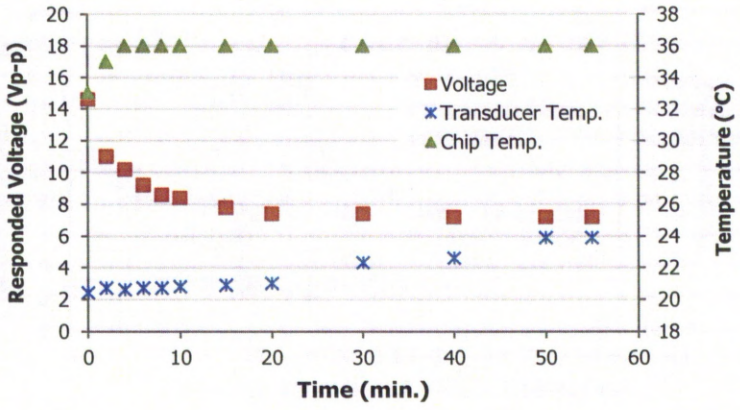

(c) Chip Temperature at Driving Voltage 190 V_{p-p}

Figure 5.7: Responded Voltages and Temperatures Records.

During the tests, it was found that the temperature of the power booster chip increased relatively when the frequency was kept changing and/or running at high levels. Then, the temperature of the chip was investigated again when the transducer was driven at frequencies around 25 kHz with a 0.1 kHz step increase every 5 minutes at 190 V. The increments of the responded voltage and temperature are given in Figure 5.8. The temperature increased from 38°C to

48°C but still remained in the acceptable range when the case temperature recommended by the manufacturer was -25°C to 85°C. These results supported the previous test that the power booster chip was working under proper conditions and not a cause of the unstable oscillations.

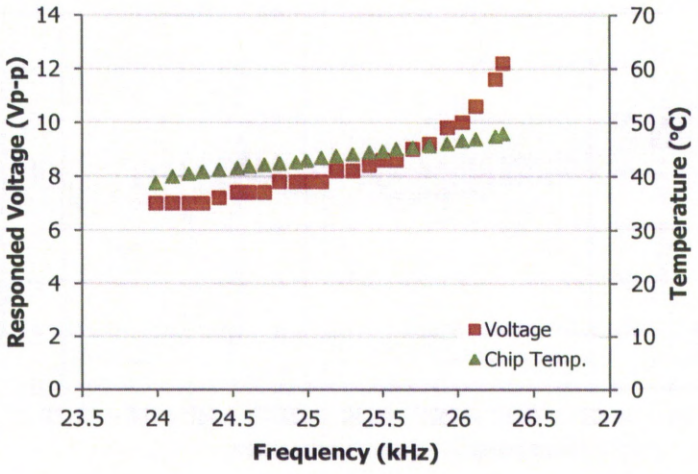

Figure 5.8: Responded Voltages and Temperatures on the Frequency Domain.

5.3.3 Mismatched Impedance

A possible major cause of non-linearity and low vibration amplitude could be impedance mismatch among various electrical components, especially the link between the HV power amplifier and transducer. In this respect, both Dubus et al. (2002) and van der Avoort et al. (2010) supported this assumption. The impedance of each component needed to be recognised in order to improve the system circuit. Initially, the impedance of the transducer was going to be estimated by calculation from the measured voltage across the known-value series resistor (Figure 5.9), but determining the impedance of the amplifier was more difficult. Moreover, the frequencies below 30 kHz were out of the technical

capability of the network analyser available. However, the impedance of the transducer and power amplifier were measured at 30 kHz and these values were used. Alternative methods using other simpler equipment instead of the impedance or network analysers were also investigated.

The first trial used LCR meters to measure electrical properties of the devices including inductance, capacitance, and resistance at a resonant frequency in order to obtain the impedance of the test object. However, the accessible LCR meters could only cater for fixed-frequencies measurements. The inductance, capacitance, and resistance of the transducer and power amplifier at 10 kHz, 20 kHz, and 40 kHz were measured but switching to the resonant frequencies of Prototype-II's components was not feasible.

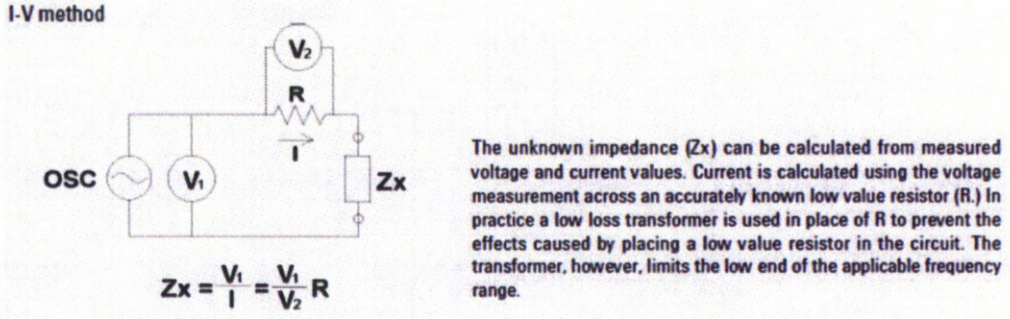

Figure 5.9: Impedance Measurement I-V Method (Agilent Technologies 2009).

In the next set of trials, a variable dummy resistor was used. For the amplifiers impedance, a reference signal level was set from the signal generator and the peak to peak signal was displayed on a digital oscilloscope. Then the amplifier box's input was connected to the output of the signal generator (connected in series). The amplifier's output was connected in series to a large variable dummy resistance which acted as a load. The output terminals of the dummy load were then connected to the oscilloscope. The resistance value was

varied until the same peak to peak voltage waveform was shown on the oscilloscope. Leaving the variable dummy load as set the impedance across the terminals of the dummy load was measured using an LCR meter at frequencies of 10 kHz and 20 kHz. The dummy load in this instance represented the output impedance offered by the amplifier box. For the transducer, the previous procedure was repeated without an amplifier box. The impedance of the transducer obtained by following this test method was relatively different from three previous methods which might be caused by too many devices connected in one test, so this setting seemed to be inappropriate.

Eventually, the set-up that appeared to be the most practicable and simple is shown in Figure 5.10. The input impedance was determined by connecting devices as presented in Figure 5.10 (a). A variable resistor was connected between the signal generator and amplifier input. An oscilloscope was connected across the transducer. The signal generator was set to generate the signal at a pre-determined frequency, and the amplitude of the signal displayed on the oscilloscope was recorded. Then, the variable resistor was adjusted from 0 Ω and increased until the output waveform monitored by the oscilloscope appeared to be half of its previous set value. At this stage the signal was shared equally between the resistor and the amplifier, so the resistance and impedance were equal. Afterwards, the circuit was switched off and the resistance of the test resistor was measured using an ohmmeter. The measured resistance represented the equivalent value to the input impedance of the amplifier. For the measurement of the output impedance, the transducer impedance, it followed the set-up as depicted in Figure 5.10 (b). The initial output from the amplifier was adjusted to be the same value as the input impedance test, but this time a transducer was not connected to the output terminals. The variable resistor, set in the maximum resistance, was connected across the output terminals. The test resistance was reduced until the display showed half the amplitude under no load condition. The resistance was measured and was supposed to have the

same value as the transducer impedance. By following these steps, the test frequency was able to be set at any value by controlling the signal generator.

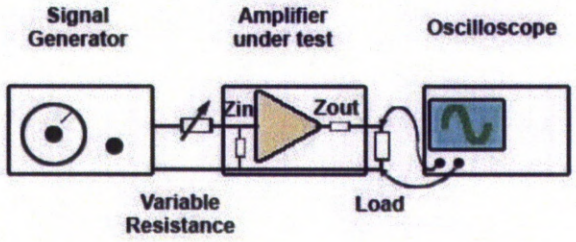

(a) Measuring Input Impedance.

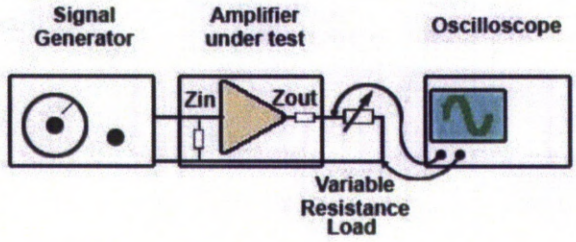

(b) Measuring Output Impedance.

Figure 5.10: Impedance Measurement Using Ohmmeter and Variable Resistor (http://www.learnabout-electronics.org 2011).

The results of the test resistance representing the impedance are shown in Table 5.5 and Table 5.6. The graphical representation of the data is shown in Figure 5.11 (a) and Figure 5.11 (b). Those values at 30 kHz were reasonable compared with the impedance obtained using the network analyser. The impedance of the amplifier varied slightly according to the change of frequency but the driving voltage had less effect. At 16 kHz and 27 kHz, the responses showed strong signals characterising the resonances. They were repeated in order to verify the minimal value of impedance for the transducer. The test

results provided extensive evidence that the input and the output impedance of the system were mismatched.

Table 5.5: HV Amplifier Impedance.

Frequency (kHz)	**Test Resistance (Ω)**	
	18 V_{p-p} Driving Voltage	**190 V_{p-p} Driving Voltage**
10	14.5	15.5
16	13.3	13.7
20	13.6	10.9
27	10.1	10.7
30	10.1	10.6

Remark: At 30 kHz, the HV power amplifier impedance obtained from a network analyser was varied between 11 Ω to 12 Ω.

Table 5.6: Transducer Impedance.

Frequency (kHz)	**Driving Voltage (V_{p-p})**	**Test Resistance (Ω)**
15.99	18	154
15.78	60	203
15.63	190	295
27.86	18	29.4
27.50	60	35.2
26.68	190	65.9

Remark: At 30 kHz, the HV amplifier impedance obtained from a network analyser was varied between 9.4 Ω to 14.5 Ω.

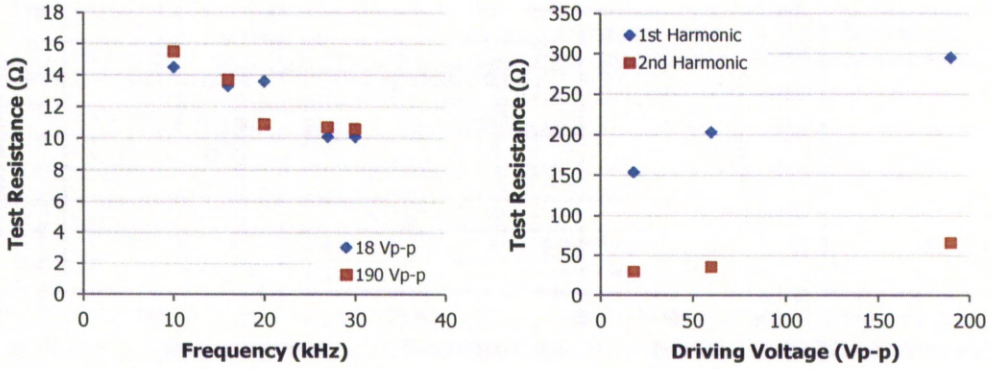

(a) (b)

Figure 5.11: Impedance of (a) HV Amplifier and (b) Transducer.

5.3.4 Selection of Impedance Matching Methods

Some results presented in Section 5.3.2 and Section 5.3.3 suggested that the electrical impedance between the excitation electronics and the proposed transducer might be mismatched. Thus, a study of impedance matching techniques suitable for the miniaturised USM was undertaken in order to maximise transmitted energy which would result in stronger resonances.

In general, there are two standard methods of ultrasonic transducer matching; using transformers and matching networks (Bowick, Blyler & Ajluni 2008; Carr 2000; Steer 2010). The classical and the simplest method is to use a transformer. The power transmitted to and from the transformer is the same but it can step voltage and current to different levels. The calculation for the transformer turns ratio is simple:

$$Turn\ Ratio = \sqrt{\frac{Load\ Resistance}{Source\ Resistance}} \qquad \text{Eq. 5-1}$$

The impedance matching transformer only matches the real part of the impedance (resistance). Since the impedance is the product of resistance and reactance (inductance and capacitance), if there is a large amount of the reactance in the load, the transformer cannot remove the reactive components so there will be power reflecting back to the signal generator and cause higher stresses on the generator components which usually results in heat.

For a simple type of impedance matching networks, the primary devices used in the networks are inductors and capacitors which are represented by the letter L and C, correspondingly. Therefore, they are frequently called LC circuits. There are numerous types of matching circuits. Therefore, they can be designed to match impedances more exactly than the transformer and in a desirable bandwidth. Unfortunately, they are generally more difficult to design and implement.

The means of using an impedance matching network is more preferable to a transformer for a miniature USM system. Axiomatic design presented in Chapter 3 suggested that simpler is better. The idea of using a transformer seemed to be easier but a simple type of networks could also be possible. In case of using a transformer, the transformer with a specified turn ratio was required but it was ruled out due to budget and time considerations. Also, the size of the transformer might not be as small as desirable. As for a matching circuit, all necessary electrical components are readily available.

Among a numbers of matching circuits (Carr 2000, 2002; Steer 2010) including L, T, and Pi-networks (they are named by the circuit topology between elements, capacitors and inductors, can look like the letter "L", "T", and "π"), one of L networks was chosen for the project. L-networks are two-element circuits. T and Pi-networks are three-element circuits. The advantages of Pi and T types are for narrow-band frequencies where a specific bandwidth can be specified. This option is preferred for radio frequency applications but it was decided that a specified bandwidth at a narrow frequency is not really necessary for USM and

the two-element circuit is simpler. There are four possible two-element L matching circuits as shown in Figure 5.12 where R_L is the load impedance (the impedance of the transducer), R_S is the source impedance (the impedance of the excitation circuit), X_L is inductive reactance, X_C is capacitive reactance, and Q is Q-factor (a measure of quality when inductance and capacitance are involved). The low-pass filter will allow all signals below a certain cut-off frequency to pass while blocking all others. A high-pass filter's action is opposite to the low-pass filter's response. The expressions can be;

$$X_L = 2\pi f L \qquad \text{Eq. 5-2}$$

$$X_C = \frac{1}{2\pi f C} \qquad \text{Eq. 5-3}$$

where f is the given frequency.

When the impedance of the transducer is significantly higher than the impedance of the excitation circuit, Carr (2000) and Garcia-Rodriguez et al. (2010) suggested the inverse-L network (see Figure 5.12(a)) can be chosen. However, at a narrow frequency or when the termination impedances are nearly the same, either low-pass or high-pass topology is feasible (Bowick, Blyler & Ajluni 2008; Carr 2002). Therefore, it was decided that high-pass low-hi L network (Figure 5.12(c)), used for matching low impedance source to high impedance load, would be used because the frequency below the cut-off frequency (around 16 kHz, data obtained from Table 5.6) was too low for USM.

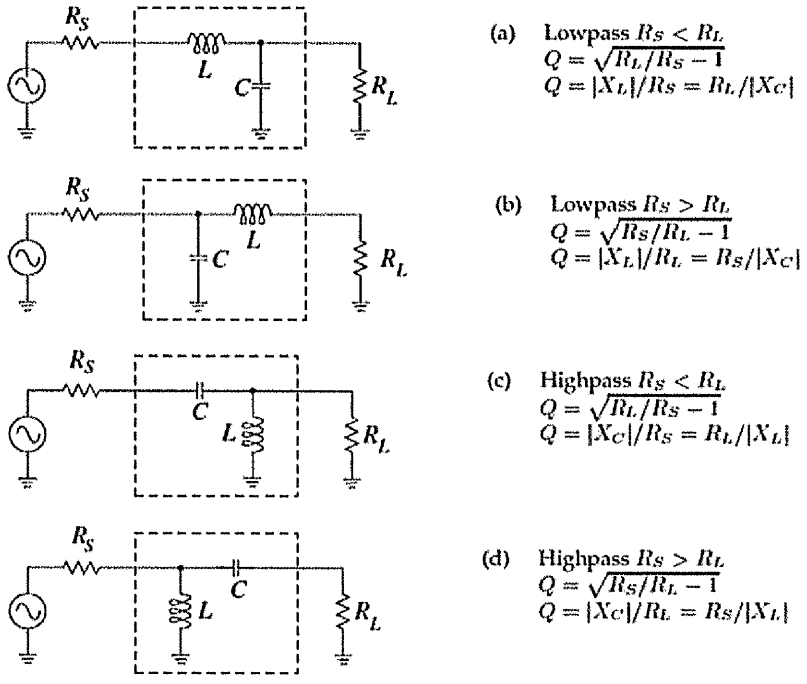

Figure 5.12: L Matching Circuits. Photos from (Steer 2010).

5.3.5 Displacement Amplitudes of Vibration

Unstable oscillations caused amplitude saturations for Prototype-II. The impedance mismatch was most likely to be the main reason for this problem. Techniques for matching electrical impedance in a high frequencies system and the selection of the type of matching circuits was reviewed and explained in Section 5.3.4. The impedance matching which is a property of a resonant or tuned circuit was designed to be an additional element for Prototype-II. Two matching circuits were applied. Firstly, it was proposed to match 10 Ω to 15 Ω input to 150 Ω to 300 Ω output at around 16 kHz. Secondly, some extra pieces of components were added for implementing at 27 kHz (30 Ω to 70 Ω output) in order to get another sampling point to study effects of the impedance matching circuits on the system. The impedance matching circuits were inductance-capacitance, LC, type which consisted of selectable series capacitors and shunt

inductors. At the resonant frequency around 16 kHz the circuit was designed to use the pair of capacitance C1 and inductance L2. Another pair of capacitance C4 and inductance L1 was used for the resonance at 27 kHz.

The vibration amplitudes generated from Prototype-II with and without the additional matching circuits were measured using the 1D-LDV. Although the voltage across the 27-Ω resistor was still irregular sine waveforms at high driving voltages and frequencies near resonance, the oscillations in the longitudinal axis were found to be sinusoidal. The vibration amplitudes measured at 1st and 2nd harmonic are shown in Figure 5.13 (a) and Figure 5.13 (b) respectively. Comparisons between Prototype-II assisted with and without the matching circuits are evident in the plots. Both figures show that the amplitude cannot be increased by applying the additional matching circuits. The amplitude saturation commenced at low power input of approximately 80 V. The vibration amplitude was higher and the system was simpler without the additional matching circuits.

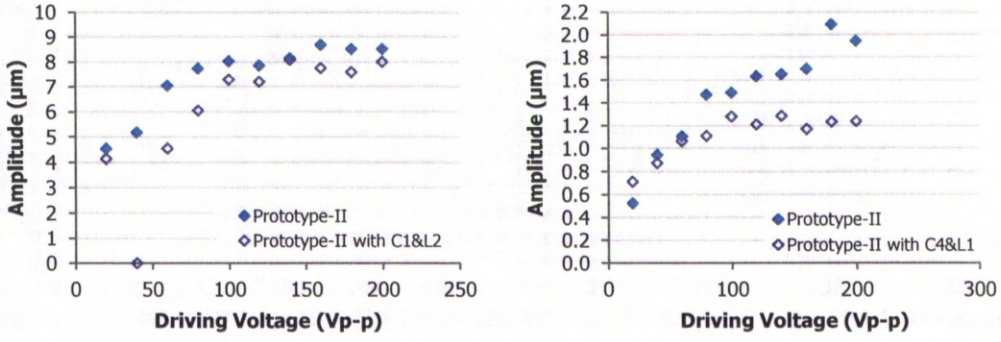

(a) At 1st Harmonic (b) At 2nd Harmonic

Figure 5.13: Effects of the Additional Impedance Matching Circuits.

5.3.6 Comparison of Displacement Amplitudes Generated from Various Shapes of Horns

Since there were limitations in time and budget for this investigation, it was decided that Prototype-II could be acceptably settled with the original design, without a matching circuit. The vibration amplitude generated from the butterfly-shape horn was compared with two conventional forms including stepped and conical horns. Both conventional horns were designed initially to reach their first longitudinal mode of resonance at an equivalent frequency with the novel horn. The experiments were set to drive the horns at the same conditions and equipment.

The vibration amplitudes obtained with a range of values of driving voltage are shown in Figure 5.14. The measured amplitude varied markedly from simulation results and such variations are very likely due to unstable and non-linear oscillations. It can be seen that the horn for Prototype-II exhibits vibration amplitude at around 20% greater than the stepped horn and more than 50% compared with the conical horn at the high levels of power input. The test results showed that the vibration amplitude produced from the stepped horn saturated very early (less than 20 V), while the butterfly-shape and conical horn experienced amplitude saturations at the exciting voltage around 80 V. Finally, this set of investigation implies that the ability of horns to cope with power handling is different.

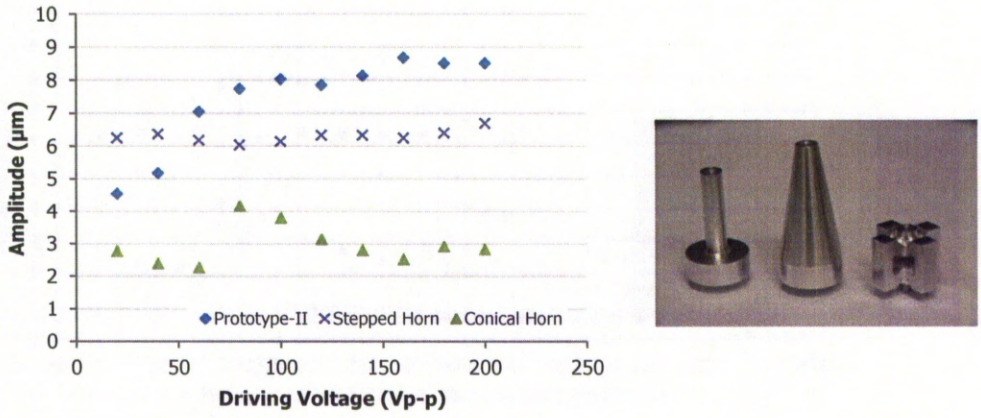

Figure 5.14: Displacement Amplitude Comparison of Different Horns.

5.4 Conclusions

The dynamic characteristics of Prototype-II assembled with the butterfly-shape horn were investigated and its electrical dynamic characteristics were studied. The results showed non-linearity behaviours. Vibrations generated from the system were not stable as the frequencies of resonance varied. The non-linearity behaviour was probably caused by electrical impedance mismatching. A means of matching electrical impedance was implemented but apparently it was not successful. The proposed additional impedance matching circuits did not seem to be beneficial to the system for maximising vibration amplitudes at resonances. Thus, it was decided to move on to the next step, machine testing, without any impedance matching system. From the experimental investigation of the dynamic characteristics of Prototype-II, the novel horn had a smaller size than conventional designs and showed higher amplification ratios under the same exciting conditions. However, the levels of amplitude were low due to the limited capacity of electrical components.

Chapter 6

Machine Performance Testing, Results, and Discussion

The machining performance of the novel USM system was observed and analysed scientifically using statistic tools and methods. Taguchi's method was chosen as a design of experiments tool in order to deal with a number of parameters involved when the experiments were conducted under the limits of time and resources. A statistics computer programme, MiniTAB, was used to generate the experiment plans and analyse the experimental results. The machining rates attained using the novel USM system on glass material was modelled empirically. A comparison between the empirical model and mathematical models proposed by other researchers as well as the comparison between the actual test results obtained using the novel USM system and a traditional USM system are also presented.

6.1 Experimental Designs

Using DOE to ensure robustness of a system follows a typical procedure (Logothetis & Wynn 1994). First, the problem needs to be defined. Then, output characteristics to be studied must be identified in order to determine the methods of measurement. After that, it is important to know which variables or factors affect the outputs and so the experimental range could be set at the appropriate levels for each factor. Next steps are the experiment plan set-up, data collection, and finally data analysis. All of these steps have been followed in the study of the machining performance of the proposed USM system.

For USM, a number of parameters are involved with its machining performance. In order to study the USM system efficiently, those parameters and

the machining performance need to be defined. Also, it is necessary to identify whether each machining parameter is controllable or uncontrollable. Usually, the performance of USM is evaluated by MRR and surface roughness (Ra). In this investigation, the MRR was calculated from the volume cut by a given cutting time and the surface roughness was measured using a white light interferometer. The controllable and uncontrollable parameters would be called control and noise factors. Typical parameters influencing on USM were presented in Figure 2.1 and discussed through MRR calculations Eq. 2-1 to Eq. 2-9. Some of these parameters and the levels of test will be explained in subsections of this chapter. Orthogonal arrays, a type of fractional factorial designs, proposed by Taguchi were chosen for experiment plans. The plans were, in practice, constructed using statistical software, MiniTAB, which was also used for data analysis.

6.2 Descriptions of Machining Set-up

6.2.1 Pilot experimentation

At the first attempt, the parameters affecting USM machining performance are presented in Table 6.1. These parameters and their levels of interest were set for the machining tests before the determination of dynamic characteristics of the system was completed. The work-piece materials, abrasive materials and sizes, and tool materials were chosen based on available resources. The selection of abrasive slurry concentrations, tool geometries, and static feeding forces was made to match the range of the values typically used as summarised in Section 2.2. The tool sizes were set at the beginning of the project to machine a size of 5 mm x 5 mm maximum. The amplitude of vibration was expected to set at the minimum, medium, and maximum of the possible levels. An L36 orthogonal array, a mixed-level design with nine factors (four factors at 2 levels and five factors at 3 levels) was used to generate the experimental plan. If a full factorial design was chosen, the number of experiments for all possible combinations

could be $2^4 \cdot 3^5 = 3888$ runs without a replication. Using the L36 orthogonal array the number of experiments was reduced to 36 runs. The noise in experimentation was the frequency of vibration since it had to be tuned to resonance during the operations.

Table 6.1: Parameters Affecting USM Performance Used for Pilot Experiments.

Control Factor		Level 1	Level 2	Level 3	Response
WM	Work-piece material	Glass	Al_2O_3		MRR
AM	Abrasive material	Al_2O_3	SiC		
AS	Abrasive size	#220	#320	#600	Surface
AC	Slurry concentration	15% wt.	25% wt.	50% wt.	roughness
TG	Tool geometry	Rectangle	Square	Round	
TS	Tool size	2 mm	5 mm		
TM	Tool material	Mild steel	Stainless steel		
SF	Static feeding force	0.5 kg	1 kg	1.5 kg	
VA	Vibration amplitude	@18V	@ 100V	@ 190V	
Noise					
Frequency of vibration					

The set-up of pilot experimentation is shown in Figure 6.1. The work-piece was fixed at the station and the tool moved downward following the guide pins under a constant weight. By this means, the static feeding force could be controlled by the given dead-weights on top of the tool. The abrasives were mixed with water in a bottle, and the abrasive slurry was squirted to the cutting zone at the beginning of each test and at a given interval. The system was kept running and machining the work-piece at resonance controlled manually by monitoring a 1-Ω test resistor connected to the electrical system circuit. The test resistor of 1 Ω was used to replace the 27 Ω to have less effect on the system. In order to determine the machining rate, it could be either the time for machining a certain depth of cut, or measuring of the depth of cut for a given duration. In practice, a fixed time was adopted based on convenience consideration as it is easier to conduct the entire experiment.

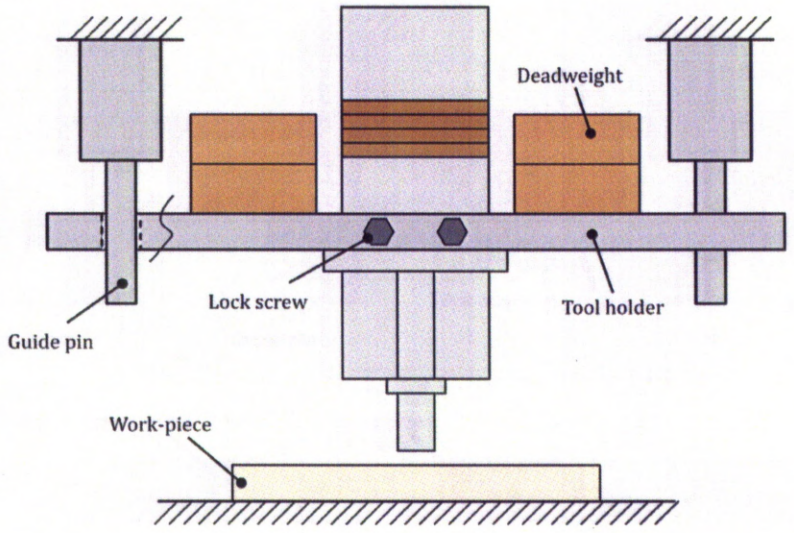

Figure 6.1: Set-Up of Pilot Experimentation.

The machining time for experiment was decided after a few pilot experiments. For the first few trials, the duration of each experiment was set to be no longer than 1 hour. The edges of the cut could not be seen clearly on the aluminium oxide ceramic work-pieces, so it was assumed that the ceramics were unable to be machined even it was run at the highest power. Besides, at 20-V driving voltage, neither alumina (Al_2O_3) nor glass work-piece could be machined. The resonant frequencies of the system with 2-mm tool bits were very fuzzy and later it was found that the fuzzy responses were caused by loosened screw joint. More tightening could not be helpful since it might risk breaking the tool bit and even breaking the horn. Also, the structure of the circular tool bits was difficult to be tightened firmly onto the horn. To solve the problems related to the tool bits, some modifications of the transducer and tool bits were required. Unfortunately, the decision was made to withdraw 2-mm

tool bits from the experimentation because the limitation of time for modifications.

Some parameters could not be involved actively in the experiments with the reasons explained above, so the final list of parameters was updated and shown in Table 6.2. For the second attempt, the control factors were reduced to six at two levels. The work material was glass only. The circular tool geometry and the tool bits of 2 mm were disregarded from the experimental plans because of assembly difficulty. The system prototype was run at the highest level, 190 V. This enabled the generation of sine waveforms from the signal generator. Three levels of the slurry concentration were reduced to two levels which was equal to the numbers of levels of other control factors to simplify the experiment plan. A fractional factorial experiment plan of 32 runs with 2 replications was used to reduce the number of all possible combinations of $2^6 = 64$ runs (128 runs if 2 replications was required). From the idea obtained at the first attempt to determine the proper duration of each experiment, each experiment was stopped after 30 minutes of cutting; otherwise the cutting time was recorded if the work-piece was cut through in less than 30 minutes.

Table 6.2: Parameters of Interest Affecting USM Performance.

Control Factor		Level 1	Level 2	Response
AM	Abrasive material	Al_2O_3	SiC	MRR
AS	Abrasive size	#220	#600	
AC	Slurry concentration	25% wt.	50% wt.	Surface
TG	Tool geometry	Rectangle	Square	roughness
TM	Tool material	Mild steel	Stainless steel	
SF	Static feeding force	1.0 kg	1.5 kg	
Noise				
Frequency of vibration				

After 8 experiments were conducted, it was decided to stop the experiments because there were signs that the tests could have been set

improperly. The MRRs of each condition were shown in Table 6.3. The tool bit sometimes got stuck or was unable to go deeper into the work-piece, for example, Experiment No.7-1. The same experiment was repeated as Experiment No.7-2, the machining speed was faster, but after 20 minutes the tool bit got stuck again. Moreover, the difference of machining rates was extraordinarily wide as shown in Figure 6.2. After further investigations, it was found that there was misalignment of the tool movement as illustrated in Figure 6.3. The plate holding the tool was unable to move vertically downwards following the guide pins. Due to the existence of this problem, it was necessary to modify the set-up in order to eliminate unsteady outputs.

Table 6.3: MRRs Determined Using the Set-up of Pilot Experimentation.

No.	AM	AS	AC	TG	TM	SF	MRR (mm^3/min.)
1	SiC	#220	15%	Square	SUS	1.0 kg	0.23
2	SiC	#220	15%	Rectangle	Mild	1.0 kg	0.52
3	SiC	#220	15%	Rectangle	Mild	1.0 kg	0.43
4	SiC	#220	15%	Square	SUS	1.0 kg	0.18
5	SiC	#220	50%	Square	Mild	1.5 kg	4.58
6	SiC	#220	50%	Rectangle	SUS	1.5 kg	1.12
7-1	SiC	#220	50%	Square	Mild	1.5 kg	2.58
7-2	SiC	#220	50%	Square	Mild	1.5 kg	3.74
8	SiC	#220	50%	Rectangle	SUS	1.5 kg	3.28

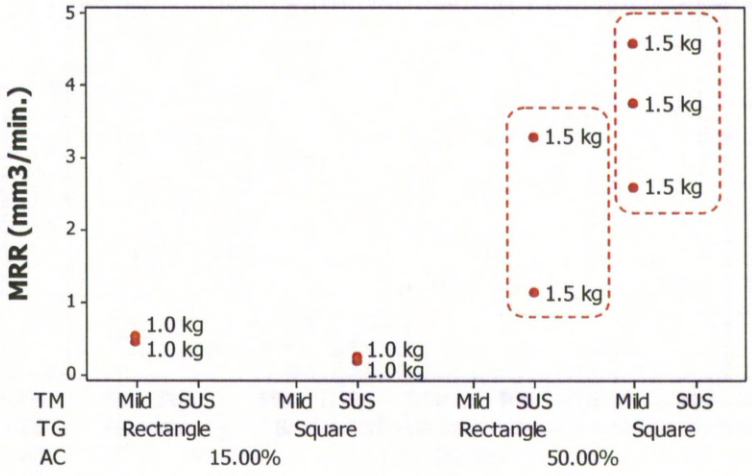

Figure 6.2: Value Plot of MRRs From Pilot Experimentation.

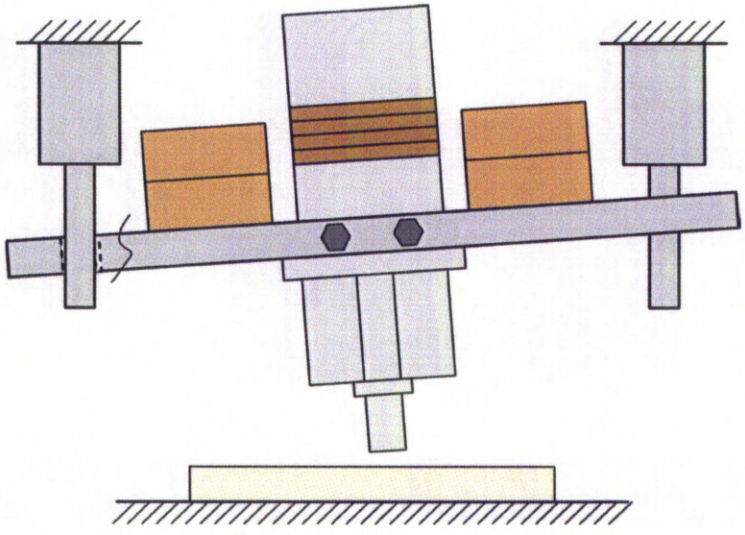

Figure 6.3: Unaligned Tool Movement.

6.2.2 Modification of the Tool Holder and Full Experimentation

Several ideas for improving the set-up for machining experiments were considered. Using three guide pins instead of two pins was one of the solutions. It was expected that the structure could be more balanced throughout the tool holding plate. To replace the guide holes on the tool holding plate with frictionless bush bearings was also considered. However, either solution was not practical given the time constraints. Moving the work material to a fixed tool was also the considered. Unfortunately, the friction of the joints of the available lift table (a scissor jack as shown in Figure 6.4) was too high. The minimum force necessary to resist the friction, when the force was sufficient to move the top plate, was higher than the minimum static feeding force required for the experiments. Accordingly, a final decision, using dead weights combining with pulleys and the profiled rail linear guide to direct the movement of the tool, was the most preferable method. The modified set-up is shown in Figure 6.5. The minimum dead weight was equal to the sum of the friction, which occurred between the sliding plate and the guide plate, and the weight of the guide plate. Any additional weights placed on top of the minimum dead weights could be equivalent to the static feeding force. In this way, the static feeding force was also controlled easily by changing the weight or numbers of the dead weights.

Figure 6.4: Modification of the Set-Up.

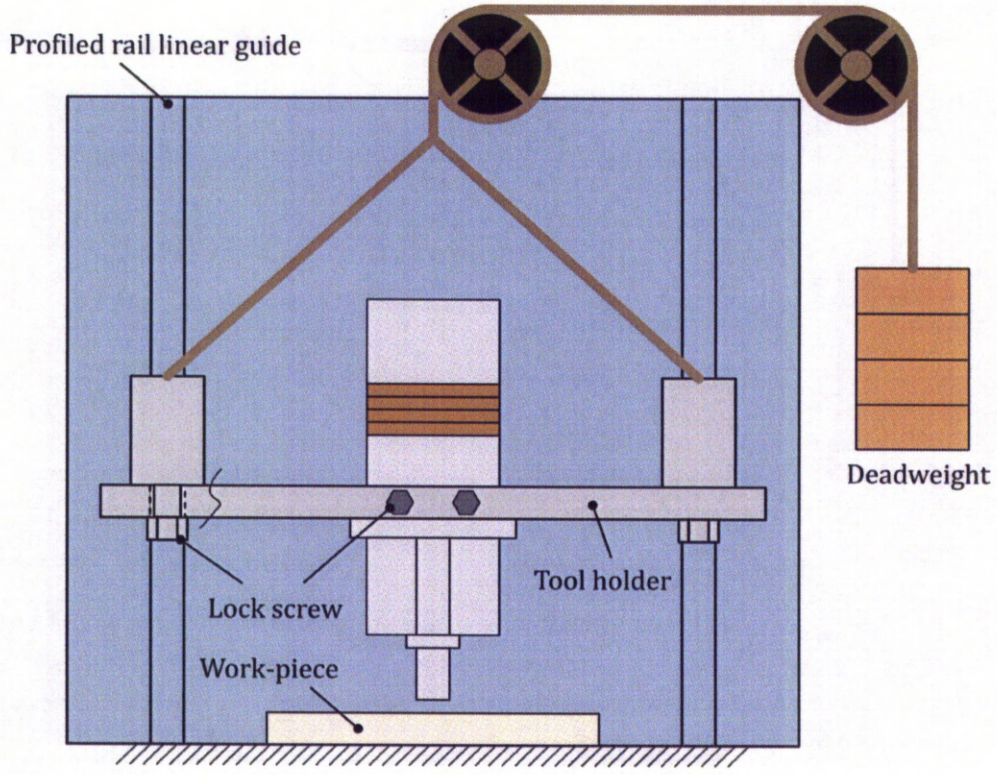

Figure 6.5: Modification of the Set-Up.

Finally, the full experimentation was conducted using the set-up as shown in Figure 6.5. The levels of the static feeding force were changed from 1.0 kg and 1.5 kg to 0.5 kg and 1.5 kg respectively. This is because the pilot experimentation showed that it was fairly difficult to adjust the driving frequency to resonance at both 1.0 kg and 1.5 kg. The reduction of 1.0 kg to 0.5 kg was expected to solve the issue of tuning and the load of 1.5 kg was kept under consideration because it seemed to have a major influence in increasing machining rates. The experimental plan of 32 runs was repeated without further incidents. The experimental results are shown in Table 6.4. The analysis of the experimental results will be explained in Section 6.3.

Table 6.4: MRRs Determined Using the Full Experimental Set-up.

No.	AM	AS	AC	TG	TM	SF	MRR (mm^3/min.)	Ra (μm)
1	SiC	#220	25%	Square	SUS	0.5 kg	0.095	1.63
2	Al_2O_3	#600	50%	Square	SUS	1.5 kg	0.026	0.82
3	Al_2O_3	#600	25%	Square	Mild	0.5 kg	0.133	0.41
4	Al_2O_3	#220	25%	Square	Mild	1.5 kg	0.674	0.94
5	Al_2O_3	#220	50%	Square	SUS	0.5 kg	0.292	2.20
6	Al_2O_3	#220	50%	Rectangle	Mild	0.5 kg	0.595	1.58
7	SiC	#220	25%	Rectangle	Mild	0.5 kg	0.557	1.10
8	SiC	#600	25%	Rectangle	Mild	1.5 kg	0.008	0.88
9	SiC	#600	25%	Square	SUS	1.5 kg	0.004	1.44
10	SiC	#600	50%	Rectangle	SUS	0.5 kg	0.026	0.75
11	Al_2O_3	#600	25%	Rectangle	SUS	0.5 kg	0.126	0.81
12	Al_2O_3	#220	50%	Square	SUS	0.5 kg	0.163	1.59
13	SiC	#220	25%	Rectangle	Mild	0.5 kg	0.493	1.80
14	Al_2O_3	#600	50%	Square	SUS	1.5 kg	0.088	1.10
15	SiC	#600	25%	Rectangle	Mild	1.5 kg	0.000	1.53
16	Al_2O_3	#220	25%	Rectangle	SUS	1.5 kg	0.097	1.31
17	Al_2O_3	#600	25%	Rectangle	SUS	0.5 kg	0.134	0.57
18	SiC	#220	25%	Square	SUS	0.5 kg	0.191	0.61
19	SiC	#220	50%	Square	Mild	1.5 kg	0.256	0.81
20	SiC	#220	50%	Rectangle	SUS	1.5 kg	0.145	1.44
21	Al_2O_3	#220	50%	Rectangle	Mild	0.5 kg	0.479	0.62
22	SiC	#600	50%	Square	Mild	0.5 kg	0.141	0.62
23	SiC	#600	25%	Square	SUS	1.5 kg	0.030	1.05
24	Al_2O_3	#600	50%	Rectangle	Mild	1.5 kg	0.012	1.35
25	SiC	#220	50%	Square	Mild	1.5 kg	0.261	1.87
26	Al_2O_3	#220	25%	Square	Mild	1.5 kg	0.203	1.28
27	Al_2O_3	#600	25%	Square	Mild	0.5 kg	0.068	0.56
28	SiC	#600	50%	Rectangle	SUS	0.5 kg	0.333	0.96
29	SiC	#220	50%	Rectangle	SUS	1.5 kg	0.195	0.84
30	Al_2O_3	#600	50%	Rectangle	Mild	1.5 kg	0.025	0.96
31	SiC	#600	50%	Square	Mild	0.5 kg	0.259	0.73
32	Al_2O_3	#220	25%	Rectangle	SUS	1.5 kg	0.044	0.91

6.3 Machining of Glass Using the Novel Design

6.3.1 Statistical Analysis

Statistical tools used for the analysis of the experimental results are explained in this section. The significant level, α, used throughout this chapter is 0.05. The objectives of using DOE to study the USM machining performances are given as follows;

- To determine the parameters affecting the mean process performance: Normal probability plot of residual was a clear and understandable tool for this analysis. Both parameters and parameter interactions that were not normally distributed would be seen readily from the straight line indicating normality of the data.
- To determine the parameters influencing performance variability: The variability of the outputs indicates the quality of the system. A system with low variability and robustness has the potential for improvement to a desired value. The statistical analysis tool used for this purpose was signal-to-noise ratio (S/N).
- To determine the parameter levels yielding the optimum performance, and whether further improvement is possible: These objectives were achievable by constructing analytical models such as regression modelling.

6.3.2 Determine the Parameters Affecting the Mean Process Performance

Since the factors of interest included both qualitative and quantitative values, they were converted to coded units before analysis. Each factor had only two levels, thus -1 and 1 were used to represent low and high levels, respectively. Table 6.5 shows coded and uncoded data.

Table 6.5: Coded vs Uncoded Data.

Coded Data	Uncoded Data					
	Abrasive Material	Abrasive Size	Abrasive Concentration	Tool Geometry	Tool Material	Feeding Force
-1	Al_2O_3	#600	25%	Square	Mild steel	0.5 kg
1	SiC	#220	50%	Rectangle	Stainless steel	1.5 kg

Figure 6.6, Figure 6.7, and Table 6.6 show the statistical analysis of the machining rates of cutting glass work-piece performed by the USM system. The normal plot (Figure 6.6) shows that tool materials, abrasive sizes, static feeding forces, and the combination of tool materials and abrasive sizes affected the MRR significantly, while the standardised effects of other parameters and interactions lie on the normal slope. Also, these significant factors and interaction were also highlighted by ANOVA (Table 6.6) as their P-values were very small. Alternatively, the significant factors and interaction showed steep slopes when the data were analysed using graphical methods such as main and interaction effects plots as shown in Figure 6.7.

The non-significant factors included abrasive materials, tool shapes, and slurry concentrations. It could be implied that the hardness of both silicon carbide and aluminium oxide was adequate for machining glass. The difference in tool shapes and variation of slurry concentrations had no significant effects on MRRs. It might be the results of the very low amplitude of vibration generated from the machining system and/or the method selected for feeding the abrasive slurry into the cutting zone. When the amplitude of vibration was very small, there was only small number of active abrasive grits operational in the machining gap. Also, for the selected method, the slurry might have less pressure to circulate and replace active abrasive particles in the machining gap.

Considering the significant effects, the smaller size of abrasives (grit no. 600) presented slower MRRs (compared with grit no. 220) agreed with previously known results (Davim & Jain 2008; Jain & Jain 2001; Kumar &

Khamba 2010). However, the effects of the tool materials and feeding forces appeared to be different. It was expected that using stainless steel as the material for a tool bit supposed to show higher MRRs than mild steel (Komaraiah & Reddy 1993; Kumar & Khamba 2010). From the properties of the materials point of view, the values of modulus of elasticity and hardness of the stainless steel (AISI 316L) are higher than the mild steel (AISI 1040) (Granta 2011). The low rates might be feasible when considering that the amplitude of vibration generated from the stainless steel tool bit is possibly smaller than from the mild steel tool bit due to the typical high damping characteristic of stainless steel. Also, in general, the MRR at the feeding force of 1.5 kg was expected to be higher than at 0.5 kg. The reason for low rates of machining at high static feeding force could be that the force of 1.5 kg might be higher than an optimum value for the system. Moreover, at the high level of feeding force, it was found very difficult to tune the system to resonance when the frequency of vibration was adjusted manually since the peak of the signal monitored could not be seen clearly. Contrary to the 1.5-kg load, at 0.5-kg, the system was able to be tuned without difficulty. In addition, the results suggested that the interaction between the tool materials and the sizes of abrasives had an effect on MRR. This means that the change of levels of these two parameters could influence the MRR.

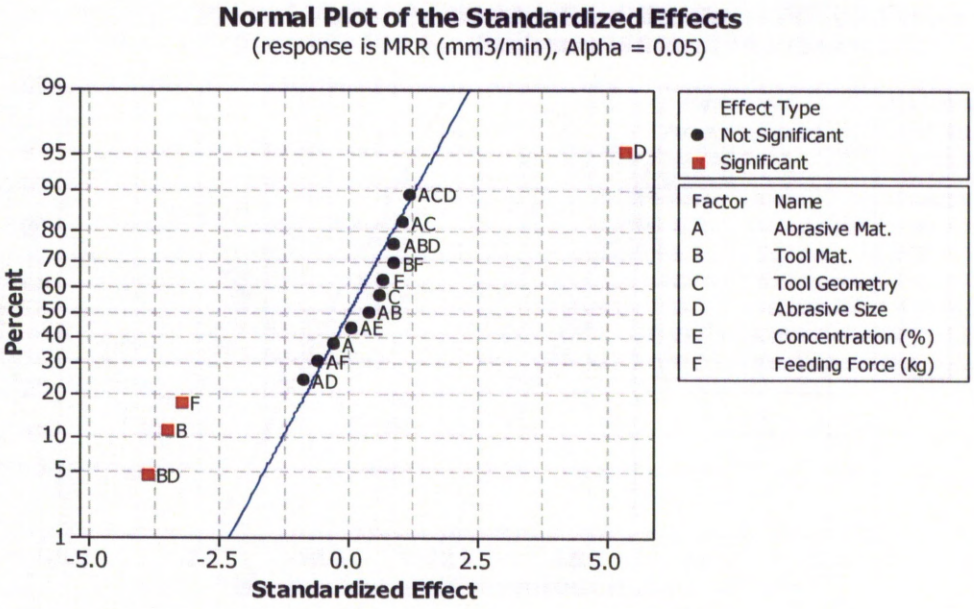

Figure 6.6: Normal Plot of Standardised Effects on MRR.

Table 6.6: ANOVA Table for MRR.

Analysis of Variance for MRR (mm3/min) (coded units)

Source	DF	Seq SS	Adj SS	Adj MS	F	P
Main Effects	6	0.63246	0.632460	0.105410	8.72	0.000
AM	1	0.00084	0.000837	0.000837	0.07	0.796
TM	1	0.14765	0.147654	0.147654	12.21	0.003
TG	1	0.00461	0.004612	0.004612	0.38	0.546
AS	1	0.34618	0.346185	0.346185	28.62	0.000
AC	1	0.00591	0.005909	0.005909	0.49	0.495
SF	1	0.12726	0.127264	0.127264	10.52	0.005
2-Way Interactions	7	0.22130	0.221304	0.031615	2.61	0.053
AM*TM	1	0.00215	0.002152	0.002152	0.18	0.679
AM*TG	1	0.01352	0.013525	0.013525	1.12	0.306
AM*AS	1	0.00925	0.009250	0.009250	0.76	0.395
AM*AC	1	0.00004	0.000038	0.000038	0.00	0.956
AM*SF	1	0.00438	0.004377	0.004377	0.36	0.556
TM*AS	1	0.18239	0.182393	0.182393	15.08	0.001
TM*SF	1	0.00957	0.009569	0.009569	0.79	0.387
3-Way Interactions	2	0.02766	0.027657	0.013829	1.14	0.343
AM*TM*AS	1	0.00991	0.009911	0.009911	0.82	0.379
AM*TG*AS	1	0.01775	0.017746	0.017746	1.47	0.243
Residual Error	16	0.19352	0.193520	0.012095		
Pure Error	16	0.19352	0.193520	0.012095		
Total	31	1.07494				

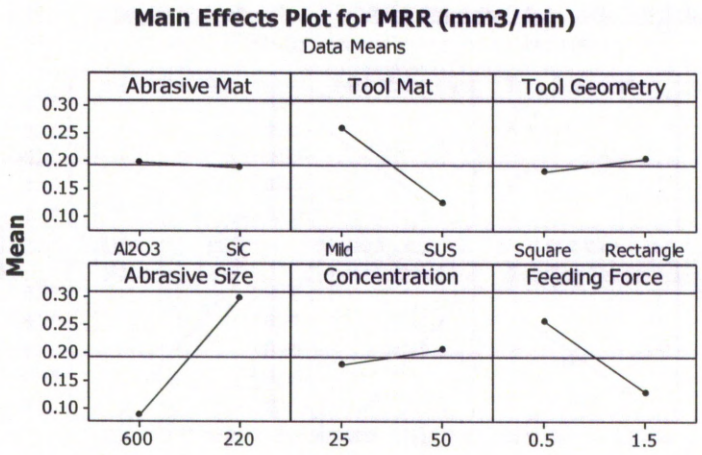

(a) Main Effects Plot

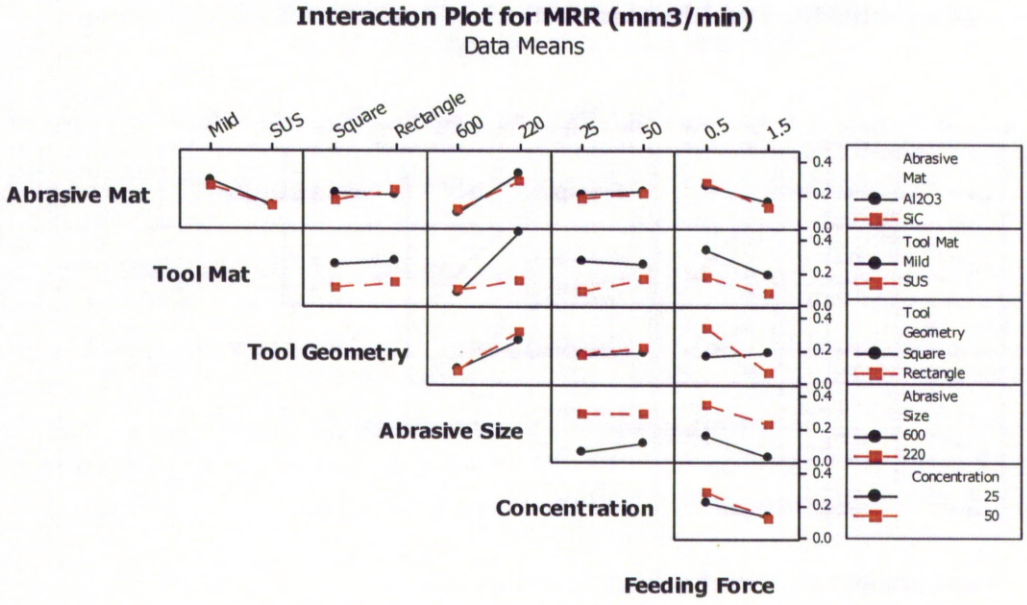

(b) Interaction Plot

Figure 6.7: Plots of Means of MRRs.

The surface roughness, Ra, was used to describe the quality of the machined surfaces which was one parameter chosen to determine the performance of the USM system. The normal plot (Figure 6.8) and ANOVA (Table 6.7) show that the sizes of abrasives, and the interaction between the abrasive materials and slurry concentrations, had a significant impact on the roughness of the machined surfaces. It was notable that all parameters relating with abrasives influenced the surface roughness, individually or interactively. Figure 6.9 (a) shows the main effects plot of the data means where increasing abrasive sizes affected the surface roughness sharply. This was commonsense because, at every hit, a bigger size of abrasives would cause more damages on the work-piece (Thoe, Aspinwall & Wise 1998). The interaction effects plot (Figure 6.9 (b)) also suggested that even though the types of abrasives and the slurry concentrations had insignificant effects on the Ra, whenever both of them were interacted, the value of surface roughness might be difficult to control.

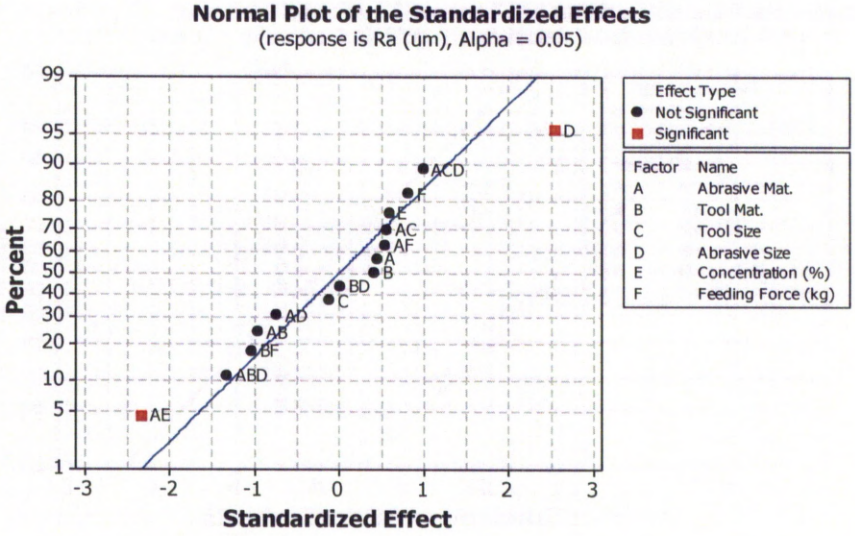

Figure 6.8: Normal Plot of Standardised Effects on Ra.

Table 6.7: ANOVA Table for Ra.

Analysis of Variance for Ra (um) (coded units)

Source	DF	Seq SS	Adj SS	Adj MS	F	P
Main Effects	6	1.37133	1.37133	0.22855	1.32	0.303
AM	1	0.03515	0.03515	0.03515	0.20	0.658
TM	1	0.03139	0.03139	0.03139	0.18	0.676
TG	1	0.00193	0.00193	0.00193	0.01	0.917
AS	1	1.12047	1.12047	1.12047	6.49	0.022
AC	1	0.06238	0.06238	0.06238	0.36	0.556
SF	1	0.12000	0.12000	0.12000	0.69	0.417
2-Way Interactions	7	1.46346	1.46346	0.20907	1.21	0.352
AM*TM	1	0.15417	0.15417	0.15417	0.89	0.359
AM*TG	1	0.05524	0.05524	0.05524	0.32	0.580
AM*AS	1	0.09071	0.09071	0.09071	0.53	0.479
AM*AC	1	0.92937	0.92937	0.92937	5.38	0.034
AM*SF	1	0.05267	0.05267	0.05267	0.30	0.588
TM*AS	1	0.00008	0.00008	0.00008	0.00	0.983
TM*SF	1	0.18122	0.18122	0.18122	1.05	0.321
3-Way Interactions	2	0.47272	0.47272	0.23636	1.37	0.283
AM*TM*AS	1	0.29858	0.29858	0.29858	1.73	0.207
AM*TG*AS	1	0.17413	0.17413	0.17413	1.01	0.330
Residual Error	16	2.76374	2.76374	0.17273		
Pure Error	16	2.76374	2.76374	0.17273		
Total	31	6.07125				

The plot of Ra and MRR is shown in Figure 6.10. Overall the data was scattered. Other researchers (Davim & Jain 2008; Jain & Jain 2001; Komaraiah et al. 1988; Kumar & Khamba 2010) noted that higher MRR was associated with inferior surface finish. For this project, the range of MRR evolved under investigation might be too narrow for its trend to be revealed clearly whilst the other researchers had studied the relationship for a wider range. Besides, there might only be a few abrasive particles actively hammering the work when the average particle diameter was greater than the vibration amplitude, so the MRRs might increase by the effects of some other parameters and made the correlation unclear. However, when the size of abrasives was proven statistically that it was the only parameter affecting both Ra and MRR, the means of data affected by abrasive sizes were reviewed (shown as a dash arrow in Figure 6.10). When the finer abrasive grit size was applied, it seemed to produce lower machining rates and smoother surfaces; when the abrasive was bigger, the response seemed to

spread into a bigger area but showed faster rates of machining and rougher surfaces.

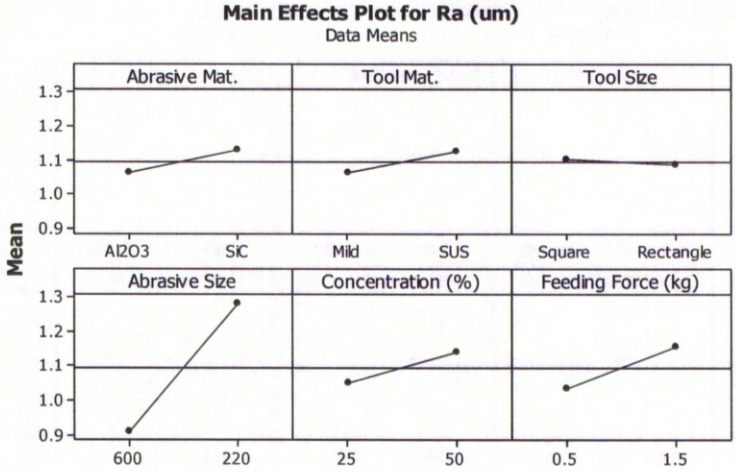

(a) Main Effects Plot

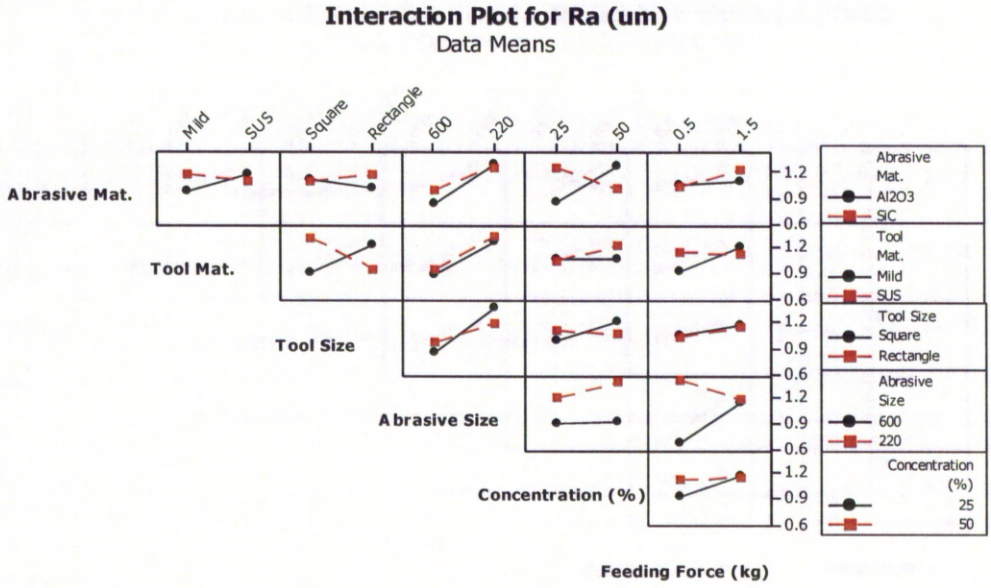

(b) Interaction Plot

Figure 6.9: Plots of Data Means of Ra.

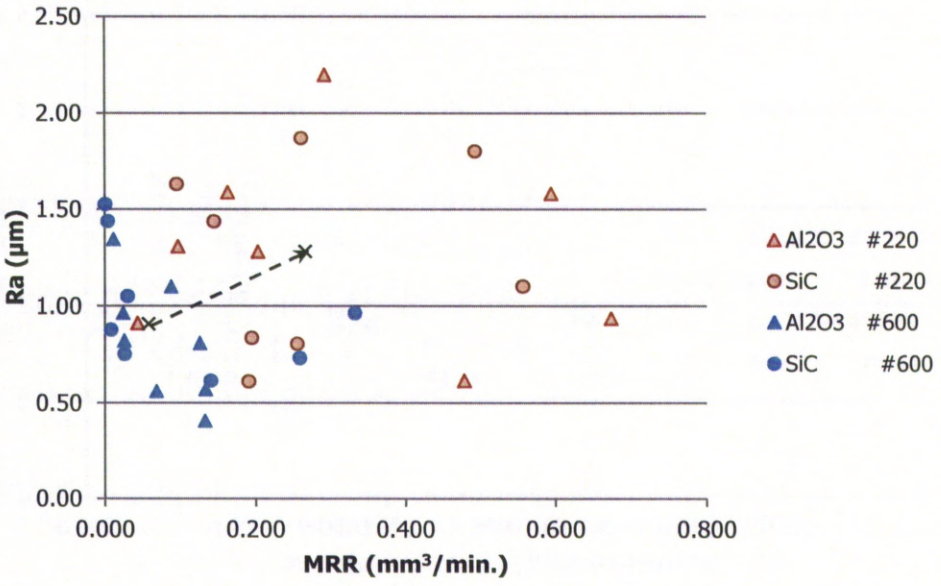

Figure 6.10: Plot of Ra vs MRR.

6.3.3 Determine the Parameters Influencing Performance Variability

To analyse the performance variability of the proposed system, Signal-to-Noise Ratio, S/N, a performance statistic devised by Taguchi, was used for this purpose. In a general term, S/N is the ratio of the mean (μ) to the standard deviation (σ) of a signal or measurement;

$$S/N = \frac{\mu}{\sigma} \qquad \text{Eq. 6-1}$$

The S/N ratios suggested by Taguchi are shown in Table 6.8 (Lawson & Erjavec 2001). The use of the ratios is dependent on the characteristics of the data y_i. s is the standard deviation of the data set, and n is the number of data in the set.

Table 6.8: Taguchi's S/N Ratios.

Characteristic	S/N Ratio
Nominal is Best	$10\ log_{10}\left(\frac{\bar{y}^2}{s^2}\right)$
Smaller the better	$-10\ log_{10}\left(\frac{\sum y_i^2}{n}\right)$
Larger the better	$-10\ log_{10}\left(\frac{\sum\left(1/y_i^2\right)}{n}\right)$

The MRR data was analysed using MiniTab and the results were given in Figure 6.11. For the S/N ratios of MRR, Figure 6.11 (a) shows that abrasive size and feeding force were distinct from the others in terms of their significant effects on MRR. Also, Figure 6.11 (b) shows that the abrasive size and feeding force had high impact with low variation on the MRR. Besides, it is evident from the plot that, when low variability of MRR is expected, the USM system would be operating with grit no. 220 aluminium oxide mixed with water to 50% weight ratio and a static feeding force of 0.5 kg.

Figure 6.12 shows the analysis of variability of the surface roughness. In this case, the abrasive size and static feeding force were the major parameters affecting the variability of surface roughness. The choice of using grit size no. 600 aluminium oxide mixed with water to 25% concentration and static feeding force of 0.5 kg is suitable for repeatedly producing a fine surface.

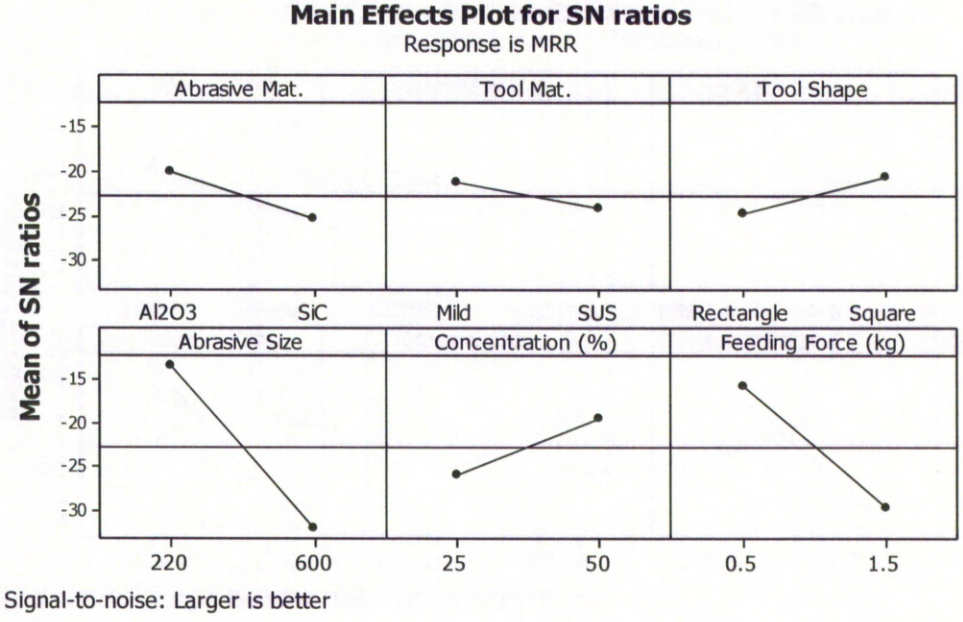

(a) Main Effects Plot

Response Table for Signal to Noise Ratios
Larger is better

Level	Abrasive Mat.	Tool Mat.	Tool Shape	Abrasive Size	Concentration (%)	Feeding Force (kg)
1	-20.02	-21.33	-24.77	-13.38	-25.97	-15.78
2	-25.47	-24.16	-20.72	-32.11	-19.52	-29.71
Delta	5.45	2.83	4.04	18.73	6.46	13.92
Rank	4	6	5	1	3	2

(b) Response Table

Figure 6.11: Analysis of Variability of MRR.

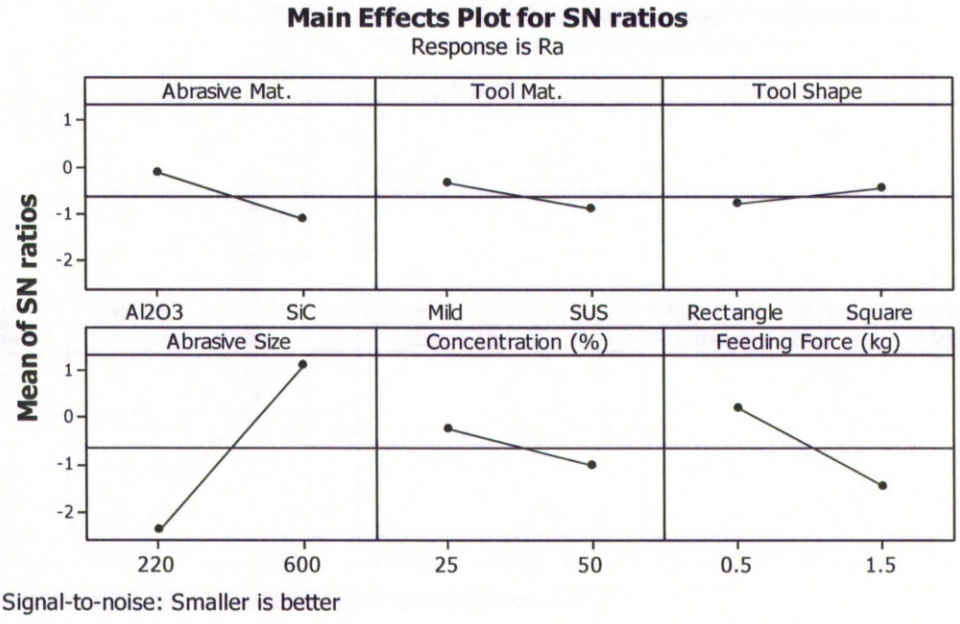

(a)Main Effects Plot

Response Table for Signal to Noise Ratios
Smaller is better

Level	Abrasive Mat.	Tool Mat.	Tool Shape	Abrasive Size	Concentration (%)	Feeding Force (kg)
1	-0.1348	-0.3649	-0.8013	-2.3936	-0.2409	0.1758
2	-1.1407	-0.9105	-0.4742	1.1182	-1.0346	-1.4513
Delta	1.0059	0.5456	0.3271	3.5118	0.7938	1.6271
Rank	3	5	6	1	4	2

(b) Response Table

Figure 6.12: Analysis of Variability of Ra.

6.3.4 Empirical modelling of MRR

In order to predict the MRR at combinations of factor settings which were not tested in the experiment, a predictive equation was developed. The equations for predicting the MRR in the form of Eq. 6-2 were constructed by regression analysis (Lawson & Erjavec 2001).

$$\hat{y} = b_0 + b_1x_1 + b_2x_2 + \cdots + b_kx_k + b_{12}x_1x_2 + b_{13}x_1x_3 + \cdots + b_{k-1,k}x_{k-1}x_k + b_{123}x_1x_2x_3 + \cdots \quad \text{Eq. 6-2}$$

where $\hat{y}$ is the predicted value of y, $x_{ijk\ldots}$ is the coded value for factor $i, j, k, \ldots$, and $b_{ijk\ldots}$ is the coefficients.

The coefficients of factors and interactions were taken from MiniTab shown in Table 6.9. In order to use the equation realistically, the coded values representing qualitative values needed to be converted to quantitative values. In this case, the qualitative factors consisted of abrasive material, tool material, and tool geometry. For the purpose of identifying types of materials, one property of materials was required to represent the material itself. According to the equations for predicting MRR summarised in Section 2.2, the hardness of materials were frequently used in machining process modelling. For the case of tool geometry, it was statistically verified that the difference in tool geometry had low effects on MRR. In addition, it was difficult to find a single index to represent the difference between geometries. For these reasons, the tool geometry was not a constituent of the MRR prediction equations. The process variables were converted to quantitative values as shown in Table 6.10.

Table 6.9: Estimated Effects and Coefficients for MRR.

Factorial Fit: MRR (mm3/min) versus AM, TM, TG, AS, AC, SF

Estimated Effects and Coefficients for MRR (mm3/min) (coded units)

Term	Effect	Coef	SE Coef	T	P
Constant		0.19231	0.01944	9.89	0.000
AM	-0.01023	-0.00511	0.01944	-0.26	0.796
TM	-0.13586	-0.06793	0.01944	-3.49	0.003
TG	0.02401	0.01200	0.01944	0.62	0.546
AS	0.20802	0.10401	0.01944	5.35	0.000
AC	0.02718	0.01359	0.01944	0.70	0.495
SF	-0.12613	-0.06306	0.01944	-3.24	0.005
AM*TM	0.01640	0.00820	0.01944	0.42	0.679
AM*TG	0.04112	0.02056	0.01944	1.06	0.306
AM*AS	-0.03400	-0.01700	0.01944	-0.87	0.395
AM*AC	0.00217	0.00109	0.01944	0.06	0.956
AM*SF	-0.02339	-0.01170	0.01944	-0.60	0.556
TM*AS	-0.15099	-0.07550	0.01944	-3.88	0.001
TM*SF	0.03459	0.01729	0.01944	0.89	0.387
AM*TM*AS	0.03520	0.01760	0.01944	0.91	0.379
AM*TG*AS	0.04710	0.02355	0.01944	1.21	0.243

S = 0.109977 PRESS = 2.76100
R-Sq = 82.00% R-Sq(pred) = 0.00% R-Sq(adj) = 65.12%

Table 6.10: Coded vs Uncoded Data.

Coded Data	Uncoded Data				
	Abrasive Material	Abrasive Size	Slurry Concentration	Tool Material	Feeding Force
-1	1630 HV (Al_2O_3)	9.3 µm (#600)	25%	208 HV (Mild steel)	0.5 kg
1	2450 HV (SiC)	58 µm (#220)	50%	195 HV (Stainless steel)	1.5 kg

The predictive equation for MRR is given as Eq. 6-3.

$$\widehat{MRR_A} = 0.192 - 0.005(AM) - 0.068(TM) + 0.104(AS) + 0.014(AC) \quad \text{Eq. 6-3}$$
$$- 0.063(SF) + 0.008(AM)(TM) - 0.017(AM)(AS)$$
$$+ 0.001(AM)(AC) - 0.012(AM)(SF) - 0.076(TM)(AS)$$
$$+ 0.017(TM)(SF) + 0.018(AM)(TM)(AS)$$

where $\widehat{MRR}_A$ is the predicted value of MRR when all factors are considered. AM, TM, AS, AC and SF are the coded values of the abrasive material, tool material, abrasive size, abrasive slurry concentration, and static feeding force.

It would be more meaningful to rewrite Eq. 6-3 in the form of uncoded values:

$$\widehat{MRR}_A = 0.192 - 0.005(AM) - 0.068\left(\frac{H_T - 201.5}{6.5}\right) \qquad \text{Eq. 6-4}$$

$$+ 0.104\left(\frac{D_A - 33.7}{24.4}\right) + 0.014\left(\frac{C - 37.5}{12.5}\right) - 0.063\left(\frac{F_S - 1}{0.5}\right)$$

$$+ 0.008\left(\frac{H_A - 2040}{410}\right)\left(\frac{H_T - 201.5}{-6.5}\right)$$

$$- 0.017\left(\frac{H_A - 2040}{410}\right)\left(\frac{D_A - 33.7}{24.4}\right)$$

$$+ 0.001\left(\frac{H_A - 2040}{410}\right)\left(\frac{C - 37.5}{12.5}\right)$$

$$- 0.012\left(\frac{H_A - 2040}{410}\right)\left(\frac{F_S - 1}{0.5}\right)$$

$$- 0.076\left(\frac{H_T - 201.5}{-6.5}\right)\left(\frac{D_A - 33.7}{24.4}\right)$$

$$+ 0.017\left(\frac{H_T - 201.5}{-6.5}\right)\left(\frac{F_S - 1}{0.5}\right)$$

$$+ 0.018\left(\frac{H_A - 2040}{410}\right)\left(\frac{H_T - 201.5}{-6.5}\right)\left(\frac{D_A - 33.7}{24.4}\right)$$

where H_A = Hardness of the abrasive material (HV)

H_T = Hardness of the tool material (HV)

D_A = Mean diameter of abrasive particles (μm)

C = Concentration of abrasive slurry (%)

F_S = Static feeding force (kg)

However, generally only significant factors and interactions are taken into account to form a predictive model because the changes of levels of insignificant parameters have less consequence to an outcome and the equation can be simpler. Based on MRR analysis discussed in Section 6.3.2, the abrasive size, feeding force, tool material, and the interaction between tool material and abrasive size were found to be statistically significant. From the coefficients obtained from Table 6.9, the coded predictive equation for MRR when only significant variables involved could be written as

$$\widehat{MRR_S} = 0.192 - 0.068(TM) + 0.104(AS) - 0.063(SF) - 0.076(TM)(AS) \quad \text{Eq. 6-5}$$

where $\widehat{MRR_S}$ is the predicted value of MRR when only significant factors are considered.

Eq. 6-5 can be written in an uncoded form as

$$\widehat{MRR_S} = 0.192 - 0.068\left(\frac{H_T - 201.5}{-6.5}\right) + 0.104\left(\frac{D_A - 33.7}{24.4}\right) - 0.063\left(\frac{F_S - 1}{0.5}\right) - 0.076\left(\frac{H_T - 201.5}{-6.5}\right)\left(\frac{D_A - 33.7}{24.4}\right) \quad \text{Eq. 6-6}$$

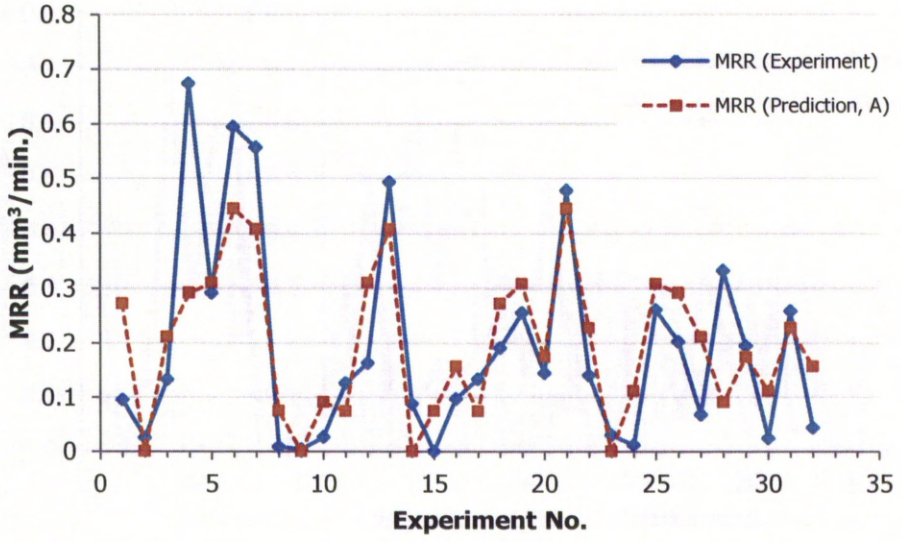

(a)

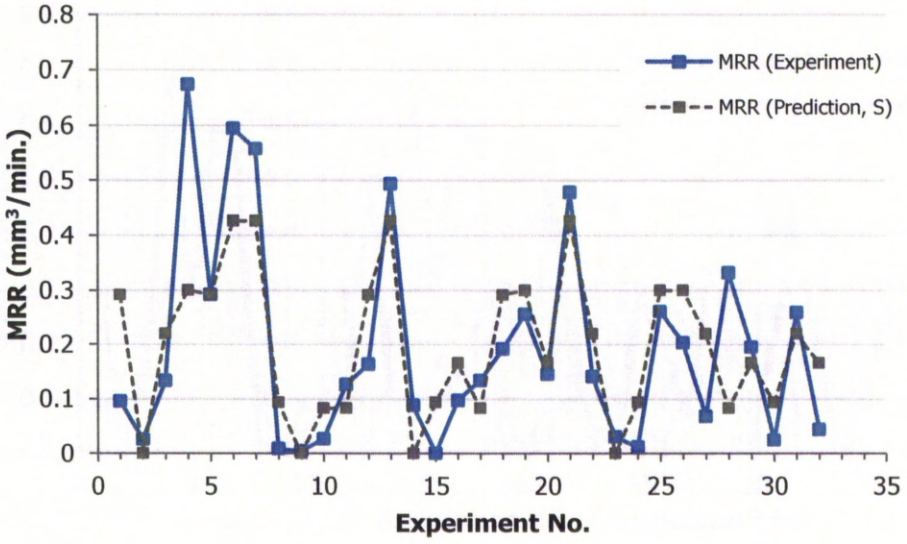

(b)

Figure 6.13: Comparison of Experiment Data with Model Predictions for MRR involved with (a) All Factors and (b) Only Significant Factors.

Figure 6.13 shows the comparison of MRRs obtained from experimentation and regression model. The MRRs predicted by the equation involving all factors (Eq. 6-4) and only the significant factors (Eq. 6-6) exhibit similar results which tend to agree with the experimental results. Eq. 6-6 was relatively simple so it was selected to be the equation for predicting MRR when using the USM for machining glass. To make the comparison between experimental and predicted result, Figure 6.14 shows the experimental MRRs that were arranged in ascending order and the margin of twice their standard deviation (indicated as dash lines) to compare with the predicted results at the same machining settings. The variation between the predicted and measured values was within the boundary of twice the standard deviation. Based on the standard normal distribution, it was 95% confident that the MRR might lie within this range if the experiments were repeated. Therefore, the model was a good fit.

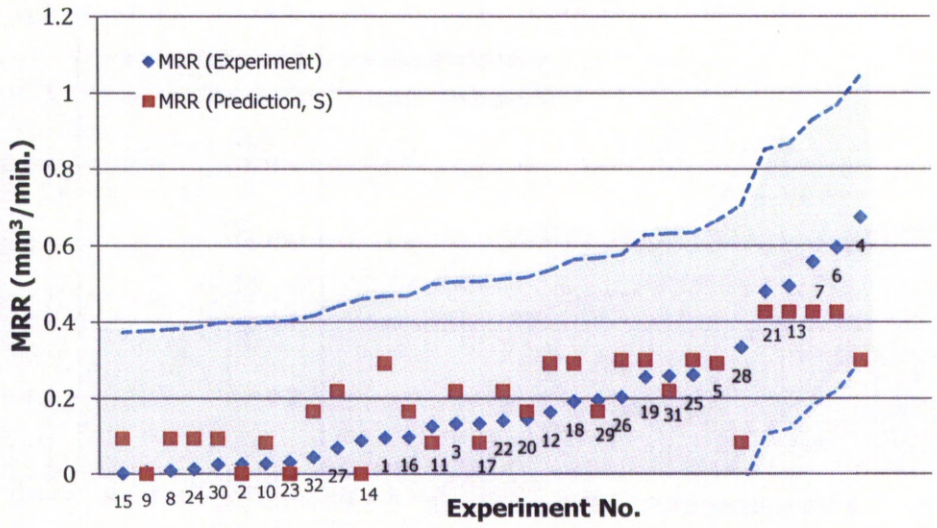

Figure 6.14: Variation between Predicted and Measured MRRs.

Another method to prove that the predicted model fitted experimental data was using statistical test. Chi-square test was suitable for this purpose (Reckase 2009). The MRRs obtained from Eq. 6-6 and experimentation were analysed. The analytical result is shown in Table 6.11. The P-value is high enough to conclude that the predicted and experimental MRRs were not significantly different. Accordingly, it was evaluated that the model adequately described the experimental data.

Table 6.11: Chi-Square Test of MRRs.

Chi-Square Goodness-of-Fit Test for Observed Counts in Variable: MRR

Using category names in Method

Category	Observed	Test Proportion	Expected	Contribution to Chi-Sq
Prediction	6.32681	0.5	6.24041	0.0011964
Experiment	6.15400	0.5	6.24041	0.0011964

N	DF	Chi-Sq	P-Value
12.4808	1	0.0023928	0.961

6.4 Comparison of the MRR

To make a comparison between the performance of the miniaturised USM system and typical USM systems, publications on machining rates obtained from mathematical models and experimentation were collected for evaluation. It was found that comparing MRR obtained from different sources were not a simple task. A direct comparison with experimental results performed by other researchers was fairly impractical because of difference in set-up and operating variables. The MRR might vary tremendously from extremely slow as 0.2 mm^3/min to tens mm^3/min (Kang et al. 2006; Komaraiah & Reddy 1993; Lee & Chan 1997) or up to hundreds mm^3/min (Boothroyd & Knight 1989; Dorf & Kusiak 1994; El-Hofy 2006; Singh 2007) depending on work-piece materials and settings.

Therefore, to compare the MRR from experimentations, the work of Komaraiah and Reddy (1993) was chosen as the key reference since their machining conditions (Table 6.12) were not so different from the conditions set in this project. Among the equations for calculating MRR, the publication of Wang and Rajurkar (1996) was chosen as another main reference. They selected glass as the work-piece material in their investigation. They made the comparison between MRR produced from their dynamic model, and other models and experimental results. Then, they claimed that their model showed good agreement with experimental results. More details on the work of Wang and Rajurkar (1996) as a reference will be explained later in this section.

Table 6.12: The Reference Machining Conditions

Parameter	Komaraiah and Reddy (1993)	Kainth, Nandy and Singh (1979)
Frequency (kHz)	22±3	25.5
Amplitude (μm)	40	62.5
Feeding force (kg)	0.5	0.93
Work material	Glass	Glass
Abrasive material	SiC	B_4C
Abrasive grit no.	220	Various sizes
Slurry concentration (% wt.)	28	16.8
Tool size (mm)	3	12.7
Tool material	Various types	Mild steel

The empirical model produced in Eq. 6-6 was modified for better forecasting the MRR under other machining conditions. Although, the machining speed was affected considerably by amplitude and frequency of vibration (as explained in Section 2.3), these two parameters were not covered in the predictive equation created in the previous section. Hence, the terms relating to amplitude, frequency, and the power of these parameters ($k1$ and $k2$), were added to Eq. 6-6. The modified MRR predictive equation is given as Eq. 6-8.

$$\widehat{MRR} = A_V^{k1} f_V^{k2} \cdot f(\text{variables involved machining}) \quad \text{Eq. 6-7}$$

$$\widehat{MRR} = A_V^{k1} f_V^{k2} (\widehat{MRR_S}) \quad \text{Eq. 6-8}$$

The values of $k1$ and $k2$ are summarised in Table 6.13. The models from Neppiras, Lee and Chan, Kazantsev and Rosenberg, and Komaraiah and Reddy were omitted from the consideration since their machining conditions were unsuitable for comparison. Neppiras (1964) stated that his model was not suitable to be applied when the feeding force was higher than an optimum value and amplitude of vibration was much smaller than the size of abrasives. The models from Kazantsev and Rosenberg (1965) and Komaraiah and Reddy (1993) had no amplitude of vibration which had a direct impact to MRR. Also, the model from Lee and Chan (1997) was created by studying the machining of ceramics which was greatly stronger than glass. The mathematical models from others including Shaw (1956) and Cook (1966) seemed to be neutral by various settings. However, Kainth, Nandy and Singh (1979) stated that Shaw's analysis did not agree with experimental results. Also, there was only little accessible information about the derivation of Cook's equation. Based on these reasons given, only the predictive equation presented by Wang and Rajurkar (1996) was selected as a main reference. Then, both $k1$ and $k2$ in Eq. 6-8 were chosen to be 8/5.

Table 6.13: List of $k1$ and $k2$.

$k1$	$k2$	Reference
$^3/_4$	1	Shaw (1956)
2	2	Neppiras (1964)
-	1	Kazantsev and Rosenberg (1965), Komaraiah and Reddy (1993)
$^1/_2$	1	Cook (1966)
$^8/_5$	$^8/_5$	Wang and Rajurkar (1996)
1	1	Lee and Chan (1997)

Figure 6.15 shows the extrapolation of MRR if the experiments were performed at vibration amplitude of 40 μm (no-loaded state) and frequency of around 22 kHz instead of 8.5 μm and 16 kHz, respectively. The figure shows that, by the association of the increments of amplitude and frequency of vibration, the MRR from each experiment conducted in this investigation could possibly increase further.

The values of each variable of interest can be substituted into Eq. 6-8 in order to compare the MRR in machining glass. The comparison with Komaraiah and Reddy (1993)'s results is shown in Figure 6.16. It can be seen that the miniaturised USM system had the potential to produce the rates of machining at 30% higher or more if it could operate at the same levels as the reference system. Another comparison was made with Kainth, Nandy and Singh (1979) as shown in Figure 6.17, the predicted MRR of the experimental USM system could only achieve half of their values. However, the hardness of glass used to produce the original plot of Kainth, Nandy and Singh (1979) was soft glass while glass supplied for this project was glass ceramic, which was significantly stronger than the soft type.

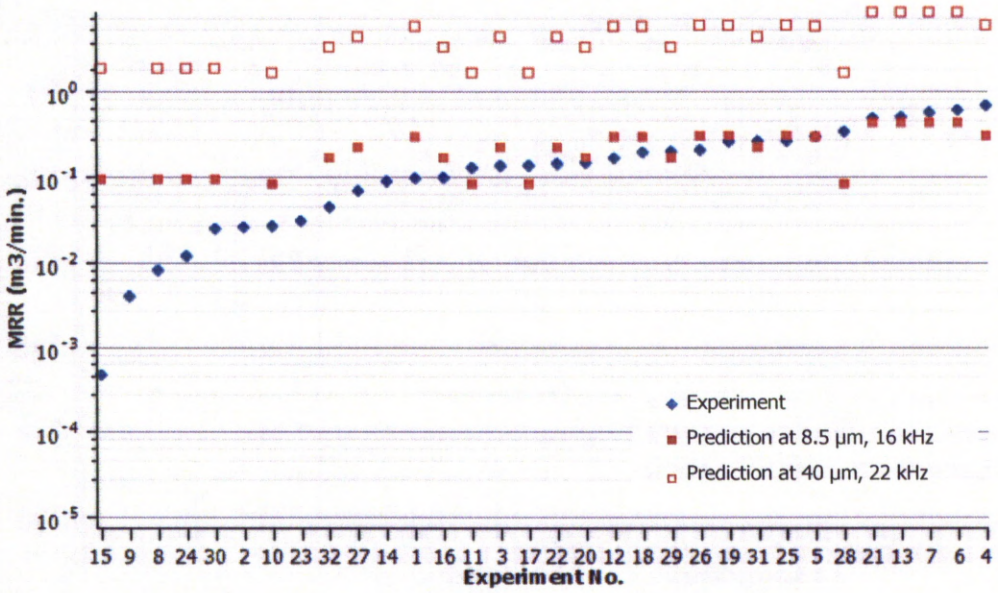

Figure 6.15: Models Comparison.

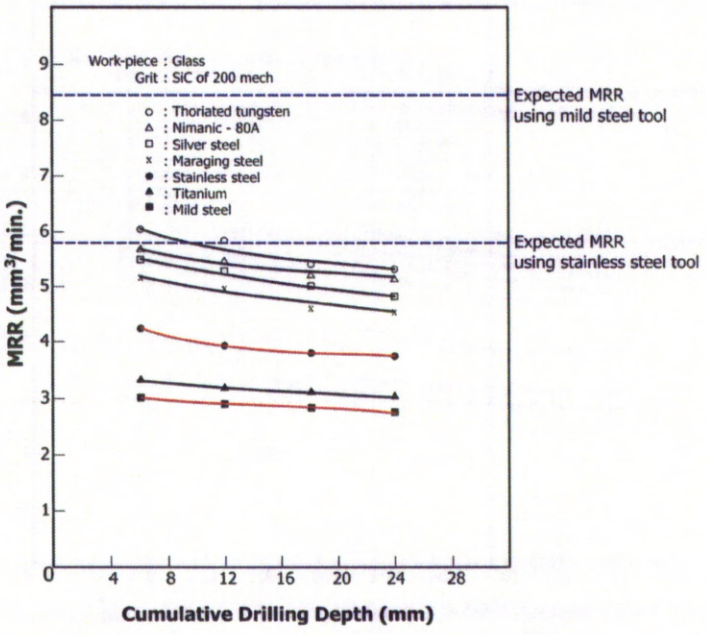

Figure 6.16: The Comparison of MRRs with Komaraiah and Reddy (1993).

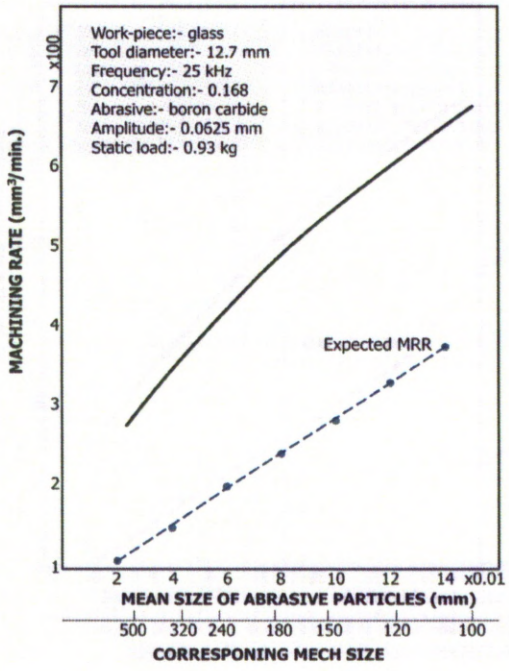

Figure 6.17: The Comparison of MRRs with Kainth, Nandy and Singh (1979).

6.5 Conclusions

It was remarkable that the mean of MRR obtained from pilot experimentation was significantly different from full experimentation as well as the variability of the data (Cf. Figure 6.18). The high MRR of pilot experimentation might be the result of high impacting force produced from the weight of the whole unit of tool and tool holder bouncing at high frequency but possibly lower than the given frequency because of damping. For the full experimentation, the tool was fixed rigidly. Therefore, the cutting action was only related to the displacement amplitude of the expansion and contraction of the tool end.

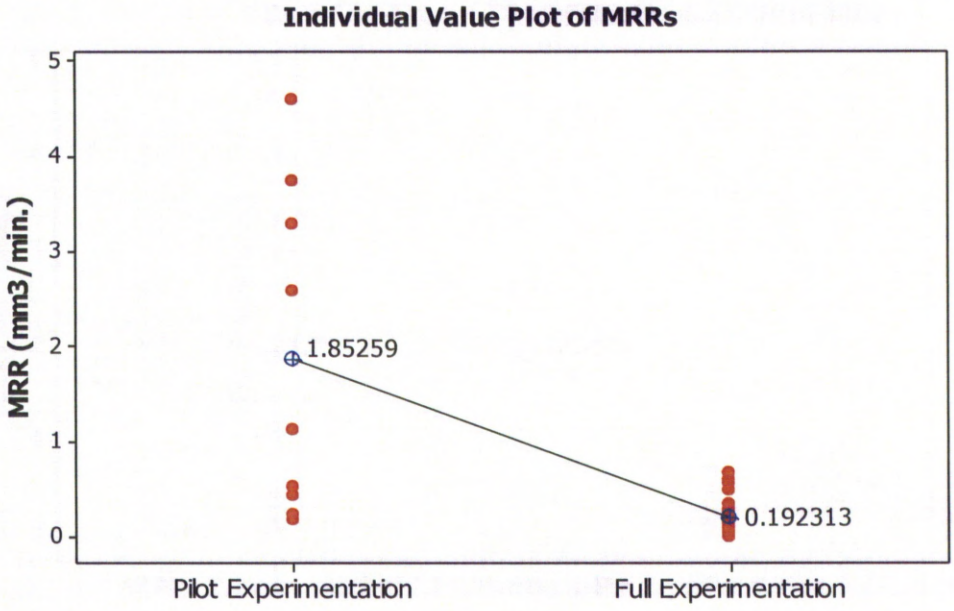

Figure 6.18: Comparison of MRR of Pilot and Full Experimentations.

Many advantages were gained with the assistance of statistical analysis methods in studying the performance a USM system with various parameters. Adequate information was obtained for a shorter duration to cope with time constraints. The MRR and surface roughness produced by the experimental USM system were investigated under the influence of abrasive materials, tool materials, tool geometries, abrasive sizes, abrasive slurry concentrations, and static feeding forces. The actual amplitude of vibration during machining was not measurable and uncontrollable. However, the amplitude was expected to be equivalent to the value measured at no-loaded condition. The amplitude had been kept at the highest level by manually tuning the excited frequency to resonance. In machining glass ceramic, tool materials, abrasive sizes, static feeding forces, and interaction between tool materials and abrasive sizes had

significant effects on MRR. Abrasive size is strongly correlated to surface roughness. Increasing rates of machining generally produced rougher surfaces.

The parameters influencing system performance variability were identified. Essentially, small abrasive sizes and low feeding forces tended to produce less process variability. A relatively simple predictive regression model for MRR was developed. An extrapolation of the model for predicting the MRR at other settings was also derived. It was also proposed that the experimental USM system had the potential to be competitive or achieve higher MRR compared with conventional USM systems.

Chapter 7

Conclusions and Recommendations for Future Work

7.1 Conclusions

USM is a non-conventional manufacturing process which utilizes vibrations for creating simple or complex cavities on a work-piece. It is very beneficial for machining extremely hard and brittle materials. The process will not generate any changes in microstructures, nor chemical, electrical, and physical properties to the work-piece. Comparing various types of non-conventional manufacturing processes, USM is one of the processes that consumes low levels of energy. Although USM has many advantages, its uses have been limited to material processing in laboratories or for specialist applications.

Nowadays, demands for miniaturisation of products are increasing because of sustainability and environment concerns. The miniaturised USM system produced in this investigation serves as a new candidate for meso/micro scale manufacturing which is normally supported by larger equipment.

The miniaturised system was designed following a number of scientific approaches. Design tools and techniques including AD, FEA, and DOEs were used for developing the system. AD was used for conceptual design. FEA was used to determine dynamic characteristics of the no-load USM system to reduce the number of prototyping stages. Statistical Analysis was applied in several stages of system development i.e. reducing the number of finite element computations, investigating machine characteristics of the prototypes, and developing the MRR prediction equation for using the proposed USM system in machining meso scale

geometries on glass material. The main achievements of this project are summarised in the following topics.

7.1.1 Axiomatic design of a miniaturised USM system

AD was used during the stage of conceptual design for understanding the complex relationships between the USM subsystems. However, it did not provide a solution for coupled components, so AD was only used for creating a framework for the design activities. AD was used for the analysis of the design of a USM proposed system and concluded that the driving unit and transducer were coupled. The coupled design indicated that the system was complicated. Design of electrical circuits and mechanical components required information from each other so the electrical circuits could be compatible to drive the mechanical components at a given level. Also, the impedance of electrical circuits and mechanical components needed to be matched in order to achieve strong excitations, so the designer needed to know the impedance of both main components in order to design a USM system that worked efficiently. Fortunately, the system could be developed as a decoupled design, if the matching system was designed separately. However, it was noted that the matching system needed to be powerful and adjustable in a wide range of impedance and frequency bandwidths.

7.1.2 Miniaturisation of a USM System and Prediction of its Dynamic Characteristics

The choice of miniaturised components for generating high power and high frequency signals was carried out. The developments of piezoelectric transformers were found interesting. However, the piezoelectric transformers for such high power level like USM application were not yet commercialised since they were developed by and under the rights of U.S. Navy and Agents, so they were impractically to be used as a component in this project. One of the

main electrical components, the power amplifier, was purposely designed and built in-house for the project.

FEA was used in the design of the transducer and the horn. Their dimensions were optimised with the aid of a statistical analysis method, i.e. response surface optimisation. By modelling and investigating characteristics of the prototypes, the results were used as a guide for tuning ultrasonic transducers and horns to a desired resonant frequency and amplitude.

- Shortening the length of an ultrasonic horn increases the longitudinal modal resonant frequencies of a system.
- Reducing the stiffness of an ultrasonic horn structure by creating cavities on a horn and reducing cross sectional area of a horn, decreases the longitudinal modal resonant frequencies of a system and increases the vibration amplitude.
- Reducing the speed of waves travelling in a horn material at microstructure levels due to impurity, imperfection, and porosity of materials, decreases both the frequencies and the amplitude.
- A long or thin section in a horn increases the number of resonant frequencies of a system and causes combinations of modes of vibrations at high frequencies which risk energy leak to a non-tuned mode. Higher amplitude of vibrations tends to develop at those sections but causes high stress concentrations which are the weakest points of the structure.

7.1.3 Investigation of Dynamic Characteristics of the Proposed USM System

The first prototype was made and its dynamic characteristics were measured. However, the horn was made of stainless steel powder by sintering instead of machining of rolled aluminium bar as the initial design. That was a

drawback regarding the resultant output. The dynamic properties of the sintered material especially at the ultrasonic range of frequency were confusing and seemed to be unsuitable for high excitation applications. Some experiments were performed to gain information to improve the computer modelling. Unfortunately, experimentation caused physical damages to the horn which strongly indicated that the SLM part was not suitable for dynamic applications.

A new prototype was designed in order to continue with the investigation. A new issue was found during the testing of the second prototype. The existence of non-linearity was detected and this was likely caused by impedance mismatching between the driving components and the transducer. In the event, the additional circuits for matching impedance were produced. Apparently, the proposed additional circuits had no relative advantage to the system. Therefore, the machine testing was conducted on glass material without a matching circuit.

7.1.4 Statistical Analysis of USM Process Parameters Affecting Machining Performance

Finally, the performance of the new USM system was investigated and compared with conventional systems. The USM process parameters for producing a meso-scale cavity on glass material were studied by considering material removal rates and surface roughness. Using statistical analysis methods, relevant information was extracted from fewer experiments. The statistical analysis results suggested that the important parameters affecting machining performance were tool materials, abrasive sizes, static feeding forces, and interaction between tool materials and abrasive sizes. Also, a predictive equation of machining rates for glass was proposed.

This work contributes to expanding the knowledge of USM for micro/meso manufacturing. The novel design showed a miniaturised system can be produced with the size of a horn being reduced by a half compared with conventional designs. It is a miniaturised system for micro/meso manufacturing

purposes and has the potential to be competitive or perform higher rates of machining compared with conventional systems.

7.2 Recommendations for Future Work

A novel miniaturised USM system had been designed and developed. Based on the experiments carried out and given the limitations imposed on the work, the performance of the miniaturised system was at least comparable to a conventional system. In addition, it has the potential to be further improved its performance. In order to achieve further improvements, future tasks on the following topics are required:

- **Improving the matching circuit for a miniaturised system.** The excitation levels could definitely be stronger if the electrical and mechanical components matched well. Different types of circuits or impedance matching techniques should be used and the values of inductor and capacitor involved should be adjustable in a wider range in order to support different transducer and horn designs.
- **Auto-tuning the exciting signal to the system resonance.** This is needed for a better design for machining performance improvement. The resonance frequency bandwidth of a USM system using piezoelectric material is reasonably narrow. Being off resonance will lower the effectiveness of a USM system. Adjusting the exciting frequencies manually is difficult in some conditions and a lack of sensitivity causes performance inconsistency. With the use of auto tracking of the resonant frequency, it could both simplify and improve the overall USM performance.
- **Increasing the variety of experiments.** The limitations on time and resources limited the number of experiments that could be carried out. Increasing the number of experiments is fundamental in taking this

work to the next level. Also, through the use of statistical design for experiments, the understanding of the USM process can be more profound if more factors and levels are taken into the experimentation. For example, the tests could be conducted for a couple of different machines, work materials, excitation levels, resonant frequencies, equipments set-ups, and slurry feeding methods, etc.

- **Integrating the components.** This thesis presented only the concept and possibility of miniaturisation of the electrical components and proposed novel ultrasonic horn designs. Further study could be made on the full integration of all of these components into a single system. Thus, the performance of the fully integrated system could be validated.
- **Testing of dynamic properties of common materials produced by additive manufacturing processes.** It was found difficult to gain information about properties of materials made by SLM. As the main-stream research in additive manufacturing is focused on producing fully dense or very complex objects, mechanical properties of objects made by additive manufacturing are rarely compared with those made by conventional cutting. It is therefore proposed that rigorous testing of parts made by additive manufacturing is essential for finite element analysis.

REFERENCES

Abdullah, A., Shahini, M. & Pak, A. (2009) 'An approach to design a high power piezoelectric ultrasonic transducer', *Journal of Electroceramics*, vol. 22, no. 4, pp. 369-382.

Adriaens, H.J.M.T.S., De Koning, W.L. & Banning, R. (2000) 'Modeling piezoelectric actuators', *Mechatronics, IEEE/ASME Transactions on*, vol. 5, no. 4, pp. 331-341.

Agilent Technologies (2009) *Agilent impedance measurement handbook: A guide to measurement technology and techniques*, Agilent Technologies, [Online], Available from: **http://cp.literature.agilent.com/litweb/pdf/5950-3000.pdf** (Accessed: 17 June 2009).

Agilent Technologies (2011) *The fundamentals of modal testing*, Agilent Technologies, [Online], Available from: **www.agilent.com/find/assist** (Accessed: 17 June 2009).

Ando, E.i. & Kagawa, Y. (1992) 'Finite-element simulation of transient heat response in ultrasonic transducers', *IEEE Transactions on Ultrasonics, Ferroelectrics, and Frequency Control*, pp. 432-440.

Antony, J. (2003) A systematic methodology for Design of Experiments, in, *Design of Experiments for Engineers and Scientists*, Butterworth-Heinemann, Oxford, pp. 29-43.

ASTM International (2004) *Standard test method for measuring vibration-damping properties of materials*, West Conshohocken.

Badescu, M., Bao, X., Bar-Cohen, Y., Chang, Z., Dabiri, B.E., Kennedy, B. & Sherrit, S. (2005a) Adapting the ultrasonic/sonic driller/corer for walking/climbing robotic applications, *Proceedings of SPIE - The International Society for Optical Engineering*, vol. 5762, ed. E.V. White, San Diego, CA, pp. 160-168.

Badescu, M., Bao, X., Bar-Cohen, Y., Chang, Z. & Sherrit, S. (2005b) Integrated modeling of the ultrasonic/sonic drill/corer - Procedure and analysis results, *Proceedings of SPIE - The International Society for Optical Engineering*, vol. 5764, ed. A.B. Flatau, San Diego, CA, pp. 312-323.

Bang, I.C. & Heo, G. (2009) 'An axiomatic design approach in development of nanofluid coolants', *Applied Thermal Engineering*, vol. 29, no. 1, pp. 75-90.

Bar-Cohen, Y., Chang, Z., Sherrit, S., Badescu, M. & Bao, X. (2005) The Ultrasonic/Sonic Driller/Corer (USDC) as a subsurface drill, sampler and lab-on-a-drill for planetary exploration applications, *Proceedings of SPIE - The International Society for Optical Engineering*, vol. 5762, pp. 152-159.

Bar-Cohen, Y., Sherrit, S., Bao, X., Badescu, M., Aldrich, J. & Chang, Z. (2007) Subsurface sampler and sensors platform using the ultrasonic/sonic driller/corer (USDC), vol. 6529, eds T. Masayoshi, Y. Chung-Bang & G. Victor, SPIE, p. 65290E.

Benedict, G.F. (1987) *Nontraditional Manufacturing Processes*, Marcel Dekker, Inc.

Benkirane, Y., Kremer, D. & Moisan, A. (1999) 'Ultrasonic machining: an analytical and experimental study on contour machining based on neural network', *CIRP Annals - Manufacturing Technology*, vol. 48, no. 1, pp. 135-138.

Bhalla, S. & Soh, C.K. (2004) 'Structural health monitoring by piezo--impedance transducers. II: Applications', *Journal of Aerospace Engineering*, vol. 17, no. 4, pp. 166-175.

Blitz, J. (1967) *Fundamentals of Ultrasonics*, 2nd edn, vol. Butterworths, London.

Boothroyd, G. & Knight, W.A. (1989) *Fundamentals of Machining and Machine Tools*, Marcel Dekker, New York.

Bowick, C., Blyler, J. & Ajluni, C. (2008) *RF Circuit Design*, 2nd Edition edn, Elsevier.

Boy, J., Andrey, E., Boulouize, A. & Khan-Malek, C. (2010) 'Developments in microultrasonic machining (MUSM) at FEMTO-ST', *The International Journal of Advanced Manufacturing Technology*, vol. 47, no. 1, pp. 37-45.

Boy, J.J., Aiguillé, M., Boulouize, A., Khan-Malek, C., Wolfgang, M., Stefan, D. & Bertrand, F. (2006) Developments in micro ultrasonic machining (MUSM), in, *4M 2006 - Second International Conference on Multi-Material Micro Manufacture*, Elsevier, Oxford, pp. 123-126.

Buchbinder, D., Schleifenbaum, H., Heidrich, S., Meiners, W. & Bültmann, J. (2011) 'High power selective laser melting (HP SLM) of aluminum parts', *Physics Procedia*, vol. 12, no. Part 1, pp. 271-278.

Bullen Inc. (2010) [Online], Available from: **http://www.bullentech.com** (Accessed: 14 May 2010).

Calderwood, J.H. (1968) High power ultrasonics, in, *Ultrasonics. Theory and Applications*, The English Universities Press, London, pp. 94-112.

Carazo, A.V. (2004) '50 Years of piezoelectric transformers. Trends in the technology', *Materials Research Society Symposium - Proceedings*, vol. 785.

Carazo, A.V. (2010) *Telephone Interview* 24 May 2010

Cardoni, A., Harkness, P. & Lucas, M. (2010) 'Ultrasonic rock sampling using longitudinal-torsional vibrations', *Ultrasonics*, vol. 50, no. 4-5, pp. 447-452.

Carr, J.J. (2000) *Secrets of RF Circuit Design*, McGraw-Hill Professional Publishing, Blacklick, OH, USA.

Carr, J.J. (2002) *RF Components and Circuits*, Oxford ; Newnes, 2002. 1st ed.

Cavique, M. & Gonçalves-Coelho, A.M. (2009) 'Axiomatic design and HVAC systems: An efficient design decision-making criterion', *Energy and Buildings*, vol. 41, no. 2, pp. 146-153.

Ceratec North America Corp. (2011) [Online], Available from: www.ceramtec.com (Accessed: 6 June 2011).

Chang, Z., Sherrit, S., Badescu, M., Bao, X. & Bar-Cohen, Y. (2005) Design and analysis of ultrasonic actuator in consideration of length-reduction for a USDC (Ultrasonic/Sonic Driller/Corer), *Proceedings of SPIE - The International Society for Optical Engineering*, vol. 5762, ed. E.V. White, San Diego, CA, pp. 72-79.

Chang, Z., Sherrit, S., Bao, X. & Bar-Cohen, Y. (2004) Design and analysis of ultrasonic horn for USDC (ultrasonic/sonic driller/corer), vol. 5388, ed. H.A. Eric, SPIE, pp. 320-326.

Claeyssen, F., Lhermet, N., Le Letty, R. & Bouchilloux, P. (1997) 'Actuators, transducers and motors based on giant magnetostrictive materials', *Journal of Alloys and Compounds*, vol. 258, no. 1-2, pp. 61-73.

Claeyssen, F., Lhermet, N. & Maillard, T. (2002) Magnetostrictive actuators compared to piezoelectric actuators, *Proceedings of SPIE - The International Society for Optical Engineering*, vol. 4763, eds B. Culshaw & P.F. Gobin, Presquile de Giens, pp. 194-200.

Clark, A.E. (1993) 'High power rare earth magnetostrictive materials', *Journal of Intelligent Material Systems and Structures*, vol. 4, no. 1, pp. 70-75.

Clark, N., Jr. (1954) 'An ultrasonic machine tool', *Ultrasonic Engineering, Transactions of the IRE Professional Group on*, vol. 2, no. 1, pp. 10-18.

Communities, C.o.t.E. (2009) *Communication from the Commission to the European Parliament, the Council, the European Economic and Social Committee and the Committee of the Regions*, Brussels

Cremer, L., Heckl, M. & Petersson, B.A.T. (2005) Damping, in, *Structure-Borne Sound*, Springer Berlin Heidelberg, pp. 149-235.

Dapino, M.J., Flatau, A.B. & Calkins, F.T. (2006) 'Statistical analysis of Terfenol-D material properties', *Journal of Intelligent Material Systems and Structures*, vol. 17, no. 7, pp. 587-599.

Davim, J.P. & Jain, V.K. (2008) Advanced (Non-traditional) Machining Processes, in, *Machining*, Springer London, pp. 299-327.

Dhilsha, K.R., Markandeyulu, G., Subrahmanyeswara Rao, B.V.P. & Rama Rao, K.V.S. (1997) 'Design and fabrication of a low frequency giant

magnetostrictive transducer', *Journal of Alloys and Compounds*, vol. 258, no. 1-2, pp. 53-55.

Dhilsha, R., Rajeshwari, P.M. & Rajendran, V. (2005) 'Advanced magnetostrictive materials for sonar applications', *Defence Science Journal*, vol. 55, no. 1, pp. 13-20.

Dorf, R.C. & Kusiak, A. (1994) *Handbook of Design, Manufacturing, and Automation*, Wiley.

Dubus, B., Haw, G., Granger, C. & Ledez, O. (2002) 'Characterization of multilayered piezoelectric ceramics for high power transducers', *Ultrasonics*, vol. 40, pp. 903-906.

Durmusoglu, M.B. & Kulak, O. (2008) 'A methodology for the design of office cells using axiomatic design principles', *Omega*, vol. 36, no. 4, pp. 633-652.

Egashira, K. & Masuzawa, T. (1999) 'Microultrasonic machining by the application of workpiece vibration', *CIRP Annals - Manufacturing Technology*, vol. 48, no. 1, pp. 131-134.

El-Haik, B. (2005) *Axiomatic Quality : Integrating Axiomatic Design with Six-Sigma, Reliability, and Quality Engineering*, Wiley, Hoboken, NJ, USA.

El-Hofy, H. (2006) *Fundamentals of Machining Processes: Conventional and Nonconventional Processes*, CRC/Taylor & Francis.

Ensminger, D. & Stulen, F.B. (2008a) Advanced designs of ultrasonic transducers and devices using finite element analysis, in, *Ultrasonics: Data, Equations and Their Practical Uses*, CRC PRESS, pp. 129-183.

Ensminger, D. & Stulen, F.B. (2008b) Properties of materials, in, *Ultrasonics: Data, Equations and Their Practical Uses*, CRC PRESS, pp. 285-322.

European Communities (2007) EU action against climate change, vol., [Online]. Available from: **http://ec.europa.eu/environment/climat/pdf/brochures/research_en.pdf** (Accessed: 14 August 2010).

Femto-st (2012) [Online], Available from: **http://www.femto-st.fr** (Accessed: 20 August 2012).

Fletcher, N.H. & Thwaites, S. (1992) 'Multi-horn matching plate for ultrasonic transducers', *Ultrasonics*, vol. 30, no. 2, pp. 67-75.

Fuji & Co. (2012) [Online], Available from: **http://www.fuji-piezo.com/** (Accessed: 26 April 2012).

Fuji Ceramics Corp. (2011).

Garcia-Rodriguez, M., Garcia-Alvarez, J., Yañez, Y., Garcia-Hernandez, M.J., Salazar, J., Turo, A. & Chavez, J.A. (2010) 'Low cost matching network for ultrasonic transducers', *Physics Procedia*, vol. 3, no. 1, pp. 1025-1031.

Gilmore, R. (1991) 'Ultrasonic machining: a case study', *Journal of Materials Processing Technology*, vol. 28, no. 1-2, pp. 139-148.

Giurgiutiu, V. & Rogers, C.A. (1997) 'Power and energy characteristics of solid-state induced-strain actuators for static and dynamic applications', *Journal of Intelligent Material Systems and Structures*, vol. 8, no. 9, pp. 738-750.

Göken, J., Bergmann, K., Baetz, W. & Steinhoff, K. (2006) 'Functional gradation of gear shafts made of cementation steel and its influence on damping and microstructure', *Materials Characterization*, vol. 57, no. 3, pp. 137-149.

Gonçalves-Coelho, A.M. & Mourão, A.J.F. (2007) 'Axiomatic design as support for decision-making in a design for manufacturing context: A case study', *International Journal of Production Economics*, vol. 109, no. 1-2, pp. 81-89.

Gooberman, G.L. (1968) *Ultrasonics: Theory and Application*.

Granta (2011) *Granta's CES EduPack*, Teaching resources for materials education.

Greenough, R.D. & Jenner, A.G.I. (1994) Rare earth-iron compounds for actuators and sensors, *Magnetic Materials for Sensors and Actuators (Digest No. 1994/183), IEE Colloquium on*, pp. 7/1-7/3.

Groover, M.P. (2011) Nontraditional machining and thermal cutting processes, in, *Principles of modern manufacturing*, 4th ed. edn, John Weiley & Sons, Inc., pp. 618-645.

Guzzo, P.L., Raslan, A.A. & De Mello, J.D.B. (2003) 'Ultrasonic abrasion of quartz crystals', *Wear*, vol. 255, no. 1-6, pp. 67-77.

Guzzo, P.L., Shinohara, A.H. & Raslan, A.A. (2004) 'A comparative study on ultrasonic machining of hard and brittle materials', *Journal of the Brazilian Society of Mechanical Sciences and Engineering*, vol. 26, no. 1, pp. 56-61.

Harris, R.W. (1970) 'Electromechanical analogies in acoustics', *Applied Acoustics*, vol. 3, no. 4, pp. 265-281.

Horsley, E.L., Foster, M.P. & Stone, D.A. (2007) State-of-the-art Piezoelectric Transformer technology, *Power Electronics and Applications, 2007 European Conference on*, pp. 1-10.

http://www.learnabout-electronics.org (2011) *Measuring impedance* [Online], Available from: **http://www.learnabout-electronics.org/ac_theory/impedance73.php** (Accessed: 19 March 2012).

Ichida, Y., Sato, R., Morimoto, Y. & Kobayashi, K. (2005) 'Material removal mechanisms in non-contact ultrasonic abrasive machining', *Wear*, vol. 258, no. 1-4, pp. 107-114.

International Organization for Standardization (2004) *Glass in building -- Glazing and airborne sound insulation -- Measurement of the mechanical impedance of laminated glass.*

Iula, A. (2009) 'Design and experimental characterization of a multifrequency flexural ultrasonic actuator', *Ultrasonics, Ferroelectrics and Frequency Control, IEEE Transactions on*, vol. 56, no. 8, pp. 1725-1730.

Iula, A., Parenti, L., Pappalardo, M. & Lamberti, N. (2005) A power ultrasonic actuator based on a displacement amplifier vibrating in flexural mode, *Ultrasonics Symposium, 2005 IEEE*, vol. 3, pp. 1534-1537.

Jahanmir, s., Ramulu, M. & Koshy, P. (1999) Ultrasonic machining of ceramics, in, *Machining of ceramics and composites*, Marcel Dekker, Inc., New York, pp. 483-524.

Jain, N.K. & Jain, V.K. (2001) 'Modeling of material removal in mechanical type advanced machining processes: a state-of-art review', *International Journal of Machine Tools and Manufacture*, vol. 41, no. 11, pp. 1573-1635.

Jain, N.K., Jain, V.K. & Deb, K. (2007) 'Optimization of process parameters of mechanical type advanced machining processes using genetic algorithms', *International Journal of Machine Tools and Manufacture*, vol. 47, no. 6, pp. 900-919.

Jalili, N. (2009) *Piezoelectric-based Vibration-control: from Macro to Micro/Nano Scale Systems*, Springer Verlag.

Jang, B.-S., Yang, Y.-S., Song, Y.-S., Yeun, Y.-S. & Do, S.-H. (2002) 'Axiomatic design approach for marine design problems', *Marine Structures*, vol. 15, no. 1, pp. 35-56.

Jianxin, D. & Taichiu, L. (2002) 'Ultrasonic machining of alumina-based ceramic composites', *Journal of the European Ceramic Society*, vol. 22, no. 8, pp. 1235-1241.

Juuti, J., Kordas, K., Lonnakko, R., Moilanen, V.P. & Leppavuori, S. (2005) 'Mechanically amplified large displacement piezoelectric actuators', *Sensors and Actuators A: Physical*, vol. 120, no. 1, pp. 225-231.

Kainth, G.S., Nandy, A. & Singh, K. (1979) 'On the mechanics of material removal in ultrasonic machining', *International Journal of Machine Tool Design and Research*, vol. 19, no. 1, pp. 33-41.

Kang, I.S., Kim, J.S., Seo, Y.W. & Kim, J.H. (2006) 'An experimental study on the ultrasonic machining characteristics of engineering ceramics', *Journal of Mechanical Science and Technology*, vol. 20, no. 2, pp. 227-233.

Kazantsev, V.F. & Rosenberg, L.D. (1965) 'The mechanism of ultrasonic cutting', *Ultrasonics*, vol. 3, no. 4, pp. 166-174.

Kellogg, R. & Flatau, A. (2004) 'Blocked-force characteristics of terfenol-D transducers', *Journal of Intelligent Material Systems and Structures*, vol. 15, no. 2, pp. 117-128.

Kellogg, R. & Flatau, A. (2008) 'Experimental investigation of terfenol-D's elastic modulus', *Journal of Intelligent Material Systems and Structures*, vol. 19, no. 5, pp. 583-595.

Kelton, W.D. (2000) Experimental design for simulation, *Simulation Conference, 2000. Proceedings. Winter*, vol. 1, pp. 32-38 vol.31.

Khairy, A.B.E. (1990) 'Assessment of some dynamic parameters for the ultrasonic machining process', *Wear*, vol. 137, no. 2, pp. 187-198.

Kim, S.-M., Wang, S. & Brennan, M.J. (2011) 'Dynamic analysis and optimal design of a passive and an active piezo-electrical dynamic vibration absorber', *Journal of Sound and Vibration*, vol. 330, no. 4, pp. 603-614.

King, T.G., Preston, M.E., Murphy, B.J.M. & Cannell, D.S. (1990) 'Piezoelectric ceramic actuators: A review of machinery applications', *Precision Engineering*, vol. 12, no. 3, pp. 131-136.

Kjær, B. (2011) *Product data Ometron Laser Doppler Vibrometer — Type 8329*, Brüel & Kjær Sound & Vibration Measurement,

Komaraiah, M., Manan, M.A., Narasimha Reddy, P. & Victor, S. (1988) 'Investigation of surface roughness and accuracy in ultrasonic machining', *Precision Engineering*, vol. 10, no. 2, pp. 59-65.

Komaraiah, M. & Narasimha Reddy, P. (1993) 'A study on the influence of workpiece properties in ultrasonic machining', *International Journal of Machine Tools and Manufacture*, vol. 33, no. 3, pp. 495-505.

Komaraiah, M. & Reddy, P.N. (1993) 'Relative performance of tool materials in ultrasonic machining', *Wear*, vol. 161, no. 1-2, pp. 1-10.

Kommepalli, H.K.R., Yu, H.G., Muhlstein, C.L., Trolier-McKinstry, S., Rahn, C.D. & Tadigadapa, S.A. (2009) 'Design, fabrication, and performance of a piezoelectric uniflex microactuator', *Microelectromechanical Systems, Journal of*, vol. 18, no. 3, pp. 616-625.

Kremer, D., Saleh, S.M., Ghabrial, S.R. & Moisan, A. (1981) 'The state of the art of ultrasonic machining', *CIRP Annals - Manufacturing Technology*, vol. 30, no. 1, pp. 107-110.

Kumar, J. & Khamba, J. (2010) 'Modeling the material removal rate in ultrasonic machining of titanium using dimensional analysis', *The International Journal of Advanced Manufacturing Technology*, vol. 48, no. 1, pp. 103-119.

Kumar, J., Khamba, J. & Mohapatra, S. (2009) 'Investigating and modeling tool-wear rate in the ultrasonic machining of titanium', *The International Journal of Advanced Manufacturing Technology*, vol. 41, no. 11, pp. 1107-1117.

Lamb, C. & Zecchino, M. (1999) *WYKO Surface profilers technical reference manual*, Report Number 980-085, Veeco Metrology Group,

Lawson, J. & Erjavec, J. (2001) Response surface methodology, in, *Modern statistics for engineering and quality improvement*, 1 edn, Duxbury, pp. 465-491.

Le Letty, R., Claeyssen, F., Lhermet, N. & Bouchilloux, P. (1997) New amplified piezoelectric actuator for precision positioning and active damping, vol. 3041, ed. M.E. Regelbrugge, SPIE, San Diego, CA, USA, pp. 496-504.

Lee, D.G. & Suh, N.P. (2005) *Axiomatic Design and Fabrication of Composite Structures : Applications in Robots, Machine Tools and Automobiles*, Oxford University Press, Cary, NC, USA.

Lee, T.C. & Chan, C.W. (1997) 'Mechanism of the ultrasonic machining of ceramic composites', *Journal of Materials Processing Technology*, vol. 71, no. 2, pp. 195-201.

Leo, D.J. (2007) *Engineering Analysis of Smart Material Systems*, John Wiley & Sons.

Lerch, R. (1990) 'Simulation of piezoelectric devices by two- and three-dimensional finite elements', *Ultrasonics, Ferroelectrics and Frequency Control, IEEE Transactions on*, vol. 37, no. 3, pp. 233-247.

Leu, M.C., Wu, J.C. & Liu, X.F. (2009) 'Axiomatic functional and object-oriented product design framework', *CIRP Annals - Manufacturing Technology*, vol. 58, no. 1, pp. 147-152.

Li, H., Lai, X., Li, C., Lin, Z., Miao, J. & Ni, J. (2008) 'Development of meso-scale milling machine tool and its performance analysis', *Frontiers of Mechanical Engineering in China*, vol. 3, no. 1, pp. 59-65.

Li, X., Wang, J. & Li, W. (2007) Current state and prospect of micro-machining, *Proceedings of the IEEE International Conference on Automation and Logistics*, pp. 1414-1419.

Liu, C. (2006) *Foundations of MEMS*, Pearson Prentice Hall.

Liu, H., Gopalkrishnan, V., Quynh, K. & Ng, W.-K. (2009) 'Regression models for estimating product life cycle cost', *Journal of Intelligent Manufacturing*, vol. 20, no. 4, pp. 401-408.

Liu, W., Zhou, L., Xia, T. & Yu, H. (2006) 'Rare earth ultrasonic transducer technique research', *Ultrasonics*, vol. 44, no. Supplement 1, pp. e689-e692.

Logothetis, N. & Wynn, H.P. (1994) *Quality Through Design: Experimental Design, Off-line Quality Control, and Taguchi's Contributions*, Oxford University Press, USA.

Louvis, E., Fox, P. & Sutcliffe, C.J. (2011) 'Selective laser melting of aluminium components', *Journal of Materials Processing Technology*, vol. 211, no. 2, pp. 275-284.

Masuzawa, T. (2000) 'State of the art of micromachining', *CIRP Annals - Manufacturing Technology*, vol. 49, no. 2, pp. 473-488.

McGeough, J.A. (1988) *Advanced Methods of Machining*, Chapman and Hall.

Melvin, J.W. & Suh, N.P. (2002) 'Simulation within the Axiomatic Design framework', *CIRP Annals - Manufacturing Technology*, vol. 51, no. 1, pp. 107-110.

Mercelis, P. & Kruth, J.-P. (2006) 'Residual stresses in selective laser sintering and selective laser melting', *Rapid Prototyping Journal*, vol. 12, no. 5, pp. 254-265.

Miller, G.E. (1957) 'Special theory of ultrasonic machining', *Journal of Applied Physics*, vol. 28, no. 2, pp. 149-156.

Montgomery, D.C. (2009) *Design and Analysis of Experiments*, 7th Edition edn, John Wiley & Sons.

Montgomery, D.C. & Runger, G.C. (2006) Tests of hypotheses for a single sample, in, *Applied Statistics and Probability for Engineers*, 4th edn, John Wiley & Sons, Inc., pp. 290-343.

Morgan technical ceramics (2011) Transducers, vol., [Online]. Available from: **http://www.morgantechnicalceramics.com** (Accessed: 23 June 2011).

Myers, R., Montgomery, D. & Anderson-Cook, C. (2009) *Response Surface Methodology: Process and Product Optimization Using Designed Experiments (Wiley Series in Probability and Statistics)*, Wiley.

Neppiras, E.A. (1960) 'Very high energy ultrasonics', *British Journal of Applied Physics*, vol. 11, no. 4, p. 143.

Neppiras, E.A. (1964) 'Ultrasonic machining and forming', *Ultrasonics*, vol. 2, no. 4, pp. 167-173.

Nicholson, N.C. & McDicken, W.N. (1996) 'A comparison of coupling horns for waveguides used in medical ultrasonics', *Ultrasonics*, vol. 34, no. 7, pp. 747-755.

Olabi, A.G. & Grunwald, A. (2008) 'Design and application of magnetostrictive materials', *Materials & Design*, vol. 29, no. 2, pp. 469-483.

Olszak, A.G., Schmit, J. & Heaton, M.G. (2001) *Interferometry: Technology and applications*,

Ouyang, P.R., Zhang, W.J. & Gupta, M.M. (2008) 'A new compliant mechanical amplifier based on a symmetric five-bar topology', *Journal of Mechanical Design*, vol. 130, no. 10, p. 104501.

Paganelli, R.P., Romani, A., Golfarelli, A., Magi, M., Sangiorgi, E. & Tartagni, M. (2010) 'Modeling and characterization of piezoelectric transducers by means of scattering parameters. Part I: Theory', *Sensors and Actuators A: Physical*, vol. 160, no. 1-2, pp. 9-18.

Park, G., Bement, M.T., Hartman, D.A., Smith, R.E. & Farrar, C.R. (2007) 'The use of active materials for machining processes: A review', *International Journal of Machine Tools and Manufacture*, vol. 47, no. 15, pp. 2189-2206.

Park, S.H. (1996) *Robust Design and Analysis for Quality Engineering*, Chapman & Hall, London [etc.].

Park, Y.W. & Kim, D.Y. (2004) 'Development of a magnetostrictive microactuator', *Journal of Magnetism and Magnetic Materials*, vol. 272-276, no. SUPPL. 1.

Park, Y.W. & Yim, M.C. (2004) 'Design and characterization of a magnetostrictive microactuator', *Physica Status Solidi (A) Applied Research*, vol. 201, no. 8, pp. 1983-1987.

Pechersky, M.J. (1991) Coherent optical methods for metallography, *24rh Annual Convention of the International Metallographic Society*, Monterey, California, p. Medium: ED; Size: 10 p.

PI Ceramics (2011) [Online], Available from: **http://www.piceramic.com** (Accessed: 23 September 2011).

Rahman, M., Lim, H.S., Neo, K.S., Senthil Kumar, A., Wong, Y.S. & Li, X.P. (2007) 'Tool-based nanofinishing and micromachining', *Journal of Materials Processing Technology*, vol. 185, no. 1-3, pp. 2-16.

Rao, S.S. (2004) Fundamentals of vibration, in, *Mechanical Vibrations*, 4th edn, Pearson Education, pp. 1-105.

Reckase, M.D. (2009) Analyzing the Structure of Test Data Multidimensional Item Response Theory, in Springer New York, pp. 179-231.

Rohatgi, P.K., Nath, D., Singh, S.S. & Keshavaram, B.N. (1994) 'Factors affecting the damping capacity of cast aluminium-matrix composites', *Journal of Materials Science*, vol. 29, no. 22, pp. 5975-5984.

Schneider, E. (1997) Ultrasonic techniques, in, *Structural and Residual Stress Analysis by Nondestructive Methods*, Elsevier Science B.V., Amsterdam, pp. 522-563.

Seah, K.H.W., Wong, Y.S. & Lee, L.C. (1993) 'Design of tool holders for ultrasonic machining using FEM', *Journal of Materials Processing Technology*, vol. 37, no. 1-4, pp. 801-816.

Sherrit, S., Askins, S.A., Gradziol, M., Dolgin, B.P., Bao, X., Chang, Z. & Bar-Cohen, Y. (2002) Novel horn designs for ultrasonic/sonic cleaning, welding,

soldering, cutting, and drilling, vol. 4701, ed. L.P. Davis, SPIE, San Diego, CA, USA, pp. 353-360.

Sherrit, S., Badescu, M., Bao, X., Bar-Cohen, Y. & Chang, Z. (2004) Novel horn designs for power ultrasonics, *Ultrasonics Symposium, 2004 IEEE*, vol. 3, pp. 2263-2266 Vol.2263.

Sherrit, S.L.C., CA, US), Askins, Stephen A. (Ledyard, CT, US), Gradziel, Michael James (Cheshire, MA, US), Dolgin, Benjamin (Los Angeles, CA, US), Bar-cohen, Yoseph (Seal Beach, CA, US), Bao, Xiaoqi (San Gabriel, CA, US), Chang, Zensheu (Irvine, CA, US), Peterson, Thomas M. (Erie, PA, US) (2004) *Folded horns for vibration actuators, US Patents*, no 20040047485, United States.

Shiomi, M., Osakada, K., Nakamura, K., Yamashita, T. & Abe, F. (2004) 'Residual stress within metallic model made by selective laser melting process', *CIRP Annals - Manufacturing Technology*, vol. 53, no. 1, pp. 195-198.

Shirwaiker, R. & Okudan, G. (2008) 'Triz and axiomatic design: a review of case-studies and a proposed synergistic use', *Journal of Intelligent Manufacturing*, vol. 19, no. 1, pp. 33-47.

Siddiq, A. & Ghassemieh, E. (2008) 'Thermomechanical analyses of ultrasonic welding process using thermal and acoustic softening effects', *Mechanics of Materials*, vol. 40, no. 12, pp. 982-1000.

Singh, M.K. (2007) Introduction of unconventional manufacturing process, in, *Unconventional Machining Processes* New Age International, pp. 1-8.

Singh, R. & Khamba, J.S. (2006) 'Ultrasonic machining of titanium and its alloys: A review', *Journal of Materials Processing Technology*, vol. 173, no. 2, pp. 125-135.

Singh, R. & Khamba, J.S. (2007) 'Taguchi technique for modeling material removal rate in ultrasonic machining of titanium', *Materials Science and Engineering: A*, vol. 460–461, no. 0, pp. 365-369.

Soundararajan, V. & Radhakrishnan, V. (1986) 'An experimental investigation on the basic mechanisms involved in ultrasonic machining', *International Journal of Machine Tool Design and Research*, vol. 26, no. 3, pp. 307-321.

Statnikov, E.S., Korolkov, O.V. & Vityazev, V.N. (2006) 'Physics and mechanism of ultrasonic impact', *Ultrasonics*, vol. 44, no. Supplement 1, pp. e533-e538.

Steer, M.B. (2010) *Microwave and RF Design - A Systems Approach*, SciTech Publishing.

Suh, N.P. (1990) *The Principles of Design*, Oxford University Press.

Suh, N.P. (1999) 'A theory of complexity, periodicity and the design axioms', *Research in Engineering Design*, vol. 11, no. 2, pp. 116-132.

Suh, N.P. (2001) *Axiomatic design : advances and applications*, New York : Oxford University Press, 2001.

Sun, X.Q., Masuzawa, T. & Fujino, M. (1996) 'Micro ultrasonic machining and its applications in MEMS', *Sensors and Actuators, A: Physical*, vol. 57, no. 2, pp. 159-164.

The University of Tokyo (2012) *MEMS Facility in THT Lab* [Online], Available from: **http://www.thtlab.t.u-tokyo.ac.jp/MEMS_Equipment/mems.html** (Accessed: 9 May 2012).

Thoe, T.B., Aspinwall, D.K. & Wise, M.L.H. (1998) 'Review on ultrasonic machining', *International Journal of Machine Tools and Manufacture*, vol. 38, no. 4, pp. 239-255.

Tutuncu, A.N., Podio, A.L., Gregory, A.R. & Sharma, M.M. (1998) 'Nonlinear viscoelastic behavior of sedimentary rocks. Part 1: Effect of frequency and strain amplitude', *Journal Name: Geophysics; Journal Volume: 63; Journal Issue: 1; Other Information: PBD: Jan-Feb 1998*, pp. Medium: X; Size: pp. 184-194.

Ueno, T., Qiu, J. & Tani, J. (2004) 'Magnetic force control based on the inverse magnetostrictive effect', *IEEE Transactions on Magnetics*, vol. 40, no. 3, pp. 1601-1605.

van der Avoort, C., van der Hout, R., Bontemps, J.J.M., Steeneken, P.G., Le Phan, K., Fey, R.H.B., Hulshof, J. & van Beek, J.T.M. (2010) 'Amplitude saturation of MEMS resonators explained by autoparametric resonance', *Journal of Micromechanics and Microengineering*, vol. 20, no. 10, p. 105012.

Venkatesh, V.C. (1983) 'Machining of glass by impact processes', *Journal of Mechanical Working Technology*, vol. 8, no. 2-3, pp. 247-260.

Wang, Z.Y. & Rajurkar, K.P. (1996) 'Dynamic analysis of the ultrasonic machining process', *Journal of Manufacturing Science and Engineering*, vol. 118, no. 3, pp. 376-381.

Wevers, M., Lafaut, J.P., Baert, L. & Chilibon, I. (2005) 'Low-frequency ultrasonic piezoceramic sandwich transducer', *Sensors and Actuators, A: Physical*, vol. 122, no. 2, pp. 284-289.

Wing Or, S., Nersessian, N. & Carman, G.P. (2003) 'Effect of combined magnetic bias and drive fields on dynamic magnetomechanical properties of Terfenol-D/epoxy 1-3 composites', *Journal of Magnetism and Magnetic Materials*, vol. 262, no. 2, pp. L181-L185.

Wong, M., Owen, I., Sutcliffe, C.J. & Puri, A. (2009) 'Convective heat transfer and pressure losses across novel heat sinks fabricated by Selective Laser Melting', *International Journal of Heat and Mass Transfer*, vol. 52, no. 1-2, pp. 281-288.

Wu, S.M. (1962) *Tool-life testing by response surface methodology*, University of Wisconsin--Madison.

Xian, X. & Lin, S. (2008) 'Study on the compound multifrequency ultrasonic transducer in flexural vibration', *Ultrasonics*, vol. 48, no. 3, pp. 202-208.

Xu, C.H., Hu, J.H. & Chan, H.L.W. (2002) 'Behavior of a PZT ring under non-uniform mechanical stress', *Ultrasonics*, vol. 39, no. 10, pp. 735-742.

Yamamoto, Y., Eda, H. & Shimizu, J. (1999) 'Application of giant magnetostrictive materials to positioning actuators', *IEEE/ASME International Conference on Advanced Intelligent Mechatronics, AIM*, pp. 215-220.

Yoon, H.S., Washington, G., Eyabi, P., Radhamohan, M., Woodard, S.W. & Dayton, R. (2006) A millimeter-stroke piezoelectric hybrid actuator using hydraulic displacement amplification mechanism, *IEEE International Symposium on Industrial Electronics*, vol. 4, Montreal, QC, pp. 2809-2813.

Yu, H.N., Kim, S.S., Suh, J.D. & Lee, D.G. (2010) 'Axiomatic design of the sandwich composite endplate for PEMFC in fuel cell vehicles', *Composite Structures*, vol. 92, no. 6, pp. 1504-1511.

Yu, Z., Hu, X. & Rajurkar, K.P. (2006) 'Influence of debris accumulation on material removal and surface roughness in micro ultrasonic machining of silicon', *CIRP Annals - Manufacturing Technology*, vol. 55, no. 1, pp. 201-204.

Zhang, C., Rentsch, R. & Brinksmeier, E. (2005) 'Advances in micro ultrasonic assisted lapping of microstructures in hard-brittle materials: A brief review and outlook', *International Journal of Machine Tools and Manufacture*, vol. 45, no. 7-8, pp. 881-890.

Zhang, J., Perez, R.J., Wong, C.R. & Lavernia, E.J. (1994) 'Effects of secondary phases on the damping behaviour of metals, alloys and metal matrix composites', *Materials Science and Engineering: R: Reports*, vol. 13, no. 8, pp. 325-389.

Zhang, Q.H., Wu, C.L., Sun, J.L. & Jia, Z.X. (2000) 'The mechanism of material removal in ultrasonic drilling of engineering ceramics', *Proceedings of the Institution of Mechanical Engineers, Part B: Journal of Engineering Manufacture*, vol. 214, no. 9, pp. 805-810.

APPENDIX

Table A.1: Complete Material Data Set PIC181.

Coefficient	Unit	Value	Coefficient	Unit	Value
Density	kg/m^3	7,85E+03	N1	Hzm	1646
			N3	Hzm	2004
Qm		2200	N5	Hzm	1222
			Np	Hzm	2265
ε11Tr		1224	Nt	Hzm	2302
ε33Tr		1135			
ε11Sr		740	d31	m/V	-1,08E-10
ε33Sr		624	d33	m/V	2,53E-10
tan δ		3,0E-3	d15	m/V	3,89E-10
k31		0,315	g31	Vm/N	-1,08E-02
k33		0,662	g33	Vm/N	2,52E-02
k15		0,629	g15	Vm/N	3,59E-02
kp		0,551			
kt		0,459	e31	N/Vm	-4,50
			e33	N/Vm	14,70
Poisson (σ)		0,35	e15	N/Vm	11,00
s11E	m^2/N	1.18E-08	c11E	N/m^2	1.52E+14
s33E	m^2/N	1.41E-08	c33E	N/m^2	1.34E+14
s55E	m^2/N	3.53E-08	c55E	N/m^2	2.83E+13
s12E	m^2/N	-4.07E-09	c12E	N/m^2	8.91E+13
s13E	m^2/N	-5.00E-09	c13E	N/m^2	8.55E+13
s44E	m^2/N	3.53E-08	c44E	N/m^2	2.83E+13
s66E	m^2/N	3.16E-08	c66E	N/m^2	3.16E+13
s11D	m^2/N	1.06E-08	c11D	N/m^2	1.55E+14
s33D	m^2/N	7.93E-08	c33D	N/m^2	1.66E+14
s55D	m^2/N	2.13E-08	c55D	N/m^2	4.69E+13
s12D	m^2/N	-5.24E-09	c12D	N/m^2	9.18E+13
s13D	m^2/N	-2.27E-09	c13D	N/m^2	7.06E+13
s44D	m^2/N	2.13E-08	c44D	N/m^2	4.69E+13
s66D	m^2/N	3.16E-08	c66D	N/m^2	3.16E+13

Source: PI Ceramics

Table A.2: Properties of Metals.

Material	Density kg/m³	Modulus of Elasticity N/m²	Shear Modulus N/m²	Poisson's Ratio	$c_{L,II}$ m/s	c_T m/s	Loss Factor		Remarks
							Flexural	Longitudinal	
Aluminium	2700	$72 \cdot 10^9$	$27 \cdot 10^9$	0.34	5200	3100	$0.3–10 \cdot 10^{-5}$	$\approx 10^{-4}$	[4.19, 20, 24]
Lead	11300	$17 \cdot 10^9$	$6 \cdot 10^9$	0.43	1250	730	$5–30 \cdot 10^{-2}$ $1–4 \cdot 10^{-3}$	$\approx 2 \cdot 10^{-2}$	[4.19] chem. pure [4.19] Antimon
Iron	7800	$200 \cdot 10^9$	$77 \cdot 10^9$	0.30	5050	3100	$1–4 \cdot 10^{-4}$	$2–6 \cdot 10^{-4}$	[4.19, 21, 24]
Steel	7800	$210 \cdot 10^9$	$77 \cdot 10^9$	0.31	5100	3100	$0.2–3 \cdot 10^{-4}$		
Gold	19300	$80 \cdot 10^9$	$28 \cdot 10^9$	0.423	2000	1200	$\approx 3 \cdot 10^{-4}$		[4.23]
Copper	8900	$125 \cdot 10^9$	$46 \cdot 10^9$	0.35	3700	2300	$2 \cdot 10^{-3}$ $2–7 \cdot 10^{-4}$	$\approx 2 \cdot 10^{-3}$	Polycrystal single crystal
Magnsium	1740	$43 \cdot 10^9$	$17 \cdot 10^9$	0.29	5000	3100		$\approx 10^{-4}$	[4.24]
Brass	8500	$95 \cdot 10^9$	$36 \cdot 10^9$	0.33	3200	2100	$0.2–1 \cdot 10^{-3}$	$< 10^{-3}$	[4.19]
Nickel	8900	$205 \cdot 10^9$	$77 \cdot 10^9$	0.30	4800	2900		$< 10^{-3}$	[4.24]
Silver	10500	$80 \cdot 10^9$	$29 \cdot 10^9$	0.37	2700	1600	$\approx 4 \cdot 10^{-4}$	$< 3 \cdot 10^{-3}$	[4.22, 23]
Bismuth	9800	$3.3 \cdot 10^9$	$1.3 \cdot 10^9$	0.38	580	360		$\approx 8 \cdot 10^{-4}$	[4.24]
Zinc	7130	$13.1 \cdot 10^9$	$5 \cdot 10^9$	0.33	1350	850		$\approx 3 \cdot 10^{-4}$	[4.24]
Tin	7280	$4.4 \cdot 10^9$	$1.6 \cdot 10^9$	0.39	780	470		$\approx 20 \cdot 10^{-4}$	[4.24]

Source: Cremer, Heckl and Petersson (2005)

Table A.3: Properties of Materials Used for Studying MRRs.

Material	Density (10^3kg/m³)	Young's Modulus (GPa)	Hardness (HV)	Poisson's ratio (-)	Source
Glass ceramic	2.6	93			Schott ROBAX®
Soda-lime glass	2.4 – 2.5	68 – 72	439 – 484		CES Edupack
Mild steel (S45C)	7.8 – 7.9	208 – 216	188 – 228	0.29 – 0.30	CES Edupack
Stainless steel (316L)	7.9 – 8.1	190 – 205	170 – 220	0.27 – 0.28	CES Edupack
Ceramic Al_2O_3	3.8 – 4.0	343 – 390	1.2e3 – 2.1e3	0.23 – 0.26	CES Edupack
Ceramic SiC	3.1 – 3.2	400 – 460	2.3e3 – 2.6e3	0.16 – 0.18	CES Edupack

Table A.4: Particle Size Conversion Chart - FEPA.

Macro grits				Micro grits	
Grit designation	Mean Diameter (μm)	Grit designation	Mean Diameter (μm)	Grit designation	Mean Diameter (μm)
F 4	4890	F 36	525	F 230	53.0 ± 3
F 5	4125	F 40	438	F 240	44.5 ± 2
F 6	3460	F 46	370	F 280	36.5 ± 1.5
F 7	2900	F 54	310	F 320	29.2 ± 1.5
F 8	2460	F 60	260	F 360	22.8 ± 1.5
F 10	2085	F 70	218	F 400	17.3 ± 1
F 12	1765	F 80	185	F 500	12.8 ± 1
F 14	1470	F 90	154	F 600	9.3 ± 1
F 16	1230	F 100	129	F 800	6.5 ± 1
F 20	1040	F 120	109	F 1000	4.5 ± 0.8
F 22	885	F 150	82	F 1200	3.0 ± 0.5
F 24	745	F 180	69	F 1500	2.0 ± 0.4
F 30	625	F 220	58	F 2000	1.2 ± 0.3